TWO-DIMENSIONAL DEPTH-AVERAGED BEACH EVOLUTION MODELLING

A THESIS SUBMITTED TO
THE GRADUATE SCHOOL OF NATURAL AND APPLIED SCIENCES
OF
MIDDLE EAST TECHNICAL UNIVERSITY

BY

CÜNEYT BAYKAL

IN PARTIAL FULFILLMENT OF THE REQUIREMENTS
FOR
THE DEGREE OF DOCTOR OF PHILOSOPHY
IN
CIVIL ENGINEERING

FEBRUARY 2012

Approval of the thesis:

TWO-DIMENSIONAL DEPTH-AVERAGED BEACH EVOLUTION MODELLING

submitted by **CÜNEYT BAYKAL** in partial fulfillment of the requirements for the degree of **Doctor of Philosophy in Civil Engineering Department, Middle East Technical University** by,

Prof. Dr. Canan Özgen
Dean, Graduate School of **Natural and Applied Sciences**   _____

Prof. Dr. Güney Özcebe
Head of Department, **Civil Engineering**   _____

Prof. Dr. Ayşen Ergin
Supervisor, **Civil Engineering Dept., METU**   _____

Examining Committee Members:

Prof. Dr. Can Elmar Balas
Civil Engineering Dept., Gazi University   _____

Prof. Dr. Ayşen Ergin
Civil Engineering Dept., METU   _____

Prof. Dr. Ahmet Cevdet Yalçıner
Civil Engineering Dept., METU   _____

Prof. Dr. İsmail Aydın
Civil Engineering Dept., METU   _____

Assoc. Prof. Dr. Utku Kânoğlu
Engineering Sciences Dept., METU   _____

                                        Date: 10.02.2012

I hereby declare that all information in this document has been obtained and presented in accordance with academic rules and ethical conduct. I also declare that, as required by these rules and conduct, I have fully cited and referenced all material and results that are not original to this work.

Name, Last name :   Cüneyt Baykal

Signature   :

ABSTRACT

TWO-DIMENSIONAL DEPTH-AVERAGED BEACH EVOLUTION MODELLING

Baykal, Cüneyt

Ph.D., Department of Civil Engineering

Supervisor: Prof.Dr. Ayşen Ergin

February 2012, 174 pages

In this study, a two-dimensional depth-averaged beach evolution numerical model is developed to study the medium and long term nearshore sea bottom evolution due to non-cohesive sediment transport under the action of wind waves only over the arbitrary land and sea topographies around existing coastal structures and formations. The developed beach evolution numerical model is composed of four sub-models: a nearshore spectral wave transformation model based on energy balance equation including random wave breaking and diffraction terms to compute the nearshore wave characteristics, a nearshore wave-induced circulation model based on the non-linear shallow water equations to compute the nearshore depth averaged wave-induced current velocities and mean water level changes, a sediment transport model to compute the local total sediment transport rates occurring under the action of wind waves and a bottom evolution model to compute the bed level changes in time due to gradients of sediment transport rates in cross-shore and longshore directions. The governing partial differential equations are solved utilizing finite difference schemes. The developed models are applied successfully to several theoretical and conceptual benchmark cases and an extensive data set of laboratory and field measurements. As an alternative approach to be used in beach evolution problems, a distributed total sediment load formula is proposed based on the assumption that the local total sediment transport rates across the surf zone are proportional to the product of the rate of dissipation of wave energies due to wave breaking and wave-induced current velocities. The proposed distribute load approach is validated with the available laboratory and field measurements.

Keywords: Spectral Wave Modelling, Nearshore Wave-Induced Circulation, Cross-shore Distribution of Longshore Sediment Transport, Numerical Modeling of Beach Evolution

ÖZ

İKİ BOYUTLU DERİNLİK ORTALAMALI KIYI DEĞİŞİMİ MODELLEMESİ

Baykal, Cüneyt

Doktora, İnşaat Mühendisliği

Tez Yöneticisi: Prof. Dr. Ayşen Ergin

Şubat 2012, 174 sayfa

Bu çalışmada düzensiz kara ve deniz taban topoğrafyası üzerinde kıyı yapıları ve oluşumları çevresindeki rüzgar dalgaları etkisindeki koheziv olmayan kum hareketlerine bağlı orta ve uzun dönemli kıyı değişimlerinin araştırılmasında kullanılmak üzere iki boyutlu derinlik ortalamalı kıyı değişimi sayısal modeli geliştirilmiştir. Geliştirilen kıyı değişimi sayısal modeli dört alt-modelden oluşmaktadır. Bu modeller sırasıyla; yakın kıyı dalga özelliklerinin belirlendiği enerji korunum denklemine bağlı düzensiz dalga kırılması ve dönmesini içeren spektral dalga dönüşüm modeli, lineer-olmayan sığ su denklemlerine bağlı yakın kıyı derinlik ortalamalı dalga kaynaklı akıntı hızları ve ortalama su seviyesi değişimlerinin elde edildiği yakın kıyı çevrim modeli, rüzgar dalgaları etkisinde oluşan toplam kum taşınım debilerinin hesaplandığı kum taşınım modeli ve kum taşınım debilerinin kıyıya dik ve paralel doğrultulardaki türevlerine bağlı zaman içindeki taban yüksekliği değişimlerinin hesaplandığı taban değişim modelidir. Geliştirilen modeller çeşitli teorik ve kavramsal durumlar, laboratuvar ve saha ölçümlerinden oluşan geniş bir veri seti ile doğrulama çalışmaları yapılmıştır. Bu çalışmada ayrıca kıyı değişimi problemlerinde kullanılmak üzere, kırılma bölgesindeki toplam kum taşınım debilerinin dalga kırılması olaylarında kaybolan enerji miktarlarına ve dalga kaynaklı akıntı hızlarına bağlı olduğu kabul edilerek geliştirilen bir yayılı toplam kum taşınım yöntemi önerilmiştir. Önerilen yayılı taşınım yaklaşımı ile laboratuvar ve saha ölçümleri arasındaki niteliksel uygunluk araştırılmış ve yöntemin doğrulaması yapılmıştır.

Anahtar Kelimeler: Spektral Dalga Modellemesi, Yakın Kıyı Dalga Kaynaklı Su Çevrimi, Kıyı Boyu Kum Taşınımının Kıyıya Dik Dağılımı, Kıyı Değişimi Sayısal Modellemesi

Dedicated to My Family

ACKNOWLEDGEMENTS

TABLE OF CONTENTS

LIST OF TABLES

LIST OF FIGURES

LIST OF SYMBOLS

A emprical dimensionless parameter (Watanabe, 1992)

*slope of the equation of straight line of equation of long term statistics

(*: Chapter 5)

A_w wave orbital semi excursion

A_{sr} surface roller area

A_x lateral mixing term in x-direction

A_y lateral mixing term in y-direction

B intercept of the equation of straight line of equation of long term

statistics in vertical axis of wave height

c suspended sediment concentration

c_f friction coefficient

C wave celerity

C_{g0} deep water wave group celerity

C_0 deep water wave celerity

D directional spreading function (Borgman, 1984)

D_b dissipation rate due to wave breaking

D_d dissipation term introduced by Mase (2001)

d water depth from mean water level

d_{50} median grain size diameter

$d_{50}*$ dimensionless median grain size diameter parameter

E total wave energy

E_{mean} mean absolute percent error

E_{sr} kinetic energy of the surface roller

f wave frequency

f_c current friction factor

f_p peak frequency

f_w wave friction factor

F_x sum of radiation stresses and stresses acting on the water body due to

surface rollers in x-direction

F_y	sum of radiation stresses and stresses acting on the water body due to surface rollers in y-direction
g	gravitational acceleration
G	directional spreading function
h	water depth from still water level
H	wave height
H_b	depth-limited maximum wave height
H_{rms}	root-mean-square wave height
$H_{rms,0}$	deep water root-mean-square wave height
$H_{rs,0}$	representative deep water significant height
H_s	significant wave height
$H_{s,0}$	deep water significant wave height
$H_{s,b}$	significant breaking wave height
i	spatial grid index in x-direction
j	spatial grid index in y-direction
k	wave number
	an assigned range to compute occurrence probability (: Chapter 5)
k_s	bed roughness (Nikuradse sand grain roughness)
K	dimensionless empirical parameter in CERC's total sediment transport formula
K_d	coefficient of diffraction of regular waves
$(K_d)_{eff}$	coefficient of diffraction of irregular waves
K_{sr}	energy dissipation rate of the surface roller
L	wave length
L_0	deep water wave length
m	bottom slope
m_{cr}	critical bottom slope (user defined wet- or dry- angle of repose)
m_0	integral (zero moment) of the directional spectrum
n	ratio of group velocity to wave celerity
	(also used as time step index)
p	in-place porosity
P_i	occurrence probability of wave with height H_i

$q_{total,x}$	total sediment transport rate in bulk volume including pores per unit longshore distance in cross-shore direction
$q_{total,y}$	total sediment transport rate in bulk volume including pores per unit cross-shore distance in longshore direction
Q	cumulative exceedance probability
Q_b	fraction of waves broken
R	relative roughness
s	degree of directional energy concentration
s_{max}	spreading parameter
s_{os}	deep water significant wave steepness
S	directional wave spectral density
S_{xx}	radiation stress acting in the x-direction along x-axis
S_{xy}	radiation stress acting in the y-direction along x-axis
S_{yx}	radiation stress acting in the x-direction along y-axis
S_{yy}	radiation stress acting in the y-direction along y-axis
T	wave period
T_s	significant wave period
T_p	peak wave period
u	depth-averaged current velocity in x-direction
u_w	wave orbit velocity
u_c	current velocity
u_{cw}	combined wave-current velocity
u_0	maximum horizontal orbital velocity
U	wind speed
v	depth-averaged current velocity in y-direction
v_x	energy flux propagation velocity in x-direction
v_y	energy flux propagation velocity in y-direction
v_ϑ	energy flux propagation velocity in θ-direction
w^*	total work needed to keep sediments in suspension per unit length in cross-shore direction
w_s	fall speed of sediment grain
W	total amount of work needed to keep the sediment in suspension

x	cross-shore direction
y	alongshore direction
z	normal direction to x-y plane
α	energy transfer coefficient
γ	peak enhancement factor for the frequency spectrum
γ_b	breaker index
δ	thickness of the surface roller in front of the breaking waves, moving with the wave celerity
Δh	bottom change in one morphological time step
Δh_a	bottom change due to avalanche in one morphological time step
Δt	time step in the nearshore circulation model
Δx	alongshore grid spacing
Δy	offshore grid spacing
Δt_m	time step in the bottom evolution model
ε	fraction of the rate of dissipation in wave energy flux due to wave breaking
$\bar{\eta}$	change in the mean water elevation
θ	approach angle
θ_{cr}	critical Shields parameter
θ_{max}	maximum approach angle in the directional domain
θ_{min}	maximum approach angle in the directional domain
θ_{peak}	peak approach angle
$\bar{\theta}$	mean approach angle
$\bar{\theta}_0$	deep water mean approach angle
κ	diffraction intensity parameter
Λ	empirical turbulent eddy viscosity constant
μ	turbulent eddy viscosity term
ν	kinematic viscosity
ρ	water density
ρ_s	sediment density
σ_m	directional spreading parameter
σ_{rms}	root-mean-square scatter
$\tau_{b,cw}$	mean bed shear stress under wave-current field over a wave-cycle

τ_c	bed shear stress due to steady current only
τ_{cr}	critical bed shear stress required to mobilize the sediment grains at the sea bed
τ_{cw}	instantaneous combined bed shear stress
$\tau_{w,max}$	maximum bed shear stress due to waves only
φ	angle between the mean wave approach angle and the steady current
ω	angular frequency

CHAPTER 1

INTRODUCTION

1.1. General Description

The continuous geomorphological evolution of coastal areas is the result of a dynamic and highly complex balance between the anthropogenic activities at coastal areas and various physical processes occurring due to the interactions between the three masses of earth: land, water and atmosphere. Among these processes, the sediment transport due to wind wave action plays an important role in this evolution. The prediction of this evolution for various temporal and spatial scales and for various types of problems such as erosion/accretion around coastal structures, navigation channels, river mouths or tidal inlets has been a great concern of scientists and engineers for decades. Advances in the numerical computing techniques and the computer technology increased the popularity of the use of numerical modeling techniques in the estimation of beach evolution problems.

Coastal erosion or accretion problems are among the major problems that almost every country with some kilometers of coastline faces and spends millions of dollars to solve as in the case of Miami Beach in Florida, USA, where $64 million USD were spent in the nourishment of the Miami Beach by 100 m in width over a length of 16 km as a remedial measure between the years 1976-1981 (Dean and Dalrymple, 2002). Miami Beach is a typical example to coastal erosion problems resulting from imbalance in the 'sediment budget' of coastal areas in the world. In Turkey, the Bafra alluvial plain, where the Kızılırmak River discharges into the Black Sea, might be given as an example to severe coastal erosion problems. Almost 1 km wide band of shoreline has vanished since 1988 under the action of storm waves and due to the flow regulation structures on the Kızılırmak River blocking the sediment supply to the alluvial plain (Kökpınar et al., 2007).

Erosion or accretion problems at coastal areas are mainly due to the imbalance between the sources and sinks (losses) of the sediment budget of the coastal areas. The weathering of cliffs by waves and other steady or quasi-steady currents like wind- or tide-induced circulation, wind-blown material from cliffs, dunes and inland, sediments carried by surface (rain waters) and groundwater flows, freeze-thaw process, sediment carried by rivers, biogenic materials resulting from the decay of organic matter such as shells and coral fragments especially in some tropical areas and human induced sources like artificial nourishment, disposal of dredged soil and industrial waste tipping are the main sources of sediment at coastal areas. Likewise, erosion by marine action (waves, tides and currents), submarine canyons, human extraction along rivers (sand mining) and at nearshore areas for commercial and navigational purposes, damming of rivers and streams, fishing by the use of explosives and trapping of sand on the upstream side of the coastal structures are the main sinks of the sediment budget at coastal areas (CIRIA, 1996; Baykal et al., 2011). Among the above given wide variety of physical processes of sources and sinks, wind waves play an important role both in the short and long term morphological evolution of coastal areas such as recession of shoreline, sedimentation around coastal structures, seasonal changes in the nearshore sea bottom topography (bathymetry) (Kamphuis, 2000; Masselink and Hughes, 2003). In temporal scale, the variation in the amount and direction of the longshore movement of sand grains under the action of wind waves is constitutive in long term changes, whereas cross-shore transport of sediment plays important role in short term changes at coastal areas.

For the purpose of understanding and prediction of temporal and spatial morphological changes at coastal areas due to the variation in the amount and direction of cross-shore and longshore sediment transport (hereafter LST) rates, starting from 1950's (Pelnard-Considere, 1956) till nowadays (Roelvink et al., 2009; Nam et al., 2009, 2010) there has been numerous attempts to model the nature physically in small or large scale laboratories or numerically in computer medium, the details of which are discussed in the following chapter.

However, these efforts are still far from the re-production of the nature within the desired limits of accuracy, computation time and cost and the numerical modeling efforts should be supported by physical modeling of governing mechanisms isolated for various wave, current, bottom topography and structural conditions to deepen our understanding in sediment motion.

1.2. Objectives of the Study

This thesis study is focused on the numerical modeling of the coastal erosion and accretion processes both in short and long terms due to sediment transport under the action of wind waves only. The main objectives of the study are;

- To develop a two-dimensional phase-averaged spectral wave transformation model based on energy balance equation for the simulation of irregular wave shoaling, refraction, diffraction and breaking processes around coastal defense structures over arbitrary bathymetries,
- To develop a two-dimensional depth-averaged numerical circulation model based on non-linear shallow water equations for the computation of wave-induced nearshore current fields and the changes in mean water level around coastal defense structures over arbitrary bathymetries,
- To investigate the relationship between the energy dissipation rates due to random wave breaking and distributed total LST rates,
- To construct a depth-averaged two-dimensional beach evolution model which is applicable to both medium-term (weeks to months) and long-term events (years to decades),
- To validate the developed beach evolution model with the available laboratory and field measurements and to apply to real a case study of beach evolution.

1.3. Contents of Chapters

In the following chapters, the work carried out for the above given objectives throughout this thesis study is presented.

The second chapter gives the available information in the literature related to each stage of the study. Starting with the types of modeling techniques of wave transformation, available methodologies focused on phase-averaged modeling of propagation of directional random waves from offshore to the shore are presented. Detailed literature survey on irregular wave breaking and diffraction is given. Regarding to the irregular wave diffraction, the methodologies used in the action/energy balance equation models are emphasized. Moreover, the studies in the literature carried out for the determination of wave-induced nearshore current velocities and mean water levels over arbitrary bathymetries are summarized. Finally, the available literature on beach evolution modeling is given within the perspective of one-line models, limitations and improvements of these models, and recent studies on two dimensional depth-averaged beach evolution models.

In the third chapter, the structure of the two-dimensional depth-averaged beach evolution model is presented in the order of the flowchart of the model structure. The main assumptions and limitations of the model are discussed first. The governing equations and the numerical structure of the two-dimensional phase-averaged spectral wave transformation model is given and followed by the surface roller model and the depth-averaged nearshore circulation model which solves non-linear shallow water equations. Later, the theoretical background and the numerical application of the sediment transport and bottom evolution modules of the beach evolution model are presented in detail.

Fourth chapter is the part where the developed models are benchmarked with the analytical solutions, several data sets of laboratory and field experiments and benchmark problems such as modeling of rip currents around beach cusps.

In the fifth chapter, a comparative study to validate the numerical beach evolution model is given and discussed. The case study area is selected as the Bafra alluvial plain where the Kızılırmak River discharges into the Black Sea. The shoreline changes measured at the groin field to the east of the river mouth between the years 1999 and 2003 are studied by the developed beach evolution model.

In the last chapter, the performed thesis work is summarized in the light of achieved and recommended future research agenda for further development of the theoretical and numerical background of the beach evolution model.

CHAPTER 2

LITERATURE SURVEY

2.1. Numerical Modeling of Random Wave Transformation

Starting from 1960s, numerical computation techniques are commonly used in solving various problems regarding water waves (Goda, 2010). Wave hindcasting and forecasting problems, including generation, growth and decay of wind waves, propagation of waves (i.e. wind waves, tsunami) from deep water to the shore, wave-structure interactions (i.e. diffraction, transmission, reflection, overtopping), wave-sediment interactions and beach morphology problems are some of these problems. Over the years, numerical techniques developed to solve these problems showed great variety with respect to the problem in concern, equations solved, techniques and approaches implemented to solve specific points (i.e. wave breaking, diffraction), areas of interest (i.e. harbor agitation, wind wave generation, tsunami propagation) and temporal and spatial scales. In the investigation of nearshore wave-induced currents and beach morphology changes, numerical methods for two dimensional wave transformations are commonly used.

Two dimensional wave transformation models (Goda, 2010) can be classified into two main groups as phase-resolving and phase-averaged models. Boussinesq models (Boussinesq, 1871, Mei and LeMehaute, 1966; Peregrine, 1967) and nonlinear or time-dependent mild slope models (Smith and Sprinks, 1975; Booij, 1981; Kirby and Dalrymple, 1983; 1984; Copeland, 1985; Tang and Quellet, 1992; Tang, 1994; Tang and Quellet, 1997) are examples to the phase-resolving models which give both spatial and temporal variations of wave profiles over a region. These models are commonly used in the applications of harbor tranquility and resonance problems. Although they provide a very high degree of sophistication in wave transformation modeling, this type of models

are not practical to be applied to large scale regions due to excessive computational load and often lack stability. The size of the computational area is limited by the computational capacity of available computer. The computational grid spacing is in the order of a few hundredths of the wavelength and the time step is a few percent of the wave period for this type of models.

Phase-averaged models give only the spatial variation of wave amplitude and direction without computing wave profiles. These models are widely used in nearshore wave transformation problems and are applicable to large scale coastal areas as coarser grid spacing (one-tenth of the wavelength or larger) can be used. Mild slope models and action/energy balance models are examples to phase averaged models (Goda, 2010).

The mild slope equation (MSE hereafter), originally in elliptic form, was first proposed by Berkhoff (1972) to analyze the transformation of regular waves due to combined wave refraction and diffraction. In deep water, MSE reduces to Helmholtz equation, which was developed to solve harbor tranquility problems for monochromatic waves in France in the 1960s, and reduces to shallow water equations (SWE hereafter) in shallower depths (Troch, 1998). Radder (1979) proposed the parabolic type of MSE, which disregards the wave reflection, yet, provides numerical efficiency and reduces the excessive computational demands of MSE. The hyperbolic form of the MSE is solved in Nishimura et al. (1983), Copeland, (1985), Madsen and Larsen (1987), Panchang et al., (1991). It includes wave reflection and requires reduced computing effort compared with the elliptic form (Bokaris and Anastasiou, 2003). A major limitation of using mild slope equations is the grid spacing that should be considered with respect to wavelengths which may lead spacing and computation time problems in large regions (larger than 1km x 1km).

Pierson et al.'s study (1952) on the evaluation of wave refraction in the northern New Jersey coast was the first attempt on the modeling of transformation of directional random waves. In 1969, Karlsson introduced the energy balance equation of directional wave spectral density for the solution of shoaling and refraction of directional random waves when they propagate from deep water toward the shore. Goda and Suzuki (1975) used Karlsson's model to compute the refraction coefficient of random waves defined

with the Mitsuyasu-type directional spreading function (Mitsuyasu et al., 1975). The energy balance equation introduced by Karlsson is only for the solution of shoaling and refraction of directional random waves, and does not include the effects of depth limited wave breaking, wave diffraction, bottom friction, nonlinear wave-wave interactions, white-capping, or ambient currents. Effects of these processes on waves were later added to the differential equation as source or sink terms (Booij et al., 1999; Mase, 2001; Holthuijsen et al., 2003).

Energy density spectrum is the distribution of energy of the sea surface composed of waves with different heights, periods and directions (Goda, 2010). In the presence of ambient currents, the energy density is not conserved as there might be an energy transfer between the wave motion and the mean fluid motion, but the action density, defined as the ratio of energy density to the relative frequency, is conserved (Bretherton and Garrett, 1968; Whitham, 1974). Therefore, the action balance equation, the evolution of action densities over arbitrary sea bottom topographies, is more commonly used in this type of models, called as action/energy balance models.

The concept of action/energy density is also used in wave generation models. WAM (WAMDI Group, 1988), HISWA (Holthuijsen et al., 1989), WAVEWATCH III (Tolman, 1991), TOMAWAC (Benoit et al., 1996), SWAN (Booij et al., 1999) and STWAVE (Smith and Zundel, 2006) are some of the wave generation and transformation models solving the action/energy balance equation with the source and sinks terms including wind stresses over the sea surface additive to the other physical sources or sinks. Except SWAN and STWAVE models, which are essentially developed for nearshore wave transformation of directional random waves including generation by winds, these models are not realistically applicable to coastal regions with horizontal scales less than 20-30 km and water depths less than 20-30 m (nearshore coastal areas i.e. estuaries, tidal inlets, barrier islands, tidal flats, channels) (Booij et al., 1999). Similar to SWAN and STWAVE models, there exist several other wave transformation models solving the action/energy balance equation such as WABED (Mase and Kitano, 2000; Mase, 2001), GHOST (Rivero et al., 1997) and CMS-Wave (Lin et al., 2008). The above given models mainly differ from each other with respect to their numerical schemes, directional

sectors of wave propagation, methods used to define the depth induced wave breaking, wave diffraction, bottom friction and other physical processes.

2.1.1. Irregular Wave Breaking

As the waves approach to the shore, they increase in steepness (ratio of wave height to the wave length) due to decreasing water depths. When the increasing wave steepness of a single wave reaches to a limiting value, the wave breaks dissipating energy and inducing nearshore currents and an increase in the mean water level at the shore (CEM, 2003). Regular waves break almost at a certain location, called as "breaking depth" approximately equal to the wave height, depending on the bottom slope, the wave steepness and the approach angle. For directional random waves composed of individual waves with different heights, periods and directions, depth-induced wave breaking becomes a continuous process of dissipation of wave energy due to bottom effect and wave steepness over a wide nearshore area, called as "surf zone."

Random wave breaking is mostly studied or modeled with either the similarity method, assuming a constant height-to-depth ratio called as "breaker index," or a statistical (individual wave or wave height distribution) approach (CEM, 2003). In the similarity method, the ratios of wave heights to the water depths are assumed to be equal to or smaller than the breaker index within the surf zone and the wave heights are determined accordingly. The STWAVE model uses such an approach, a modified Miche Criterion (Miche, 1951), to represent the depth-induced wave breaking for directional random waves.

Statistically, waves in nature can be described using the Rayleigh distribution outside the surf zone. The distribution of waves within the surf zone can be obtained transforming the waves individually and re-evaluating their distribution (Dally, 1990; Larson and Kraus, 1991; Dally, 1992) or assuming a truncated/modified distribution (Collins, 1970; Battjes, 1972; Goda, 1975a; Battjes and Janssen, 1978; Thornton and Guza, 1983; Baldock et al., 1998; Goda, 2004; Janssen and Battjes, 2007).

As it is given in Goda (2010), Collins (1970) was the first to truncate the Rayleigh distribution beyond the breaker height. Battjes (1972) and Goda (1975a) followed the same methodology using different approaches to deform the probability density function (*pdf*) of the wave heights. Goda (1975a-b) used a gradational breaker index, providing for a smoother cut-off of the *pdf* of the waves compared to others, to represent the variation in breaker heights due to the variation of individual wave periods and other characteristics. In this approach, for a given incident offshore wave height, M levels of wave heights are set by equally dividing the Rayleigh cumulative distribution. Breaker index values are computed for each level of wave height considering bottom slope (negative or positive in propagation direction) Corresponding dissipated wave energy for each level of wave height is then computed. The method has been verified with several laboratory and field data (Goda, 1975a-b) and has been later improved to be used also for two dimensional varying bathymetries (Goda, 2004).

Battjes and Janssen (1978) (BJ78 hereafter) used the bore-type analogy, originally suggested by LeMehaute (1962), to approximate the dissipated energy due to wave breaking similar to the head loss due to hydraulic jump in a uniform flow. BJ78 assumed that the wave heights of the breaking or broken waves at a certain depth are equal to a maximum depth limited wave height and the distribution of waves would like a clipped version of Rayleigh distribution. Battjes and Stive (1985) and Nairn (1990) further calibrated BJ78's model with an extensive data set of laboratory and field measurements, also relating the breaker index parameter used in the model to the incident wave steepness, and the authors found the model applicable for a wide range of wave conditions. Although describing the distribution of waves within the surf zone with a clipped Rayleigh distribution does not reflect the reality in nature (Thornton and Guza, 1983), BJ78's approach is still used in the prediction of the bulk dissipation rates for random waves within the surf zone. SWAN model, one of the most well-verified and widely used random wave transformation models, uses BJ78's approach for modeling the depth-induced wave breaking phenomenon in the nearshore areas.

Thornton and Guza (1983) (TG83 hereafter) observed in the field experiments carried out at Torrey Pines Beach at California that the distribution of the wave heights within surf zone is similar to a full Rayleigh distribution rather than a clipped one. Based on the

observations, the authors proposed a weighting function describing the fraction of waves breaking for each wave class in the *pdf*. Baldock et al., (1998) (Ba98 hereafter) followed the same approach proposed by TG83 to improve BJ78's model for steep beaches as it under-estimates the dissipation rates at the inner surf zone for steep slopes and thus over-estimates the fraction of breaking waves (even greater than 1). To avoid from such an unrealistic condition, BJ78 used a depth limited wave decay approach to estimate the wave heights at the inner surf zone after the saturation is reached (the root mean square wave height is assumed to be equal to the maximum depth limited wave height to satisfy fraction of wave broken is less than or equal to unity).

As a matter of fact, the surf zone on steep beaches is frequently very narrow and there is insufficient time for all the incident wave energy to be dissipated and an unsaturated breaking condition exists (the root mean square wave height is smaller than the maximum depth limited wave height) (Baldock et al., 1998). In order to improve the BJ78's model for steep beaches, Ba98 used a non-clipped Rayleigh distribution with a weighting function which assumes the fraction of waves breaking for the wave classes greater than a maximum depth limited wave height is equal to unity and for the smaller wave classes is equal to zero. This assumption also assures that the fraction of waves broken cannot exceed unity at the shoreline. The difference between the BJ78 and Ba98 is given by Janssen (2011) that BJ78 assumes that all the breaking waves have a fixed depth limited breaking wave height (H_b), which results in a delta function at H_b in the *pdf* for breaking waves, whereas in Ba98 (and in JB07), the complete Rayleigh distribution is used, but waves where $H > H_b$ are assumed as broken.

Janssen and Battjes (2007) followed the approach proposed by Ba98 and removed the algebraic simplification made by Ba98 in the derivation of dissipation rate and obtained a more consistent formula for the energy losses due to wave breaking. JB07 states that "the resulting parameterization predicts vanishing wave height as the shoreline is approached, even in the presence of 'shore breaks' that can dominate the surf in the nearshore on steep beaches." This approach solves the above mentioned inconsistency in Ba98 and provides a more unified solution for the irregular wave breaking

phenomenon. Therefore, JB07 is used in the numerical nearshore wave model developed in this study.

Recently, Apotsos et al. (2008) give an inter-comparison of some of the widely used parametric wave breaking models including above given approaches, except Goda's (1975a or 2004), using six field experiments: SandyDuck (Elgar et al., 2001), Duck94 (Raubenheimer et al., 1996), Egmond (Ruessink et al., 2001), Terschelling (Ruessink et al., 2003; Ruessink et al., 1998), NCEX (Thomson et al., 2006) and SwashX measurements (Raubenheimer, 2002). The authors tested the models using the field data for both the default values of breaker index values as given by authors and the tuned values using the available data. They have stated that all the models show similar accuracy with the median root-mean-square wave height errors between 10% and 20% and model errors might be reduced by roughly 50% tuning the breaker indexes with the field data. It is also stated that none of the models predicts the wave heights in the surf zone with the highest accuracy for all cases in all of the field experiments.

2.1.2. Irregular Wave Diffraction

As the waves encounter to an obstacle such as breakwaters or islands, some of their energy is blocked and reflected back and the rest of their energy is dissipated on the obstacle. The waves passing through the edge of the obstacle or the openings on the obstacle (i.e. series of offshore breakwaters) tend to turn around and enter into the shadow zone of the obstacle. The wave heights inside the shadow zone of the obstacle differ from the incoming wave heights. The diffracted wave heights of regular waves can be computed using the Sommerfeld's (1896) solution which is originally developed for the diffraction of light passing the edge of a semi-infinite screen (Goda, 2010). Penny and Price (1952) applied the Sommerfeld's solution to linear surface waves propagating at a constant depth and past a semi-infinite obstacle. Wiegel (1962) summarized the solution of Penny and Price (1952) and tabulated the diffraction coefficients for regular waves around a semi-infinite breakwater and prepared graphs for the diffraction coefficients with different approach angles given in Wiegel (1962) and the Shore Protection Manual (1984) (SPM, 1984 hereafter). As the sea surface in nature is composed of waves with different heights, periods and directions, the direct application

of these graphs to real situations is not recommended and may lead to erroneous results (Goda, 2010). Goda et al. (1978) followed the same methodology as in Wiegel (1962) to obtain the diffraction coefficients of irregular waves with different directional spreading properties. The authors computed the regular diffraction coefficients of each wave class in the directional wave spectrum and divided the sum of diffracted wave energy densities to the incoming wave energy density to find the effective or irregular wave diffraction coefficient. They prepared diffraction diagrams for random waves with different directional spreading parameters.

As discussed in earlier sections, the wave diffraction around coastal structures is readily accounted for in the mild-slope or Boussinesq type models which are widely used in harbor agitation problems. As for the action/energy balance models, various methods have been proposed for the implementation of wave diffraction. Holthuijsen et al. (2003) categorize these methods into two such that one approach is the introduction of a spatial or spectral diffusion into the model (Resio, 1988; Booij et al., 1997; Mase, 2001) to take the diffraction process into account. This method is simply smoothing of the wave energy with respect to spatial coordinates. The second approach is the modification of group velocity components (both geographical and directional group velocities) based on mild slope equation (Booij et al., 1997; Rivero et al., 1997; Holthuijsen et al., 2003). The second method changes the energy balance equation from a second-order differential equation to a fourth-order equation and thus requires higher order numerical schemes and more computational load. However, compared to the mild slope approximation, the smoothing approach lacks turning of the wave directions in the sheltered zones of the obstacles and also suffers from numerical diffusion.

The wave diffraction process in SWAN is solved using the mild slope approximation given by Holthuijsen et al. (2003). STWAVE model uses the smoothing method proposed by Resio (1988). CMS-Wave and WABED models follow Mase's approach (2001) that considers the wave diffraction with a dissipation term formulated from parabolic mild slope equation. Although above mentioned methods have improved the capability of the action/energy balance models to solve wave diffraction around obstacles like breakwaters, headlands or islands, the wave diffraction in these models still needs

detailed consideration to be used instead of MSE or Boussinesq models for more complex diffraction problems.

An important note in the literature about modeling of wave diffraction given by O'Reilly and Guza (1991) states that, in the case of very broad directional spreading, diffraction effects become unimportant, and in such situations a simpler spectral refraction model with a sink term to account wave breaking would be more preferable to the more complex refraction-diffraction model.

2.2. Numerical Modeling of Nearshore Wave-Induced Currents

As the waves approach to the shore, they change in height and direction due to shoaling, refraction, diffraction, breaking and other processes related to site specific conditions. Accordingly, the radiation stresses related to the wave momentum flux vary spatially and the variation of radiation stresses, as the main forcing mechanism, generates nearshore currents in longshore and cross-shore directions and changes in the local mean water levels (Goda, 2010). Moreover, Ruessink et al. (2001) note that winds (Whitford and Thornton, 1993), tidal forcing (Feddersen et al., 1998; Houwman and Hoekstra, 1998) and bottom shear stresses may contribute significantly to the nearshore currents, though the breaking waves govern the nearshore circulation in the surf zone in storm conditions.

The changes in the local mean water levels and the depth-averaged nearshore wave-induced current velocities can be obtained by solving one conservation of mass and two conservation of momentum equations, which are called as the non-linear shallow water equations (NSWE hereafter), also called as Saint-Venant (1871) equations derived from the Navier-Stokes equations. After Longuet-Higgins and Stewart (1964) introduced the radiation stress concept, numerous analytical and numerical models have been developed for the prediction of wave-induced currents and mean water levels utilizing one dimensional (1D) or two dimensional (2D) and linearized or nonlinear forms of the shallow water equations.

Longuet-Higgins (1970) computed longshore current velocities induced by regular waves at planar beaches using the radiation stress concept. He also introduced the turbulent eddy viscosity concept to take horizontal (lateral) mixing into account and to avoid from physically unrealistic and discontinuous variation of longshore current velocity around the breaker depth.

Battjes (1972) computed the longshore current velocities for random waves and showed that, contrary to the Longuet-Higgins's solution for regular waves, the cross-shore variation of longshore current velocities is continuous even if the lateral mixing is disregarded. Thornton and Guza (1986) compared the longshore current velocities measured at Leadbetter Beach, at Santa Barbara, California, in 1980 with the analytical and numerical models derived using their irregular wave breaking model (Thornton and Guza, 1983). Reiner and Battjes (1997) investigated the longshore current velocities on barred and non-barred planar beaches with the laboratory measurements for regular and random waves.

Kraus and Larson (1991) developed the NMLong (and later NMLong-CW by Larson and Kraus, 2002) model for computing the nearshore wave heights, mean water levels and the longshore current velocities including wind-induced set-up and set-down and the effects of interaction between waves and currents (occurring independently by winds and tides) are considered within the model.

Balas et al., (2006) compared the results of a 2D-NSWE nearshore current model, solved numerically using the Runge-Kutta-Fehlberg method and coupled with a MSE wave transformation model, with the laboratory measurements carried out for the Obaköy coastal waters located at the Mediterranean coast of Turkey for regular waves. Tang et al. (2008) carried out a similar study coupling the NSWE with a MSE wave model and compared the computed longshore current velocities with the laboratory measurements for irregular waves.

Goda (2006) examined the available irregular wave breaking models and turbulent eddy viscosity formulations on the longshore currents induced by irregular waves and

demonstrated the importance of the random wave model and the surface roller concept (Svendsen, 1984) for reliable predictions of longshore current velocities.

Surface roller concept was introduced by Svendsen (1984) to explain the increase of return flow velocity observed in the surf zone, relative to the value suggested by balancing the purely wave-associated volume flux given (Tajima and Madsen, 2006). Inclusion of the variation of the kinetic energies of the surface rollers in the surf zone in the computations of nearshore currents and mean water levels shifts the location of the maximum longshore currents toward the shoreline and increases the current speeds as observed especially in case of barred beaches (Goda, 2006). Surface rollers are simply the white foams (vortices) in front the breaker with a kinetic energy proportional to the celerity of the breaker and surface area of the roller. They gradually grow by absorbing a part of the energy dissipated through the wave breaking process, and then decay by losing its energy by turbulence (Goda, 2006). Dally and Osiecki (1994) and Dally and Brown (1995), Tajima and Madsen (2003) give mathematical expressions for the growth and decay of the kinetic energy of the surface rollers similar to the energy balance equation.

De Vriend and Stive (1987) developed a quasi-3D model for nearshore currents which combines the two dimensional depth integrated nearshore circulation with the effects of vertical distribution of nearshore currents. Similarly, Van Dongeren et al. (1994) developed a quasi-3D nearshore circulation model called as SHORECIRC capable of simulating a wide variety of nearshore phenomena, such as surf beats, longshore currents, infragravity waves, shear waves, flows around detached breakwaters and rip currents (Svendsen et al., 2004).

Determination of depth-averaged nearshore current velocities and mean water levels by means of numerical solution of NSWE requires a separate run of wave transformation for the determination of forcing mechanisms. The reliability of the results of the NSWE models mostly depends on the wave transformation model coupled with and the numerical techniques used in the NSWE solution. In addition to this approach, coupling of wave and current models, the time-dependent (phase-resolving) extended Boussinesq equations are also used in the wave-induced nearshore circulation problems.

As an example, FUNWAVE, developed by Kirby et al. (1998) based on the fully nonlinear Boussinesq model of Wei et al. (1995), is capable of simulating surf zone hydrodynamics as it includes energy dissipation due to wave breaking based on Kennedy et al., (2000). Extended Boussinesq equations remove the necessity of coupling the wave transformation with the nearshore current models, and give the depth-averaged current velocities in time for the respective the water surface elevations of regular or irregular wave trains. However, the extensive computational time required for large scale and long term applications stands as a major limitation of such models.

2.3. Sediment Transport in the Surf Zone

Sediment transport in the surf zone occurs mainly in two modes as suspended and bed loads both in cross-shore and longshore directions. Komar (1997) gives that the ratio of suspended to the total sediment load varies from 0.07 to 1.0 based on the available field data. For the storm conditions, it can be said that the suspended sediment transport, which is mainly due to breaking waves, governs the process of sediment transport and beach evolution (Goda, 2010). The short term changes in the beach morphology such as bar formation after a storm event or severe erosion at beaches in seasonal scale are governed mainly by cross-shore sediment transport processes, whereas the long term changes such as continuous recession of a shoreline or accretion/erosion of sediments around coastal structures are mainly due to the LST processes occurred during successive storm events over the years (Kamphuis, 2000; Masselink and Hughes, 2003).

Over the years, numerous formulas have been developed for the prediction of LST rates within the surf zone due to waves and/or currents. Inman and Bagnold (1963), U.S. Army Engineers Waterways Experiment Station's Coastal Engineering Research (hereafter CERC) formula (SPM, 1984), and Kamphuis (1991) formulas are the most well-known and utilized formulas for the prediction of total LST rates within the surf zone due to breaking waves for the problems where the knowledge of cross-shore distribution of LST is not the primary concern (i.e. one-line models).

Both Inman and Bagnold (1963) and CERC formulas relate the total LST to the breaking wave energy flux. Inman and Bagnold (1963) also incorporate the ratio of the mean

longshore current velocity to the maximum horizontal orbital wave velocity to the total LST. Kamphuis's (1991) formula, on the other hand, is based on the dimensional analysis of the results of the three-dimensional model tests carried out for both regular and random waves. Wang et al. (2002c) state that Kamphuis's formula (1991) predicts the total LST rates more consistently compared to the CERC formula for both spilling and plunging breaking wave conditions as it includes the effect of wave period in the expression. It is also stated in Wang et al. (2002c) that Kamphuis's formula works better for the low-energy events compared to the CERC formula, but not for the high energy events.

Recently, Bayram et al. (2007) proposed a formula for the total LST rate based on field measurements including storm conditions. The authors assumed that the suspended load dominates in the surf zone, steady states conditions prevail and the total work needed to keep sediments in suspension is done by the wave energy flux before wave breaking. Bayram et al.'s formula (2007) showed higher correlation with the used data points compared to other commonly used total LST formulas.

Advances in computer technology and numerical modeling encouraged the development and use of more sophisticated formulas and approaches for the computation of spatial and temporal distribution of sediment transport rates in the nearshore environments focusing on the different modes of transport such as bed or suspended loads to be used mostly in complex numerical models for sediment transport and bottom evolution problems. Bijker (1967, 1971), Engelund and Hansen (1967), Ackers and White (1973), Bailard and Inman (1981), Van Rijn (1984), Watanabe (1992) and more recently Camenen and Larson (2005, 2007 and 2008), Kobayashi et al. (2007) and Kuriyama (2010) are some of these local sediment transport rate formulas. Bodge (1989) states that almost all the distributed load transport approaches shares the same concept that the sediment is mobilized with a mechanism and transported with the existing current velocities. These approaches are mainly divided into two categories; the "energetics" models, which assume the mobilizing mechanism is a function of wave energy dissipation, and "stress" models, in which shear stress exerted on the bottom by waves and currents mobilize sediment.

Bayram et al. (2001) gives an evaluation of the former six of above given local sediment transport formulas and compares their capabilities in predicting the cross-shore distribution of LST rates for the selected data sets from DUCK85, SUPERDUCK and SANDYDUCK experiments which are carried out at the U.S. Army Corps of Engineers' Field Research Facility at Duck, NC. Van Maanen et al. (2009) compared the longshore transport formulas given by Bailard (1981) and Van Rijn (1984) with the field measurements carried out at Egmond site, in Netherlands. According to the comparisons of Bayram et al. (2001) and Van Maanen et al. (2009), Van Rijn's formula performed the best overall measurements despite the fact that its application requires a comprehensive understanding of sediment transport processes. On the contrary, Camenen and Larroude (2003) states that the Bijker and Van Rijn formulae consider only current related sediment transport and should not be used in nearshore morphology models. Another disadvantage of Van Rijn's formula is that it requires the integration of suspended load over the depth increasing the computational load (Camenen and Larroude, 2003). Among the above mentioned local sediment transport formulas, Watanabe's (1992) formula provides the most simplistic approach based on the exceedance of critical shear stress at the bottom for the prediction of total local sediment transport rates. As stated in Bayram et al. (2001), it has "yielded the best predictions for the storm conditions, but markedly overestimated the transport rates for swell waves."

Katayama and Goda (1999, 2000) studied the suspended sediment transport due to breaking waves estimating the mean suspended sediment concentration based on CERC expression and the sediment pick-up rate by breaking waves based on authors' energetics model. The authors (2002) later modeled the morphological changes around several detached breakwaters considering "only the process of advection and diffusion of suspended sediment that has been picked up by breaking waves."

Kobayashi et al. (2007) developed a model to simulate the suspended sediment transport caused by the roller dissipation rate and energy dissipation rate due to bottom friction from outside the surf zone to the lower swash zone. The model was compared with a very limited field data (Thorton and Guza, 1986) and the laboratory tests of Wang et al. (2002a).

Kuriyama (2010) assumed that the total LST is composed of suspended sediment load induced by surface roller energy dissipation rate and bed load due to near-bottom velocity (Bailard, 1981) and near-bottom acceleration (Hoefel and Elgar, 2003). The developed formula was examined with Ribberink's formula (1998) given for steady flows, Bayram et al.'s total LST formula (2007) and the field measurements of Miller (1998). The approach was found to be able to predict the LST rates measured in the field almost completely within a factor of 4 (Kuriyama, 2010).

Camenen and Larson (2005, 2007, 2008) (hereafter CL08) developed a general formula for the bed and the suspended loads in the surf zone under the action of waves and currents. The authors disregarded the contribution of waves for the bed load and assumed that the suspended load is governed by the energy dissipation due to wave breaking and bottom friction due to currents and waves. The authors also applied their formula to an extensive data set of laboratory and field measurements and obtained overall better predictions compared to the other existing widely used formulae. Moreover, Nam et al., (2009) computed the bed load using CL08 formula and the suspended load solving the advection-diffusion equation and also the sediment transport in the swash zone with the formula given by Larson and Wamsley (2007) and obtained reasonable predictions for the laboratory tests of Gravens and Wang (2007).

2.4. Beach Evolution Modeling

De Vriend et al. (1993) say that "coastal behaviour is the result of a large number of processes and mechanisms which act and interact on a variety of space and time scales." Requejo et al. (2008) gives the classification of space and time scales as "micro-scale (centimeters, decimeters), meso-scale (tens-hundreds of meters) and macro-scale (kilometers) according to the space scale; and as short-term (hours to days), medium-term (weeks to months) and long-term (years to decades) according to the time scale." Usually, the applicability of a beach evolution model is limited with the active physical processes within respective time and space scales, number and size of the input parameters, efficiency of the numerical solution techniques and the available computational capacity. Hanson et al. (2003) state that "there is still no universal model

for analyzing and predicting coastal evolution and its governing processes to be used for the complete scale range, from the short-term to the long-term." As an example, the long term changes in the shoreline could be studied fastest using one-line models, whereas dune erosion, bar formation or seasonal changes in the shoreline, swash zone dynamics could be studied with medium- or short-term beach evolution models.

Numerical modeling of beach evolution was first studied by Pelnard-Considere (1956), who introduced the one-line theory for the prediction of shoreline changes next to a groin. In one-line theory, it is assumed that the spatial and temporal changes along the bottom profile such as storm-induced erosion, bar formation, or shoreline changes due to seasonal variation of the wave climate cancel over the longer periods of time. It is also assumed that the bottom profile along the shoreline can be represented with a single equilibrium beach profile defined between two boundaries: depth of closure at sea and berm height on land, where the sediment transport processes take place. In this concept, the shoreline changes are assumed to be due to the variation of LST rates and local sources or sinks along the coast only. The one-line theory has been verified and further improved with the addition of combined wave refraction-diffraction theory (Dabees and Kamphuis, 1998), sediment transport due to tidal and wind-induced local currents, and tombolo formation behind T-shaped or detached breakwaters (Hanson et al., 2006).

Over the years, the applicability of one-line models over a wide range of spatial and temporal scales, lesser computational load compared to 2D or 3D models, and easiness in calibration to actual problems have made them preferable for preliminary research and design purposes in many coastal engineering applications. Several models based on one-line theory exist in the literature (Hanson and Kraus, 1989; Dabees and Kamphuis, 1998; DHI, 2001). Moreover, Şafak (2006), Artagan (2006), Baykal (2006) and Esen (2007) mainly studied the available methods used in wave transformation of one-line models, determination of the representative wave data and the effects of the order in series of wave events on the shoreline changes around various types of coastal defense structures, and they developed a one-line numerical shoreline change model, CSIM (acronym for Numerical Model for Coastline-Structure Interaction). The developed numerical model was applied to the shoreline changes observed at Kızılırmak River

Mouth, and in several other research studies (Ergin et al., 2006; Güler et al., 2008; Baykal et al., 2011).

A major limitation of one-line models, which is due to its basic assumption of equilibrium beach profile concept, is that these models disregard the spatial and temporal changes in the bottom profile and thus are used in long-term shoreline evolution problems only. To cope with this limitation and increase the applicability of one-line models to medium- to short-term events, one-line models including cross-shore sediment transport terms (Hanson et al., 1997; Hanson and Larson, 1998), one-line models coupled with one dimensional beach profile evolution models (Larson et al., 1990), multiple-line models (Hanson and Larson, 2000; Dabees and Kamphuis, 2000) or one-line models linked to two dimensional depth averaged (2DH) models (Shimizu et al., 1996; DHI, 2001) were developed.

Another major problem of the one-line models is that they are not easily applicable to the irregular shorelines, and they tend to smooth the existing irregularities in the shoreline throughout the simulations. This limitation was remedied by Hanson et al. (2001) introducing a fixed representative contour line or later by Larson et al., (2002) and Larson et al., (2006) introducing regional contour orientation that the waves are transformed accordingly. As a result the shoreline without any structure evolves preserving its orientation rather than transforming into a straight line (Hanson and Kraus, 2011). The above given limitation is also encountered in the application of one-line models to shoreline changes around complex coastal structures as these models usually use geometrical or empirical approximations for the variation of wave heights around these structures. To overcome these limitations, a phase-averaged type random wave model based on either mild slope or action/energy balance might be used to predict the wave height gradients in the surf zone and around the coastal structures. A recent study by Hoan (2010) utilizes the Mase's (2001) energy balance model to compute the wave heights inshore to be used in a one-line model applied to several real case studies.

Advances in computer technology and numerical modeling techniques encouraged the development of more sophisticated 2D or 3D tools for the prediction of morphological

changes in medium- to short-term and to overcome the above given limitations of one-line models. Basically, 2D or 3D models are composed of several separate models for the computation of wave transformation, nearshore current, sediment transport and bottom evolution. Quasi-3D (Q3D) models or fully 3D models are more preferable for short term events (less than a year) where the vertical distribution of current velocities and concentrations become important for accurate modeling. A Q3D model is simply a 2DH model with an additional one dimensional vertical profile model (1DV) to include the effects of return flows (undertow) in cross-shore dynamics (Briand and Kamphuis, 1993). A fully 3D model solves the governing hydrodynamic equations in three dimensions (Warner et al., 2008). 2DH or 2DV models require less computational loads compared to 3D models and provide the simulation of longer term events (Shimizu et al., 1996). Some of the recent studies on 2DH modeling of beach evolution are Militello et al. (2004), Buttolph et al. (2006), Bruneau et al. (2007), Roelvink et al. (2009), Nam et al. (2009, 2010).

Militello et al. (2004) and later Buttolph et al. (2006) developed the M2D model (later called as CMS-M2D) for simulating the nearshore hydro- and morpho-dynamics such as currents due to waves, tide, wind, and rivers, sediment transport and morphology changes. The model is a two dimensional depth averaged (2DH) model solving NSWE for nearshore currents and including sediment transport, hard-bottom and avalanching modules. The model is coupled with STWAVE or WABED for the wave forcings.

Bruneau et al. (2007) constructed a 2DH nearshore morphology model coupling the spectral wave model SWAN with a NSWE model MARS (Perenne, 2005) and a sediment transport module based on MORPHODYN (Saint-Cast, 2002). The authors applied their model only to some theoretical cases with complex bathymetrical features.

Roelvink et al. (2009) developed a 2DH numerical nearshore model, called as XBeach, to simulate hydrodynamics and morphological changes in the surf and swash zones during storms and hurricanes, including dune erosion, overwash and breaching. XBeach consists of a wave transformation model based on action balance equation, a flow model based on NSWE, a sediment transport model solving the advection-diffusion equation for the depth averaged concentrations, bottom evolution and avalanching

modules to predict the morphological changes during storm events. The model has been validated through several analytical, laboratory and field case studies (Roelvink et al., 2009).

Recently, Nam et al. (2009, 2010) developed a 2DH nearshore morphology model for simulating nearshore waves, currents, and sediment transport and bottom changes. The authors used Mase's (2001) spectral wave model with the Dally et al.'s (1985) energy dissipation term, a surface roller (Dally and Brown, 1995; Larson and Kraus, 2002) and a nearshore current model (Militello et al., 2004). Sediment transport rates within the surf and swash zones are included as discussed earlier. The developed model is applied to the laboratory measurements of Gravens et al. (2006), Gravens and Wang, (2007) in Large-scale Sediment Transport Facility (LSTF) at the US Army Corps of Engineer Research and Development Center in Vicksburg, Mississippi, USA.

CHAPTER 3

MODEL DEVELOPMENT

In this chapter, the theoretical and the numerical background of the developed two-dimensional depth-averaged beach evolution model is presented.

3.1. Model Structure

The two-dimensional depth-averaged (2DH) BeaCh EvOlution Numerical MoDel (COD) developed is composed four main sub-models:

- Nearshore Spectral Wave Model (NSW)
- NearShore Circulation Model (NSC)
- Sediment Transport Model (SED)
- Bottom EVOlution Model (EVO).

The numerical model COD is developed in MATLAB® environment utilizing finite difference schemes to numerical solutions of governing equations of the above given sub-models. The main inputs of the COD are the offshore/nearshore wave conditions (wave height, period, approach angle and directional spreading), the initial two-dimensional sea bottom and land topographies (including information about existing/planned coastal structures) and controlling parameters based on site and case specific conditions such as spacing in time and space, breaker index, diffraction intensity parameter, kinematic viscosity, sediment porosity, median grain size diameter, densities of sediment and water, bottom roughness and friction parameters, lateral mixing coefficient and energy transfer factor for surface rollers. The model structure is given in Figure 3.1.
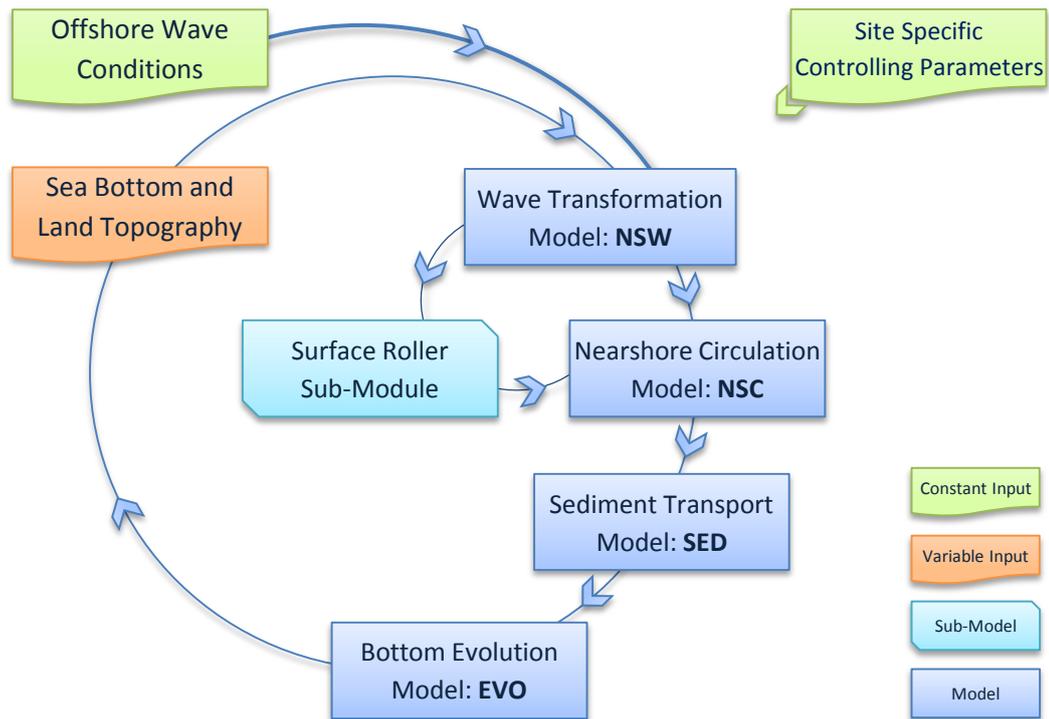
Figure 3.1 Beach Evolution Numerical Model (COD) Structure

As shown in Figure 3.1, in numerical modeling of beach evolution, the first step is to set the site and case specific controlling parameters, the initial bathymetry and offshore wave conditions.

Second step is to compute the nearshore significant (or root mean square as *rms* hereafter) wave heights, mean wave directions, dissipated energies due to random wave breaking, fraction of broken waves, maximum orbital velocities at the bottom, radiation stress terms for the given wave condition around existing coastal defense structures over the initial arbitrary bathymetry. The computed wave related parameters are assumed to be constant during the given wave condition. Therefore, it is called as phase-averaged or stationary approach.

Third step is to compute the growth and decay of the kinetic energies of the surface rollers, the friction and radiation terms obtained from the outputs of the wave and surface roller models. Using these terms, the time-averaged local nearshore wave-

induced current velocities and mean water level changes for the given wave condition over the initial arbitrary bathymetry are computed in this step.

In the fourth step, the computed nearshore current velocities and wave-related parameters are used in the computation of depth-averaged total sediment transport rates both in cross-shore and longshore directions.

In the last step, the computed sediment transport rates are used in a continuity equation to update the bathymetry and new bathymetry is used for the preceding wave conditions.

3.2. Model Assumptions and Limitations

Almost every numerical model is based on some assumptions to simplify and optimize the computational work needed for the solution of actual problem. For the developed numerical model, the basic assumptions made can be listed as given below.

3.2.1. Nearshore Spectral Wave Transformation

Nearshore wave parameters are computed as phase-averaged which means that the variation of wave parameters within a wave period or during the time series of irregular wave trains is disregarded. Nearshore wave parameters are assumed to be constant during the duration of the wave condition which might be selected as an hour or the duration of a single storm or the occurrence in hours in a year from a particular direction.

Along the offshore boundary (not the lateral sea boundaries), the wave conditions (wave height and period, mean approach angle and the directional spreading) are assumed to remain constant (Smith et al., 2001).

To reduce the computational work in the numerical modeling of wave transformation, the energy distribution over the frequency domain is disregarded, and the directional random waves are represented with a single significant or peak wave period only.

Therefore, the transfer of wave energy flux in frequency domain is not considered (wave-wave interactions).

The directional domain of the spectrum of the directional waves is defined from $-\pi/2$ to $+\pi/2$ with a directional spreading parameter given by Mitsuyasu et al. (1975). Therefore, waves can propagate within this directional domain only.

Wave transformation over the arbitrary bathymetry and around structures considers linear wave shoaling and refraction, depth-induced random wave breaking and irregular wave diffraction processes only.

The random waves in the surf zone are assumed to possess a full Rayleigh distribution (Figure 3.2) where the wave classes in the distribution greater than a maximum depth limited wave height are assumed to be broken (Baldock et al., 1998; Janssen and Battjes, 2007). Figure 3.2 shows the distribution of waves and portion of the waves breaking when $H/H_{rms} \geq H_b/H_{rms} = 0.8$, where H is the individual wave height, H_{rms} is the root-mean-square wave height and H_b is the maximum depth-limited wave height.
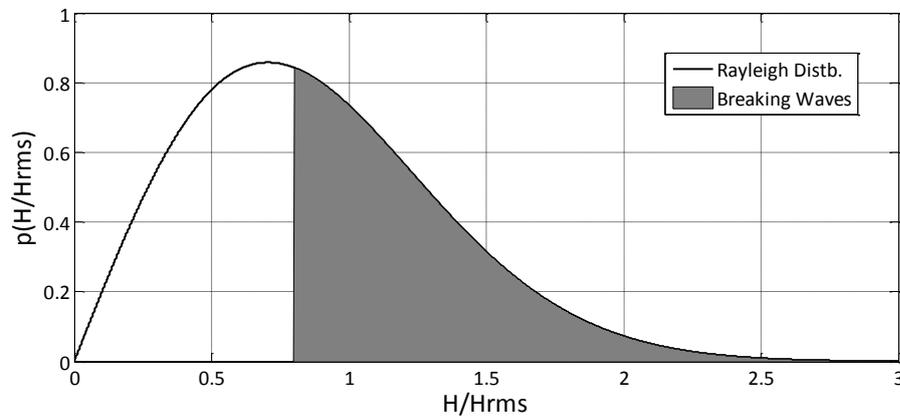
Figure 3.2 Theoretical distributions of non-breaking (solid line) and breaking wave heights (shaded area: $H/H_{rms} \geq H_b/H_{rms}$) (Baldock et al., 1998)

Wave-current interactions that can be observed at the river mouths or tidal inlets or at locations with strong ocean, wind-induced or tidal currents are not considered in the wave transformation computations. Inclusion of the wave-current interactions might be done by the adoption of the action balance equation which is also recommended as future work.

Wave reflection from shore due to sharp bottom gradients and coastal structures, dissipation due to bottom friction, white-capping (steepness controlled dissipation in deep water) and bottom vegetation, transfer of wind energy and Coriolis effects are not considered in the wave transformation model.

3.2.2. Nearshore Circulation

Nearshore local current velocities and mean water level changes are computed solving the depth-averaged non-linear shallow water equations, of which main assumption is the water depth "h" is small compared to the wavelength "L", (L/h>20) in addition to the inviscid and incompressible assumptions. It means that the vertical accelerations of the fluid particles are negligible and the pressure distribution is hydrostatic over the flow depth. This assumption is often violated for short waves in shallow water depths.

Vertical structure of the cross-shore current velocities is disregarded and thus undertow (seaward return of the wave-induced) velocity in the surf zone that significantly affect the bar formation is not taken into consideration. This assumption limits the model applicability where the cross-shore movements of sediments govern the morphological changes such as short term events. Goda (2010) states that "detailed observations have revealed the presence of the onshore flow (mass transport) near the surface within the surf zone, and the offshore return flow which compensates the mass transport in the middle to the lower layer of water body." Therefore, the effects of undertow or the 3D structure of flow (Figure 3.3) is considered as a recommended subject for future work. Similarly, Luijendijk et al. (2010) state that "as depth-averaged computations do not resolve the 3D effects in the surf zone, like e.g. undertow, the balance between offshore and onshore-directed transports is not accurately solved. As a result, the development and evolution of breaker bars, largely governed by the delicate balance of wave asymmetry and skewness related onshore transport and undertow related off-shore transport, cannot be modeled accurately with a purely 2DH approach. Cross-shore profiles in depth-averaged computations typically have the tendency to flatten out."
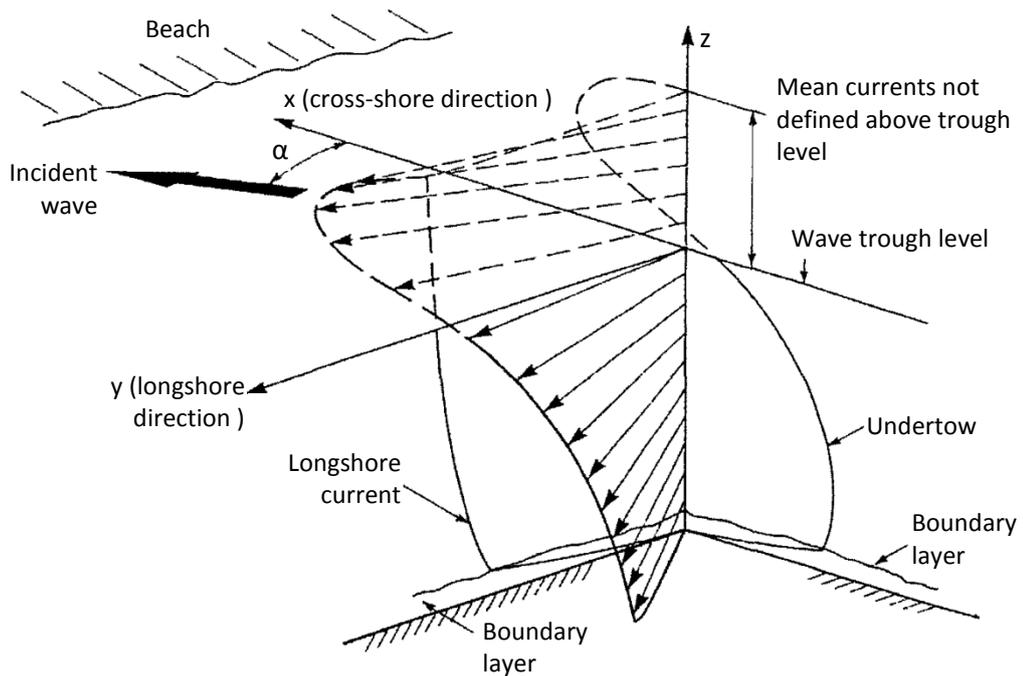
Figure 3.3 The three-dimensional structure of the nearshore flow velocities in the surf zone (Svendsen and Lorenz, 1989)

In the surf zone, a fraction of the dissipated wave energies due to wave breaking is assumed to be used in the growth and decay of kinetic energies of the surface rollers: vortices (white foams) in front of the breaking waves (Figure 3.4). Effects of surface rollers both in cross-shore and longshore directions are included in the nearshore circulation computations to obtain better representations of flow conditions near bar formations in the surf zone.

Effects of tidal, wind and Coriolis terms are disregarded as the effects of these mechanisms are often negligible compared to wave forcing over small to medium scale areas respectively (up to tens of kilometers).

In the numerical model, the non-linear shallow water equations are solved till reaching a steady state solution for a given wave condition as during which the nearshore wave conditions are assumed to be constant. The solution of the NSWE gives the depth- and time-averaged values of nearshore current velocities and mean water level changes.
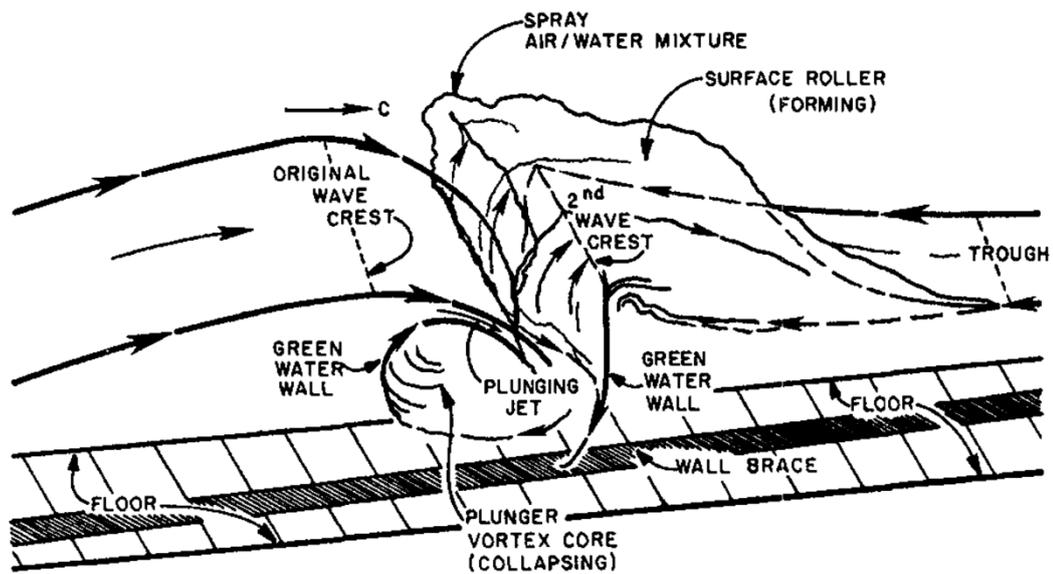
Figure 3.4 Formation of surface rollers in front of breaking waves (Basco and Yamashita, 1986)

3.2.3. Sediment Transport

Sediment transport rates are computed as time-averaged values which mean that steady conditions prevail during the wave conditions. Briand and Kamphuis (1993) say that "the time-averaged approach omits two aspects of sediment transport under an oscillatory flow. It ignores the presence of phase shift between sediment and water motions. This aspect is not expected to affect the calibrated time-averaged transport results significantly. It also ignores the asymmetry in the oscillatory flow (a higher peak velocity in the direction of wave propagation than in the reverse direction). This effect is mostly noticeable outside the surf zone under relatively calm weather conditions, when small waves carry sediment toward the shore and reconstruct the beach profile."

The sediment transport computations are carried out for non-cohesive sediments only (i.e. quartz sand). The non-cohesive-cohesive mixtures or cohesive bed material transport is not covered in this study and recommended as a future study for further development of the sediment model.

3.2.4. Bottom Evolution

The morphological evolution of coastal areas is assumed to be governed by the continuity equation depth-averaged longshore and cross-shore sediment transport mechanisms induced by the wind waves only.

Non-erodible bottoms are disregarded. The overall beach area where the sediment transport rates are computed (all the wet points and the wet-dry boundary) is assumed to be eroded infinitely till the end of the simulation and there exist no hard substrate under the surface of the bathymetry. This assumption is not realistic for most of the beaches and should be considered as a recommended work in future studies.

Based on above the given assumptions, a numerical model of depth-averaged two-dimensional beach evolution composed of several sub-models for wave transformation, surface rollers, nearshore circulation, sediment transport and bottom evolution is developed in MATLAB® environment applying finite difference schemes in the numerical solutions of governing equations of sub-models.

3.3. Nearshore Spectral Wave Model: NSW

In this part, the theoretical and numerical background of the two-dimensional nearshore spectral wave transformation model is given.

3.3.1. Energy Balance Equation

The temporal and spatial scales of the problem under consideration and the numerical complexity and stability of the schemes applied to solve the governing equations impose the methodologies and assumptions followed. As an example, the phase-averaged models for nearshore random wave transformation are more preferable for the medium- to long-term beach evolution models as they require less computational demands compared to the phase-resolving models or numerical stability of action/energy balance models are less dependent on the grid spacing compared to mild-slope models and therefore possess high numerical stability.

Determination of nearshore wave parameters is the primary step in the modeling of beach evolution under the wave action. Therefore, a numerical model for the nearshore transformation of directional random wind waves is developed. For this purpose, a numerical model solving the energy balance equation is written based on the above mentioned considerations and assumptions. The original version of the energy balance equation is a first-order homogeneous linear partial differential equation. It gives the variation of the energy flux at every location over an arbitrary bathymetry and in angular domain. It was introduced by Karlsson (1969) to investigate the shoaling and refraction of directional random waves. Mase (2001) gives the energy balance equation with the additional terms for breaking and diffraction as

$$\frac{\partial(v_x S)}{\partial x} + \frac{\partial(v_y S)}{\partial y} + \frac{\partial(v_\theta S)}{\partial \theta} = D_b - D_d \qquad (3.1)$$

where S is the directional wave spectral density (in m^2/Hz/rad) that varies in x and y horizontal coordinates (cross-shore and longshore directions respectively, Figure 3.5) and with respect to θ, the angle measured counterclockwise from x-axis and f, the wave frequency. D_b is the dissipation rate due to random wave breaking (Janssen and Battjes, 2007) and D_d is the diffraction term introduced by Mase (2001). The propagation velocities (v_x, v_y, v_θ) are given as

$$(v_x, v_y) = (C_g \cos\theta, C_g \sin\theta) \qquad (3.2)$$

$$v_\theta = \frac{C_g}{C}\left(\sin\theta\frac{\partial C}{\partial x} - \cos\theta\frac{\partial C}{\partial y}\right) \qquad (3.3)$$

where C_g is the group velocity and C is the wave celerity (both in m/s), both of which can be computed with the following equations

$$C = \frac{gT}{2\pi}tanh(kh) \qquad (3.4)$$

$$C_g = \frac{1}{2}\frac{gT}{2\pi}tanh(kh)\cdot\left(1 + \frac{2kh}{sinh(2kh)}\right) \qquad (3.5)$$

$$k = 2\pi / L \qquad\qquad (3.6)$$

where g is the gravitational acceleration (taken as 9.81 m/s^2), k is the wave number (in rad/m) and L is the wavelength (in meters) which can be found iteratively with the following dispersion equation for a given wave period of T (in seconds) and at a water depth of h (in meters).

$$L = \frac{g}{2\pi} T^2 \, tanh(\,kh\,) \qquad\qquad (3.7)$$
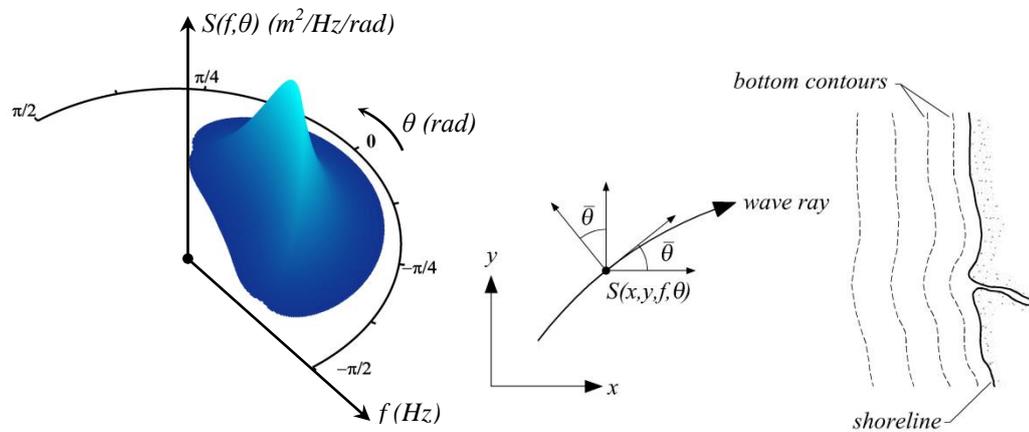
Figure 3.5 Coordinate system used in the numerical model (Mase, 2001)

3.3.2. Directional Wave Spectra

The directional wave spectral density, *S(f,θ)* (m^2/Hz/rad), describes the energy distribution of the random sea waves in both frequency and direction domain (Figure 3.5). It is often described applying a directional spreading function, *G(θ|f)*, to a frequency spectrum, *S(f)*.

$$S(\,f,\theta\,) = S(\,f\,) \cdot G(\,\theta / f\,) \qquad\qquad (3.8)$$

There exist several standard expressions for the frequency spectrum, *S(f)*, of the random sea waves, e.g., Pierson-Moskovitz (1964), Bretschneider-Mitsuyasu (Bretschneider, 1968; Mitsuyasu, 1970; Goda, 1988) and JONSWAP (Joint North Sea Wave Project;

34

Hasselmann et al., 1973). As an example, the frequency spectrum given by Goda (1988) and also used in the numerical model is as follows,

$$S(f) = 0.257 \cdot H_{s,0}^2 \cdot T_s^{-4} \cdot f^{-5} \cdot exp\left[-1.03 \cdot (T_s \cdot f)^{-4} \right]$$ (3.9)

where $H_{s,0}$ is the significant wave height, T_s is the significant wave period (for $T_p=1.05 \cdot T_s$) and f is the frequency. The directional spreading function defines the relative magnitude of directional spreading of wave energy in variation with the frequency and is normalized as

$$\int_{\theta_{min}}^{\theta_{max}} G(\theta / f) \cdot d\theta = 1$$ (3.10)

Mitsuyasu et al. (1975) gives the following cosine power '2s' distribution as the directional spreading function, which is originally introduced by Longuet-Higgins et al. (1963) and also used in the numerical model,

$$G(\theta / f) = G_0 \cos^{2s}(\theta / 2)$$ (3.11)

$$G_0 = \left[\int_{\theta_{min}}^{\theta_{max}} \cos^{2s}(\theta / 2) \cdot d\theta \right]^{-1}$$ (3.12)

where G_0 is a constant defined within the limits of directional domain, θ_{min} and θ_{max}, s is the degree of directional energy concentration taking a peak value at the spectral peak frequency, f_p. Goda and Suzuki (1975) relates the spreading parameter to the peak frequency, f_p, and its maximum value, s_{max}, at the peak frequency as follows.

$$s = \begin{cases} (f / f_p)^5 s_{max} & : f \leq f_p \\ (f / f_p)^{-2.5} s_{max} & : f > f_p \end{cases}$$ (3.13)

Mitsuyasu et al. (1975) relates the maximum spreading parameter (s_{max}) to the wind speed (U) as follows.

$$s_{max} = 11.5 \cdot (2\pi \cdot f_p \cdot U / g)^{-5/2}$$ (3.14)

$$f_p \approx 1/(1.05 \cdot T_s)$$ (3.15)

Goda (2010) gives the relation between the deep water wave steepness relates (the ratio of deep water wave height to the deep water wave length, H_0/L_0) and s_{max} value in Figure 3.6 utilizing Wilson's formula (1965) given for the growth of wind waves. For engineering applications, the typical values of s_{max} parameter for wind waves and swell waves with different range of decay distances are given in Table 3.1 (Goda, 2010).
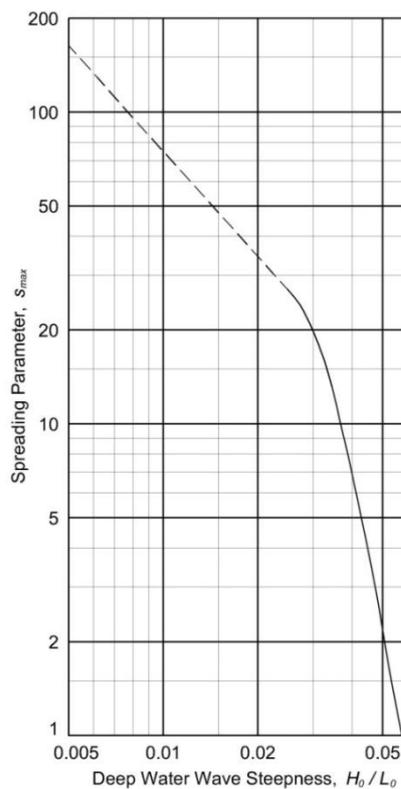
Figure 3.6 Relationship between spreading parameter and deep water wave steepness (Goda, 2010)

Table 3.1 Directional spreading parameter in deep water (s_{max}) for different wave types (Goda, 1985)

Wave Type	s_{max}
Wind waves	10
Swell with short to medium decay distance (with relatively large wave steepness)	25
Swell with medium to long decay distance (with relatively small wave steepness)	75

In the numerical, the total wave energy is assumed to be concentrated in a single representative frequency (peak frequency) and distributed over the directional domain (directional bin) which is bounded between -π/2 and π/2 (Figure 3.7).
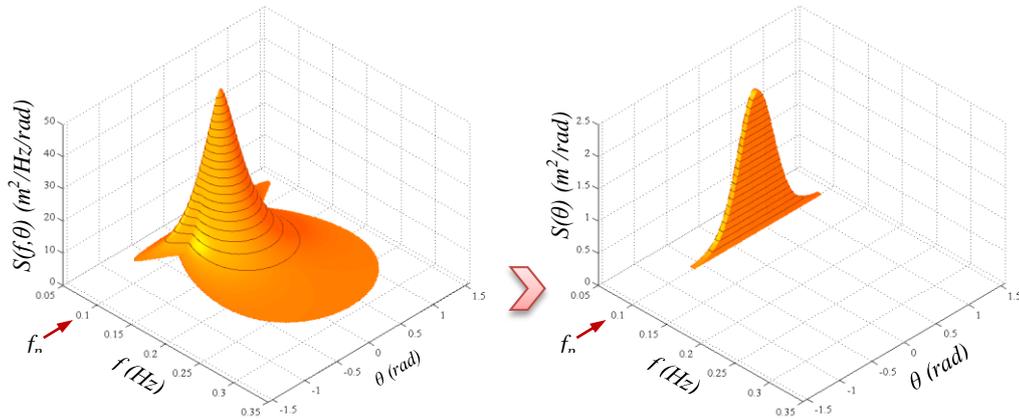
Figure 3.7 The directional bin used to represent the directional wave spectrum in the numerical model

The fact that the peak wave period of the random waves may slightly vary as they approach to the shore due to wave-wave interactions is disregarded. The peak wave period is assumed to be representative and constant. Therefore, the directional wave spectral density is defined as $S(\theta)$ (in m^2/rad) which is simply the integration of $S(f,\theta)$ over the frequency domain.

$$S(\theta) = \int_0^\infty S(f,\theta) \cdot df \tag{3.16}$$

The significant wave height (H_s) can be calculated by the following equation,

$$H_s = 4.004\sqrt{m_0} \tag{3.17}$$

where the m_0 is the total wave energy density that can be found integrating the $S(\theta)$ over the direction domain:

$$m_0 = \int_{-\pi/2}^{\pi/2} S(\theta) \cdot d\theta$$ (3.18)

Kuik et al (1988) defines the mean wave direction ($\bar{\theta}$) for directional random waves with the below given equation.

$$\bar{\theta} = arctan \left[\frac{\int_{-\pi/2}^{\pi/2} sin\,\theta \cdot S(\theta) \cdot d\theta}{\int_{-\pi/2}^{\pi/2} cos\,\theta \cdot S(\theta) \cdot d\theta} \right]$$ (3.19)

3.3.4. Random Wave Diffraction

Wave diffraction around land features (i.e. headland, islands) or the man-made coastal structures such as breakwaters or groins plays an important role in the nearshore wave transformation and related processes: circulation and sediment transport. Based on the parabolic mild-slope equation (Radder, 1979), Mase (2001) introduced the wave diffraction term, D_d, to include the wave diffraction process in action/energy balance models as

$$D_d = \frac{\kappa}{2\omega} \left((CC_g \cos^2\theta \cdot S_y)_y - \frac{1}{2} CC_g \cos^2\theta \cdot S_{yy} \right)$$ (3.20)

where κ (≥ 0) is the diffraction intensity parameter, the subscripts y and yy are the first and second order derivatives of spectral densities, respectively, with respect to y-direction and ω is the angular frequency given below.

$$\omega^2 = gk\,tanh\,kh$$ (3.21)

The diffraction intensity parameter, κ, is a free parameter controlled with respect to the intensity of the diffraction. If the κ is taken as equal to 0, the diffraction term is disregarded in the equation. This condition might be faced with the waves with a very wide directional spreading where the diffraction process become insignificant (O'Reilly and Guza, 1991). Mase (2001) used a constant value of κ equal to 2.5 in the application

of the proposed term to wave diffraction through narrow and wide gaps between the breakwaters and laboratory experiments of Vincent and Briggs (1989) on wave transformation over elliptical shoal. In the absence of field or laboratory data for the intensity of wave diffraction, the recommended value for the κ is given as 2.5 by Mase (2001).

3.3.5. Random Wave Breaking

Dissipation of wave energy flux due to random wave breaking is described using the methodology given by Janssen and Battjes (2007), based on the method proposed by Baldock et al. (1998). In this method, the distribution of random waves in the surf zone is assumed to be a full Rayleigh distribution with a weighting function which assumes the waves greater than a maximum depth limited wave height are broken. The given method satisfies that the fraction of broken waves cannot exceed unity at the shoreline even for the steep beaches where there is not enough time for all the incident wave energy to be dissipated and an unsaturated breaking condition exists.

The dissipation rate of wave energy flux (D_b) due to random wave breaking given by Janssen and Battjes (2007) is as follows

$$D_b = \frac{3\sqrt{\pi}}{16} f_p \frac{H_{rms}^3}{h} \left\{ 1 + \frac{4}{3\sqrt{\pi}} \left[\left(\frac{H_b}{H_{rms}} \right)^3 + \frac{3}{2} \left(\frac{H_b}{H_{rms}} \right) \right] \cdot exp \left[-\left(\frac{H_b}{H_{rms}} \right)^2 \right] - erf \left(\frac{H_b}{H_{rms}} \right) \right\}$$

(3.22)

where H_{rms} is the root mean square wave height at water depth h, f_p is the peak frequency, erf is the error function and H_b is the maximum depth-limited wave height.

$$H_b = \gamma_b h$$

(3.23)

The selection of the correct breaker index parameter is an important step in the wave transformation modeling, the results of which significantly affect the nearshore current velocities and sediment transport rates. The breaker index, γ_b, might be taken as 0.78 for

flat beaches and might exceed 1.0 depending on beach slope (Weggel, 1972). Janssen and Battjes (2007) uses the following equation given by Nairn (1990) for the breaker index which is related to deep water wave steepness value ($H_{rms,0}/L_0$)

$$\gamma_b = 0.39 + 0.56\,tanh(\,33H_{rms,0}\,/\,L_0\,)$$ (3.24)

where L_0 is the deep water wave length (L_0=1.56·T_p^2). The fraction of waves broken, Q_b, is given explicitly with the following formula by Baldock et al. (1998).

$$Q_b = exp\left[-\left(\frac{H_b}{H_{rms}}\right)^2\right]$$ (3.25)

The above given expression is the integration of the Rayleigh distribution, $p(H/H_{rms})$, over all waves for which $H/H_{rms} \geq H_b/H_{rms}$. Therefore, as the ratio of H_b/H_{rms} increases, the fraction of waves breaking, Q_b, approaches to 0 and as the ratio of H_b/H_{rms} decreases to 0, Q_b approaches to 1. Furthermore, if H_b/H_{rms} is equal to 1, Q_b becomes 0.4, in contrary to BJ78 model which enforces a saturated surf zone ($H_b=H_{rms}$) and gives that all the waves are broken (Q_b=1). Over-estimation of the fraction of waves in BJ78 model is mainly due to the fact that BJ78 underestimates of the dissipation rates, predicts the H_{rms} greater than H_b and obtain Q_b=1 before reaching to the shoreline which is physically unrealistic.

3.3.6. Numerical Solution of Energy Balance Equation

In order to estimate the nearshore wave parameters, the energy balance equation (Eq.3.1) is solved numerically utilizing finite difference schemes. The arbitrary bathymetry is discretized using a Cartesian coordinate system where x is the cross-shore direction and y is the longshore direction. Similarly, the angular domain of the spectral density is discretized into finite angular grids. The grid system used in the numerical solution is shown in Figure 3.8.
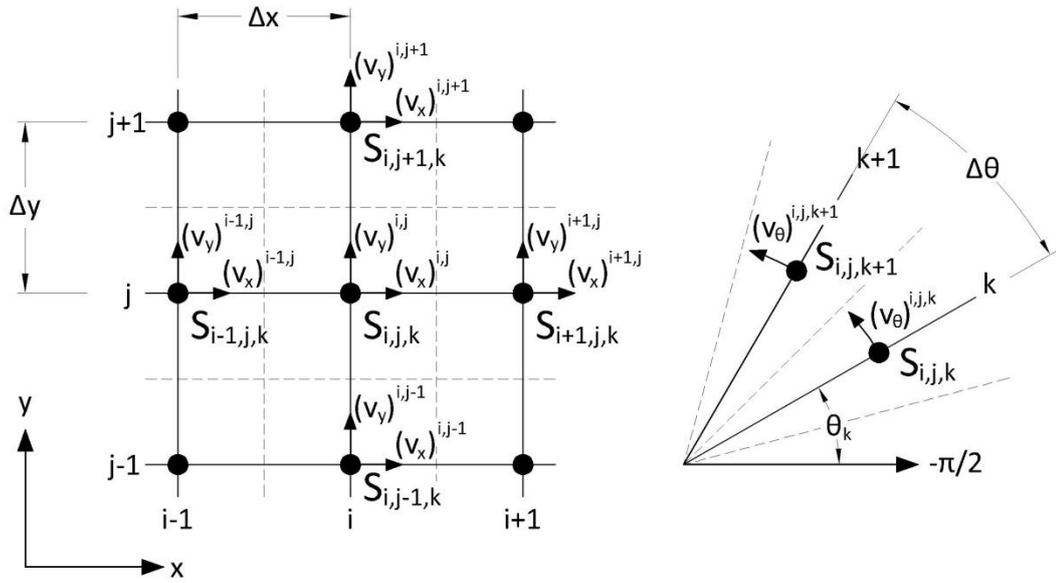
Figure 3.8 The grid system used in the numerical solution

As it is seen from Figure 3.8, the propagation velocities (v_x, v_y, v_θ) and the spectral densities, $S(\theta)$, are defined at the same grid points where the water depths ($h_{i,j}$) are defined and wave celerities ($C_{i,j}$), group velocities ($C_{g,i,j}$) and angular frequencies ($\omega_{i,j}$) are computed at the respective water depths using the representative peak frequency. In Figure 3.8, indices i and j are the grid numbers in x and y coordinates respectively, k is the angular component number, Δx, Δx and $\Delta\theta$ are the grid spacing in x and y coordinates and angular domain, respectively.

In the numerical solution, first order backward scheme in x direction, and first order centered schemes are utilized in y direction and angular domains which yields an explicit upwinding scheme in cross-shore direction and an implicit scheme for the unknown density components in longshore direction and angular domain. The numerical solution of the equation can be given as

$$\frac{(v_x S)_{i,j,k} - (v_x S)_{i-1,j,k}}{\Delta x} + \frac{(v_y S)_{i,j+1,k} - (v_y S)_{i,j-1,k}}{2\Delta y} + \frac{(v_\theta S)_{i,j,k+1} - (v_\theta S)_{i,j,k-1}}{2\Delta \theta} =$$

$$\frac{\kappa}{2\omega_{i,j}} C_{g,i,j} \cos^2 \theta_k \left(\frac{C_{i,j+1} - C_{i,j-1}}{2\Delta y} \right) \left(\frac{S_{i,j+1,k} - S_{i,j-1,k}}{2\Delta y} \right) +$$

$$\frac{\kappa}{2\omega_{i,j}} C_{i,j} \cos^2 \theta_k \left(\frac{C_{g,i,j+1} - C_{g,i,j-1}}{2\Delta y} \right) \left(\frac{S_{i,j+1,k} - S_{i,j-1,k}}{2\Delta y} \right) + \tag{3.26}$$

$$\frac{\kappa}{2\omega_{i,j}} C_{g,i,j} C_{i,j} 2\cos\theta_k \sin\theta_k \left(\frac{\theta_{i,j+1,k} - \theta_{i,j-1,k}}{2\Delta y} \right) \left(\frac{S_{i,j+1,k} - S_{i,j-1,k}}{2\Delta y} \right) +$$

$$\frac{\kappa}{2\omega_{i,j}} \frac{1}{2} C_{g,i,j} C_{i,j} \cos^2 \theta_k \left(\frac{S_{i,j+1,k} - 2S_{i,j-1,k} + S_{i,j-1,k}}{(\Delta y)^2} \right) - D_b(S_{i-1,j,k})$$

where $D_b(S_{i-1,j,k})$ is the rate of dissipation due wave breaking of each angular component of spectral density at a particular location (x_{i-1}, y_j). The rate of dissipation due wave breaking, D_b, is computed for the sum of spectral densities of each angular component using the Eq.3.19. Based on several laboratory observations, Eldeberky and Battjes (1995) states that the shape of the spectrum is barely sensitive to the depth induced random wave breaking. They define the rate of dissipation due to random wave breaking for each angular component of spectral density at a particular location (x_i, y_j) with the following equation

$$D_b(S_{i,j,k}) = S_{i,j,k} \frac{D_b}{\sum\limits_{k=1}^{N_d} S_{i,j,k}} \tag{3.27}$$

where N_d is the number of components in angular domain from $-\pi/2$ to $\pi/2$.

Regarding the boundary conditions applied in the numerical solution of the wave transformation model, there are three types of boundary conditions: offshore, open sea and dissipative beach boundary conditions (Figure 3.9).
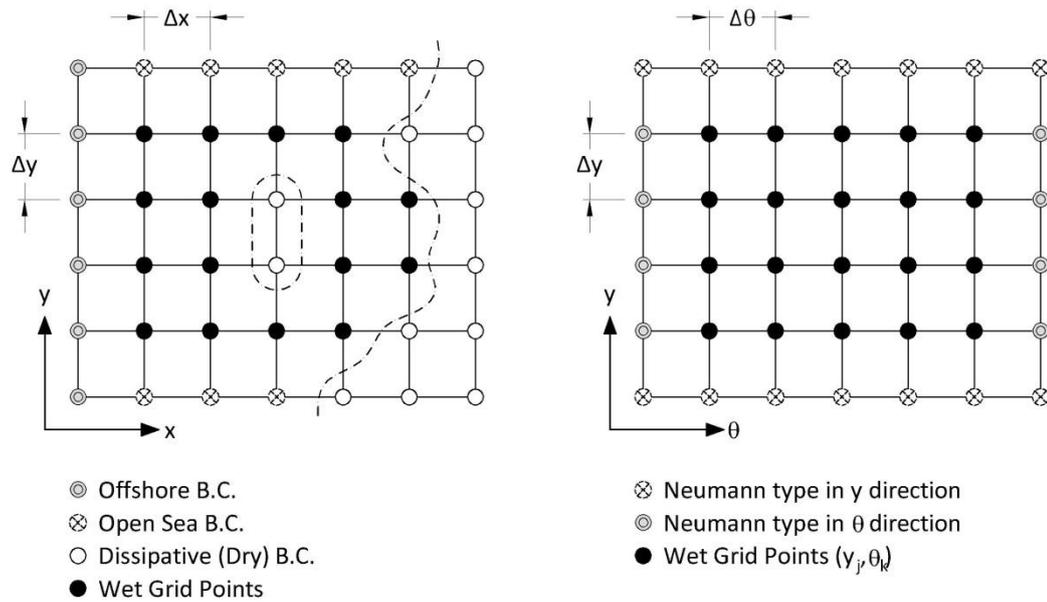
Figure 3.9 Boundary conditions used the wave transformation model

The offshore boundary condition is a Dirichlet type boundary condition where the wave conditions are pre-defined. The open sea boundary condition is applied where there exists no pre-defined wave conditions and the water depth is greater than a minimum water depth (h_{min}) at the boundary of the computational area. It is a Neumann type boundary condition that the spectral densities outside the computational area are assumed to be equal to the ones at the edge of the computational area. The dissipative beach boundary condition (dry points: land, islands and structures) is applied at the grid cells where the water depth is less than a minimum water depth (h_{min}) at any location of the computational area. The spectral densities at these boundaries are assumed to be fully dissipated and are equal to zero. In the numerical model, wave reflection from structures and beaches is disregarded; hence, no specific boundary condition is applied at reflective boundaries such as coastal structures or steep beaches. Instead, dissipative beach boundary condition is applied at such boundaries.

3.4. Nearshore Circulation Model: NSC

In this part, the theoretical and numerical background of the two-dimensional depth-averaged nearshore circulation model is given.

43

3.4.1. Non-linear Shallow Water Equations and Governing Stress Terms

Wave-induced nearshore current velocities and changes in mean sea level at a particular location at the nearshore can be found solving the nonlinear shallow water equations which are conservation of mass and momentum in x and y directions. The nonlinear shallow water equations are given as

$$\frac{\partial \bar{\eta}}{\partial t} + \frac{\partial}{\partial x}\left[u(h+\bar{\eta})\right] + \frac{\partial}{\partial y}\left[v(h+\bar{\eta})\right] = 0 \tag{3.28}$$

$$\frac{\partial u}{\partial t} + u\frac{\partial u}{\partial x} + v\frac{\partial u}{\partial y} + g\frac{\partial \bar{\eta}}{\partial x} + \frac{1}{\rho(h+\bar{\eta})}\left[\tau_{bx} + F_x\right] - A_x = 0 \tag{3.29}$$

$$\frac{\partial v}{\partial t} + u\frac{\partial v}{\partial x} + v\frac{\partial v}{\partial y} + g\frac{\partial \bar{\eta}}{\partial y} + \frac{1}{\rho(h+\bar{\eta})}\left[\tau_{by} + F_y\right] - A_y = 0 \tag{3.30}$$

where t is time (in seconds), u and v are the depth averaged current velocities in x (cross-shore) and y (longshore) directions respectively, $\bar{\eta}$ is the change in mean sea level, h is the water depth from still water level (Figure 3.10), ρ is the density of water (might be taken as ρ=1025 kg/m^3 for salt water and ρ=1000 kg/m^3 for fresh water), g is the gravitational acceleration (g=9.81 m/s^2), τ_{bx} and τ_{by} are the bottom shear stresses, F_x and F_y are the sum of radiation stresses and stresses acting on the water body due to surface rollers, A_x and A_y are the lateral mixing stresses. F_x and F_y terms are the governing stress terms in these set of equations. Sample cross-shore distributions of these terms for two different bottom profiles (uniform slope and bar-profile) are given in Appendix A.
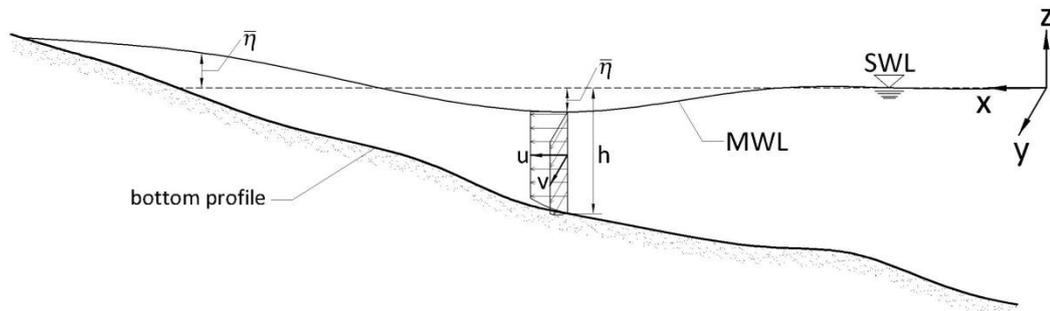
Figure 3.10 Definition sketch for the depth-averaged current velocities and the changes in the mean water level

Eq.3.28 is the equation of conservation of mass which means that the net change in mass in a water column is proportional to the difference between the influxes and outfluxes both in x and y directions. Effects of tide and wind-induced stresses and Coriolis forces are disregarded. Goda (2010) gives the wave-induced stress terms, F_x and F_y, as

$$F_x = \left[\left(\frac{\partial S_{xx}}{\partial x} + \frac{\partial S_{xy}}{\partial y} \right) + \frac{\partial}{\partial x} (2E_{sr} \cos^2 \bar{\theta}) + \frac{\partial}{\partial y} (E_{sr} \sin 2\bar{\theta}) \right] \tag{3.31}$$

$$F_y = \left[\left(\frac{\partial S_{yx}}{\partial x} + \frac{\partial S_{yy}}{\partial y} \right) + \frac{\partial}{\partial x} (E_{sr} \sin 2\bar{\theta}) + \frac{\partial}{\partial y} (2E_{sr} \sin^2 \bar{\theta}) \right] \tag{3.32}$$

where S_{xx} is the radiation stress acting in the x direction along the x axis, S_{xy} is the radiation stress acting in the y direction along x axis, S_{yx} is the radiation stress acting in the x direction along y axis and S_{yy} is the radiation stress acting in the y direction along y axis, E_{sr} is the kinetic energy of the surface roller, $\bar{\theta}$ is the mean approach angle with respect to the x axis, positive in counter-clockwise direction. The radiation stress terms, S_{xx}, S_{xy}, S_{yx} and S_{yy} are computed as

$$S_{xx} = \rho g \cdot \int_{-\pi/2}^{\pi/2} S(\theta) \cdot \left[n(\cos^2 \theta + 1) - 0.5 \right] \cdot d\theta \tag{3.33}$$

$$S_{yy} = \rho g \cdot \int_{-\pi/2}^{\pi/2} S(\theta) \cdot \left[n(\sin^2 \theta + 1) - 0.5 \right] \cdot d\theta \tag{3.34}$$

$$S_{xy} = S_{yx} = 0.5 \cdot \rho g \cdot \int_{-\pi/2}^{\pi/2} S(\theta) \cdot (n \cdot \sin 2\bar{\theta}) \cdot d\theta \tag{3.35}$$

where n is the ratio of group velocity to wave celerity and can be computed at a given depth (h) for a given wave period (T_p) using the below given equation.

$$n = \frac{C_g}{C} = \frac{1}{2} \left(1 + \frac{2kh}{\sinh 2kh} \right) \tag{3.36}$$

Surface rollers are the vortices (white foams) with a thickness of δ occurring in front of the breaking waves and moving with the wave celerity (Figure 3.11) and the bottom part

moves with the depth- and phase-averaged velocity (u). Tajima and Madsen (2003) give the kinetic energy of the surface roller (E_{sr}) with the following equation,

$$E_{sr} = \frac{\rho A_{sr} C}{2T}$$

(3.37)

where A_{sr} is the surface roller area, C is the wave celerity, T is the wave period which is taken as the peak wave period (T_p) in the numerical model.
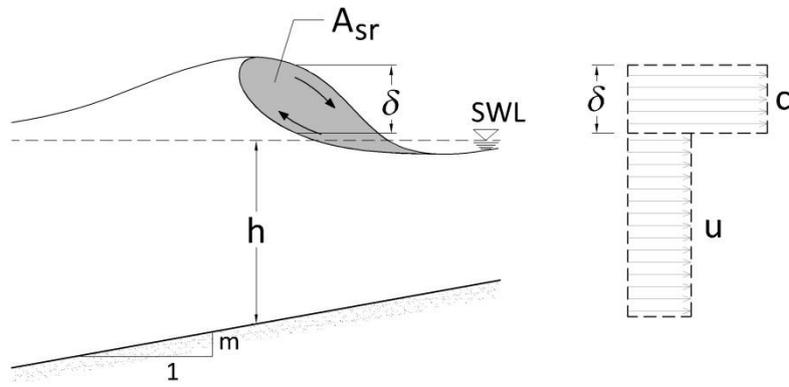
Figure 3.11 The surface roller in front of a breaking wave and the assumed phase-averaged velocity profile (Svendsen, 1984)

The evolution of the kinetic energy of surface roller over an arbitrary bathymetry is given as

$$\alpha \rho g \left[\frac{\partial}{\partial x}(m_0 C_g \cos \overline{\theta}) + \frac{\partial}{\partial y}(m_0 C_g \sin \overline{\theta}) \right] + \left[\frac{\partial}{\partial x}(E_{sr} C \cos \overline{\theta}) + \frac{\partial}{\partial y}(E_{sr} C \sin \overline{\theta}) \right]$$
$$= -\frac{K_{sr} E_{sr} C}{h}$$

(3.38)

where α is the energy transfer coefficient (taking values between 0 and 1) controlling the transferred energy to the surface roller, m_0 is the total energy density, K_{sr} is the energy dissipation rate of the surface roller. Tajima and Madsen (2003) relate the K_{sr} to the bottom slope, m, as follows.

$$K_{sr} = \frac{3}{8}(0.3 + 2.5m)$$

(3.39)

In the numerical model, the bottom shear stress terms, τ_{bx} and τ_{by}, are computed with the following equations given by Longuet-Higgins (1970) due to their simplicity in use compared to many other expressions.

$$\tau_{bx} = \frac{4}{\pi} \cdot \rho \cdot c_f \cdot u \cdot u_0$$

(3.40)

$$\tau_{by} = \frac{2}{\pi} \cdot \rho \cdot c_f \cdot v \cdot u_0$$

(3.41)

In the above given equations, c_f is the friction coefficient varying between 0.005 and 0.010, u and v are the depth averaged wave-induced current velocities, u_0 is the maximum horizontal orbital velocity at the sea bed and is computed with the below given equation

$$u_0 = \frac{\pi \cdot H_{rms}}{T \cdot \sinh(kh)}$$

(3.42)

where H_{rms} is the root-mean-square wave height which is approximately equal to $1/\sqrt{2}$ times the significant wave height (H_s). Although the ratio of H_{rms} to H_s slightly changes in shallow water and the breaking zone ($h/H_s \leq 3$) (Battjes and Groenendijk, 2000), it is kept constant from deep water to shoreline in the numerical model.

Regarding to the use of above given expressions for bottom shear stress terms, Goda (2008) says that "the various factors such as the selection of the wave model, evaluation of eddy viscosity, inclusion of surface roller etc., exercise far greater influence on the predicted longshore current velocity than the formulation of bottom shear stress. Adjustment of the bottom friction coefficient can also compensate any inadequacy in the linear approximation, as indicated by Thornton and Guza (1986)."

The lateral mixing terms, A_x and A_y, in x and y directions respectively are given with the following equations

$$A_x = \frac{\partial}{\partial x}\left[\mu\frac{\partial u}{\partial x}\right] + \frac{\partial}{\partial y}\left[\mu\frac{\partial u}{\partial y}\right] \qquad (3.43)$$

$$A_y = \frac{\partial}{\partial x}\left[\mu\frac{\partial v}{\partial x}\right] + \frac{\partial}{\partial y}\left[\mu\frac{\partial v}{\partial y}\right] \qquad (3.44)$$

where μ is the turbulent eddy viscosity term, u and v are the depth averaged current velocities in x and y directions respectively. Goda (2006) compares the effect of the available expressions for turbulent eddy viscosity (Longuet-Higgins, 1970; Battjes, 1975; Larson and Kraus, 1991) on the cross-shore profiles of longshore currents on planar beaches, and he recommends the empirical expression given by Larson and Kraus (1991) for practical applications,

$$\mu = \Lambda u_0 H_{rms} \qquad (3.45)$$

where Λ is an empirical constant taking values between 0.1-3.0 (Ding et al., 2006).

3.4.2. Numerical Solution of Non-linear Shallow Water Equations

NSWE give the variation of nearshore current velocities and local mean water levels both in time and space considering the varying stresses acting on the water mass. If the stress terms are kept constant such that an average sea state throughout a storm event occurs and respective wave-induced stresses are assumed to act constantly on the water mass, then a steady state solution exists for the given set of equations that gives the time-averaged values of the nearshore current velocities and local mean water level changes.

As mentioned in previous sections, the two dimensional depth-averaged nearshore circulation model is used to determine time-averaged values of the nearshore current velocities and local mean water level changes at a specific site during each storm event over the years. The obtained velocity components are used to compute the sediment fluxes and later bed level changes due to sediment flux gradients.

In the nearshore circulation model, the above mentioned governing equations are solved numerically utilizing finite difference methods. In order to solve the NSWE, the stress terms are evaluated first. The radiation stress terms, maximum horizontal orbital velocities, the total wave energy densities, mean approach angles, significant and root-mean-square wave heights are obtained from the wave transformation model outputs.

As a second step, the variation of kinetic energy of surface rollers over the arbitrary bathymetry is evaluated solving the equation of evolution of surface roller kinetic energy numerically (Eq.3.38). An implicit finite difference scheme is employed in the numerical solution of surface roller kinetic energies such that for all grid points with the same x_i and the water depth greater than the minimum water depth (h_{min}), a system of linear equations (in the form of $Ax=B$) is obtained and solved.

$$\alpha \rho g \left[\frac{(m_0 C_g \cos \bar{\theta})_{i,j} - (m_0 C_g \cos \bar{\theta})_{i-1,j}}{\Delta x} + \frac{(m_0 C_g \sin \bar{\theta})_{i,j+1} - (m_0 C_g \sin \bar{\theta})_{i,j-1}}{2 \Delta y} \right] +$$

$$\left[\frac{(E_{sr} C \cos \bar{\theta})_{i,j} - (E_{sr} C \cos \bar{\theta})_{i-1,j}}{\Delta x} + \frac{(E_{sr} C \sin \bar{\theta})_{i,j+1} - (E_{sr} C \sin \bar{\theta})_{i,j-1}}{2 \Delta y} \right]$$

$$= -\left(\frac{K_{sr} E_{sr} C}{h} \right)_{i,j}$$

(3.46)

At the offshore boundary condition, E_{sr} is assumed to be equal to zero as the random wave breaking has not started yet. At the lateral (open sea) boundaries, the rates of change of E_{sr} in x and y directions are assumed to be constant. At dry points where the water depth is less than h_{min}, E_{sr} is assumed to be equal to zero again.

In the numerical solution of NSWE, an explicit scheme of two time step Lax-Wendroff finite difference method on a staggered grid system, which is second order accurate and recommended especially for nonlinear problems, is used (Burkardt, 2010). Two time step Lax-Wendroff method divides the spacing in time and space into two, thus there exists three time levels (n, n+1/2, n+1) and the current velocity components, *u* and *v* and

the change in mean water level, $\bar{\eta}$, are evaluated at the cell faces (i+1/2,j and i,j+1/2) at n+1/2 time levels. The grid system used in time and space is illustrated in Figure 3.12.
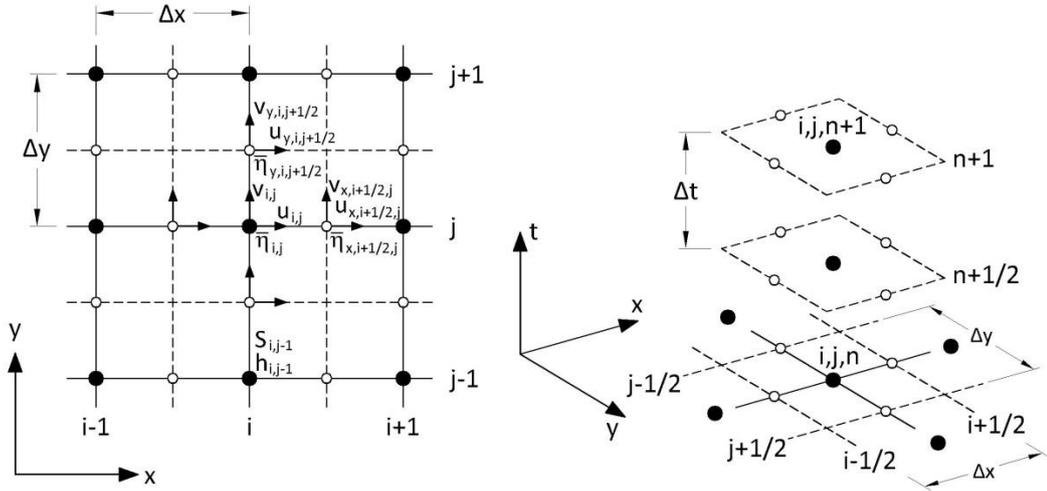
Figure 3.12 The grid system used in the nearshore circulation model (Burkardt, 2010)

The solution scheme consists of two half time steps. At the first half time step (n+1/2), NSWE are solved for the mid-points of cell faces (i+1/2,j and i,j+1/2) using the values at initial time step (n). For the mid-points of cell faces in *x* direction (i-1/2, i+1/2, i+3/2), Eq.3.47-3.49 are used. For the mid-points of cell faces in *y* direction (j-1/2, j+1/2, j+3/2), Eq.3.50-3.52 are used. At the second half time step (n+1), NSWE are solved (Eq.3.53-3.55) for the grid points (i,j) using the values computed at the first time step initial time step (n+1/2) for the derivatives of the unknown *u*, *v* and $\bar{\eta}$.

$$
\frac{\bar{\eta}_{i+1/2,j}^{n+1/2} - (\bar{\eta}_{i,j}^{n} + \bar{\eta}_{i+1,j}^{n})/2}{\Delta t} +
$$

$$
\frac{(u_{i,j}^{n} + u_{i+1,j}^{n})}{2} \frac{(h+\bar{\eta})_{i+1,j}^{n} - (h+\bar{\eta})_{i,j}^{n}}{\Delta x} + \frac{\left[(h+\bar{\eta})_{i,j}^{n} + (h+\bar{\eta})_{i+1,j}^{n}\right]}{2} \frac{(u_{i+1,j}^{n} - u_{i,j}^{n})}{\Delta x} = 0
$$

$$(3.47)$$

$$\frac{u_{i+1/2,j}^{n+1/2} - (u_{i,j}^n + u_{i+1,j}^n)/2}{\Delta t} + \frac{(u_{i,j}^n + u_{i+1,j}^n)}{2}\frac{(u_{i+1,j}^n - u_{i,j}^n)}{\Delta x} + g\frac{(\overline{\eta}_{i+1,j}^n - \overline{\eta}_{i,j}^n)}{\Delta x} +$$

$$\frac{1}{\rho}\frac{2}{\left[(h+\overline{\eta})_{i,j}^n + (h+\overline{\eta})_{i+1,j}^n\right]}\left[\frac{4}{\pi}\cdot\rho\cdot c_f\cdot\frac{(u_{i,j}^n + u_{i+1,j}^n)}{2}\cdot\frac{(u_{0,i,j}^n + u_{0,i+1,j}^n)}{2}\right] +$$

$$\frac{1}{\rho}\frac{2}{\left[(h+\overline{\eta})_{i,j}^n + (h+\overline{\eta})_{i+1,j}^n\right]}\left[\frac{S_{xx,i+1,j}^n - S_{xx,i,j}^n}{\Delta x} + \frac{(2E_{sr}\cos^2\overline{\theta})_{i+1,j}^n - (2E_{sr}\cos^2\overline{\theta})_{i,j}^n}{\Delta x}\right] -$$

$$\frac{\mu_{i+1,j}^n - \mu_{i,j}^n}{\Delta x}\frac{(u_{i+1,j,n} - u_{i,j}^n)}{\Delta x} - \frac{\mu_{i+1,j}^n + \mu_{i,j}^n}{2}\frac{(u_{i+2,j}^n - u_{i+1,j}^n - u_{i,j}^n + u_{i-1,j}^n)}{(\Delta x)^2} = 0$$

$$(3.48)$$

$$\frac{v_{i+1/2,j}^{n+1/2} - (v_{i,j}^n + v_{i+1,j}^n)/2}{\Delta t} + \frac{(u_{i,j}^n + u_{i+1,j}^n)}{2}\frac{(v_{i+1,j}^n - v_{i,j}^n)}{\Delta x} +$$

$$\frac{1}{\rho}\frac{2}{\left[(h+\overline{\eta})_{i,j}^n + (h+\overline{\eta})_{i+1,j}^n\right]}\left[\frac{2}{\pi}\cdot\rho\cdot c_f\cdot\frac{(v_{i,j}^n + v_{i+1,j}^n)}{2}\cdot\frac{(u_{0,i,j}^n + u_{0,i+1,j}^n)}{2}\right] +$$

$$\frac{1}{\rho}\frac{2}{\left[(h+\overline{\eta})_{i,j}^n + (h+\overline{\eta})_{i+1,j}^n\right]}\left[\frac{S_{yx,i+1,j}^n - S_{yx,i,j}^n}{\Delta x} + \frac{(E_{sr}\sin 2\overline{\theta})_{i+1,j}^n - (E_{sr}\sin 2\overline{\theta})_{i,j}^n}{\Delta x}\right] -$$

$$\frac{\mu_{i+1,j}^n - \mu_{i,j}^n}{\Delta x}\frac{(v_{i+1,j}^n - v_{i,j}^n)}{\Delta x} - \frac{\mu_{i+1,j}^n + \mu_{i,j}^n}{2}\frac{(v_{i+2,j}^n - v_{i+1,j}^n - v_{i,j}^n + v_{i-1,j}^n)}{(\Delta x)^2} = 0$$

$$(3.49)$$

$$\frac{\overline{\eta}_{i,j+1/2}^{n+1/2} - (\overline{\eta}_{i,j}^n + \overline{\eta}_{i,j+1}^n)/2}{\Delta t} +$$

$$\frac{(v_{i,j}^n + v_{i,j+1}^n)}{2}\frac{(h+\overline{\eta})_{i,j+1}^n - (h+\overline{\eta})_{i,j}^n}{\Delta y} + \frac{\left[(h+\overline{\eta})_{i,j}^n + (h+\overline{\eta})_{i,j+1}^n\right]}{2}\frac{(v_{i,j+1}^n - v_{i,j}^n)}{\Delta y} = 0$$

$$(3.50)$$

$$\frac{u_{i,j+1/2}^{n+1/2} - (u_{i,j}^n + u_{i,j+1}^n)/2}{\Delta t} + \frac{(v_{i,j}^n + v_{i,j+1}^n)}{2}\frac{(u_{i,j+1}^n - u_{i,j}^n)}{\Delta y} +$$

$$\frac{1}{\rho}\frac{2}{\left[(h+\overline{\eta})_{i,j}^n + (h+\overline{\eta})_{i,j+1}^n\right]}\left[\frac{4}{\pi}\cdot\rho\cdot c_f\cdot\frac{(u_{i,j}^n + u_{i,j+1}^n)}{2}\cdot\frac{(u_{0,i,j}^n + u_{0,i,j+1}^n)}{2}\right] +$$

$$\frac{1}{\rho}\frac{2}{\left[(h+\overline{\eta})_{i,j}^n + (h+\overline{\eta})_{i,j+1}^n\right]}\left[\frac{S_{xy,i,j+1}^n - S_{xy,i,j}^n}{\Delta y} + \frac{(E_{sr}\sin 2\overline{\theta})_{i,j+1}^n - (E_{sr}\sin 2\overline{\theta})_{i,j}^n}{\Delta y}\right] +$$

$$-\frac{\mu_{i,j+1}^n - \mu_{i,j}^n}{\Delta y}\frac{(u_{i,j+1}^n - u_{i,j}^n)}{\Delta y} - \frac{\mu_{i,j+1}^n + \mu_{i,j}^n}{2}\frac{(u_{i,j+2}^n - u_{i,j+1}^n - u_{i,j}^n + u_{i,j-1}^n)}{(\Delta y)^2} = 0$$

$$(3.51)$$

$$\frac{v_{i,j+1/2}^{n+1/2} - (v_{i,j}^{n} + v_{i,j+1}^{n})/2}{\Delta t} + \frac{(v_{i,j}^{n} + v_{i,j+1}^{n})}{2}\frac{(v_{i,j+1}^{n} - v_{i,j}^{n})}{\Delta y} + g\frac{(\overline{\eta}_{i,j+1}^{n} - \overline{\eta}_{i,j}^{n})}{\Delta y} +$$

$$\frac{1}{\rho}\frac{2}{\left[(h+\overline{\eta})_{i,j+1,n} + (h+\overline{\eta})_{i,j}^{n}\right]}\left[\frac{2}{\pi}\cdot\rho\cdot c_f\cdot\frac{(v_{i,j}^{n} + v_{i,j+1}^{n})}{2}\cdot\frac{(u_{0,i,j}^{n} + u_{0,i,j+1}^{n})}{2}\right] +$$

$$\frac{1}{\rho}\frac{2}{\left[(h+\overline{\eta})_{i,j}^{n} + (h+\overline{\eta})_{i,j+1}^{n}\right]}\left[\frac{S_{yy,i,j+1}^{n} - S_{yy,i,j}^{n}}{\Delta y} + \frac{(2E_{sr}\sin^2\overline{\theta})_{i,j+1}^{n} - (2E_{sr}\sin^2\overline{\theta})_{i,j}^{n}}{\Delta y}\right] +$$

$$-\frac{\mu_{i,j+1}^{n} - \mu_{i,j}^{n}}{\Delta y}\frac{(v_{i,j+1}^{n} - v_{i,j}^{n})}{\Delta y} - \frac{\mu_{i,j+1}^{n} + \mu_{i,j}^{n}}{2}\frac{(v_{i,j+2}^{n} - v_{i,j+1}^{n} - v_{i,j}^{n} + v_{i,j-1}^{n})}{(\Delta y)^2} = 0$$

$$(3.52)$$

$$\frac{\overline{\eta}_{i,j}^{n+1} - \overline{\eta}_{i,j}^{n}}{\Delta t} + \frac{(u_{i+1/2,j}^{n+1/2} + u_{i-1/2,j}^{n+1/2})}{2}\frac{(h+\overline{\eta})_{i+1/2,j}^{n+1/2} - (h+\overline{\eta})_{i-1/2,j}^{n+1/2}}{\Delta x} +$$

$$\frac{\left[(h+\overline{\eta})_{i+1/2,j}^{n+1/2} + (h+\overline{\eta})_{i-1/2,j}^{n+1/2}\right]}{2}\frac{(u_{i+1/2,j}^{n+1/2} - u_{i-1/2,j}^{n+1/2})}{\Delta x} +$$

$$\frac{(v_{i,j+1/2}^{n+1/2} + v_{i,j-1/2}^{n+1/2})}{2}\frac{(h+\overline{\eta})_{i,j+1/2}^{n+1/2} - (h+\overline{\eta})_{i,j-1/2}^{n+1/2}}{\Delta y} +$$

$$\frac{\left[(h+\overline{\eta})_{i,j+1/2}^{n+1/2} + (h+\overline{\eta})_{i,j-1/2}^{n+1/2}\right]}{2}\frac{(v_{i,j+1/2}^{n+1/2} - v_{i,j-1/2}^{n+1/2})}{\Delta y} = 0$$

$$(3.53)$$

$$\frac{u_{i,j}^{n+1} - u_{i,j}^{n}}{\Delta t} + \frac{(u_{i+1/2,j}^{n+1/2} + u_{i-1/2,j}^{n+1/2})}{2}\frac{(u_{i+1/2,j}^{n+1/2} - u_{i-1/2,j}^{n+1/2})}{\Delta x}$$

$$+ \frac{(v_{i,j+1/2}^{n+1/2} + v_{i,j-1/2}^{n+1/2})}{2}\frac{(u_{i,j+1/2}^{n+1/2} - u_{i,j-1/2}^{n+1/2})}{\Delta y} + g\frac{(\overline{\eta}_{i+1/2,j}^{n+1/2} - \overline{\eta}_{i-1/2,j}^{n+1/2})}{\Delta x} +$$

$$\frac{1}{\rho}\frac{1}{(h+\overline{\eta})_{i,j}^{n}}\left(\frac{4}{\pi}\cdot\rho\cdot c_f\cdot u_{i,j}^{n}\cdot u_{0,i,j}^{n}\right) + \frac{1}{\rho}\frac{1}{(h+\overline{\eta})_{i,j}^{n}}\left[\frac{S_{xx,i+1,j}^{n} - S_{xx,i-1,j}^{n}}{2\Delta x} + \frac{S_{xy,i,j+1}^{n} - S_{xy,i,j-1}^{n}}{2\Delta y}\right] +$$

$$\frac{1}{\rho}\frac{1}{(h+\overline{\eta})_{i,j}^{n}}\left[\frac{(2E_{sr}\cos^2\overline{\theta})_{i+1,j}^{n} - (2E_{sr}\cos^2\overline{\theta})_{i-1,j}^{n}}{2\Delta x}\right] +$$

$$\frac{1}{\rho}\frac{1}{(h+\overline{\eta})_{i,j}^{n}}\left[\frac{(E_{sr}\sin 2\overline{\theta})_{i,j+1}^{n} - (E_{sr}\sin 2\overline{\theta})_{i,j-1}^{n}}{2\Delta y}\right] -$$

$$\frac{\mu_{i+1,j}^{n} - \mu_{i-1,j}^{n}}{2\Delta y}\frac{(u_{i+1/2,j}^{n+1/2} - u_{i-1/2,j}^{n+1/2})}{\Delta x} - \mu_{i,j}^{n}\frac{(u_{i+3/2,j}^{n+1/2} - u_{i+1/2,j}^{n+1/2} - u_{i-1/2,j}^{n+1/2} + u_{i-3/2,j}^{n+1/2})}{(\Delta x)^2} -$$

$$\frac{\mu_{i,j+1}^{n} - \mu_{i,j-1}^{n}}{2\Delta y}\frac{(u_{i,j+1/2}^{n+1/2} - u_{i,j-1/2}^{n+1/2})}{\Delta y} - \mu_{i,j}^{n}\frac{(u_{i,j+3/2}^{n+1/2} - u_{i,j+1/2}^{n+1/2} - u_{i,j-1/2}^{n+1/2} + u_{i,j-3/2}^{n+1/2})}{(\Delta y)^2} = 0$$

$$(3.54)$$

$$\frac{v_{i,j}^{n+1} - v_{i,j}^{n}}{\Delta t} + \frac{(u_{i+1/2,j}^{n+1/2} + u_{i-1/2,j}^{n+1/2})}{2} \frac{(v_{i+1/2,j}^{n+1/2} - v_{i-1/2,j}^{n+1/2})}{\Delta x}$$

$$+ \frac{(v_{i,j+1/2}^{n+1/2} + v_{i,j-1/2}^{n+1/2})}{2} \frac{(v_{i,j+1/2}^{n+1/2} - v_{i,j-1/2}^{n+1/2})}{\Delta y} + g \frac{(\bar{\eta}_{i,j+1/2}^{n+1/2} - \bar{\eta}_{i,j-1/2}^{n+1/2})}{\Delta y} +$$

$$\frac{1}{\rho} \frac{1}{(h+\bar{\eta})_{i,j}^{n}} \left(\frac{2}{\pi} \cdot \rho \cdot c_f \cdot v_{i,j}^{n} \cdot u_{0,i,j}^{n} \right) + \frac{1}{\rho} \frac{1}{(h+\bar{\eta})_{i,j}^{n}} \left[\frac{S_{yx,i+1,j}^{n} - S_{yx,i-1,j}^{n}}{2\Delta x} + \frac{S_{yy,i,j+1}^{n} - S_{yy,i,j-1}^{n}}{2\Delta y} \right] +$$

$$\frac{1}{\rho} \frac{1}{(h+\bar{\eta})_{i,j}^{n}} \left[\frac{(E_{sr} \sin 2\bar{\theta})_{i+1,j}^{n} - (E_{sr} \sin 2\bar{\theta})_{i-1,j}^{n}}{2\Delta x} \right] +$$

$$\frac{1}{\rho} \frac{1}{(h+\bar{\eta})_{i,j}^{n}} \left[\frac{(2E_{sr} \sin^2 \bar{\theta})_{i,j+1}^{n} - (2E_{sr} \sin^2 \bar{\theta})_{i,j-1}^{n}}{2\Delta y} \right] -$$

$$\frac{\mu_{i+1,j}^{n} - \mu_{i-1,j}^{n}}{2\Delta y} \frac{(v_{i+1/2,j}^{n+1/2} - v_{i-1/2,j}^{n+1/2})}{\Delta x} - \mu_{i,j}^{n} \frac{(v_{i+3/2,j}^{n+1/2} - v_{i+1/2,j}^{n+1/2} - v_{i-1/2,j}^{n+1/2} + v_{i-3/2,j}^{n+1/2})}{(\Delta x)^2} -$$

$$\frac{\mu_{i,j+1}^{n} - \mu_{i,j-1}^{n}}{2\Delta y} \frac{(v_{i,j+1/2}^{n+1/2} - v_{i,j-1/2}^{n+1/2})}{\Delta y} - \mu_{i,j}^{n} \frac{(v_{i,j+3/2}^{n+1/2} - v_{i,j+1/2}^{n+1/2} - v_{i,j-1/2}^{n+1/2} + v_{i,j-3/2}^{n+1/2})}{(\Delta y)^2} = 0$$

(3.55)

At time t=0, all the unknown parameters u, v and $\bar{\eta}$, are assumed to be equal to zero. The below given equations are solved till a steady state is reached for the unknowns. The steady state is controlled with a user defined accuracy limit such that the difference between the values of unknown parameter for the two time steps (n and n+1) is less than the limit value for each unknown parameter.

The time increment, Δt, for the solution is selected to satisfy the numerical stability in the solution, which is defined with the following equation for two-dimensional square grids (Syme, 1991)

$$\Delta t \leq \frac{min(\Delta x, \Delta y)}{\sqrt{2g \, max(h)}}$$

(3.56)

where Δx and Δy are the grid spaces in x and y directions respectively, g is the gravitational acceleration and h is the water depth (positive for wet points). The above given equation satisfies the speed of the numerical solution is less than the maximum

physical speed in the problem which is also known as Courant-Friedrichs-Lewy (CFL) condition.

As for the boundary conditions, at the offshore boundary where the wave conditions are defined, the mean water level is set to zero. At the offshore and open sea boundaries, the velocity component gradients are set to zero. At the dry cells, u, v and $\bar{\eta}$ are assumed to be equal to zero. Moreover, at the wet cells neighboring dry cells such as shoreline or the wet cells around structures and the wet cells with a very steep bottom slope which is also controlled by the user (such as bottom slopes steeper than 1:10), u, v and $\bar{\eta}$ are assumed to be the average of the values of the neighboring cells. Thus, instability problems close to the structures and the moving boundary condition at the shoreline due to the run-up of waves is achieved although the physical phenomenon is not fully reflected. Detailed studies for both the moving boundary condition at the shoreline and the instability problems faced around the structures, where the bottom slopes are steep due to uniform discretization (constant grid spacing in x and y directions over the arbitrary bathymetry), are required in future.

3.5. Sediment Transport Model: SED

The sediment transport model computes the local sediment transport rates under the action of wind waves over the arbitrary bathymetry to be used in the computation of bottom evolution. As mentioned in the literature survey, there exist various approaches for the computation of sediment transport rates in the surf zone. In the sediment transport model, the Watanabe (1992) formulation is used to compute the local total sediment transport rates. The method is based on the shear stress concept (or power model concept) that the total load both in cross-shore and longshore directions ($q_{total,x}$ and $q_{total,y}$ in bulk volume including pores) is proportional to the residual between the mean bed shear stress under wave-current field ($\tau_{b,cw}$) over a wave-cycle and the critical bed shear stress (τ_{cr}) that is required to mobilize the sediment grains at the sea bed.

$$q_{total,x} = \frac{A \cdot \left[\tau_{b,cw} - \tau_{cr} \right] \cdot u}{\rho \cdot g} \qquad (3.57)$$

$$q_{total,y} = \frac{A \cdot \left[\tau_{b,cw} - \tau_{cr} \right] \cdot v}{\rho \cdot g}$$ (3.58)

The Watanabe formula has been widely used for the prediction of beach evolution around coastal structures, sand deposition in harbors and navigation channels. It has been calibrated and verified for a variety of laboratory and field data sets (Watanabe, 1987; Watanabe et al, 1991; Bayram et al., 2001; Buttolph et al., 2006; Nam et al., 2009). However, the dependency of the empirical parameter (A) in the formula has not been well established and is given as 0.5 for monochromatic waves and 2.0 for random waves. The current velocities u and v are the depth-averaged wave-induced current velocities in cross-shore and longshore directions. The critical shear stress for incipient motion is given as

$$\tau_{cr} = (\rho_s - \rho) \cdot g \cdot d_{50} \cdot \theta_{cr}$$ (3.59)

where ρ_s and ρ are the densities of sediment grains and water respectively, (ρ=2650 kg/m^3 for quartz sand, ρ=1025 kg/m^3 for salt water and ρ=1000 kg/m^3 for fresh water), g is the gravitational acceleration (g=9.81 m/s^2), d_{50} is the median grain diameter and θ_{cr} is the critical Shields parameter. Soulsby and Whitehouse (1997) defines the critical Shields parameters based on a dimensionless median grain size diameter parameter (d_{50}^*) as

$$\theta_{cr} = \frac{0.3}{1 + 1.2 d_{50}^*} + 0.055 \cdot \left[1 - exp(-0.02 d_{50}^*) \right]$$ (3.60)

$$d_{50}^* = d_{50} \cdot \left[\frac{g \cdot (\rho_s / \rho - 1)}{v^2} \right]^{1/3}$$ (3.61)

where v is the kinematic viscosity ($1 \cdot 10^{-6}$ m^2/s at 20°C water temperature).

The bed shear stresses acting on the sand grains mainly consist of two different velocity components as existing steady currents (u_c) and the oscillatory motions of the water body due to progressive waves (u_w). The instantaneous combined wave-current velocity over a wave cycle is the vectoral sum of these two components (u_{cw}). The schematic diagram of instantaneous velocity is shown in Figure 3.13.
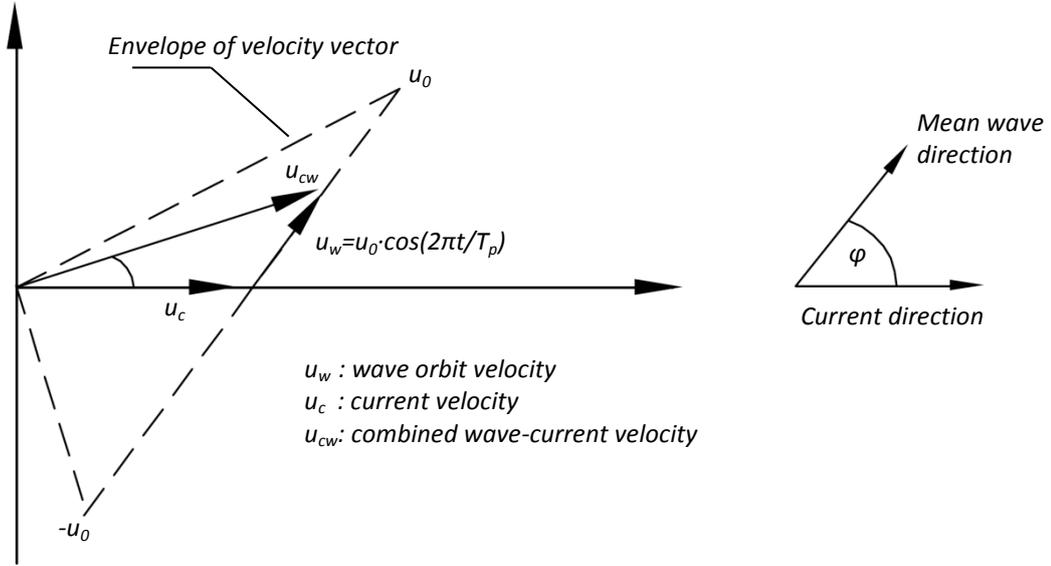
Figure 3.13 Schematic diagram of instantaneous velocity at the sea bed on top of the wave boundary layer (Liu, 2001)

In Figure 3.13, u_c is the steady current velocity which is the vectoral sum of depth-averaged wave-induced current velocities ($\vec{u}_c = \vec{u} + \vec{v}$), u_w is the wave orbital velocity in the direction of mean wave approach angle, u_0 is the maximum horizontal orbital velocity at the sea bed which can be found using Eq.3.42, φ is the angle between the mean wave approach angle and the steady current and u_{cw} is the instantaneous combined wave-current velocity defined as:

$$u_{cw} = \sqrt{u_c^2 + u_w^2 + 2u_w u_c \cos \phi}$$

(3.62)

The instantaneous combined bed shear stress (τ_{cw}) is

$$\tau_{cw} \propto \rho \cdot u_{cw}^2$$

(3.63)

Bijker (1971) gives the mean bed shear stress over a wave-cycle as

$$\tau_{b,cw} = \frac{1}{T} \int_0^T \tau_{cw} \cdot dt \approx \tau_c + \frac{1}{2}\tau_{w,max}$$

(3.64)

where T is the wave period, τ_c is the bed shear stress due to steady current u_c and $\tau_{w,max}$ is the maximum bed shear stress due to waves only. The bed shear stress due to depth-averaged wave-induced resultant current (u_c) is given as

$$\tau_c = \frac{1}{8} \rho \cdot f_c \cdot (u_c)^2 \tag{3.65}$$

where f_c is the current friction factor defined by Van Rijn (1998) as

$$f_c = 0.24 \log^{-2}\left(12\frac{d}{k_s}\right) \tag{3.66}$$

in which d is the total water depth ($d=h+\bar{\eta}$) and k_s is the bed roughness (Nikuradse sand grain roughness) might be taken as equal to $k_s=2.5 \cdot d_{50}$ flat beds. The maximum bed shear stress due to waves is given by

$$\tau_{w,max} = \frac{1}{2} \rho \cdot f_w \cdot (u_0)^2 \tag{3.67}$$

where f_w is the wave friction factor given by Nielsen (1992) as:

$$f_w = exp\left[5.5 \cdot R^{-0.2} - 6.3\right] \tag{3.68}$$

R is the relative roughness defined as:

$$R = \frac{A_w}{k_s} \tag{3.69}$$

where A_w is the wave orbital semi excursion defined as:

$$A_w = \frac{u_0 T_p}{2\pi} \tag{3.70}$$

3.5.1. An Alternate Approach for the Distributed Total Longshore Sediment Transport

To develop an alternative approach to be implemented in the beach evolution models, the cross-shore distribution of the total LST rate is investigated with the available laboratory and field measurements based on an energetics type of approach within the scope of this thesis study. The main assumption of the proposed approach is that the local total sediment transport rates across the surf zone are proportional to the rate of dissipation of wave energies due to wave breaking and wave-induced current velocities.

The proposed approach follows similar assumptions as given in Bayram et al. (2007). Suspended sediment transport is assumed to be the governing mode of transport in the surf zone where the strong the wave action mobilize the sediment and keep in suspension so that transported by the currents. The sediment transport outside the surf zone is assumed to be insignificant compared to the surf zone. The total amount of work (W) needed to keep the sediment in suspension is related to a certain portion of the energy flux of the breaking waves ($W=\varepsilon \cdot E_b \cdot C_{gb} \cdot cos\theta_b$).

Similarly, in the proposed approach, the total work (w^*) needed to keep sediments in suspension per unit length in cross-shore direction is done by a certain part (ε) of the rate of dissipation in wave energy flux due to wave breaking ($w^*=\varepsilon D_b$), and the steady state conditions prevail for the respective unit length and the sediment concentration in the water column is carried with a depth-averaged longshore current velocity (v).

The total amount of work (w^*) needed to keep the sediment in suspension per unit length (Δx) in cross-shore direction is given by the Bayram et al. (2007) as the product of the concentration (c) of the submerged weight of the particle with the fall speed (w_s),

$$w^* = \int_{x}^{x+\Delta x} \int_{-d(x)}^{0} c(x,z) \cdot (\rho_s - \rho) \cdot g \cdot w_s \cdot dz \cdot dx \qquad (3.71)$$

where x is a cross-shore coordinate originating at the shoreline and taken positive offshore, z is the vertical coordinate originating at the still-water level, $d(x)$ is the water depth including mean water level change at x. Ahrens (2000) gives the fall speed with the following set of equations:

$$S_* = \frac{d_{50}}{4\nu}\sqrt{(s-1)\rho g} \tag{3.72}$$

$$C_1 = 1.06\, tanh\big[0.064 S_* \exp(-7.5/S_*^2)\big] \tag{3.73}$$

$$C_2 = 0.22\, tanh\big[2.34 S_*^{-1.18} \exp(-0.0064 S_*^2)\big] \tag{3.74}$$

$$w_s = \sqrt{(s-1)\rho g}\cdot\big[C_1 + C_2\cdot S_*\big] \tag{3.75}$$

The total LST rate per unit length in cross-shore direction can be expressed as the product of concentration (c) and longshore current velocity (v):

$$q_{total,y} = \int_x^{x+\delta x}\int_{-d(x)}^0 c(x,z)\cdot v(x,z)\cdot dz\cdot dx \tag{3.76}$$

Using a depth averaged longshore velocity (v) varying in cross-shore direction only and replacing the integral in Eq.3.76 with a certain fraction (ε) of rate of dissipation in wave energy flux due to wave breaking (D_b) similarly varying in cross-shore direction as the depth changes and irregular wave breaking occurs, the following expression is obtained,

$$q_{total,y} = \frac{\varepsilon\cdot D_b\cdot v}{(\rho_s - \rho)\cdot(1-p)\cdot w_s\cdot g} \tag{3.77}$$

where $q_{total,y}$ is the local total LST rate in bulk volume per time per unit length in cross-shore direction and p is the in-place sediment porosity. Bayram et al. (2007) defines the ε parameter (hereafter ε_{Ba07}) for their total LST formulae through dimensional analysis based on an extensive data set of laboratory and field experiments as

$$\varepsilon_{Ba07} = \left(4 + 9\frac{H_{s,b}}{T_p w_s}\right)\cdot 10^{-5} \tag{3.78}$$

where $H_{s,b}$ is the significant breaking wave height, T_p is the peak wave period and w_s is the fall velocity of the median grain size diameter.

In order to test the above given proposed approach and determine the ε parameter to be used in Eq.3.78, the laboratory measurements carried out at Large-scale Sediment Transport Facility (LSTF) at the U.S. Army Engineer Research and Development Center (Wang et al., 2002a; Gravens and Wang, 2007) and field measurements carried out at Duck site, North Carolina, USA between years 1995-1998 (Miller, 1999) where the breaking wave conditions dominates the sediment transport are used. For the available data sets of the measured transport rates, it is found that the ε parameter ranges between 0.0018-0.0026. The proposed approach where the ε parameter is taken as constant (i.e. ε=0.002) is denoted as 'SED1' approach and for $\varepsilon=\varepsilon_{Ba07}$ it is denoted as 'SED2' approach. The detailed information about the experiments and comparisons of results for the wave heights, longshore current velocities, mean water level changes, and LST rates are given in the following chapter where the different features and components of the numerical model are benchmarked for various cases.

3.6. Bottom Evolution Model: EVO

In the bottom evolution model (EVO), the gradients of the computed local total sediment transport rates including pores at the cell boundaries both in longshore and cross-shore directions are used to the compute the bed level changes in time. The depth change in time can be given with the following continuity equation,

$$h_{i,j}^{n+1} = h_{i,j}^{n} + \Delta t_m \cdot \left(\frac{q_{total,x_{i+1,j}}^{n} - q_{total,x_{i,j}}^{n}}{\Delta x} + \frac{q_{total,y_{i,j+1}}^{n} - q_{total,y_{i,j}}^{n}}{\Delta y} \right) \qquad (3.79)$$

where Δt_m is the time step used in the bottom evolution in terms of hours, $q_{total,x}$ and $q_{total,y}$ are the phase-averaged local total sediment transport rates in terms of bulk volume transported per unit area at the cell, Δx and Δy are the grid spacing in the x and y directions, respectively.

As the changes in the water depths are computed, the bottom slopes over the arbitrary bathymetry are controlled against the exceedance of a limiting slope at which the sand grains begin to roll. This critical slope is called as the angle of repose (or internal angle of

friction). The angle of repose is given as 32-34° for dry sands and may reduce up to 18° under wave action (Reeve et al., 2004; Roelvink et al., 2009).

The exceedance of the critical slope results in bottom avalanche at the sea bottom. In order to take the bottom avalanching into account in the beach evolution model, an algorithm based on Buttolph et al. (2006) and Roelvink et al. (2009) is followed. After every morphological time step (Δt_m), for all cells where the water depth is defined in the middle of the cell, the bottom slopes in four directions (in positive and negative x and y directions) using the neighboring cells are computed. Starting the from the bottom slope in the negative x-direction in clockwise direction, the four bottom slopes are checked. If one of the four bottom slopes is greater than or equal to the user-defined critical slope and the other three slopes, the avalanching is assumed to take place in the direction of the steepest slope and the water depths of the respective slope are re-computed, and the four slopes of these two cells are re-computed. This control process is repeated iteratively until all the critical slopes are eliminated and the water depths where avalanching took place are re-evaluated for the respective morphological time step.

When the bottom slope between two cells exceeds the user-defined critical slope (m_{cr}),

$$\left| \frac{\Delta h}{\Delta x} \right| = \left| \frac{h_{i,j} - h_{i-1,j}}{\Delta x} \right| > m_{cr} \tag{3.80}$$

an avalanching is assumed take place and the bed update (Δh_a) due to avalanching is given by

$$\Delta h_a = \left(\left| \frac{\Delta h}{\Delta x} \right| - m_{cr} \right) \cdot \Delta x \tag{3.81}$$

and the water depths in the respective cells are re-computed as follows:

$$h_{i,j}^a = h_{i,j}^a - \Delta h_a \left.\right\} \qquad for \quad \frac{\Delta h}{\Delta x} > 0 \qquad\qquad (3.82)$$
$$h_{i-1,j}^a = h_{i-1,j}^a + \Delta h_a$$

$$h_{i,j}^a = h_{i,j}^a + \Delta h_a \left.\right\} \qquad for \quad \frac{\Delta h}{\Delta x} < 0 \qquad\qquad (3.83)$$
$$h_{i-1,j}^a = h_{i-1,j}^a - \Delta h_a$$

The computation of bottom topography and the control for bottom avalanching is carried on until a user defined maximum bottom level change occurs and the wave and current fields are recomputed according to the updated bathymetry. The computations are carried out till the end of the wave condition under consideration.

CHAPTER 4

MODEL BENCHMARKING

In this chapter, the validity of the developed numerical wave transformation, wave-induced circulation, sediment and bottom evolution models are tested with the linear wave theory, a fully-spectral wave model (SWAN by TU Delft, The Netherlands) and several laboratory and field experiments available in the literature. The details of the model validation study are given in the following parts.

4.1. Theoretical Comparisons of the Wave Transformation Model

In this part, the NSW model is compared with the linear wave theory and the SWAN model, a fully-spectral wave model, for various basic wave processes: shoaling, refraction, random breaking and diffraction.

4.1.1. Wave Shoaling

Wave shoaling is defined as the "the change in the wave height due to varying depth" by Goda (2010). As the wave enters into shallower depths, it start to feel the bottom and decrease in length and celerity, thus, increase in height till reaching to maximum wave steepness (height-to-length ratio) or maximum height-to-depth ratio where wave breaking takes place and it starts to dissipate its energy.

In order to test the performance of the NSW model for pure wave shoaling, a series of runs on planar bottom slopes is carried out for different bottom slopes (1/20, 1/50 and 1/100) and spreading parameter values, s_{max} (10, 25 and 75). The deep water mean approach angle ($\bar{\theta}_0$) is taken as zero degrees.

In the comparisons, the original energy balance equation given by Karlsson (1969) is solved numerically in x coordinate only with a very small grid spacing ($\Delta x \leq 1$ m) to obtain the shoaling characteristics of waves with respect to linear wave theory for different bottom slopes and s_{max} values. The equation solved is

$$\frac{\partial(\,EC_g\,cos\,\theta\,)}{\partial x} = 0 \qquad\qquad (4.1)$$

where C_g is the group velocity, θ is the approach angle measured with respect to x (cross-shore) axis. E is the total wave energy given as

$$E = \frac{\rho g H_{rms}^2}{8} \qquad\qquad (4.2)$$

where ρ is the density of water (might be taken as ρ=1025 kg/m³ for salt water and ρ=1000 kg/m³ for fresh water), g is the gravitational acceleration (g=9.81 m/s²), H_{rms} is the root-mean-square wave height, which is approximately equal to $1/\sqrt{2}$ times the significant wave height (H_s) in deep water. In the comparisons, the numerical solution of the above given one-dimensional equation (Eq.4.1) is called as 1D.

The shoaling performance of the numerical wave transformation model is also compared with the SWAN model (version 40.51) for the same wave conditions. In the simulations, Pierson-Moskowitz (1964) type frequency spectrum and '$cos^m(\theta-\theta_{peak})$' type directional spreading function are used. The directional domain is defined from $-\pi/2$ to $\pi/2$ with 5 degrees directional resolution. The frequency domain is defined between 0.04 and 1.0 Hz.

The deep water significant wave steepness ($H_{s,0}/L_0$) values are taken as 0.0358, 0.0264 and 0.0105 for the runs with s_{max} values equal to 10, 25 and 75 respectively using Figure 3.6 that adds up nine simulations in total. Applied wave conditions are given from deep water and summarized in Table 4.1. For all simulations, the spatial resolution in SWAN, 1D and NSW is taken as 1 meter. The directional spectrum used in the NSW model is

obtained from the given two-dimensional (defined in both direction and frequency domains) offshore spectrum in SWAN using Eq.3.16. The variation of the significant wave height with respect to depth is presented in Figure 4.1 and Figure 4.3 for the selected three of the nine simulations. The depth-induced wave breaking is turned off for three models.

Table 4.1 The applied wave conditions in the simulations of pure shoaling

Deep Water Significant Wave Height, $H_{s,0}$ (m)	4.0
Deep Water Significant Wave Steepness, $H_{s,0}/L_0$	0.0358, 0.0264 and 0.0105 (for smax=10, 25 and 75 respectively)
Deep Water Mean Approach Angle, $\bar{\theta}_0$ (degrees)	0
Maximum Directional Spreading Parameter, s_{max}	10, 25 and 75
Bottom Slopes (m)	1/20, 1/50 and 1/100
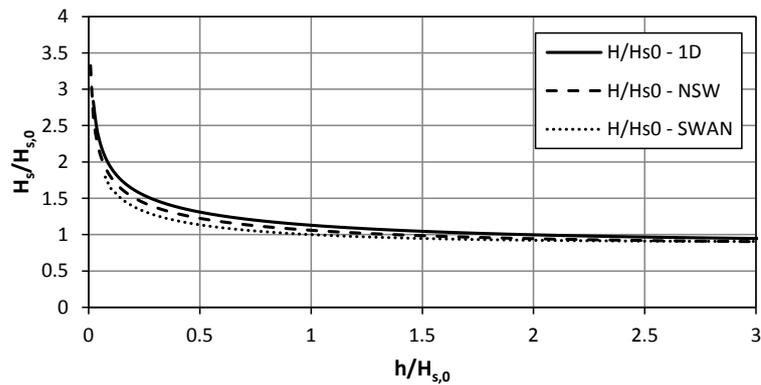
Figure 4.1 The variation of significant wave height in case of pure shoaling on planar bottom slope of 1:20 for directional spreaded waves with s_{max}=10
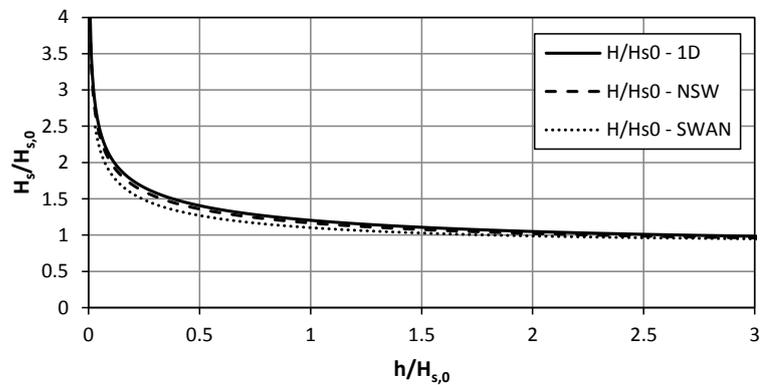
Figure 4.2 The variation of significant wave height in case of pure shoaling on planar bottom slope of 1:50 for directional spreaded waves with s_{max}=25
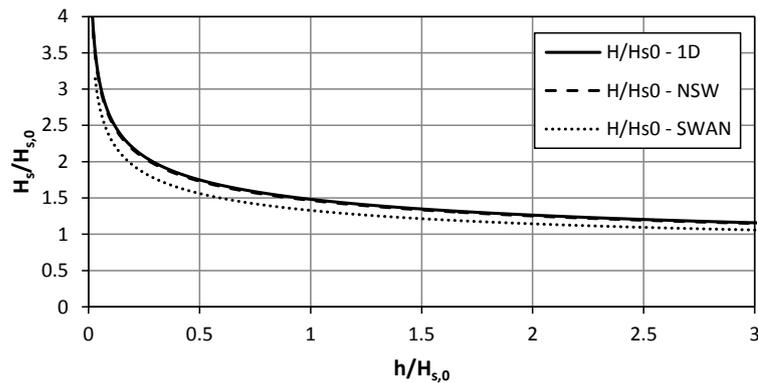
Figure 4.3 The variation of significant wave height in case of pure shoaling on planar bottom slope of 1:100 for directional spreaded waves with s_{max}=75

In Figure 4.1 and Figure 4.3, the horizontal axis is the relative depth (h) with respect to the deep water significant wave height ($H_{s,0}$) and the vertical axis gives the variation of significant wave height with respect to deep water significant wave height. As observed from the simulations carried out for pure shoaling, the difference between 1D and NSW solutions gets smaller as s_{max} increases and the two solutions are close to each other as only directional spreading is considered in NSW solution. The difference between the NSW and SWAN solutions increase as the s_{max} increase as the directional spreading gets narrower, waves become more uni-directional and the NSW solution gets close to the 1D solution. It is also observed that difference between NSW and SWAN solutions increase as the bottom slope gets milder, whereas no significant difference is observed between the 1D and 2D solutions. For all cases, the maximum error in the relative significant wave height ($H_s/H_{s,0}$) at the relative depth, $h/H_{s,0}$=0.1, is 6.8% between 1D and 2D solutions and 14.3% between SWAN and NSW solutions.

4.1.2. Wave Shoaling, Refraction and Breaking

The NSW model is tested with the one-dimensional solution and SWAN for various deep water approach angles to observe the performance of the model where shoaling, refraction and depth-induced random wave breaking are active in the transformation of waves.

Refraction of water waves is the change in the direction of a wave moving in shallow water at an angle to the depth contours. The part of the wave advancing in shallow

66

water moves more slowly than that part still advancing in deeper water, causing the wave crest to bend toward alignment with the underwater contours. As the approach angle in deep water increases the effect of refraction gets stronger and the wave heights change more rapidly. Each angular component in a directional spectrum is subjected to wave refraction differently with respect to its angular value in deep water. Hence, irregular wave refraction has stronger influence on multi-directional waves compared to uni-directional waves. Similarly, as the wave period increases, the effect of refraction is felt more strongly by the waves. Each frequency component in a directional spectrum is subjected to wave refraction differently with respect to its frequency. Therefore, irregular wave refraction differs also from regular wave refraction with respect to the frequency spectrum.

In order to test the performance of the numerical wave transformation model for the cases where shoaling is active with both refraction and depth-induced breaking, a series of runs on a planar bottom with a bottom slope of 1/50 is carried out for different deep water mean approach angles ($\bar{\theta}_0$=0, 15, 30, 45, and 60 degrees) and the maximum spreading parameter, s_{max}=25.

In the comparisons, the right hand side of the original energy balance equation (Eq.4.1) is assumed to be equal to (=$D_b.g.\rho$) to include the dissipation of depth-induced wave breaking. For the computation of the breaker index, γ_b, used in the computation of D_b values in 1D and NSW models, Eq.3.24 is used.

SWAN model utilizes Battjes and Janssen (1978) method for the depth-induced wave breaking with a recommended value of 0.73 for the breaker index parameter. The variation of the ratio of nearshore significant wave height to the deep water wave height ($H_s/H_{s,0}$) and nearshore mean approach angles ($\bar{\theta}$) with respect to relative water depth ($h/H_{s,0}$) is given for the deep water mean approach angles, $\bar{\theta}_0$=15, 30, 45, and 60 degrees, in Figure 4.4 and Figure 4.7.
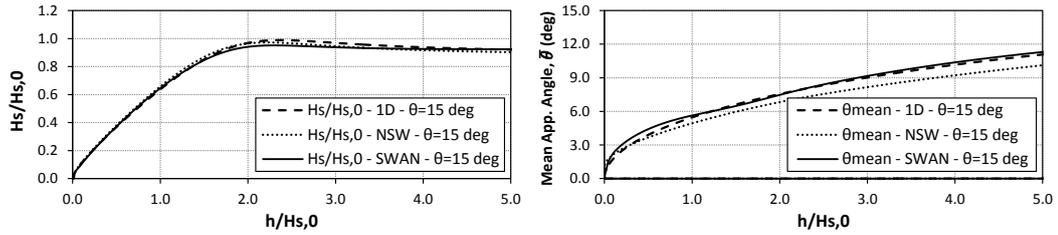
Figure 4.4 The variation of significant wave height (left) and mean approach angle (right) on planar bottom slope of 1:50 for s_{max}=25 and $\overline{\theta}_0$=15°
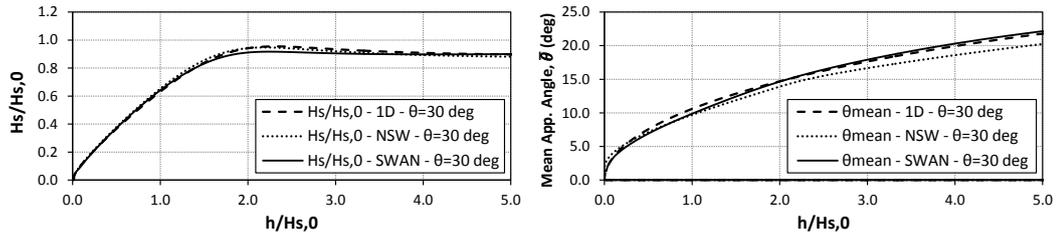
Figure 4.5 The variation of significant wave height (left) and mean approach angle (right) on planar bottom slope of 1:50 for s_{max}=25 and $\overline{\theta}_0$=30°
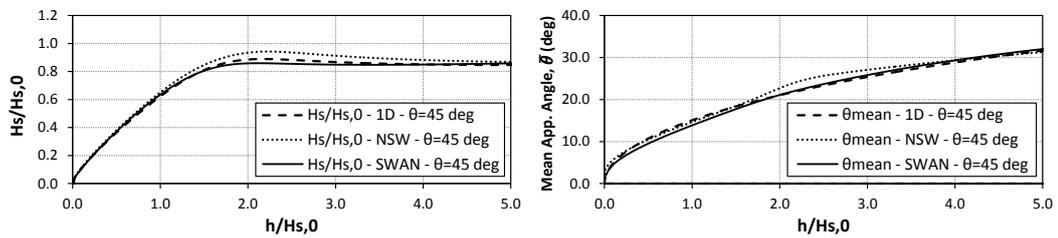
Figure 4.6 The variation of significant wave height (left) and mean approach angle (right) on planar bottom slope of 1:50 for s_{max}=25 and $\overline{\theta}_0$=45°
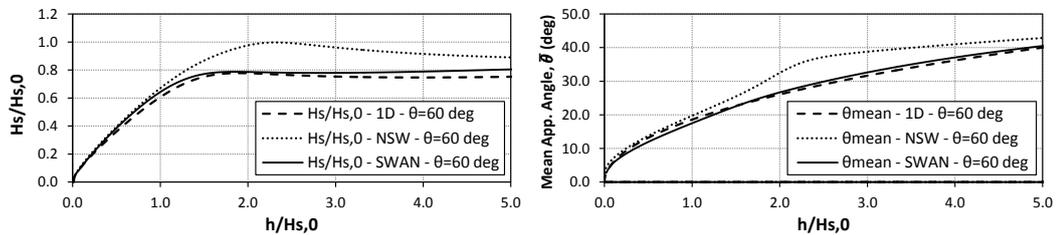
Figure 4.7 The variation of significant wave height (left) and mean approach angle (right) on planar bottom slope of 1:50 for s_{max}=25 and $\overline{\theta}_0$=60°

Figure 4.4 and Figure 4.7 show that, the differences between 1D and NSW solutions and between SWAN and NSW solutions increase as the deep water mean approach angle ($\bar{\theta}_0$) increases. For all cases, the maximum percent error in the relative significant wave height ($H_s/H_{s,0}$) at the relative depths, $h/H_{s,0}$=0.1-5.0, is 6.1% for $\bar{\theta}_0 \leq 45°$ and increases up to 30.0% for $\bar{\theta}_0$=60° between 1D and NSW solutions. The maximum percent error in the relative significant wave height ($H_s/H_{s,0}$) at the relative depths, $h/H_{s,0}$=0.1-5.0, is 9.8% for $\bar{\theta}_0 \leq 45°$ and increases up to 27.6% for $\bar{\theta}_0$=60° between SWAN and NSW solutions. Similarly, the maximum percent error in the nearshore mean approach angle ($\bar{\theta}$) at the relative depths, $h/H_{s,0}$=0.1-5.0, is in between 17.5-28.9% for $15° \leq \bar{\theta}_0 \leq 60°$ between 1D and NSW solutions. The maximum percent error between SWAN and NSW solutions at the relative depths, $h/H_{s,0}$=0.1-5.0, is in between 16.8-25.4% for $15° \leq \bar{\theta}_0 \leq 60°$.

As it is seen from the results, up to 45° of deep water approach angles, the percent error between three models is less than 10% for the significant wave heights nearshore. The percent error in the mean approach angles, however, is greater than 10% and increases up to 30% which might be considered as a limitation of the numerical scheme applied in wave transformation model.

4.1.3. Wave Diffraction

As mentioned in previous sections, wave diffraction is the decrease in wave energy due to an obstacle (i.e. islands, headlands, breakwaters etc.) in the direction of propagation of waves. In the shadow zone of such obstacles, the diffracted wave heights can be computed using the available charts given for regular (Wiegel, 1962) or irregular waves (Goda et al., 1978). In benchmarking the numerical wave transformation model for the case of pure wave diffraction, the charts given for irregular wave by Goda et al., (1978) is used.

Goda et al.'s (1978) computes the diffraction coefficients of irregular waves represented with a directional spectrum, $S(f,\theta)$, with the below given formula.

$$(K_d)_{eff} = \left[\frac{1}{m_0} \cdot \int_0^\infty \int_{\theta_{min}}^{\theta_{max}} S(f,\theta) \cdot K_d^2(f,\theta) \cdot d\theta \cdot df \right]^{1/2} \tag{4.3}$$

where $(K_d)_{eff}$ denotes the irregular diffraction coefficient (the ratio of diffracted to incident wave height), $K_d(f,\theta)$, is the regular diffraction coefficient computed for a given spectral energy density component $S(f,\theta)$ with frequency, f, and direction, θ, and m_0 is the total wave energy (zero moment of the directional spectrum), θ_{max} and θ_{min} are the limits of the directional domain (Goda, 2010).

In the benchmark study, the wave diffraction charts given by Goda et al., (1978) for irregular waves behind a semi-infinite breakwater defined within the limits of -10≤x/L≤10 and 0≤y/L≤20, where the water depth is constant, x/L is the distance along the breakwater from the tip, y/L is the distance perpendicular to the breakwater alignment from the tip of the breakwater and L is the wavelength corresponding to the significant wave period and water depth, are used. The given charts are digitized in 0.1 increments of x/L and y/L.

In the simulations of the NSW and SWAN models, the deep water significant wave height is taken as 1.0 meter, the significant wave periods are determined with respect to the maximum directional spreading parameters, s_{max}=10, 25 and 75. The water depth over the two dimensional bathymetry is taken as greater than the deep water limit ($h \geq 0.78 \cdot T_s^2$). The grid spacing in x and y directions, Δx and Δy, are taken as variable (5, 10, 20, 50 and 100 meters) for simulations of the NSW model. The grid spacing in SWAN is taken as the minimum grid spacing that gives a stable solution. In the NSW model, various values for the diffraction intensity parameter, ($\kappa \geq 0$), is taken between 0 and 5. For κ is equal to zero, the diffraction term (D_d) in Eq.3.1 is disregarded, hence, the irregular wave diffraction is not considered in the solution. The relative mean percent errors between the diffraction coefficient, $(K_d)_{eff}$, given at Goda et al.'s (1978) diffraction charts and the diffraction coefficients computed with the NSW and SWAN models are given in Table 4.2.

Table 4.2 The relative mean percent errors in the diffraction coefficient $(K_d)_{eff}$ in the domain of -10<x/L<10 and 0<y/L<20

κ	s_{max}=10, Δx (m)					s_{max}=25, Δx (m)					s_{max}=75, Δx (m)				
	5	10	20	50	100	5	10	20	50	100	5	10	20	50	100
0.0	5.8	5.5	6.0	13.7	30.9	9.0	8.9	9.2	17.2	44.3	16.5	12.4	11.7	11.8	12.4
0.5	4.5	4.3	5.5	13.6	30.7	7.4	7.8	8.4	17.0	44.2	13.4	9.6	9.3	10.4	12.2
1.0	4.0	3.9	5.2	13.4	30.5	6.7	7.4	8.2	17.0	44.2	12.1	8.6	8.6	10.3	12.4
1.5	3.8	3.7	5.0	13.3	30.4	6.4	7.3	8.2	17.1	44.2	11.3	8.1	8.3	10.4	12.7
2.0	3.7	3.7	4.9	13.3	30.3	6.2	7.3	8.3	17.2	44.2	10.8	7.9	8.3	10.7	13.1
2.5	3.6	3.6	4.8	13.2	30.1	6.2	7.4	8.5	17.3	44.3	10.5	7.8	8.4	11.0	13.4
3.0	3.6	3.7	4.8	13.2	30.0	6.2	7.5	8.7	17.5	44.3	10.3	7.9	8.6	11.3	13.8
3.5	3.6	3.7	4.8	13.2	29.9	6.3	7.6	8.9	17.6	44.3	10.3	8.1	8.8	11.7	14.2
4.0	3.7	3.7	4.9	13.1	29.8	6.4	7.8	9.1	17.8	44.4	10.3	8.3	9.0	12.1	14.6
4.5	3.7	3.8	4.9	13.1	29.7	6.6	8.0	9.3	18.0	44.4	10.4	8.5	9.3	12.5	15.0
5.0	3.7	3.8	4.9	13.1	29.6	6.7	8.2	9.6	18.1	44.4	10.5	8.8	9.6	12.9	15.5
SWAN		3.5					6.4								10.6

As it is seen from Table 4.2, the relative percent error in the decrease as the grid spacing decrease for s_{max} equal to 10 and 25. The relative percent error is within an acceptable limit of 10% up to a grid spacing of 20 meters (for both Δx and Δy). SWAN model gives also similar mean percent errors. It is also seen from Table 4.2 that the mean percent error is minimum for κ=2.0-2.5. Mase et al. (2001) state that κ value should be less than 15 to minimize the error and they use a constant value of κ=2.5 in several comparisons. Lin et al. (2008) and Demirbilek et al. (2009) give that κ=4 is appropriate for the cases of strong diffraction e.g. semi-infinite breakwater and narrow gaps (inlets) with openings equal or less than one wavelength. For wider gaps with the opening greater than one wavelength, κ=3 is recommended. For various types of structural geometry, bathymetry and incident wave conditions, κ value need to be calibrated with the actual field data to minimize the error in diffraction computation. The results of diffraction simulations of NSW and SWAN models are shown in Figure 4.8 and Figure 4.9 together with the digitized diffraction charts of Goda et al. (1978). In these figures, the tip of the semi-infinite breakwater is at the point of x/L=0 and y/L=0. The semi-infinite breakwater extends along the positive x/L direction.
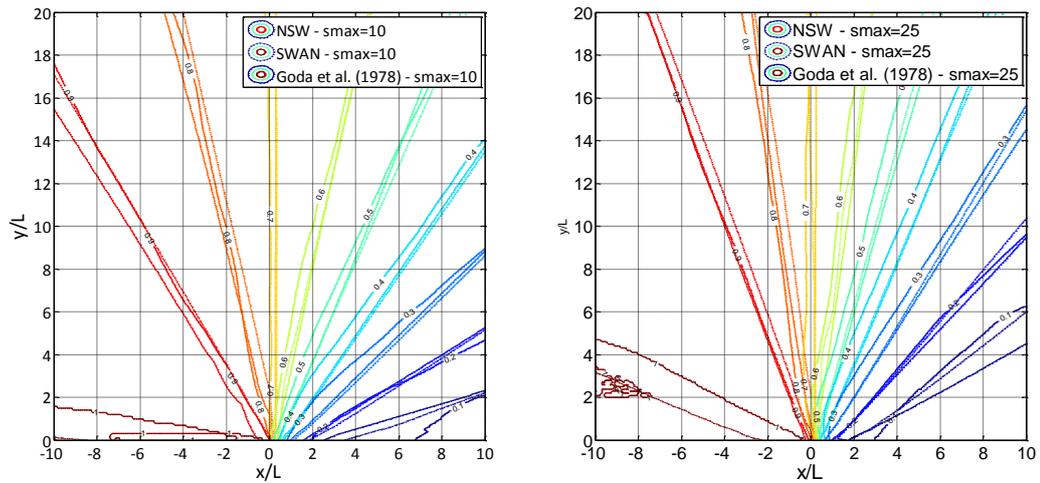
Figure 4.8 Diffraction diagrams of a semi-infinite breakwater for s_{max}=10 (left) and s_{max}=25 (right)
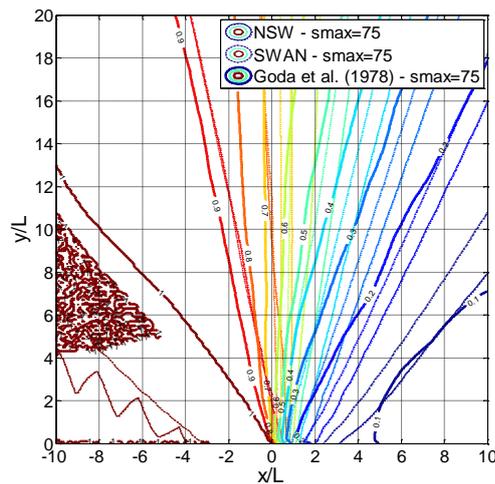
Figure 4.9 Diffraction diagrams of a semi-infinite breakwater for s_{max}=75

As shown from Figure 4.8 and Figure 4.9, the contours of diffraction coefficients computed using NSW and SWAN are in good agreement both qualitatively and quantitatively with the diffraction coefficients given by Goda et al. (1978). Although, these two models are not sufficient for detailed analysis of harbor agitation problems, they are quite capable of simulating the diffraction process around coastal structures. Further detailed analyses of the NSW model with the laboratory measurements such as elliptic and circular shoal experiments where shoaling, refraction and diffraction processes are important in the transformation of waves.

4.2. Laboratory Experiments

The three main modules of the two-dimensional depth-averaged beach evolution model (COD), spectral wave transformation (NSW), nearshore circulation (NSC) and sediment (SED) models, are tested with the laboratory experiments available in the literature (Okayasu and Katayama, 1992; Baldock et al., 1998; Battjes and Janssen, 1978; Vincent and Briggs, 1989; Chawla et al., 1998; Hamilton and Ebersole, 2001; Tang et al., 2008; Reniers and Battjes, 1997; Wang et al., 2002a; Gravens and Wang, 2007). The laboratory data set used in this part is categorized as given in Table 4.3.

Table 4.3 Characteristics of the laboratory data set used in the model benchmarking

Laboratory Data Set	Wave Processes	Waves	Type of Data	Bottom Profile	Test No
Okayasu and Katayama (1992)	Shoaling, Breaking	Uni-Directional Random	H	Uniform, 1/20	Case-2
				Barred Beach	Case-3
Baldock et al. (1998)	"	"	H	Mixed Uniform	J2 & J3
Battjes and Janssen (1978)	"	"	H and $\bar{\eta}$	Uniform, 1/20	R2 & R3
				Barred Beach	R13 & R15
Vincent and Briggs (1989)	Shoaling, Refraction, Diffraction and Breaking	Multi-Directional Random	H	Elliptic Shoal	N1 & B1
Chawla et al. (1998)	"	"	"	Circular Shoal	T3, T4, T5 & T6
Hamilton and Ebersole (2001)	Shoaling, Breaking, Refraction	Uni-Directional Random	H, $\bar{\eta}$ and v	Uniform, 1/30	TEST-8E
Tang et al. (2008)	"	"	"	Uniform, 1/40	Case-1
				Uniform, 1/100	Case-2
Reniers and Battjes (1997)	"	"	"	Barred Beach	SO014
Wang et al. (2002a)	"	"	H, $\bar{\eta}$, v, and $q_{total,y}$	Irregular	T1-C1, T3-C1, T5-C1, & T6C1
Gravens and Wang (2007)	"	"	"	Irregular	TEST-BC1
Gravens and Wang (2007)	Shoaling, Refraction, Diffraction and Breaking	"	H, v, u and h	Irregular, a single offshore breakwater	Test1-Case1

Table 4.3 gives the characteristics of the laboratory data set used in the model benchmarking. As it is seen from Table 4.3, the selected laboratory data set consists of

variety of wave and bottom conditions where different wave transformation mechanisms are active. The data set is categorized with respect to the effective wave transformation processes (shoaling, refraction, breaking and diffraction), types of spreading of waves (uni-directional or multi-directional), the types of data measured in the experiments and used in the benchmarking study, the channel or basin bottom configuration and the name of the test used in this study. The first five of the nine data sets (Okayasu and Katayama, 1992; Baldock et al., 1998; Battjes and Janssen, 1978; Vincent and Briggs, 1989; Chawla et al., 1998) are used in benchmarking the wave transformation model, NSW. The next three of the data sets (Hamilton and Ebersole, 2001; Tang et al., 2008; Reniers and Battjes, 1997) are used in benchmarking both the NSW and NSC models. The last two of the data sets (Wang et al., 2002a; Gravens and Wang, 2007) are used to investigate the performance of the NSW, NSC and SED models. For the SED model, different approaches are used to compute the local total longshore sediment transport rates. These approaches are the Watanabe (1992) formulation which utilizes the critical shear stress concept, SED1 ($\varepsilon=0.002$) and SED2 ($\varepsilon=\varepsilon_{Ba07}$) approaches which utilize the dissipation rates of wave energies due to random wave breaking. The data set of Gravens and Wang (2007) experiments on the morphology change around the offshore breakwater is used to the validate the COD model.

The bottom friction (c_f), eddy viscosity constant (Λ) and the energy transfer coefficient (α) used in the nearshore circulation computations to obtain mean water elevations and current velocities are given in Table 4.4. Tang et al. (2008) gives the values of these parameters for their experiments. For Reniers and Battjes (1997) and Hamilton and Ebersole (2001) experiments, these values are taken from Goda (2006). For Gravens and Wang (2007), these values are taken from Nam et al. (2009) and similar values are used for Wang et al. (2002a) experiments. For Battjes and Janssen (1978) experiments, these values are taken according to the experimental set-up.

Table 4.4 The computational data given in the literature for the laboratory data set

Laboratory Data Set	Test No	Bottom Friction Coefficient, c_f	Eddy Viscosity Constant, Λ	Energy Transfer Coef., α
Battjes and Janssen (1978)	R2, R3, R13 and R15	0.007	0.50	0.5
Hamilton and Ebersole (2001)	TEST-8E	0.007	0.50	0.5
Tang et al. (2008)	Case-1	0.009	0.85	0.5
	Case-2	0.0065	0.85	0.5
Reniers and Battjes (1997)	SO014	0.015	0.30	0.5
Wang et al. (2002a)	T1-C1, T3-C1, T5-C1, & T6C1	0.015	0.50	0.5
Gravens and Wang (2007)	TEST-BC1 TEST1-CASE1	0.015	0.50	0.5

4.2.1. Okayasu and Katayama (1992) Experiments

Okayasu and Katayama (1992) carried out laboratory measurements on cross-shore wave height distributions in the surf zone on a 17 m long and 0.5 m wide wave flume with both regular and random waves for perpendicular wave approach (wave orthogonals are perpendicular to the bottom contours). The wave heights across the surf zone were obtained applying zero-down crossing method to the time series of surface elevation measured with the capacitance-type wave gauges. The uni-directional random waves were generated with a Bretschneider-Mitsuyasu type frequency spectrum. The experiment conditions are summarized in Table 4.3 and Table 4.5 and the set-up is shown in Figure 4.10.

Table 4.5 Summary of laboratory incident wave conditions for Okayasu and Katayama (1992)

Test No	Offshore Water Depth, h (m)	Offshore Sig. Wave Height, H_s (m)	Sig. Wave Period, T_s (sec)	Deep Water Sig. Wave Height, $H_{s,0}$ (m)	Peak Wave Period, T_p (sec)	Deep Water Wave Steepness, s_{os}	Breaker Index, $\gamma_{br,N90}$
Case-2	0.35	**0.083**	**1.26**	0.090	1.323	0.036	0.753
Case-3	0.32	**0.057**	**0.945**	0.059	0.992	0.042	0.79

$s_{os}=H_{s,0}/1.56 \cdot T_s^2$
$T_p=T_s \cdot 1.05$
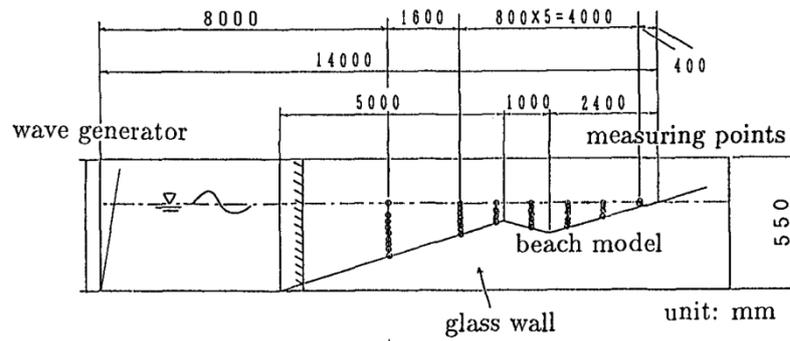
Figure 4.10 Side view of the wave flume of Okayasu and Katayama (1992) Experiments

The NSW model is compared with the two of the measurements given in Okayasu and Katayama (1992). One of these measurements (Case-2) was carried out for a uniform bottom slope of 1/20 and the other one (Case-3) had a barred type beach profile as shown in Figure 4.10. In the NSW model computations, wave are given from deep water assuming that the beach has the same bottom slope up to the respective deep water wave limit of the experiment. The given deep water wave heights in Table 4.5 are obtained dividing the measured wave heights at offshore gauge to the respective shoaling coefficients computed for the respective depth and peak period. For the computation of wave heights across the surf zone in the wave model, two breaker index values are used, one of which is equal to 0.78 and the other one is found using Nairn's (1990) equation (Eq.3.24, hereafter $\gamma_{br,N90}$). In the numerical model, the directional spectrum of the waves is assumed to have a triangular shape where the energy density has a peak value at $\theta=0°$ and zero elsewhere. The computed nearshore wave heights with the NSW model and the measurements are given in Figure 4.11 and Figure 4.12.
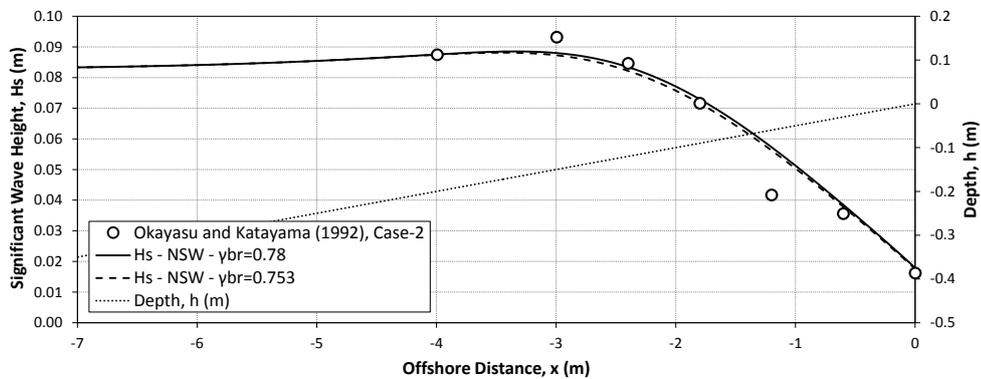
Figure 4.11 Measured and computed significant wave heights for Case-2 (Okayasu and Katayama, 1992)
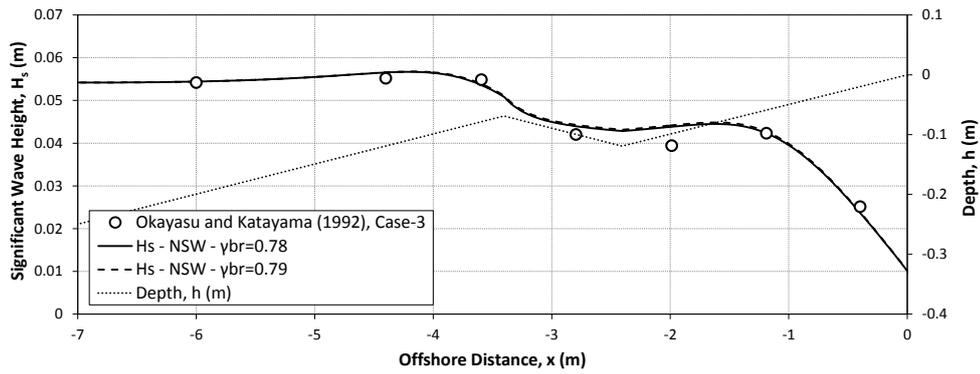
Figure 4.12 Measured and computed significant wave heights for Case-3 (Okayasu and Katayama, 1992)

As seen from Figure 4.11 and Figure 4.12, the computed wave heights are in good agreement with the measurements for both experiments.

4.2.2. Baldock et al. (1998) Experiments

Baldock et al. (1998) studied the cross-shore variation of wave heights at steep beaches to investigate the fraction of waves breaking and the distribution of waves in unsaturated surf zones. They carried out the experiments in a 50 m long, 3 m wide and 0.9 m deep wave flume of which the last 6 m is sub-divided into three sections and a 0.9 wide channel is formed for the measurements. The wave approach is perpendicular for all cases. The experiment conditions are summarized in Table 4.3 and Table 4.6. Figure 4.13 shows the plan and side views of the wave flume of Baldock et al. (1998) experiments.

Table 4.6 Summary of laboratory incident wave conditions for Baldock et al. (1998)

Test No	Offshore Water Depth, h (m)	Offshore RMS Wave Height, H_{rms} (m)	Sig. Wave Period, T_s (sec)	Deep Water Sig. Wave Height, $H_{s,0}$ (m)	Peak Wave Period, T_p (sec)	Deep Water Wave Steepness, s_{os}	Breaker Index, $\gamma_{br,N90}$
J2	0.45	**0.074**	1.429	0.114	**1.5**	0.036	0.749
J3	0.45	**0.046**	0.952	0.069	**1.0**	0.049	0.823

$s_{os}=H_{s,0}/1.56 \cdot T_s^2$
$T_s=T_p/1.05$
$H_s=H_{rms} \cdot \sqrt{2}$

The given deep water wave heights for the experiments in Table 4.5 are obtained dividing the measured wave heights at offshore gauge to the respective shoaling coefficients computed for the respective depth and peak period.
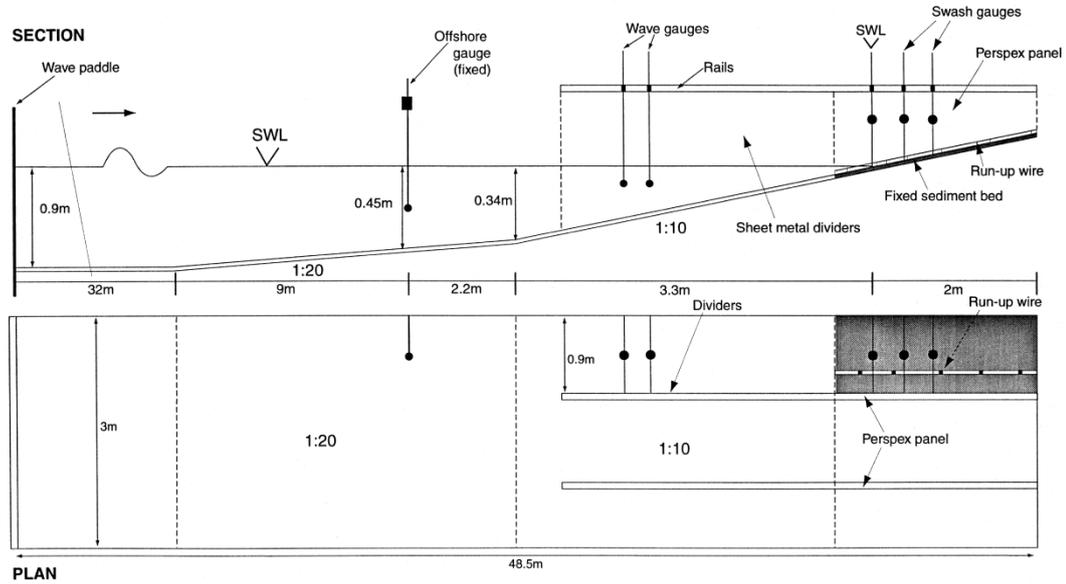
Figure 4.13 The side and plan views of the wave flume of Baldock et al. (1998) experiments

The uni-directional random waves were generated based on Jonswap spectrum with varying H_s and T_p and measured with resistance-type wave gauges. The given offshore wave conditions in Table 4.6 are measured at the offshore wave gauge at 0.45 m water depth (Figure 4.13). Both experiments (J2 and J3) were carried out for the same mixed-uniform bottom as shown in Figure 4.13 for different offshore wave steepness values s_{os}=0.036 for J2 experiment and s_{os}=0.049 for J3 experiment. In the 2D wave model computations, wave are given from deep water assuming that the beach has the same bottom slope up to the respective deep water wave limit of the experiment. The given deep water wave heights in Table 4.5 are obtained dividing the measured wave heights at offshore gauge to the respective shoaling coefficients computed for the respective depth and peak period. The NSW model is compared with the two of the measurements, J2 and J3, given in Baldock et al. (1998). In the comparison of J2 measurements, two breaker index values are used, one of which is taken as 0.78 and the $\gamma_{br,N90}$. In the comparison of J3 measurements, the results of three simulations with different breaker index values are shown, 0.78, $\gamma_{br,N90}$ and 1.2 as both the waves and the bottom slope is so steep that unsaturated breaking condition occurs close to shoreline. The comparisons

of the 2D wave model with the wave measurements are given in Figure 4.14 and Figure 4.15.
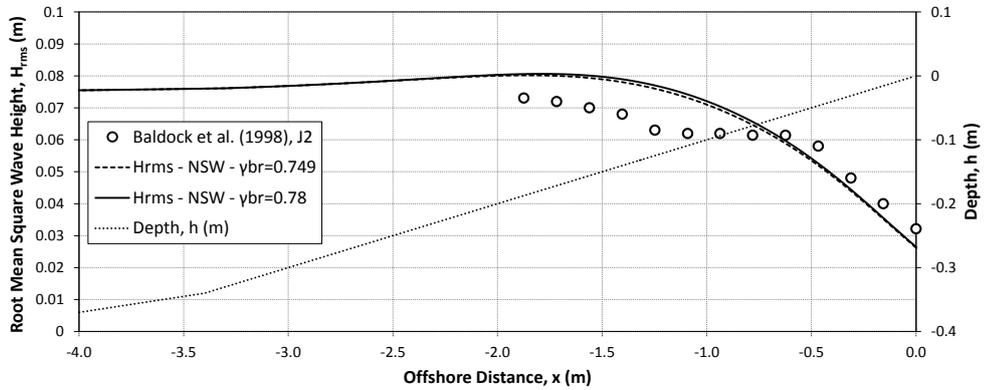
Figure 4.14 Measured and computed root-mean-square wave heights (H_{rms}) for J2 experiment (Baldock et al., 1998)
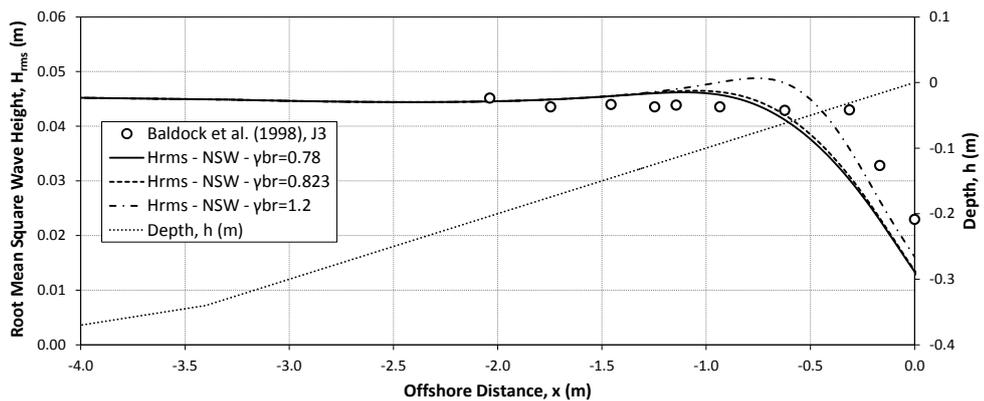
Figure 4.15 Measured and computed root-mean-square wave heights (H_{rms}) for J3 experiment (Baldock et al., 1998)

As it is seen from Figure 4.14 and Figure 4.15, the measured wave heights close to shoreline are greater than the computed wave heights due to unsaturated breaking wave conditions, where the root mean square wave height is smaller than the maximum depth limited wave height. It is seen that the breaking method used in the wave model over-estimates the dissipation rates for steep beaches.

4.2.3. Battjes and Janssen (1978) Experiments

Battjes and Janssen (1978) studied the estimation of energy dissipation in random waves due to depth-induced wave breaking, introduced an irregular breaking model and

compared the model with laboratory experiments carried out in 45 m long, 0.8 m wide and 1.0 deep wave flume. Figure 4.16 shows the side view of the wave flume of Battjes and Janssen (1978) experiments. The incident wave spectrum used in experiments is given in Battjes and Janssen (1978) as a "narrow (half-power bandwidth about %25 of peak frequency), virtually unimodal except a bulge in the range of frequencies twice the peak frequency." In the experiments, the wave heights and mean water elevations are measured during the experiments. The time series of surface elevations along the bottom profile were measured with resistance-type wave gauges and the mean water elevations at beach face were measured by means of piezometer tappings. The deep water wave heights given in Table 4.7 by Battjes and Janssen (1978) are obtained dividing the measured wave heights at the reference gauge 1.5 m offshore from the toe of the bottom slope to the respective shoaling coefficients. R2 and R3 experiments were carried out on a uniform bottom slope of 1/20 on a smooth cement-sand mortar layer. R13 and R15 experiments were carried out with the addition of a bar to the uniform profile as shown in Figure 4.16. The experiment conditions are summarized in Table 4.3 and Table 4.7.
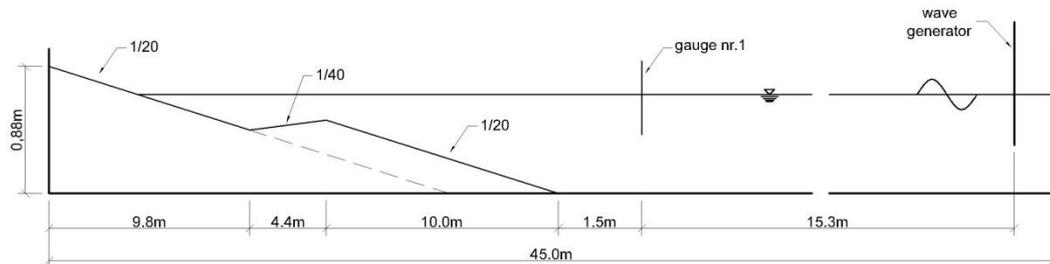
Figure 4.16 The side view of the wave flume of Battjes and Janssen (1978) experiments

Table 4.7 Summary of laboratory incident wave conditions for Battjes and Janssen (1978)

Test No	Offshore Water Depth, h (m)	Deep Water RMS Wave Height, $H_{rms,0}$ (m)	Sig. Wave Period, T_s (sec)	Deep Water Sig. Wave Height, $H_{s,0}$ (m)	Peak Wave Period, T_p (sec)	Deep Water Wave Steepness, s_{os}	Breaker Index, $\gamma_{br,N90}$
R2	0.705	**0.157**	1.75	**0.222**	**1.838**	0.046	0.812
R3	0.697	**0.126**	2.34	**0.177**	**2.457**	0.021	0.621
R13	0.762	**0.113**	1.916	**0.160**	**2.012**	0.028	0.687
R15	0.616	**0.154**	1.796	**0.219**	**1.886**	0.043	0.797

$s_{os}=H_{s,0}/1.56 \cdot T_s^2$
$T_s=T_p/1.05$
$H_s=H_{rms} \cdot \sqrt{2}$

In the computations, the water depths are extended considering a 1/20 bottom slope to the deep water limit of the experiment. Both the root-mean-square wave heights (H_{rms}) and the mean water elevations ($\bar{\eta}$) computed with the numerical wave and circulation models are compared with the measurements of R2, R3, R13 and R15. The computations are carried out for three different breaker index values, which are 0.78, $\gamma_{br,N90}$ and another breaker index value that gives the best result. The computed and measured wave heights and mean water elevations are given in dimensionless form as given in Battjes and Janssen (1978) in Figure 4.17 - Figure 4.20. The computed wave heights with the two-dimensional wave transformation model are denoted by 'NSW' and the computed mean water elevations with the two-dimensional depth-averaged nearshore circulation model are denoted by 'NSC'.
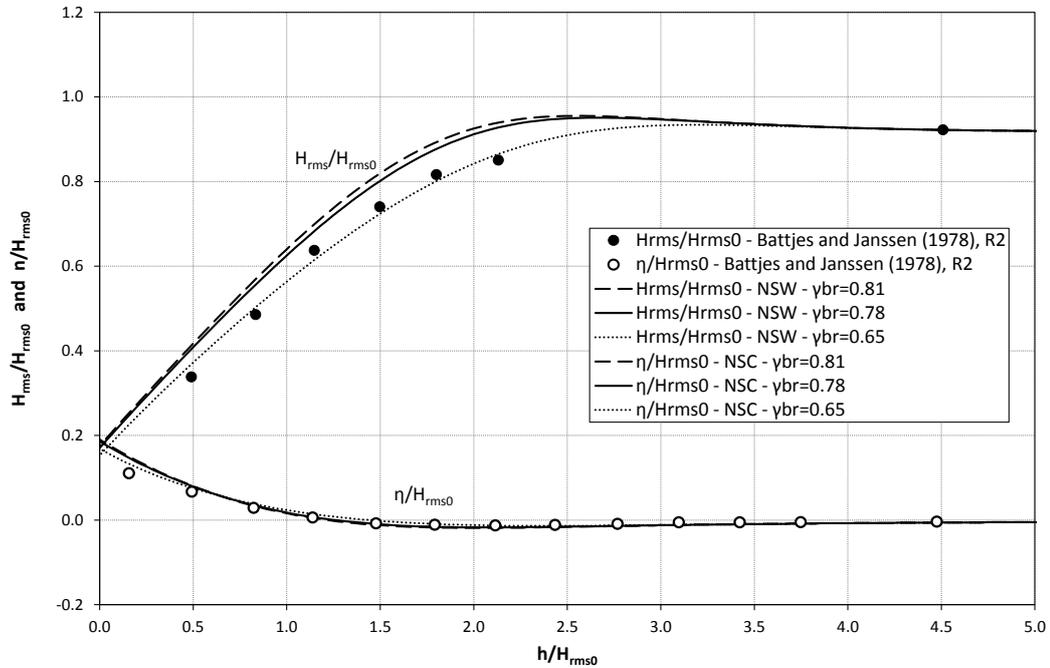
Figure 4.17 Measured and computed root-mean-square wave heights (H_{rms}) and mean water elevations ($\bar{\eta}$) for R2 experiment (Battjes and Janssen, 1978)
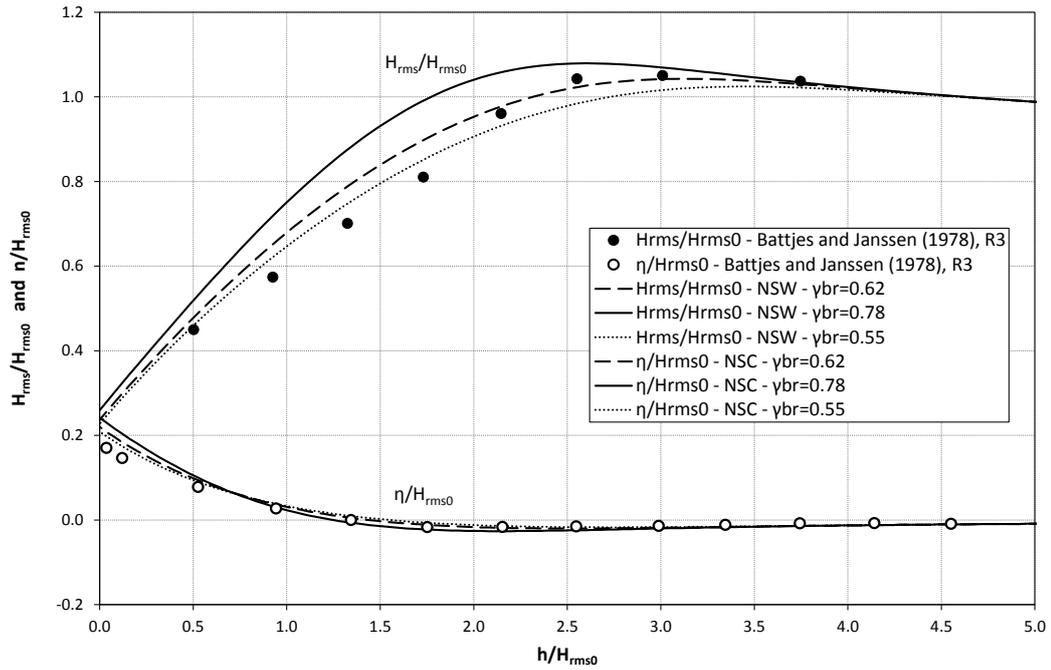
Figure 4.18 Measured and computed root-mean-square wave heights (H_{rms}) and mean water elevations ($\overline{\eta}$) for R3 experiment (Battjes and Janssen, 1978)
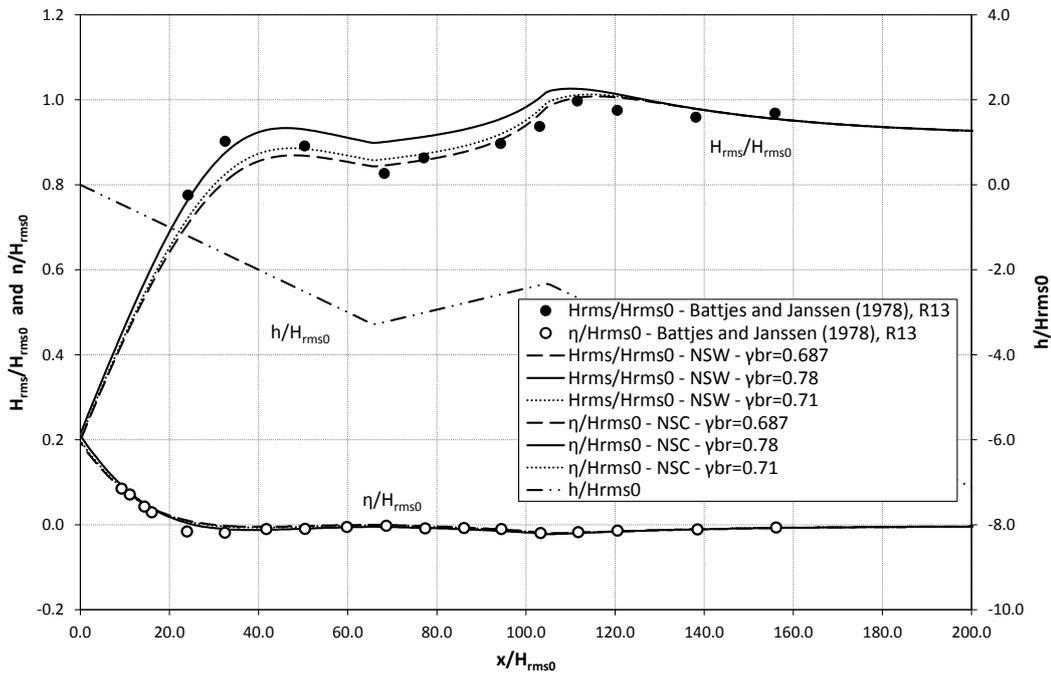
Figure 4.19 Measured and computed root-mean-square wave heights (H_{rms}) and mean water elevations ($\overline{\eta}$) for R13 experiment (Battjes and Janssen, 1978)
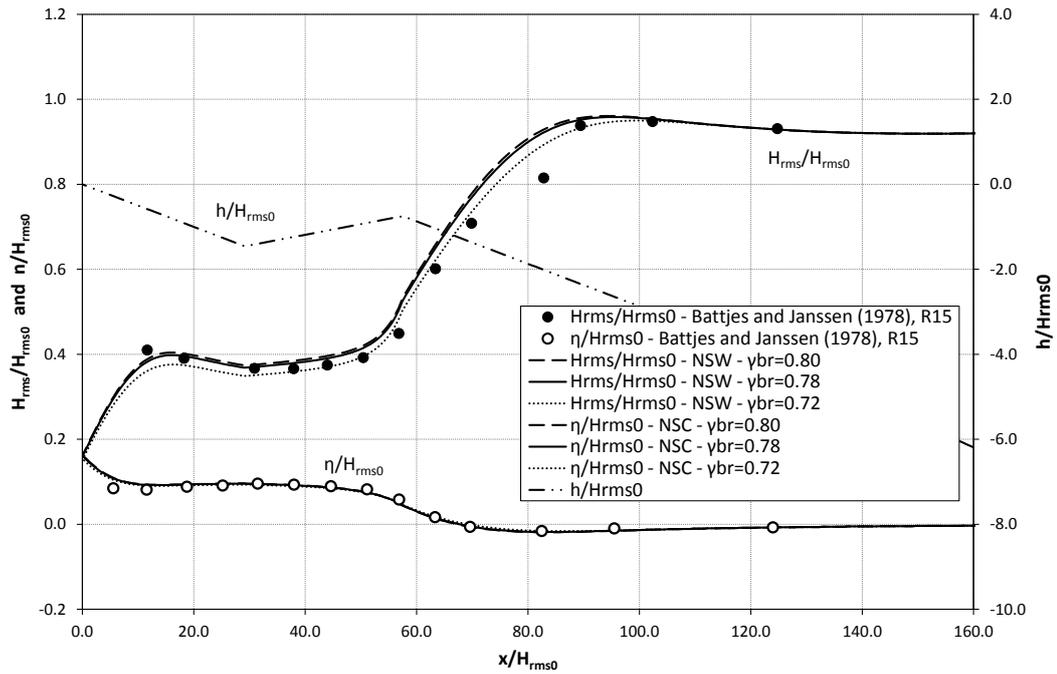
Figure 4.20 Measured and computed root-mean-square wave heights (H_{rms}) and mean water elevations ($\overline{\eta}$) for R15 experiment (Battjes and Janssen, 1978)

Figure 4.17 and Figure 4.18 shows that the wave heights computed for the experiments R2 and R3 using both the default breaker index value of 0.78 and $\gamma_{br,N90}$ are overestimated in the surf zone. It is also seen that as the wave steepness decreases the error due to breaker index value used increases and smaller values for breaker index need to be used for better estimation of breaking wave heights.

In the bar-profile experiments, R13 and R15, Figure 4.19 and Figure 4.20 shows that the computed wave heights using $\gamma_{br,N90}$ are in good agreement with the measured ones both qualitatively and quantitatively. For better prediction of breaking wave heights, the breaker index may be selected considering the deep water wave steepness ratio and the bottom slope.

4.2.4. Vincent and Briggs (1989) Experiments

Vincent and Briggs (1989) studied the wave transformation (shoaling, refraction and diffraction) of regular and multi-directional random waves passing over an elliptic shoal

through laboratory experiments carried out in 35 m wide 29 m long directional spectral basin at U.S. Army Engineers Waterways Experiment Station's Coastal Engineering Research Center (CERC). The water depth in the experiments is given as 0.4572 m. The center of the shoal is at x=6.10 m and y=13.72 m. The perimeter of the shoal is defined as

$$(x' / 3.05)^2 + (y' / 3.96)^2 = 1 \tag{4.4}$$

where x' and y' are the local coordinates centered on the shoal, denoting minor and major axes, respectively. The water depths (h) over the shoal are given with the following equation which gives the water depth at the center of the shoal is 15.24 cm.

$$h = -0.4572 + 0.7620 \left\{ 1 - \left(\frac{x'}{3.81} \right)^2 - \left(\frac{y'}{4.95} \right)^2 \right\}^{0.5} \tag{4.5}$$

The experiment conditions are summarized in Table 4.3 and Table 4.8. Figure 4.21 shows the plan view of the CERC's directional wave flume and the layout of the experimental set-up of Vincent and Briggs (1989) experiments.

Table 4.8 Summary of incident wave conditions for Vincent and Briggs (1989) Experiments

Test No	Water Depth, h (m)	Significant Wave Height, H_s (m)	Peak Wave Period, T_p (sec)	Sig. Wave Period, T_s (sec)	Peak Enhancement Factor, γ	Dir. Spread. Par., σ_m (deg) (Borgman, 1984)
N1	0.4572	**0.078**	**1.300**	1.24	**2**	10
B1	0.4572	**0.078**	**1.300**	1.24	**2**	30

$T_s = T_p / 1.05$
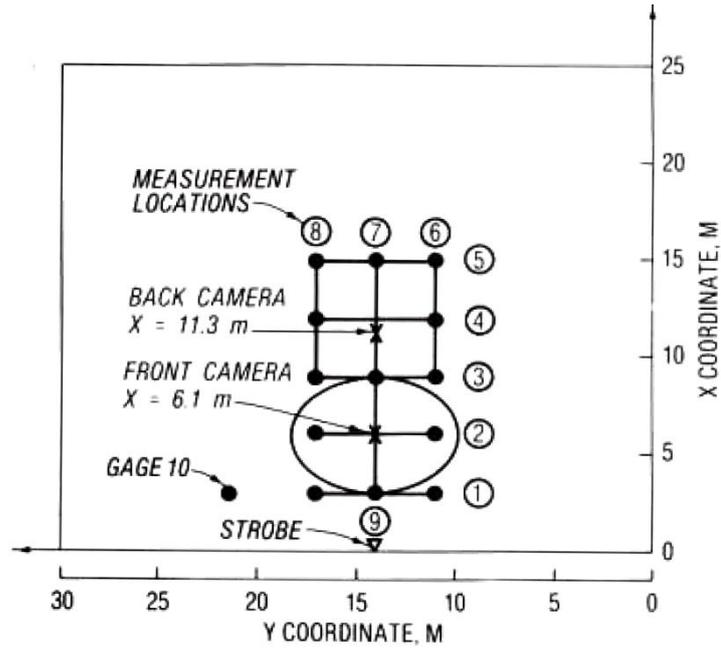
Figure 4.21 The plan view of the directional wave basin of CERC and experiment set-up in Vincent and Briggs (1989) experiments

The frequency spectrum in the experiments is selected as the TMA shallow water spectrum (Bouws et al., 1985). For the directional spreading of the waves, a wrapped normal function is used (Borgman, 1984),

$$D(\theta) = \frac{1}{2\pi} + \frac{1}{\pi} \sum_{j=1}^{J} \left\{ exp\left[-\frac{(j\sigma_m)^2}{2} \right] cos\, j(\theta - \theta_m) \right\}$$
(4.6)

where J is the number of arbitrary number of harmonics chosen to represent the Fourier series, σ_m is the spectral width parameter, θ_m is the mean approach angle. For broad directional spreading, the spectral width parameter is selected as σ_m=30° (s_{max}≈13.5) and for narrow spreading σ_m=10° (s_{max}≈130). The time series of surface elevations around the shoal as shown in Figure 4.21 were measured with resistance-type wave gauges. In the 2D wave model computations, the breaker index value is taken as 0.78 and the diffraction intensity parameter, κ, is taken as 2.5.

The measured (N1 and B1) and computed (NSW) normalized wave height ratios are contoured as a function of (x,y) in Figure 4.22 and Figure 4.23. The dashed lines on the measured contour plots at below given figures are the perimeter of shoals.
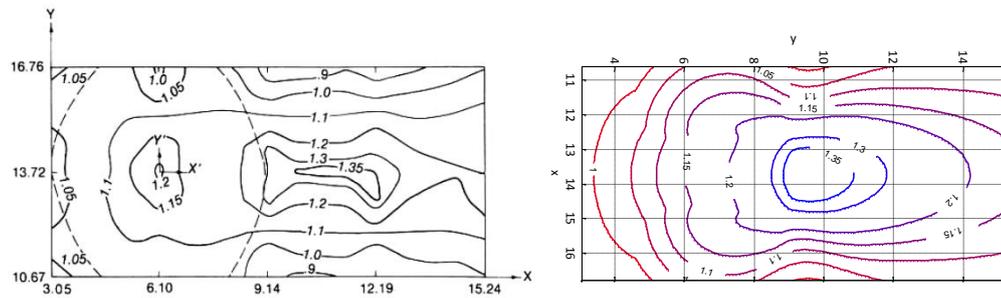
Figure 4.22 The measured (left) and computed (right) normalized wave height ratios for the N1 experiment (Vincent and Briggs, 1989)
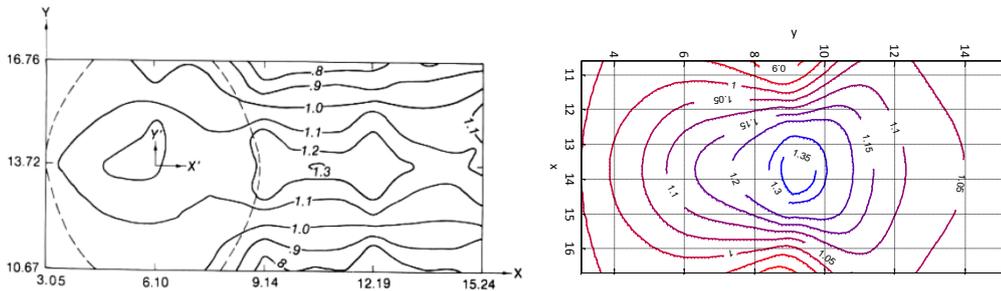
Figure 4.23 The measured (left) and computed (right) normalized wave height ratios for the B1 experiment (Vincent and Briggs, 1989)

As it is seen from Figure 4.22 and Figure 4.23, the computed wave height ratios are in agreement with the measured wave heights to some extent. Although, there exist differences between the computed and measured wave height ratios especially at the center of the shoal where the waves are blocked and increase in height, the location of the second peak and the order of magnitude in the normalized wave height ratios are predicted well in computed results.

4.2.5. Chawla et al. (1998) Experiments

Chawla et al. (1998) developed a parabolic nearshore wave transformation model (REF/DIF-S) for multi-directional random waves and compared the numerical model with the results of laboratory experiments of multi-directional random waves passing over an circular shoal carried out in a 18 m long and 18.2 m wide directional wave basin. The water depth in the experiments is given as 0.40 m. The center of the shoal is at x=5.0 m and y=8.98 m. The perimeter of the shoal is defined as

$$(x - 5)^2 + (y - 8.98)^2 = (2.57)^2 \tag{4.7}$$

and the water depths (h) over the shoal are given with the following equation which gives the water depth at the center of the shoal is 3.0 cm.

$$h = 0.40 + 8.73 - \sqrt{82.81 - (x - 5)^2 - (y - 8.98)^2} \tag{4.8}$$

The experiment conditions are summarized in Table 4.3 and Table 4.9. Figure 4.24 shows the plan view of transects of wave gauge positions and the layout of the experimental set-up of Chawla et al. (1998) experiments.

Table 4.9 Summary of incident wave conditions for Chawla et al. (1998) Experiments

Test No	Water Depth, h (m)	Deep Water Sig. Wave Height, $H_{s,0}$ (m)	Peak Wave Period, T_p (sec)	Significant Wave Period, T_s (sec)	Deep Water Wave Steepness, s_{os}	Dir. Spreading Par., σ_m (deg) (Borgman, 1984)
T3	0.40	**0.014**	**0.730**	0.695	0.019	**5**
T4	0.40	**0.016**	**0.730**	0.695	0.021	**20**
T5	0.40	**0.023**	**0.730**	0.695	0.031	**5**
T6	0.40	**0.025**	**0.710**	0.676	0.035	**20**

$T_s = T_p/1.05$
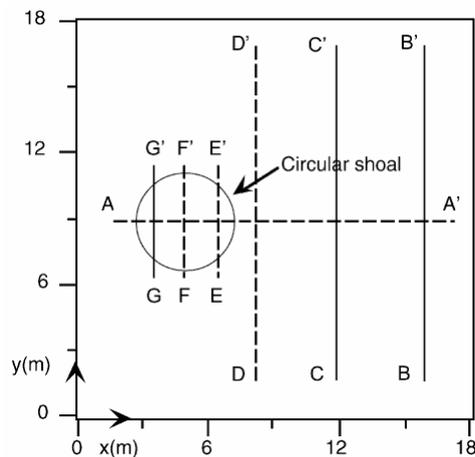
Figure 4.24 The plan view of the directional wave basin and experiment set-up in Chawla et al. (1998) experiments

The spectral sea state is defined by using a TMA shallow water frequency spectrum (Bouws et al., 1985) with a spectral width parameter of γ=10 and a wrapped normal

function (Borgman, 1984) for the directional spreading of spectral waves. For broad directional spreading, the spectral width parameter is defined as σ_m=5° (s_{max}≈550; almost unidirectional) and for narrow spreading σ_m=20° (s_{max}≈31.5). The time series of surface elevations along the transects shown in Figure 4.24 were measured with capacitance-type wave gauges on a movable frame. In the 2D wave mode computations, the breaker index value is taken as 0.78 and the diffraction intensity parameter, κ, is taken as 2.5. The measured and computed normalized significant wave height ratios ($H_s/H_{s,0}$) are given for transects A-A', B-B', C-C', D-D', E-E', F-F' and G-G' in Figure 4.25 and Figure 4.26. The circles in these figures represent the measured data and the solid lines are the computed normalized significant wave height ratios along these transects computed by the 2D wave model.
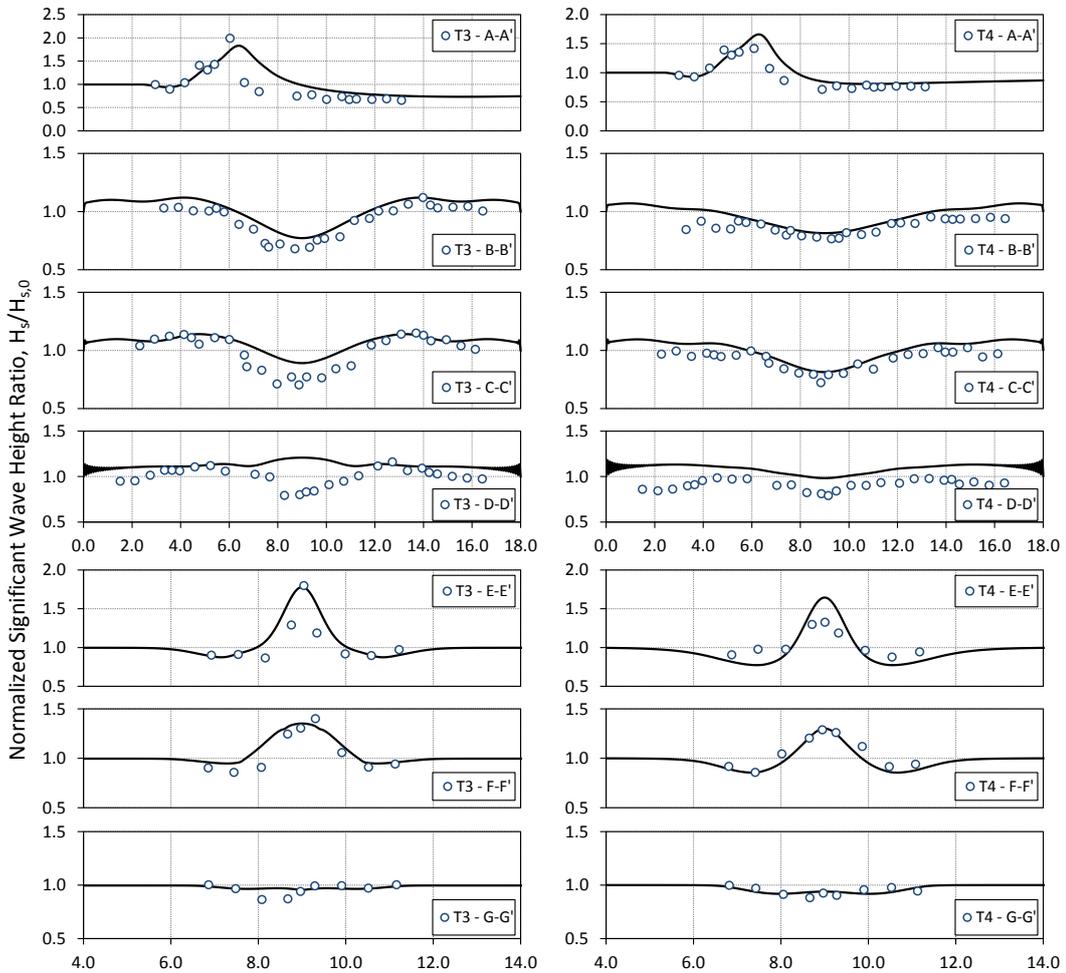
Figure 4.25 The measured and computed (solid line) normalized wave height ratios for the T3 and T4 experiments (Chawla et al., 1998)
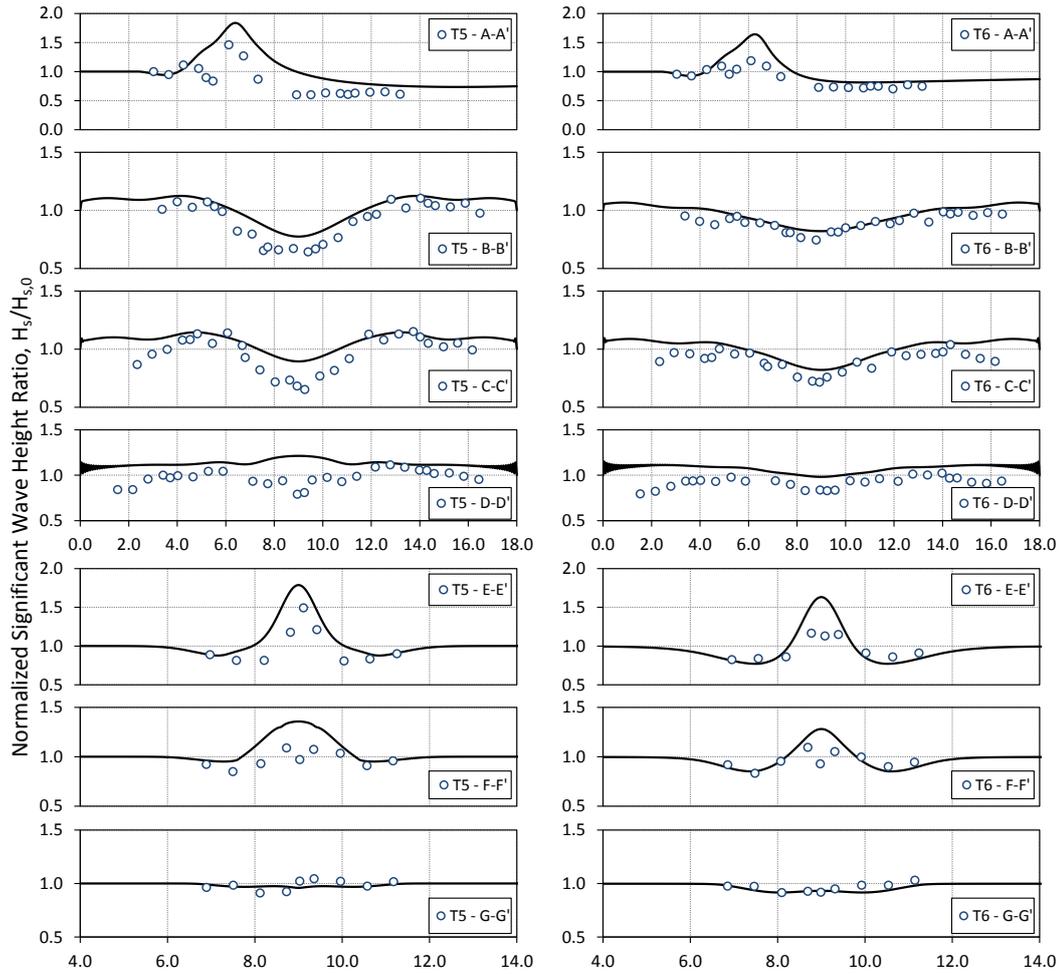
Figure 4.26 The measured and computed (solid line) normalized wave height ratios for the T5 and T6 experiments (Chawla et al., 1998)

As it seen from Figure 4.25 and Figure 4.26, the computed wave heights are in agreement with the measurements both qualitatively and quantitatively, except for the D-D' transect where Chawla et al. (1998) point out a severe wave focusing at this region which is more apparent for narrow spreaded waves (T3 and T5). It is also seen that as the deep water wave steepness increases, the numerical model tends to overestimate the wave heights which might be also due to depth-induced random wave breaking method and the breaker index value taken as constant for all simulations. The breaking method used in the wave model is not originally derived for the cases where the water depths get deeper and waves stop breaking and reform. In the numerical wave model, the non-linear wave-wave interactions are taken into account. These interactions are stated as to be responsible of growth of higher harmonics around the shoal where focusing occurs by Chawla et al. (1998). The disparity between the measured and

computed wave heights might be due to the lack of non-linear wave-wave interactions in the wave model. It should also be noted that more accurate description of the diffraction around the shoal might be achieved with the use of a more sophisticated wave model such as Boussinesq-type of time dependent non-linear mild slope models.

4.2.6. Hamilton and Ebersole (2001) Experiment: TEST-8E

Hamilton and Ebersole (2001) conducted physical model experiments at the Large-scale Sediment Transport Facility (hereafter LSTF) at CERC to evaluate the performance of the recirculation system in the laboratory and to obtain uniform longshore current conditions as seen on long straight beaches before the sediment transport experiments. The LSTF is given as to have dimensions of approximately 30 m cross-shore by 50 m longshore by 1.4 m deep (Hamilton and Ebersole, 2001). The plan view of the LSTF is given in Figure 4.27.
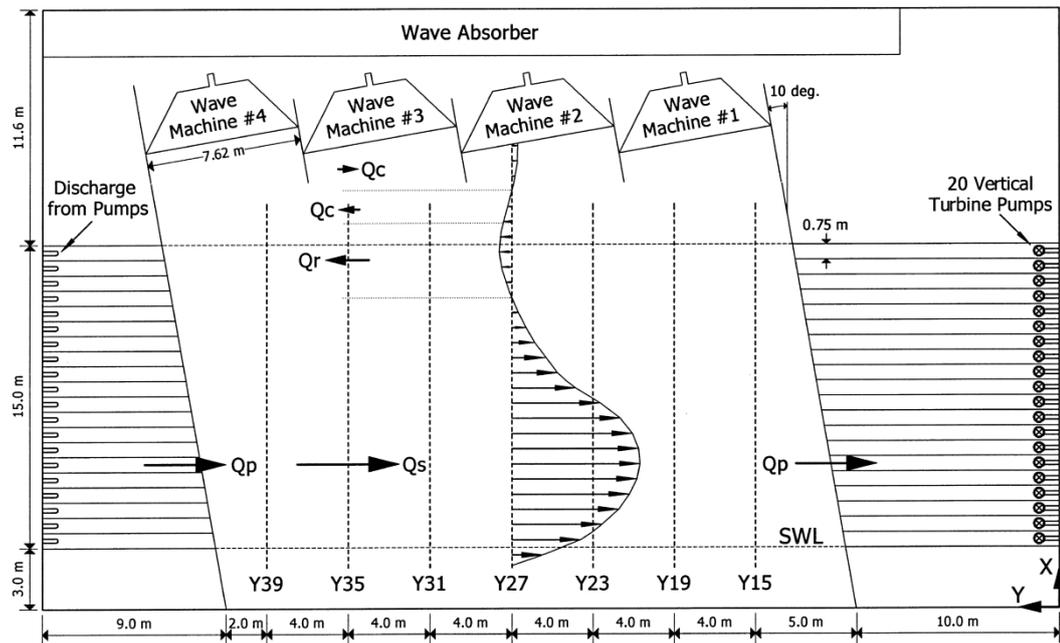
Figure 4.27 The plan view of the LSTF and a conceptual diagram of longshore flow conditions (Hamilton and Ebersole, 2001)

In the experiments, the uni-directional random waves are generated with four piston type wave makers making 10 degrees to the beach. The concrete beach had a uniform slope of 1:30. In the experiments, significant wave heights, longshore current velocities

and the mean water elevations were measured across the bathymetry at several locations alongshore to evaluate the uniformity of flow and wave conditions. The wave and current measurements were carried out with ten capacitance-type wave gauges and ten acoustic-doppler velocitimeters (ADV) co-located in a cross-shore array on the instrumentation bridge at the sections as Y15-Y39 given in Figure 4.27. They have also put wave gauges in front of wave pistons. The mean water elevations were obtained from the time series recorded by the wave gauges. The ADV's were set at elevations approximately one third of the water depth above the bed which is near the elevation of depth-averaged current velocity if a logarithmic velocity profile is assumed to take place. For the unidirectional random waves, a TMA spectrum was used to define the frequency spectrum with a spectral width parameter of γ=3.3. The experiment conditions are summarized in Table 4.3 and Table 4.10.

Table 4.10 Summary of incident wave conditions of TEST-8E (Hamilton and Ebersole, 2001)

Test No	Offshore Water Depth, h (m)	Offshore Mean Approach Angle, $\bar{\theta}$ (deg)	Offshore Sig. Wave Height, H_s (m)	Peak Wave Period, T_p (sec)	Deep Water Sig. Wave Height, $H_{s,0}$ (m)	Sig. Wave Period, T_s (sec)	Deep Water Sig. Wave Steepness, s_{os}	Breaker Index, $\gamma_{br,N90}$
TEST-8E	0.67	10	**0.225**	**2.500**	**0.233**	2.38	0.026	0.69

$s_{os}=H_{s,0}/1.56\cdot T_s^2$
$T_s=T_p/1.05$

The computations are carried out for two different breaker index values, which are 0.78 and $\gamma_{br,N90}$. For the computational parameters (bottom friction and energy transfer coefficients and eddy viscosity constant) used in the circulation model, the values given in Goda (2010) are used which are previously listed in Table 4.4. The computed and measured wave heights, mean water elevations and longshore current velocities are given in Figure 4.28. The data used in the comparisons is the average of the measured data at the sections Y19-Y35. The computed wave heights with the two-dimensional wave transformation model are denoted by 'NSW' and the computed mean water elevations and longshore current velocities with the two-dimensional depth-averaged nearshore circulation model are denoted by 'NSC'.
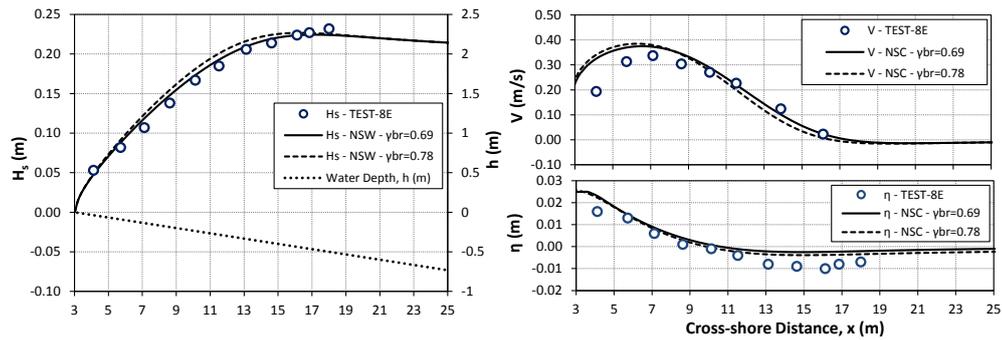
Figure 4.28 The measured and computed significant wave heights (H_s), mean water elevations ($\overline{\eta}$) and longshore current velocities (V) for the TEST-8E experiment (Hamilton and Ebersole, 2001)

Figure 4.28 shows that the computed results are in agreement with the measured data and the accuracy of estimation for $\bar{\eta}$ and V increases as the wave heights and mean approach angles in the surf zone are predicted well with the selection of an appropriate breaker index parameter considering the deep water wave steepness ratio and the bottom slope.

4.2.7. Tang et al. (2008) Experiments

Tang et al. (2008) studied the propagation of random waves and wave-induced nearshore currents both numerically and physically. The authors developed a wave transformation model based on parabolic mild-slope equation and a two-dimensional depth-averaged nearshore circulation model. They have compared the numerical models with the measurements of laboratory experiments conducted at a 55 m long and 34 m wide wave basin as shown in Figure 4.29. The experiment conditions are summarized in Table 4.3 and Table 4.10. In the experiments, the uni-directional random waves are generated with a wave generator making 30 degrees to the beach. In the experiments, significant wave heights, longshore current velocities and the mean water elevations were measured across the bathymetry at several locations. The mean water elevations were obtained from the time series recorded by the wave gauges. The ADV's were set at elevations approximately one third of the water depth above the bed (Tang, 2011). For the uni-directional random waves, JONSWAP spectrum was used to define the frequency spectrum. The experiment conditions are summarized in Table 4.3 and Table 4.11.
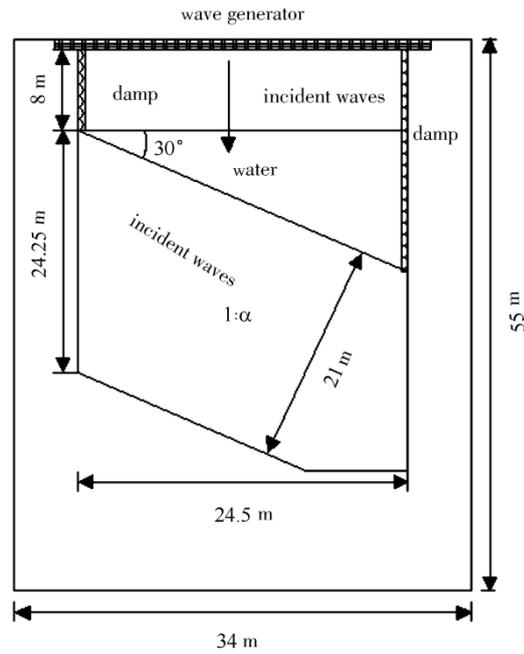
Figure 4.29 The plan view of the wave basin (Tang et al., 2008)

Table 4.11 Summary of incident wave conditions for Tang et al. (2008) Experiments

Test No	Offshore Water Depth, h (m)	Offshore Mean Approach Angle, $\bar{\theta}$ (deg)	Offshore Significant Wave Height, H_s (m)	Deep Water Significant Wave Height, $H_{s,0}$ (m)	Peak Wave Period, T_p (sec)	Sig. Wave Period, T_p (sec)	Deep Water Sig. Wave Steepness, s_{os}	Breaker Index, $\gamma_{br,N90}$
Case-1	0.45	**30**	**0.050**	0.061	2.10	**2.00**	0.010	0.51
Case-2	0.18	**30**	**0.030**	0.035	1.05	**1.00**	0.022	0.64

$s_{os}=H_s/1.56 \cdot T_s^{2}$
$T_s=T_p/1.05$

The computations are carried out for two different breaker index values, for each case, such that γ_{br}=0.78, γ_{br}=0.51 and $\gamma_{br,N90}$=0.64 for Case-1 and Case-2, respectively. For the computational parameters (bottom friction and energy transfer coefficients and eddy viscosity constant) used in the circulation model, the values given in Tang et al. (2008) are used which are previously listed in Table 4.4. The computed and measured wave heights, mean water elevations and longshore current velocities for Case-1 and Case-2 are given in Figure 4.30 and Figure 4.31. The computed wave heights with the two-dimensional wave transformation model are denoted by 'NSW' and the computed mean water elevations and longshore current velocities with the two-dimensional depth-averaged nearshore circulation model are denoted by 'NSC'.
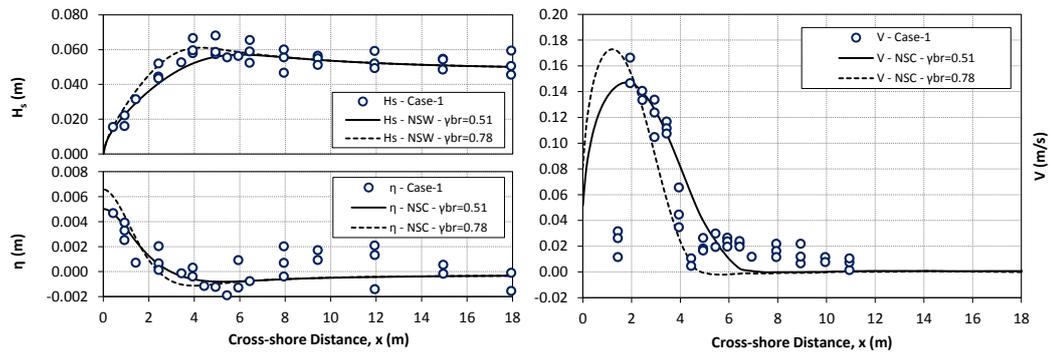
Figure 4.30 The measured and computed significant wave heights (H_s), mean water elevations ($\overline{\eta}$) and longshore current velocities (V) for Case-1 (Tang et al., 2008)
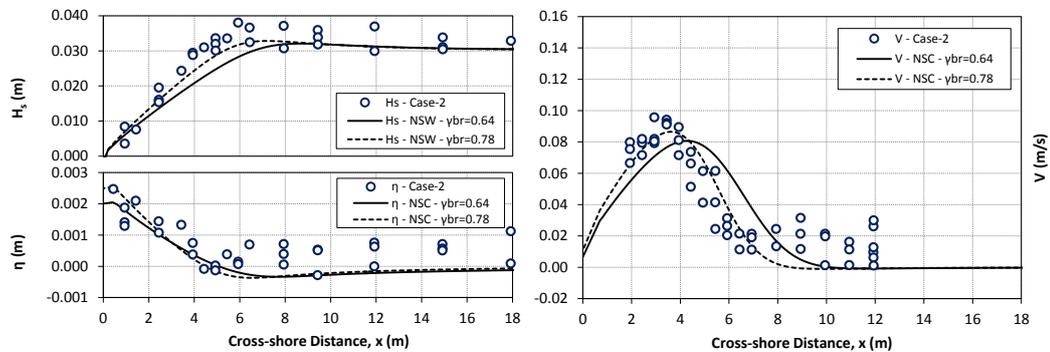
Figure 4.31 The measured and computed significant wave heights (H_s), mean water elevations ($\overline{\eta}$) and longshore current velocities (V) for Case-2 (Tang et al., 2008)

Figure 4.30 and Figure 4.31 show that the computed results are in agreement with the measured data and the accuracy of estimation for $\overline{\eta}$ and V increases as the wave heights and mean approach angles in the surf zone are predicted better with the selection of an appropriate breaker index parameter considering the deep water wave steepness ratio and the bottom slope. On the contrary to the Hamilton and Ebersole (2001) experiment, the computed H_s, $\overline{\eta}$ and V using the default value of breaker index (0.78) represent the nearshore wave and current conditions more accurately.

4.2.8. Reniers and Battjes (1997) Experiment: SO014

Reniers and Battjes (1997) conducted laboratory experiments on wave-induced longshore currents on both barred and non-barred beaches with uni-directional obliquely incident random waves in a directional wave basin, approximately 25 m wide

94

and 40 m long as shown in Figure 4.32. The experiment conditions are summarized in Table 4.3 and Table 4.10.
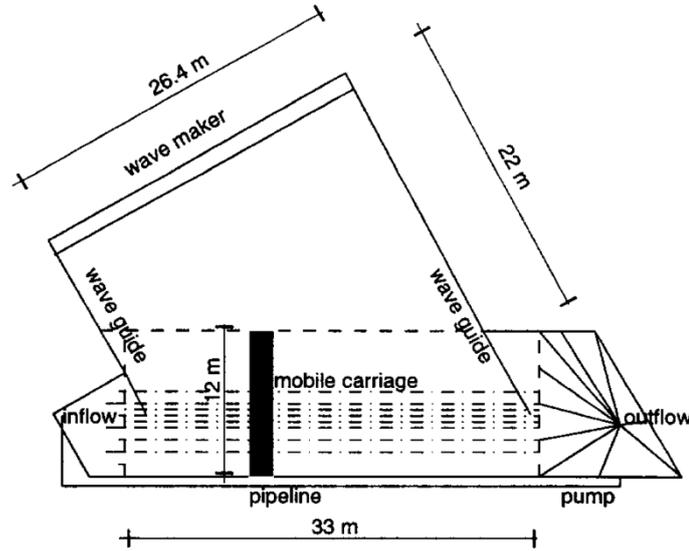
Figure 4.32 The plan view of the wave basin (Reniers and Battjes, 1997)

Table 4.12 Summary of incident wave conditions of SO014 (Reniers and Battjes, 1997)

Test No	Offshore Water Depth, h (m)	Offshore Mean Approach Angle, $\bar{\theta}$ (deg)	Offshore RMS Wave Height, H_{rms} (m)	Peak Wave Period, T_p (sec)	Deep Water Sig. Wave Height, $H_{s,0}$ (m)	Sig. Wave Period, T_s (sec)	Deep Water Sig. Wave Steepness, s_{os}	Breaker Index, $\gamma_{br,N90}$
SO014	0.55	30	0.07	1.200	0.108	1.14	0.053	0.84

$s_{os}=H_s/1.56{\cdot}T_s^2$
$T_s=T_p/1.05$
$H_s=H_{rms}{\cdot}\sqrt{2}$

In the experiments, the uni-directional random waves are generated with multi-flap wave maker making 30 degrees to the beach. The measurements used in the comparison (SO014) with the wave and circulation models were performed on a barred concrete slope with a 1:20 slope offshore on which a Gaussian bar profile with a crest height of about 0.1 m was superimposed, resulting in a slope of approximately 1/8 on the seaward side of the bar (Reniers and Battjes, 1997). In the experiments, wave heights, longshore current velocities and the mean water elevations were measured across the bathymetry at several locations alongshore. The alongshore uniformity of flow conditions were obtained by a pump recirculation system (Visser, 1980). The wave and current measurements were carried out at five different cross-sections with ten

resistance-type wave gauges and eight electromagnetic flow meters (EMF) co-located on a mobile carriage. The mean water elevations were obtained from the time series recorded by the wave gauges. The current velocity measurements are held at elevations approximately one third of the water depth above the bed.

The computations are carried out for two different values of breaker index, γ_{br}=0.78 and $\gamma_{br,N90}$=0.84. For the computational parameters (bottom friction and energy transfer coefficients and eddy viscosity constant) used in the circulation model, the values given in Goda (2006) are used which are previously listed in Table 4.4. The computed and measured wave heights, mean water elevations and longshore current velocities for the experiment SO014 are given in Figure 4.33. The computed wave heights with the two-dimensional wave transformation model are denoted by 'NSW' and the computed mean water elevations and longshore current velocities with the two-dimensional depth-averaged nearshore circulation model are denoted by 'NSC'.
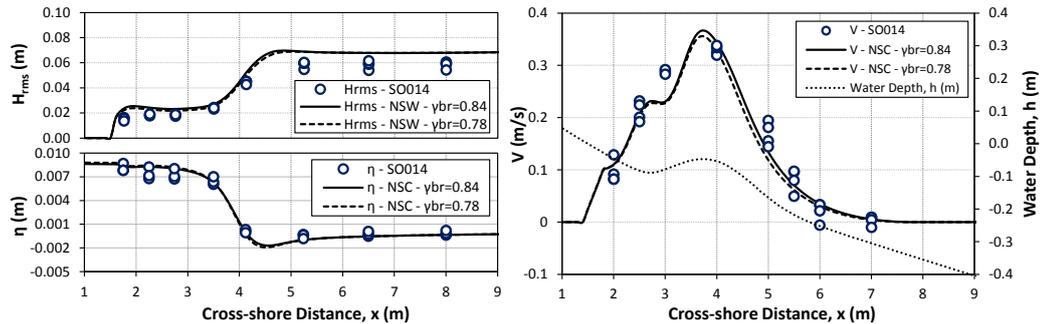
Figure 4.33 The measured and computed root-mean-square wave heights (H_{rms}), mean water elevations ($\bar{\eta}$) and longshore current velocities (V) for SO014 (Reniers and Battjes, 1997)

Figure 4.33 shows that the computed results are in agreement with the measured data and the accuracy of estimation for $\bar{\eta}$ and V increases as the wave heights and mean approach angles in the surf zone are predicted well with the selection of an appropriate breaker index parameter considering the deep water wave steepness ratio and the bottom slope. Similar to the Tang et al. (2008) experiments, the computed H_{rms}, $\bar{\eta}$ and V values using the default value of breaker index (0.78) represent the nearshore wave and current conditions more accurately.

4.2.9. LSTF Movable Bed Experiments: Wang et al. (2002a) and Gravens and Wang (2007)

Wang et al. (2002a) and Gravens and Wang (2007) conducted series of physical model experiments at the LSTF at CERC to generate data sets for testing and validation of sediment transport formulas in the presence of waves and currents. The experiments were carried on movable bed with well-sorted quartz sand having a median grain size (d_{50}) of 0.15 mm for various flow and wave conditions. The beach profile was constructed based on the equilibrium profile of the incident wave conditions and sediment properties. In this study, the measurements of the Test1-Case1, Test3-Case1, Test5-Case1 and Test6 from Wang et al. (2002a) and Test-BC1 from Graven and Wang (2007) are used. The data sets of Wang et al.'s (2002a) experiments are obtained from the website of Coastal and Hydraulics Laboratory of U.S. Army Corps of Engineers (URL-1) and Smith (2006). The data set for the Test-BC1 experiment is kindly provided by Marc B. Gravens (2011). The alongshore locations of measurements are slightly different than the Hamilton and Ebersole (2001) and are shown in Figure 4.34.
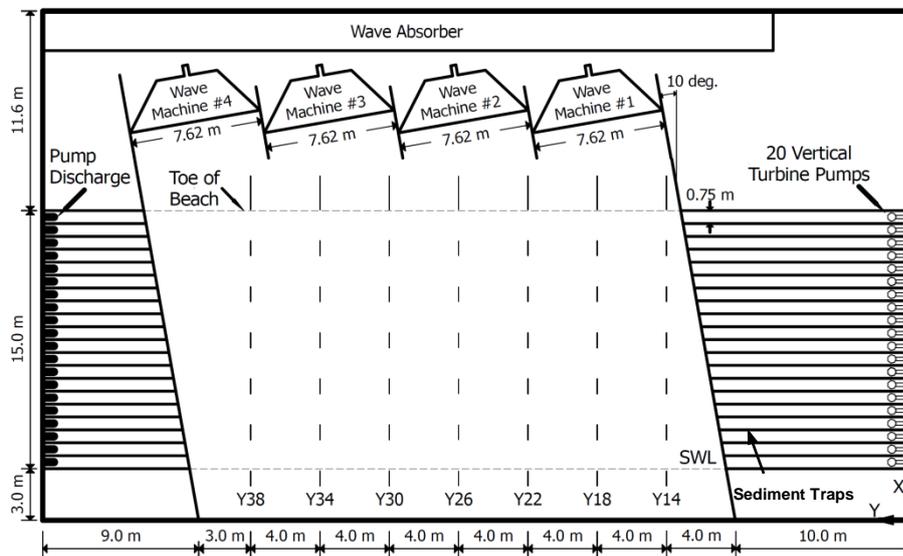
Figure 4.34 The plan view of the LSTF and alongshore locations of measurements (Wang et al., 2002a; Gravens and Wang, 2007)

During the experiments, nearshore wave heights, longshore current velocities, the mean water elevations and the total longshore sediment fluxes were measured across the bathymetry at several alongshore locations (from Y14 to Y38) with the capacitance-type

wave gauges, acoustic-doppler velocitimeters (ADV), fiber optical backscatter (FOBS) sensors co-located in a cross-shore array on the instrumentation bridge and the sediment traps at the downstream of the basin. In selected experiments, no external longshore current is applied to wave conditions and only the wave-induced longshore currents are generated and measured. The mean water elevations were obtained from the time series recorded by the wave gauges. The ADV's were set at elevations approximately one third of the water depth above the bed. In the experiments, the cross-shore distribution of total longshore sediment fluxes are also measured with the use of sediment traps at the downstream end of the beach. The mean approach angles in front of wave pistons (offshore) for all experiments are given as 10°. The data used in the comparisons is the average of the measured data between the sections Y14-Y38. The experiment conditions, the water depths and the incident wave conditions in front of the wave pistons are summarized in Table 4.3, Table 4.13 and Table 4.13.

Table 4.13 Summary of incident wave conditions of the selected LSTF Movable Bed Experiments

Test No	Offshore Water Depth, h (m)	Offshore Sig. Wave Height, H_s (m)	Peak Wave Period, T_p (sec)	Deep Water Sig. Wave Height, $H_{s,0}$ (m)	Sig. Wave Period, T_s (sec)	Deep Water Sig. Wave Steepness, s_{os}
T1-C1	0.9	**0.25**	**1.5**	0.293	1.435	0.091
T3-C1	0.9	**0.27**	**3.0**	0.262	2.517	0.027
T5-C1	0.9	**0.16**	**1.5**	0.172	1.412	0.055
T6	0.9	**0.19**	**3.0**	0.194	2.727	0.017
TEST-BC1	0.67	**0.225**	**1.459**	0.243	1.39[*]	0.081

[*]: $T_s=T_p/1.05$
$s_{os}=H_s/1.56 \cdot T_s^2$

Table 4.14 Summary of breaking conditions and breaker index values of the selected LSTF Movable Bed Experiments

Test No	Breaker Type	Sig. Breaking Wave Height, $H_{s,b}$ (m)	Breaker Index, γ_{br} (best-fit)	Breaker Index, $\gamma_{br,N90}$
T1-C1	Spilling	0.26	0.78	0.928
T3-C1	Plunging	0.27	0.62	0.620
T5-C1	Spilling	0.18	0.78	0.847
T6	Plunging	0.21	0.50	0.565
TEST-BC1	Spilling	0.26	0.78	0.914

The NSW model computations are carried out for different breaker index values, which are 0.78, $\gamma_{br,N90}$ and the best fitting value of γ_{br}. For the computational parameters

(bottom friction and energy transfer coefficients and eddy viscosity constant) used in the NSC model, the values given in Nam et al. (2009) are used which are previously listed in Table 4.4. The computed and measured H_s, $\bar{\eta}$ and V are given in Figure 4.35 - Figure 4.39. In Figure 4.35 - Figure 4.39, the computed nearshore significant wave heights with the two-dimensional wave transformation model are denoted by 'NSW', the computed mean water elevations and longshore current velocities with the two-dimensional depth-averaged nearshore circulation model are denoted by 'NSC'.
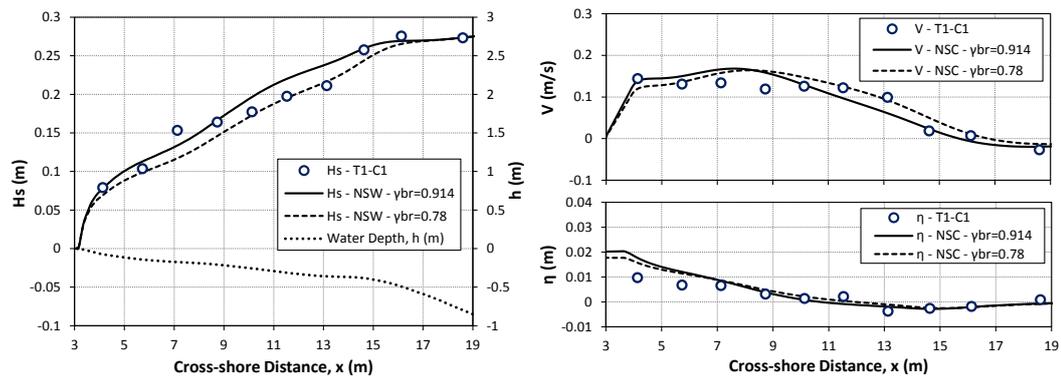
Figure 4.35 The measured and computed significant wave heights (H_s), mean water elevations ($\overline{\eta}$) and longshore current velocities (V) for T1-C1 (Wang et al., 2002a)
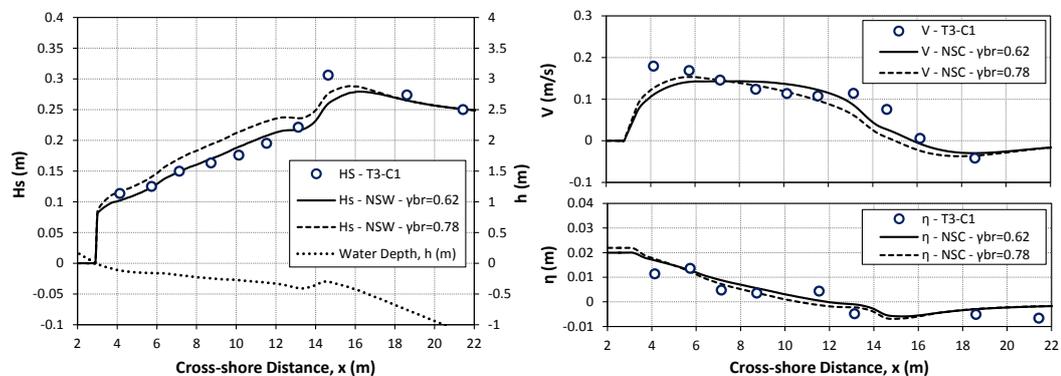
Figure 4.36 The measured and computed significant wave heights (H_s), mean water elevations ($\overline{\eta}$) and longshore current velocities (V) for T3-C1 (Wang et al., 2002a)
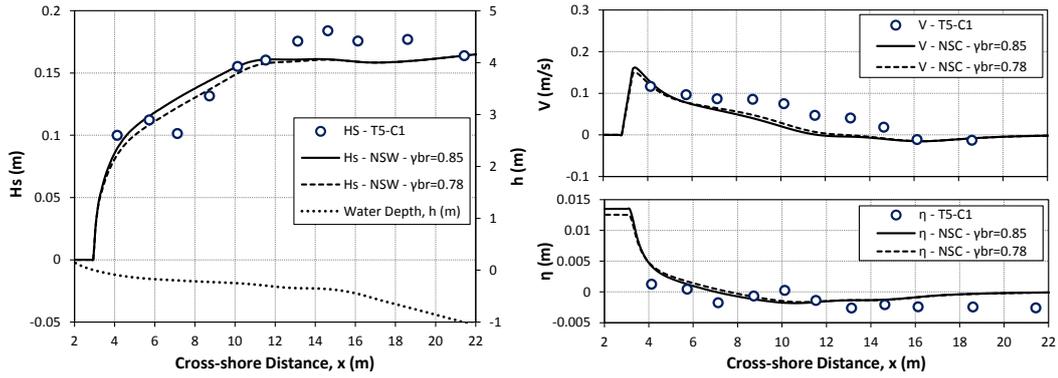
Figure 4.37 The measured and computed significant wave heights (H_s), mean water elevations ($\overline{\eta}$) and longshore current velocities (V) for T5-C1 (Wang et al., 2002a)
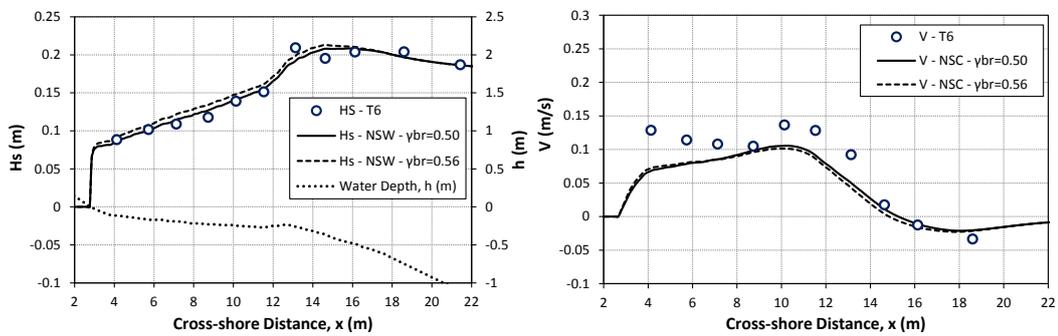
Figure 4.38 The measured and computed significant wave heights (H_s), and longshore current velocities (V) for T6 (Wang et al., 2002a)
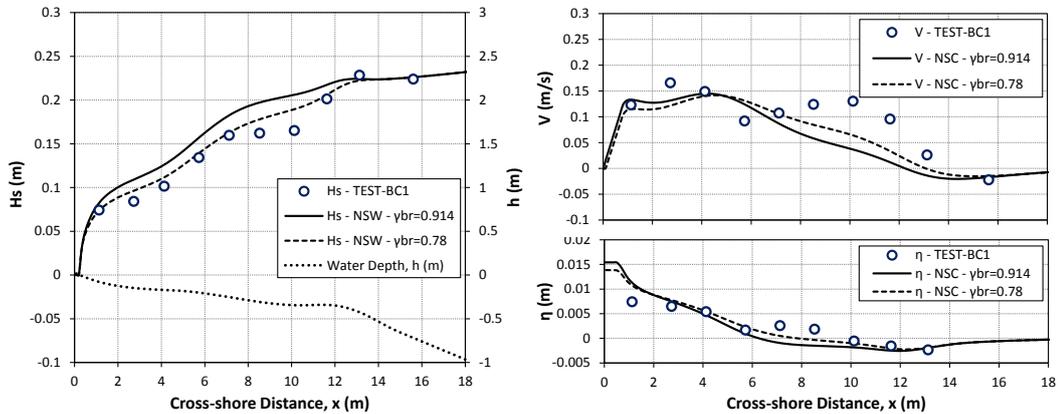

Figure 4.39 The measured and computed significant wave heights (H_s), mean water elevations ($\overline{\eta}$) and longshore current velocities (V) for TEST-BC1 (Gravens and Wang, 2007)

Figure 4.35 - Figure 4.39 shows that the computed results are in agreement with the measured data and the accuracy of estimation for $\overline{\eta}$ and V increases as the wave heights and mean approach angles in the surf zone are predicted better by selecting an

100

appropriate breaker index parameter considering the deep water significant wave steepness for all cases except T3-C1.

For the computation of local total sediment fluxes, the significant or *rms* wave heights, maximum orbital velocities at the bottom, mean approach angles and the rates of dissipation of wave energies due to random wave breaking computed with the NSW model together with the measured current velocities interpolated at the respective positions of the measured sediment transport rates are used. The A coefficient in the Watanabe (1992) formulation is given as 0.5 for regular waves and 2.0 for the random waves. For the LSTF movable bed experiments where the waves are uni-directional random waves, the A is set to be equal to 1.0 (Nam et al., 2009). The computed local total longshore sediment fluxes ($q_{total,y}$) in bulk volumes (m^3/s/m) using the Watanabe (1992), SED1 (ε=0.002) and SED2 ($\varepsilon=\varepsilon_{Ba07}$) approaches for the LSTF movable bed experiments are given in Figure 4.40 - Figure 4.42.
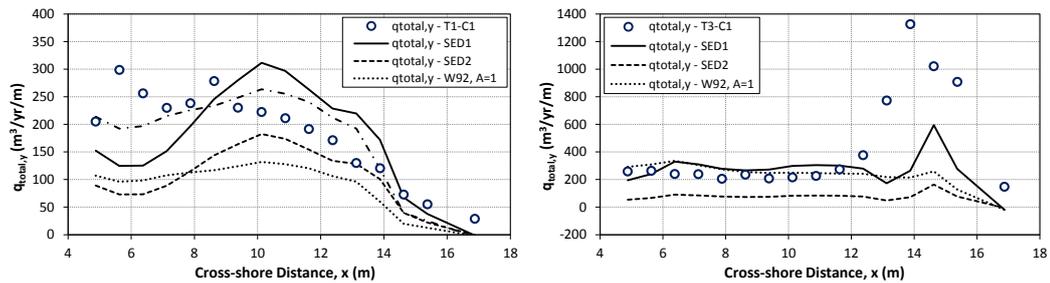
Figure 4.40 The measured and computed local total sediment transport rates (q$_{total,y}$) for T1-BC1 (left) and T3-C1 (right) experiments (Wang et al., 2002a)
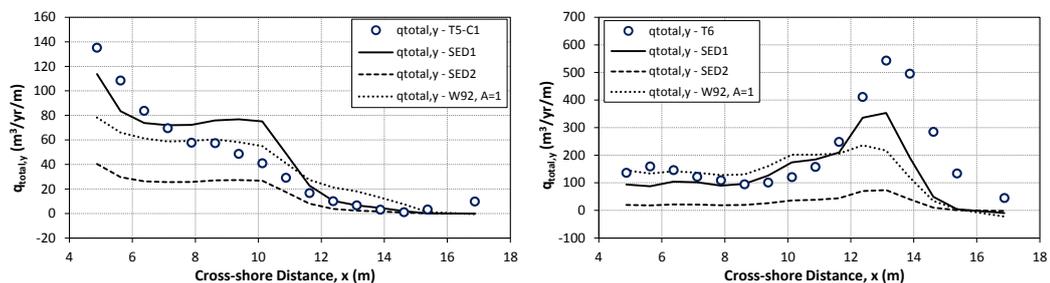
Figure 4.41 The measured and computed local total sediment transport rates (q$_{total,y}$) for T5-BC1 (left) and T6 (right) experiments (Wang et al., 2002a)
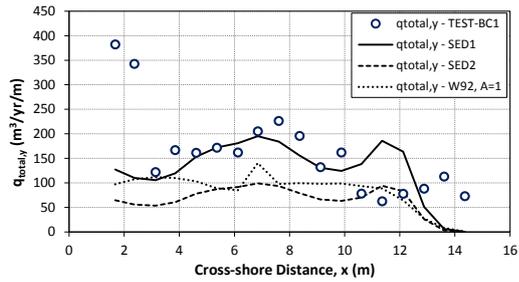
Figure 4.42 The measured and computed local total sediment transport rates ($q_{total,y}$) for for TEST-BC1 (Gravens and Wang, 2007)

As it is seen from Figure 4.40 - Figure 4.42, the predicted flux values with the SED1 approach are in good agreement with the measured data both qualitatively and quantitatively especially for the plunging breaker cases (T3-C1 and T6) up to where the abrupt changes in wave heights are observed close to bar locations due to maximized dissipation rates of breaking waves. The differences between the measured and computed fluxes where the dissipation rates are maximized can be explained by Figure 4.36 and Figure 4.38 which indicate that the dissipation rates of such steep waves are not computed accurately by the NSW model. For the spilling breaker cases (T1-C1, T5-C1 and TEST-BC1), the differences between the measured and computed flux values close to the swash zone (at the shoreline from the limit of wave run-down to the limit of wave run-up) for all approaches might be due to the fact that the increased sediment concentrations and the net transport resulting from onshore-offshore sediment movements in this zone are not fully covered in the applied approaches. Thus, the improvement of the predictive capability of the SED model for the modeling of sediment transport in the swash and inner surf zones should be considered in future studies. The overall quantitative performance of the SED2 approach is observed to be low as the ε parameter used in this approach actually depends on the ratio of mobilizing forces to the resisting forces. The wave conditions in the experiments are less effective to exceed the critical stresses to mobilize the sediment grains used in the experiments which is also noted as a scale effect by Smith (2006) in the LSTF experiments.

The computed sediment flux values with the Watanabe formulation is also in agreement with the measured values qualitatively except for the cross-shore locations where the dissipation rates of breaking waves are maximized (T3-C1 and T6) even with higher discrepancy compared to SED1 results.

To investigate the relation between the measured transport rates and the computed $D_b \cdot v/(\rho_s-\rho)/(1-p)/w_s$ values, the measured transport rates are plotted against the computed $D_b \cdot v/(\rho_s-\rho)/(1-p)/w_s$ values and using the least squares approach, the slope of the best fitting line (y=mx) for the data gives the ε parameter to be equal to 0.0026 (Figure 4.43). Predicted flux values with the Watanabe (1992), SED1 and SED2 approaches are plotted against the measured flux values in Figure 4.44 - Figure 4.46.
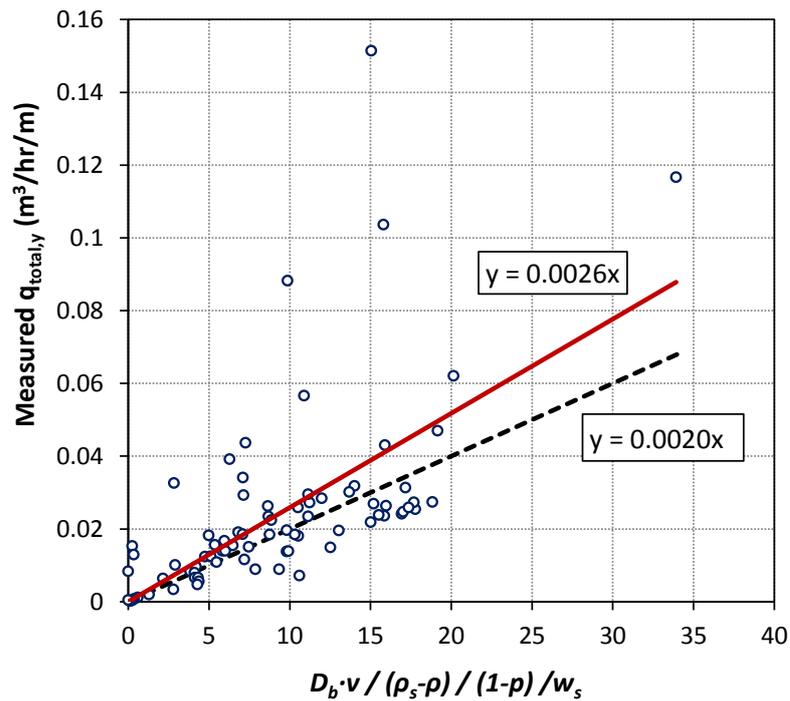
Figure 4.43 Measured flux values are plotted against $D_b \cdot v/(\rho_s-\rho)/(1-p)/w_s$ values for LSTF Movable Bed Experiments (Gravens and Wang, 2007 and Wang et al., 2002a)
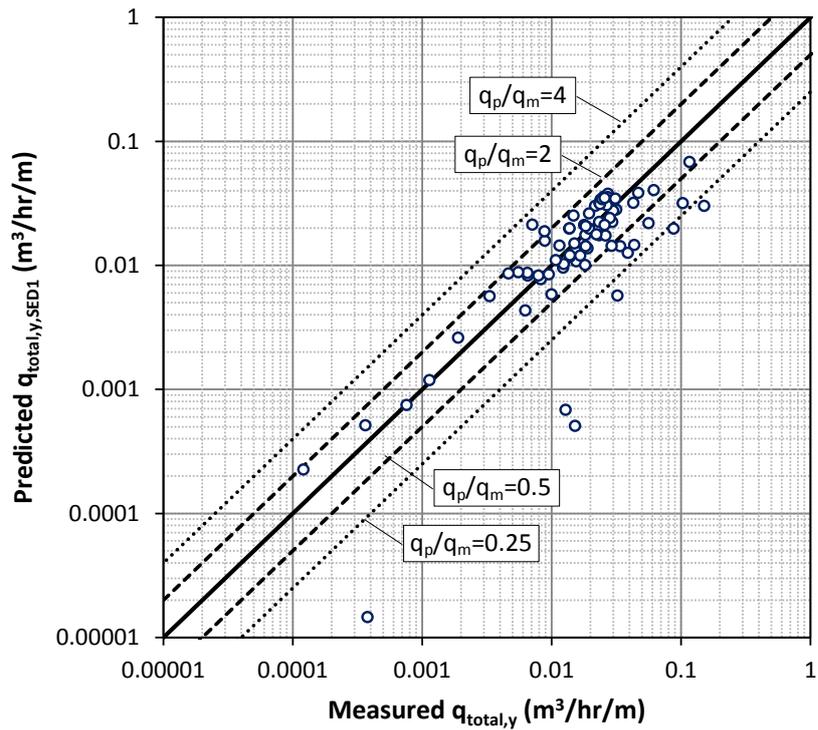
Figure 4.44 Measured transport rates versus predicted by the proposed approach ($\varepsilon=0.002$) for LSTF Movable Bed Experiments (Gravens and Wang, 2007 and Wang et al., 2002a)
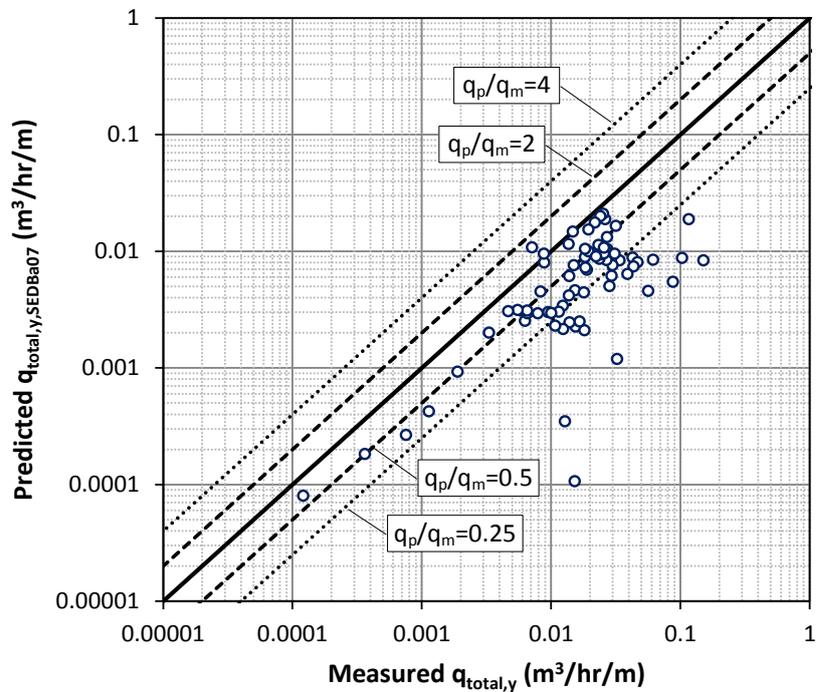
Figure 4.45 Measured transport rates versus predicted by the proposed approach ($\varepsilon=\varepsilon_{Ba07}$) for LSTF Movable Bed Experiments (Gravens and Wang, 2007 and Wang et al., 2002a)
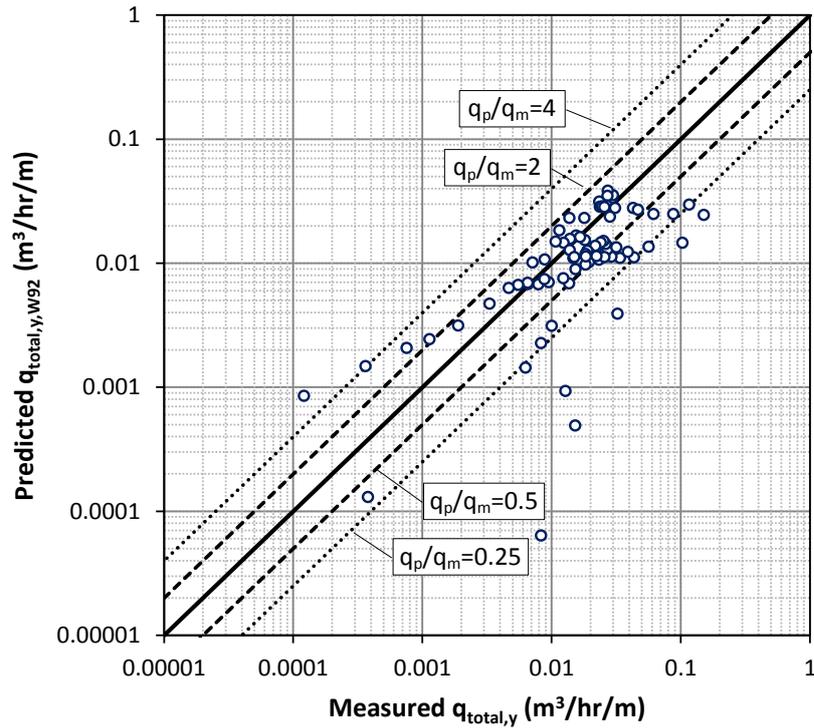
Figure 4.46 Measured transport rates versus predicted by the Watanabe (1992) approach (A=1.0) for LSTF Movable Bed Experiments (Gravens and Wang, 2007 and Wang et al., 2002a)

Quantitative and qualitative comparisons are made through computing the mean absolute percent error (E_{mean}), scatter (σ_{rms}) and the percent discrepancy ratios which gives the percentage of the number of data points outlying the limits of 0.5-2.0, 0.25-4.0 and 0.2-5.0 of the measured flux values (Table 4.15). The mean absolute error and the scatterness (as given in Bayram et al. 2007) are computed with the below given equations respectively where N is the number of data used.

$$E_{mean} = 100 \cdot \overline{\left[\frac{\left| q_{total,y,measured} - q_{total,y,predicted} \right|}{q_{total,y,measured}} \right]}$$

(4.9)

$$\sigma_{rms} = \left[\frac{\sum \left[log(q_{total,y,measured}) - log(q_{total,y,predicted}) \right]^2}{N-1} \right]^{1/2}$$

(4.10)

105

Table 4.15 Summary of accuracy of the formulas for the LSTF Movable Bed Experiments
(Gravens and Wang, 2007 and Wang et al., 2002a)

Formula	Mean Absolute Percent Error, E_{mean} (%)	Scatter, σ_{rms}	Discrepancy Ratio (%)		
			1/2 - 2.0	1/4 - 4.0	1/5 – 5.0
SED1 (ε=0.002)	39.5	0.49	19.2	9.0	7.7
SED2 (ε=ε_{Ba07})	62.6	0.77	75.6	32.1	25.6
Watanabe (1992) (A=1.0)	56.0	0.47	35.9	12.8	9.0

As it is seen from Table 4.15, the SED1 has the smallest mean absolute error and discrepancy ratio such that 80% (1-Disc.Ratio) of the predicted data lies within a factor of 0.5-2.0 of the measured values, yet, it has a 40% mean absolute error which may be decreased with further calibration through measurements carried out for a particular site under consideration. Watanabe (1992) approach shows similar scatter with the SED1 and has the mean a similar high mean absolute percent error of 56% which might be decreased further with the adjustment of the coefficient A. As it is seen from the mean absolute errors and the discrepancy ratios, there exists a high uncertainty in predicting the sediment transport rates, which is a commonly known fact that almost any type of sediment transport formulas as all of them depend on calibrating an approach with the available data set. The A coefficient given in the Watanabe (1992) formulation is an example for this uncertainty as it may have 0.5 for regular waves and 2.0 for random waves. As another typical example to this uncertainty, the K coefficient in the CERC formula is given 0.39 in SPM (1984) based on field study of Komar and Inman (1970) whereas Schoonees and Theron (1993, 1996) gives the K equal to 0.2 based on the most reliable field measurements, and Miller (1998) indicates the value of K might be higher than 0.39 for storm conditions. Furthermore, Smith et al. (2004) compares the measured total longshore sediment transport rates of Wang et al. (2002) experiments with the CERC (1984) formula and states that the CERC formula overestimates the transport rates by a factor up to 8 for K=0.39 and by a factor of up to 4 using the method of Bailard (1981, 1984) which computes the K value as a function of breaker angle and the ratio of velocity magnitude to sediment fall speed.

4.2.10. LSTF Experiments on Morphology Changes around Headland Structures: Test1-Case1, Gravens and Wang (2007)

Gravens and Wang, (2007) carried out series of experiments in the LSTF basin at CERC to generate data sets to be used in the validation of predictive numerical models for the morphology changes around headland type structures (T-head groin and offshore breakwater). The experiments were carried on movable bed with well-sorted quartz sand having a median grain size (d_{50}) of 0.15 mm. In this study, the measurements of the first case (Case1) of the second series of experiments (Test1) are used. Test1 experiment is composed of eight separate runs of approximately 190 min each on a natural beach with a 4-m-long impermeable rubble-mound breakwater with a 0.3 m height from still water level centrally located in the alongshore direction of the model beach and positioned 4 m offshore of the initial shoreline (between alongshore position Y=22 m and Y=26 m and at cross-shore position X=7 m, 4 m offshore of the initial shoreline position at X=3 m; Figure 4.47). During Test1-Case1 (a 185 min run), wave and current conditions, and the bottom topography before and after the run were measured at 13 cross-shore transects as shown (alongshore positions 14, 18, 30, 34, and at 1-m intervals between alongshore position 20 and 28) using the same equipment as in the Test-BC1 experiment where no structures exists. The data set for the Test1-Case1 experiment is kindly provided by Marc B. Gravens (2011).

The experimental wave conditions for the Test1-Case1 are given same with Test-BC1 (Gravens and Wang, 2007) as given in Table 4.13. The significant wave height measured in front of the wave pistons is around 0.23 m, the peak period is 1.46 sec, and the wave pistons make an angle of 10° with the shoreline. The breaker index and the controlling parameters are taken as the same with the values used in Test-BC1, given in Table 4.4 and Table 4.14. The measured bathymetries before and after the Test1-Case1 are discretized to a 0.2x0.2 m rectangular grids from Y14 to Y34 and from X=1.6 to X=21.4 where the offshore gauges are located. The diffraction intensity parameter is taken κ=2.5 for the run. The computed and measured significant wave heights are given in Figure 4.48. The computed nearshore current field and the measured average current velocities are given in Figure 4.49. For the computation of the beach evolution after 185 min, Watanabe (1992) total distributed load formulation (A=1) is used. The computed and measured bathymetry after 185 min is given in Figure 4.50.
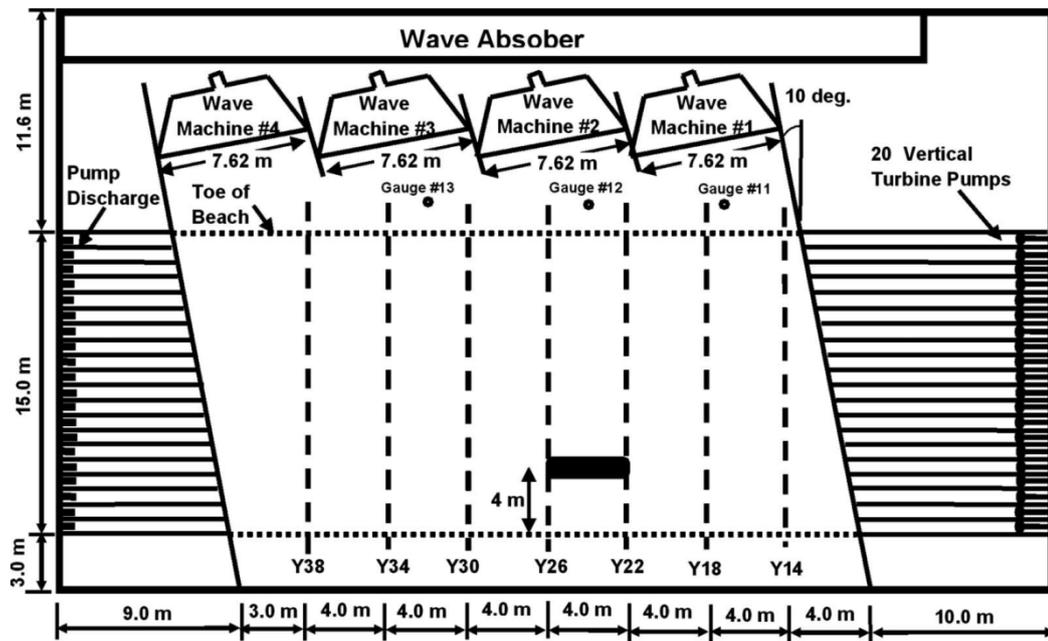
Figure 4.47 The plan view of the LSTF basin and the location of offshore breakwater for Test1-Case1 (Gravens and Wang, 2007)
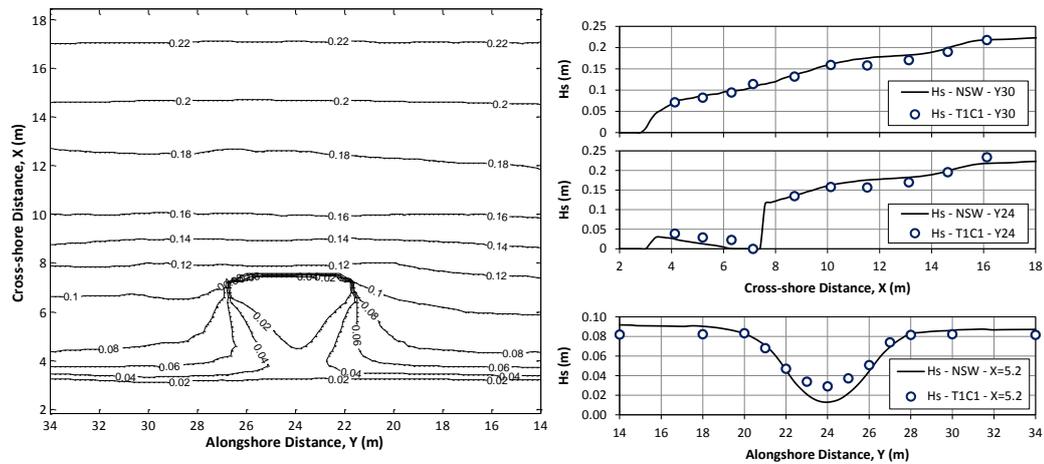
Figure 4.48 The measured (right) and computed (left) significant wave heights (H_s) by the NSW model for Test1-Case1 (Gravens and Wang, 2007)
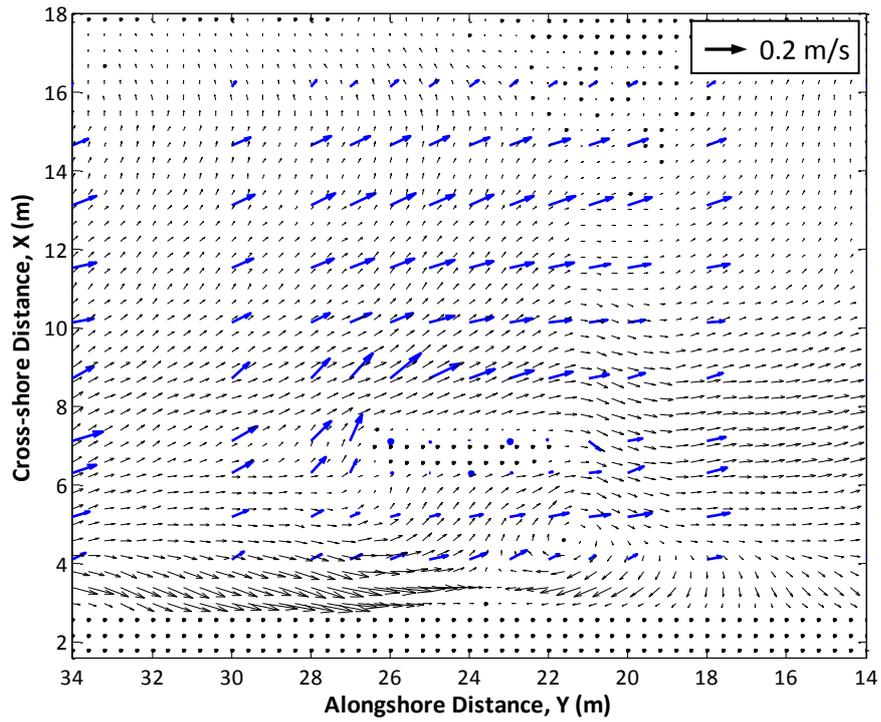
Figure 4.49 The vectorial representation of the measured (blue) and computed (black) nearshore current field (*u* and *v*) by the NSC model for Test1-Case1 (Gravens and Wang, 2007)
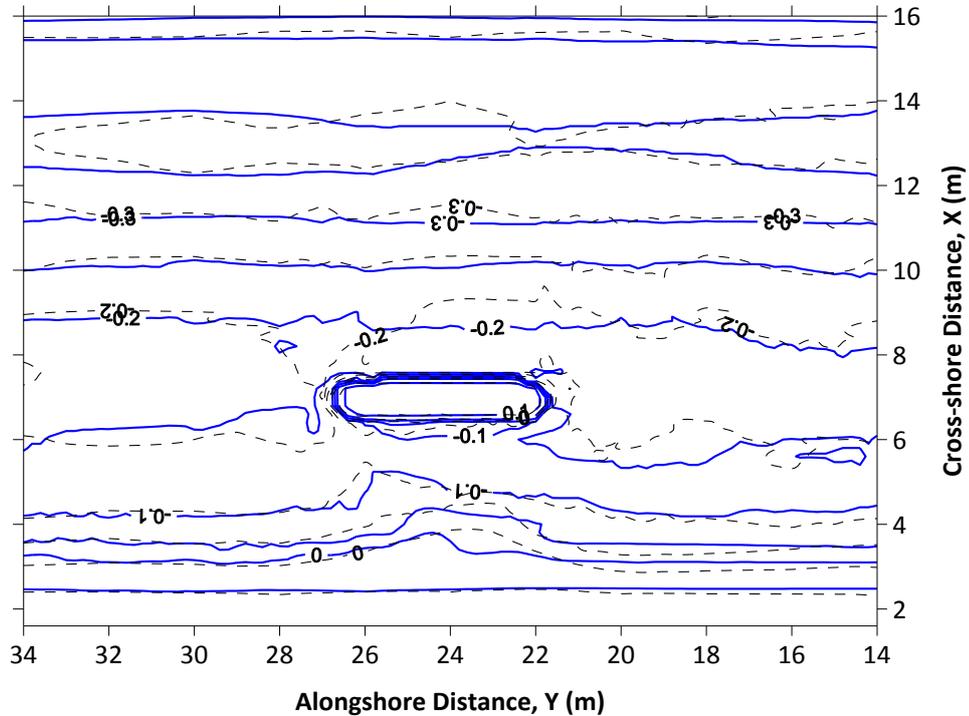
Figure 4.50 The measured (---) and the computed bottom (blue) topography by the COD model after 185 minutes for Test1-Case1 (Gravens and Wang, 2007)

As it is seen from Figure 4.48, the computed significant wave heights are in agreement with the measurements. The wave height contours in the lee of the offshore breakwater has a shift towards the downstream of the basin (Y14) as expected due to the oblique wave approach in the experiment. Figure 4.49 shows that the computed current field is in agreement with the measured current velocities (bold blue arrows) qualitatively. The separation of the flow field at the upstream end of the breakwater (Y26), and the general trend in the current field are represented well in the model result. Besides, the diverted flow at the downstream end of the structure (Y22) slows down and creates a return flow directed to the lee of the structure which might be also expected for such structures. These return flow conditions directed to the lee of the structure or slowed down flows are the governing mechanisms in the formation of salients and tombolos behind headland type structures. At the region from the structure to the offshore boundary the computed current velocities are not in agreement with the measured velocities quantitatively. The computed current velocities decrease at this region similar to the results of comparison of the NSC model with the measured current velocities of the experiment TEST-BC1 (Gravens and Wang, 2007) in Figure 4.39.

The computed current velocities might be improved further by improving the numerical schemes and controlling the friction terms in shallower water depths and around structures where the bottom slope changes rapidly used for the solution of NSWE in the NSC model. As it is seen from Figure 4.50, the computed bottom contour lines by the COD model are in agreement with the measurements qualitatively reflecting the beach evolution pattern behind the offshore breakwater. Progress of shoreline towards the structure with a shift towards upstream and erosion of beach at downstream end, changes in the contour lines of 0.05 and 0.10 m water depths in accordance with the measured bathymetry, the initiation of scour at the upstream end of the breakwater are the prominent results of the EVO model.

4.3. Field Experiments

The third stage in the model benchmarking studies is to test the performance of the three main modules of the two-dimensional depth-averaged beach evolution model; NSW, NSC and SED models are tested with the field measurements available in the

literature (Kuriyama and Ozaki, 1993; Thornton and Kim, 1993; Smith et al., 1993; Miller, 1999).

4.3.1. HORF Experiments (Kuriyama and Ozaki, 1993)

The first data set of field experiments used in the comparisons is the field experiments conducted by Kuriyama and Ozaki (1993) at the Hazaki Oceanographical Research Facility (HORF), at Kashima-nada coast which faces to the Pacific Ocean on March 28 and April 4, 1989. The field measurements are carried along the HORF Pier of 427 m long and 6.9 m above the low water level. The data of bathymetry, nearshore and deep water wave parameters and the longshore current velocities were kindly provided by Prof.Dr. Yoshimi Goda (2009). The controlling parameters used in NSC computations are taken from Goda (2008). The wave measurements were carried out by ultrasonic wave gauges before and after the longshore current measurements. The longshore current velocities were measured 1 m below the water surface with a spherical float having a diameter of 0.2 m. The location of the HORF Pier and the nearshore bathymetry on March 31, 1989 is given in Figure 4.51. The deep water and nearshore wave conditions and the controlling parameters used in the simulations are given in Table 4.16, Table 4.17 and Table 4.18 respectively.

Table 4.16 Offshore Wave Conditions for the HORF Measurements (Kuriyama and Ozaki, 1993)

Date	Mean Bottom Slope, 1/m	Offshore Water Depth, h (m)	Offshore Sig. Wave Height, H_s (m)	Offshore Mean Approach Angle, $\overline{\theta}$ (deg)	Sig. Wave Period, T_s (sec)	Dir. Spread. Par., s_{max}
March 28, 1989	1:59.9	6.1	2.47	25	8.86	40
April 04, 1989	1:59.9	6.1	2.03	10	8.40	45

Table 4.17 Deep Water Wave Conditions for the HORF Measurements (Kuriyama and Ozaki, 1993)

Date	Deep Water Sig. Wave Height, $H_{s,0}$ (m)	Sig. Wave Period, T_s (sec)	Deep Water Mean Approach Angle, $\overline{\theta}$ (deg)	Deep Water Sig. Wave Steepness, s_{os}	Breaker Index, γ_{br}
March 28, 1989	2.68	8.86	47.6	0.022	0.63*
April 04, 1989	2.05	8.40	18.7	0.019	0.53

*: Computed with Nairn's (1990) formula
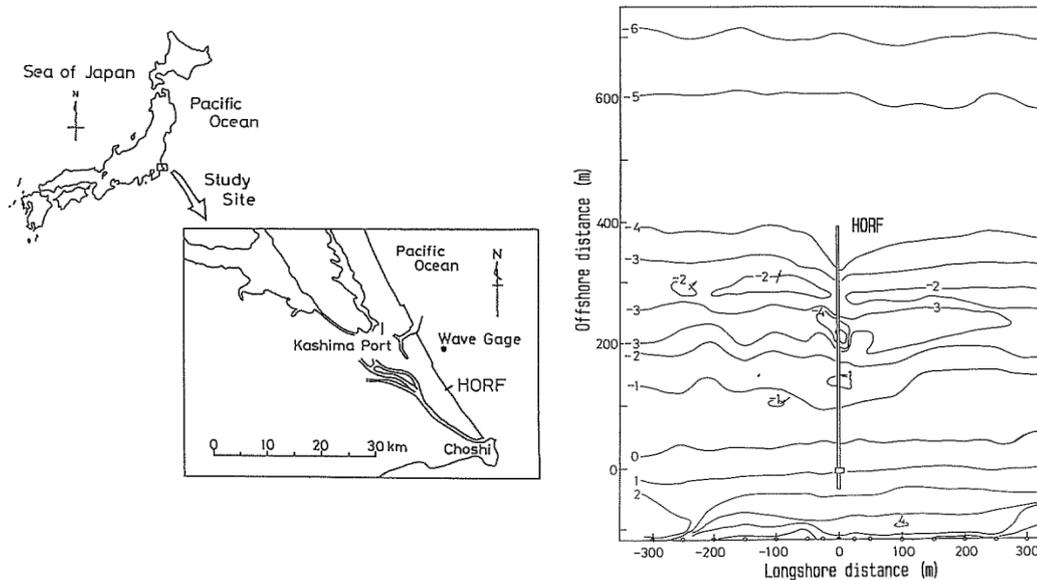
Figure 4.51 Location of HORF Pier (left) and the bathymetry on March 31, 1989 (right) (Kuriyama and Ozaki, 1993)

Table 4.18 Controlling parameters used in the NSW and NSC simulations for the HORF Measurements (Goda, 2008)

Date	Bottom Friction Coefficient, c_f	Energy Transfer Coef., α	Eddy Viscosity Constant, Λ
March 28, 1989	0.0075	0.5	1.0
April 04, 1989	0.0075	0.5	1.0

The computations are carried out for different values of breaker index, γ_{br}=0.78, $\gamma_{br,N90}$ and the best fitting γ_{br}. The computed and measured nearshore significant wave heights and longshore current velocities for the experiments are given in Figure 4.52 and Figure 4.53. The computed wave heights with the two-dimensional wave transformation model are denoted by 'NSW' and the computed longshore current velocities with the two-dimensional depth-averaged nearshore circulation model are denoted by 'NSC'.
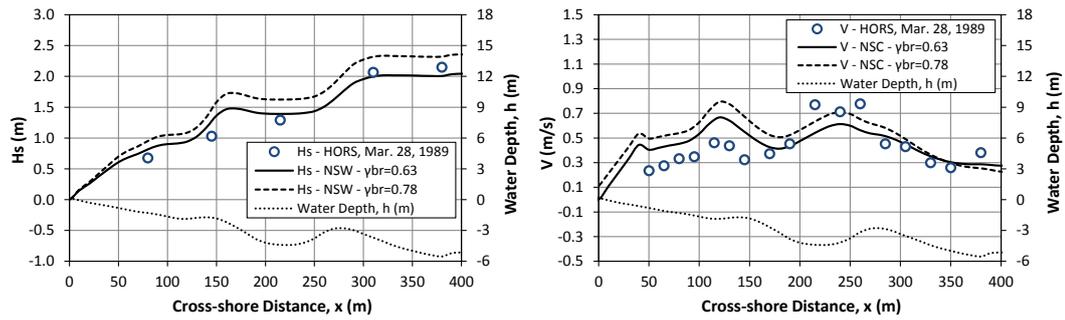
Figure 4.52 The measured and computed significant wave heights (H_s) and longshore current velocities (V) for the HORF March 28, 1989 Measurements (Kuriyama and Ozaki, 1993)
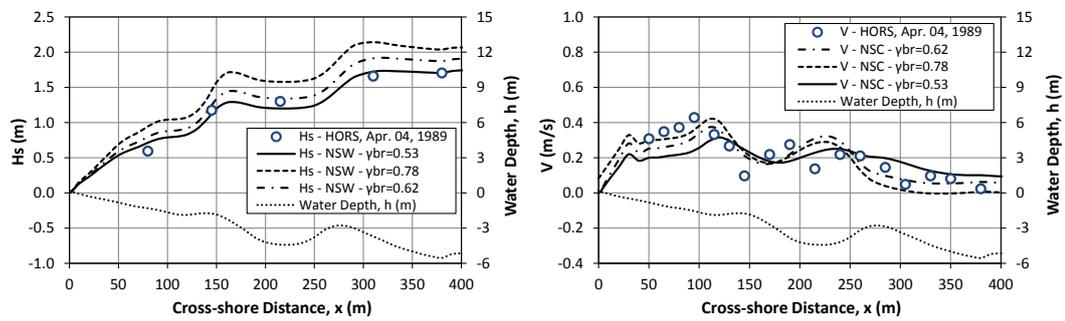
Figure 4.53 The measured and computed significant wave heights (H_s) and longshore current velocities (V) for the HORF April 04, 1989 Measurements (Kuriyama and Ozaki, 1993)

Figure 4.52 and Figure 4.53 shows that the computed results are in agreement with the measured data and the accuracy of estimation for V increases as the wave heights and mean approach angles in the surf zone are predicted better with the selection of an appropriate breaker index parameter between 0.4-0.8 (even higher for steeper beaches) considering the deep water wave steepness (April 04, 1989 measurements) by a trial-error process. As it is seen from above given Figure 4.53, the nearshore wave heights in the surf zone are slightly overestimated for $\gamma_{br}=\gamma_{br,N90}$ as the deep water wave steepness is very small (swell wave conditions) for the given wave conditions.

4.3.2. DELILAH Experiments (Thornton and Kim, 1993; Smith et al., 1993)

The second set of field experiments used in the benchmark studies is the DELILAH (Duck Experiment on Low-frequency and Incident-band Longshore and Across-shore Hydrodynamics) measurements conducted on October 11 and 14, 1990, at the U.S.

Army Engineer Waterways Experiment Station, Coastal Engineering Research Center (USACE), Field Research Facility (FRF) located in Duck, North Carolina, which faces the Atlantic Ocean on a long, sandy, barrier island beach (Figure 4.54). The beach is aligned from north-west to south-east making an angle of 69.7 degrees clockwise with the north direction. The wave climate at the site, dominated by the violent 'nor'easters' (Dolan and Davis, 1992) and the close passage of tropical hurricanes, is noted as one of the most energetic on the U.S. East Coast by Leffler et al. (1996). The tides at the FRF are given as semi-diurnal with a spring range of 1.2 m (Miller, 1999).

The wave measurements were carried out by pressure gauges and the current measurements were carried out by electromagnetic current meters. The nearshore bathymetry was surveyed daily with an amphibious buggy (called as CRAB). The data of bathymetry, nearshore wave heights, deep water wave parameters and the longshore current velocities for the measurements carried on October 11 and 14, 1990 were kindly provided by Prof.Dr. Yoshimi Goda (2009). The location of the FRF Pier and the nearshore bathymetry together with the positions of current meters and wave gauges are given in Figure 4.54. The wave conditions provided by Goda (2009) and the controlling parameters (Goda, 2008) used in the simulations are given in Table 4.16 and Table 4.18.

Table 4.19 Wave Conditions for the DELILAH Measurements (Birkemeier et al., 1997; Goda, 2008)

Date	Mean Bottom Slope, 1/m	Deep Water Sig. Wave Height, H_s (m)	Deep Water Mean Approach Angle, $\overline{\theta}$ (deg)	Peak Wave Period, T_p (sec)	Deep Water Sig. Wave Steepness, s_{os}	Dir. Spread. Par., s_{max}
October 11, 1990	1:75.2	1.55	39	8.60	0.015	50
October 14, 1990	1:75.2	1.15	20	12.0	0.006	100

$T_s=T_p/1.05$
$s_{os}=H_s/1.56 \cdot T_s^2$

Table 4.20 Controlling parameters used in the NSW and NSC simulations for the DELILAH Measurements (Goda, 2008)

Date	Breaker Index, γ_{br} (best fit)	Breaker Index, $\gamma_{br,N90}$	Bottom Friction Coefficient, c_f	Energy Transfer Coef., α	Eddy Viscosity Constant, Λ
October 11, 1990	0.67	0.56	0.005	0.5	1.0
October 14, 1990	0.56	0.46	0.005	0.5	1.0
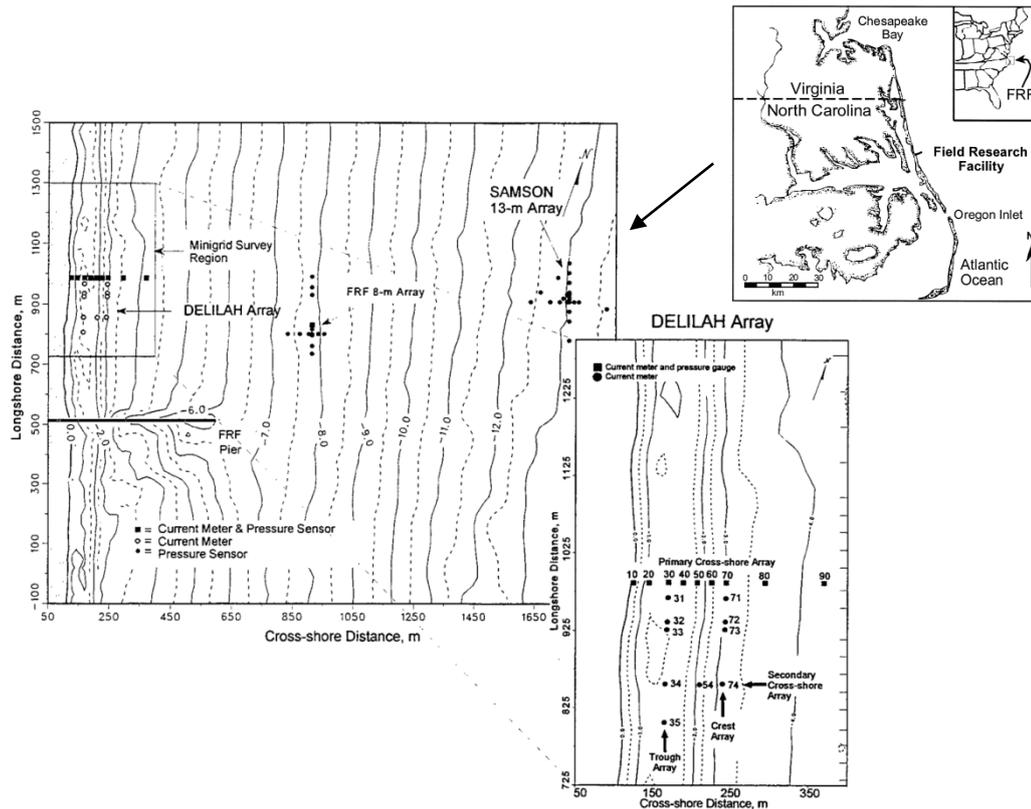
Figure 4.54 Location of Duck Site and FRF, the nearshore bathymetry and the positions of the sensors (Birkemeier et al., 1997; Miller, 1999)

The computations are carried out for different values of breaker index, γ_{br}=0.78, $\gamma_{br,N90}$ and the best fitting γ_{br}. The computed and measured wave heights and longshore current velocities for the experiments are given in Figure 4.55 and Figure 4.56. The computed wave heights with the two-dimensional wave transformation model are denoted by 'NSW' and the computed longshore current velocities with the two-dimensional depth-averaged nearshore circulation model are denoted by 'NSC'.
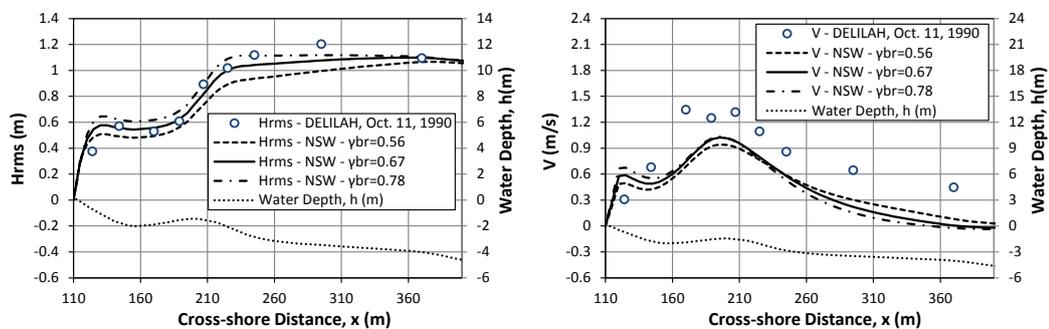
Figure 4.55 The measured and computed significant wave heights (H_s) and longshore current velocities (V) for the DELILAH October 11, 1990 Measurements
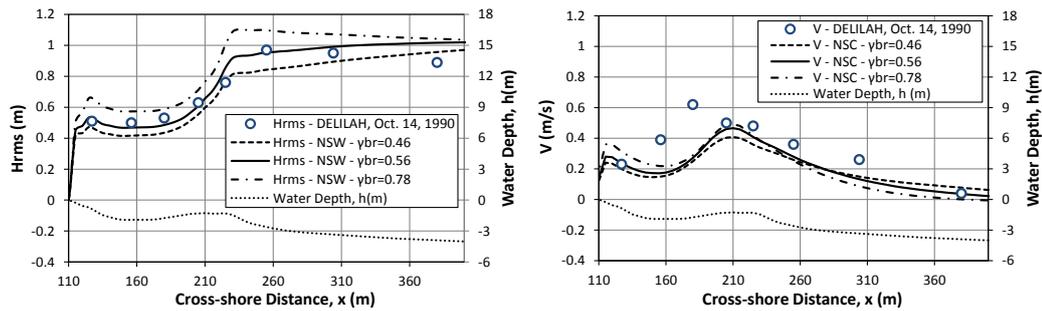
Figure 4.56 The measured and computed significant wave heights (H_s) and longshore current velocities (V) for the DELILAH October 14, 1990 Measurements

Figure 4.55 and Figure 4.56 shows that the computed results are in agreement with the measured data and the accuracy of predicted data increase with the selection of an appropriate breaker index parameter considering the deep water wave steepness for both cases by a trial-error process.

4.3.3. SANDYDUCK Experiments (Miller, 1999)

The SANDYDUCK experiments were conducted at the same location as the DELILAH measurements at the FRF Pier of the USACE, at the Duck site, North Carolina, USA (Miller, 1999) to investigate nearshore sediment transport processes during moderate storm conditions (individual wave heights up to 5 m and spilling breakers). The sediment grain size distribution for the site is given as bimodal with a main component around 0.25 mm and a secondary component near 1.0 mm. In the bar-trough region, sediment grain size distribution is given as uni-modal with a median grain size of 0.17 mm. At the seaward of the bar-trough region, the sediments are well sorted with a median diameter of 0.12 mm (Miller, 1999). The sediment density is given as 2650 kg/m^3, the sea water density is given as 1025 kg/m^3 and the porosity is given as 0.4. The overall bed slope in the surf zone between the shoreline and the 6 m water depth is around 1:73. During the experiments, the bed load and sediment load in the swash zone are not measured, yet, it is likely that the measured transport rates in the sampled zone include most of the transport. Bayram et al. (2001) state that the sediment transport for all SANDYDUCK experiments is in the sheet flow regime (highly concentrated suspended sediment transport) in the surf zone, which occurs under storm conditions.

During the experiments, the wave heights, longshore and cross-shore current velocities and suspended sediment concentrations at various depths along the cross-shore profile 15 m away from the pier pilings and up to 9 m water depth were measured by a vertical array of instruments attached to the lower boom of a track-mounted crane (Sensor Insertion System, SIS; Figure 4.57 and Figure 4.58). To minimize effects of water level variations due to tides, experiments were made within 1.5 hours before and after the high or low tide, whichever occurred during daylight hours. Along the cross-shore profile next to the pier, the wave and water level measurements were carried out by pressure gauges, the current velocity measurements were carried out by electromagnetic current meters (EMCM), the sediment concentrations were measured by the optical backscatter sensors (OBS) where the lowest (bottom) sensor was nominally 3 cm above the bed, within a range of 2-5 cm, and the depths from the measurement array to the bottom are measured by a sonar device. The OBS sensors were calibrated against suspended sediment samples collected during the storms streamer traps mounted on the SIS after the experiments. The measured sediment fluxes were obtained time-averaging the products of instantaneous current and concentration signals of each pairing of EMCM and OBS sensors and integrating through the water column. Turbidity caused by the suspended microscopic organisms and very fine organic and inorganic matter was removed from the concentration signals prior to computation of fluxes.

Figure 4.57 Sensor Insertion System (SIS) on the FRF Pier (URL-2)

Figure 4.58 Vertical array of instruments mounted on the lower boom of SIS (Miller, 1999)

During the experiments, the offshore wave conditions were measured from a (directional) pressure gauge array located at a depth of 8 m (8 m Array; slightly offshore and north of the FRF pier) and approximately at a cross-shore distance of 915 m with respect to FRF coordinate system (Figure 4.54) and a directional waverider 3 km offshore at 17.4 m water depth. The offshore wave conditions based on 8 m Array measurements are given in Table 4.21 (Miller, 1999; van Rijn, 2009; Bayram, 2011, URL-2).

The data of nearshore bathymetry (actual depths from mean water levels), wave heights and parameters, the depth-averaged longshore current velocities and sediment transport rates (in bulk volumes including pores) of the measurements carried on between the dates March 11, 1996 and February 5, 1998 were kindly provided by Prof.Dr. Yoshimi Goda (2009), Prof.Dr. Leo van Rijn (2009) and Atilla Bayram (2011). In the benchmark studies, both the NSW and NSC computations are carried out starting from deep water. The deep water wave conditions resulting the offshore wave conditions (Table 4.21) are given in Table 4.22.

Table 4.21 Offshore wave conditions based on 8 m Array Wave Measurements (Miller, 1999; van Rijn, 2009; Bayram, 2011, URL-2)

Date	Mean Bottom Slope, 1/m	Offshore Sig. Wave Height, H_s (m)	Peak Wave Period, T_p (sec)	Offshore Mean Approach Angle, $\bar{\theta}$ (deg)
March 11, 1996	1:74.8	2.8	7	10
March 27, 1996	1:71.6	1.8	6.7	25
April 2, 1996	1:85.3	1.6	7	26
March 31, 1997*	1:69.7	1.5	7	39
April 1, 1997	1:71.6	2.7	9	18
October 19, 1997	1:73	3	10	20
October 20, 1997*	1:76.8	2.2	11	7
February 4, 1998	1:60.1	3.8	11	20
February 5, 1998*	1:77.2	3.1	12	8

*: Wave parameters for these dates are approximated from the available 8 m Array and 17 m Waverider measurements.

Table 4.22 Deep water wave conditions used in the NSW model simulations

Date	Deep Water Sig. Wave Height, H_s (m)	Deep Water Mean Approach Angle, $\bar{\theta}$ (deg)	Peak Wave Period, T_p (sec)	Deep Water Sig. Wave Steepness, s_{os}	Direc. Spread. Par., s_{max}
March 11, 1996	3.02	16.0	7	0.044	3.8
March 27, 1996	2.42	34.0	6.7	0.038	8.2
April 2, 1996	1.82	37.0	7	0.026	24.2
March 31, 1997	1.7	51.0	7	0.025	26.6
April 1, 1997	3.2	29.5	9	0.028	22.0
October 19, 1997	3.66	33.4	10	0.026	24.7
October 20, 1997	2.16	13.4	11	0.013	57.5
February 4, 1998	3.82	35.0	11	0.022	30.1
February 5, 1998	3.58	17.1	12	0.018	40.1

Note: The directional spreading parameters are found from Figure 3.6 for the respective significant deep water wave steepness values.

The ε parameter used in the SED2 approach depends on the significant breaking height, the peak period and the fall velocity of the sediment grains. For random waves, van Rijn (2004) defines the incipient significant wave breaking height as the significant wave height where the fraction of breaking waves is equal to 5% which in fact corresponds approximately to the wave heights where the dissipation rates and thus the changes in wave heights becomes significant visually. For the experiments listed in Table 4.21, nearshore wave heights are computed by the NSW model for the best fitting breaker index values and the significant breaking wave heights and the corresponding breaker

angles are determined considering the computed nearshore significant wave heights with 5% percent fraction of breaking waves and the measured wave heights. The fall velocity of the sand grains having a 0.17 mm median grain size diameter is computed using the method given by Ahrens (2000) method. The bottom friction and surface roller energy transfer coefficients and eddy viscosity constant are selected as to give the best predictions of the longshore current velocities both qualitatively and quantitatively. The breaker index values, the controlling parameters and the significant breaking heights and the corresponding breaker angles used in the NSW, NSC and SED models are given in Table 4.23.

Table 4.23 The controlling parameters used in the NSW and NSC model simulations

Date	Breaker Index, γ_{br} (best fit)	Breaker Index, $\gamma_{br,N90}$	Bottom Friction Coef., c_f	Eddy Viscosity Constant, Λ	Energy Transfer Coef., α	Sig. Breaking Wave Height, H_s (m)	Mean Breaking Approach Angle, $\overline{\theta}$ (deg)
March 11, 1996	0.60	0.797	0.003	1.0	0.8	2.29	5.3
March 27, 1996	0.60	0.764	0.005	0.5	0.3	2.12	18.2
April 2, 1996	0.69	0.673	0.008	0.8	0.4	1.60	17.5
March 31, 1997	0.64	0.657	0.008	0.8	0.4	1.48	31.2
April 1, 1997	0.72	0.687	0.0035	0.8	0.2	2.71	12.8
October 19, 1997	0.60	0.669	0.0035	1.2	0.8	3.02	15.2
October 20, 1997	0.60	0.536	0.0025	1.1	0.4	2.30	5.6
February 4, 1998	0.62	0.636	0.006	1.2	0.8	3.36	14.3
February 5, 1998	0.45	0.589	0.003	0.5	0.5	2.54	6.8

The NSW computations are carried out for the best fitting breaker index values given in Table 4.23 and the longshore currents are computed using the results of NSW model and for the controlling parameters (c_f, Λ and α) given in Table 4.23. The computed and measured nearshore significant wave heights and longshore current velocities are given in Figure 4.59 - Figure 4.67. The computed wave heights with the two-dimensional wave transformation model are denoted by 'NSW' and the computed longshore current velocities with the two-dimensional depth-averaged nearshore circulation model are denoted by 'NSC' in Figure 4.59 - Figure 4.67.
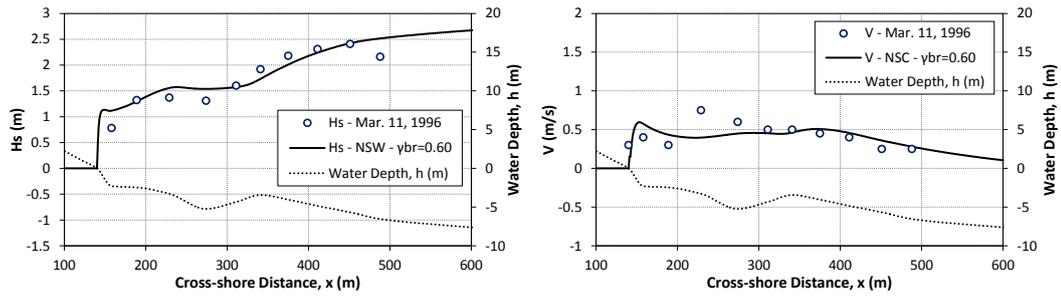
Figure 4.59 The measured and computed significant wave heights (Hs) and longshore current velocities (V) for the SANDYDUCK, March 11, 1996 Experiment
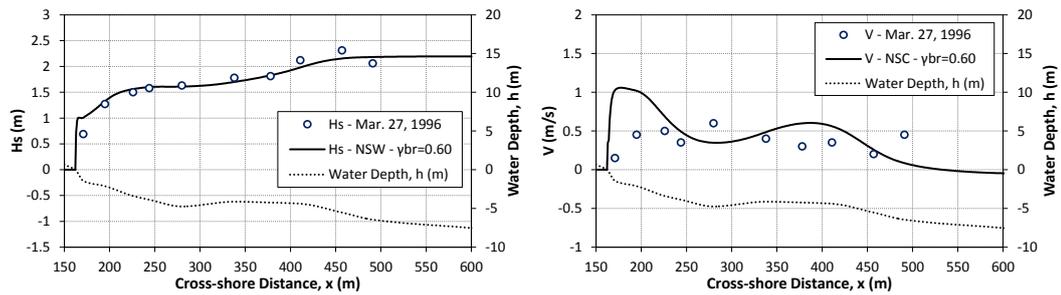
Figure 4.60 The measured and computed significant wave heights (*Hs*) and longshore current velocities (*V*) for the SANDYDUCK, March 27, 1996 Experiment
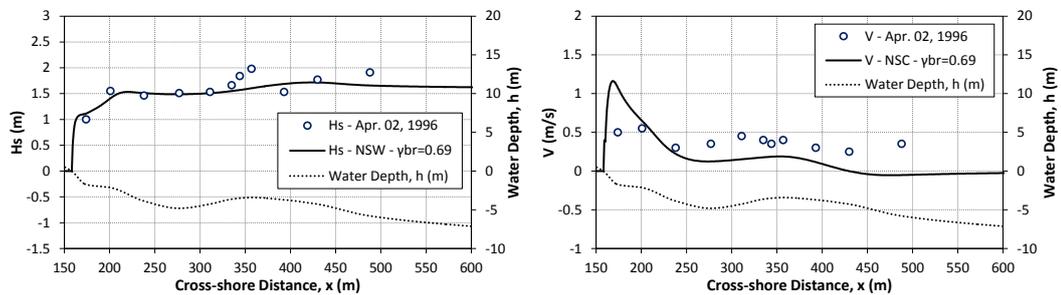
Figure 4.61 The measured and computed significant wave heights (*Hs*) and longshore current velocities (*V*) for the SANDYDUCK, April 02, 1996 Experiment
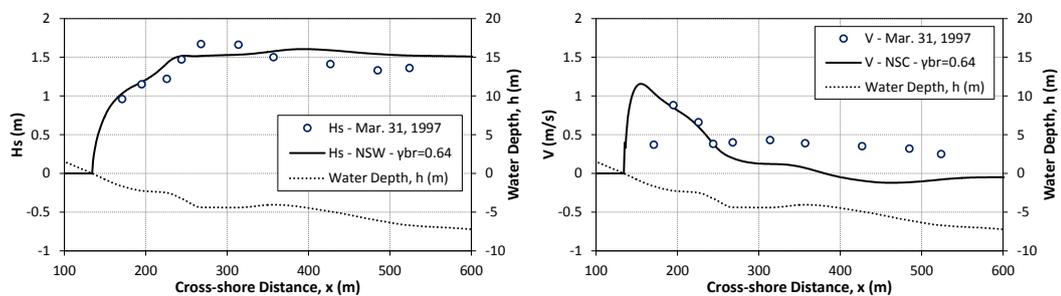
Figure 4.62 The measured and computed significant wave heights (*Hs*) and longshore current velocities (*V*) for the SANDYDUCK, March 31, 1997 Experiment
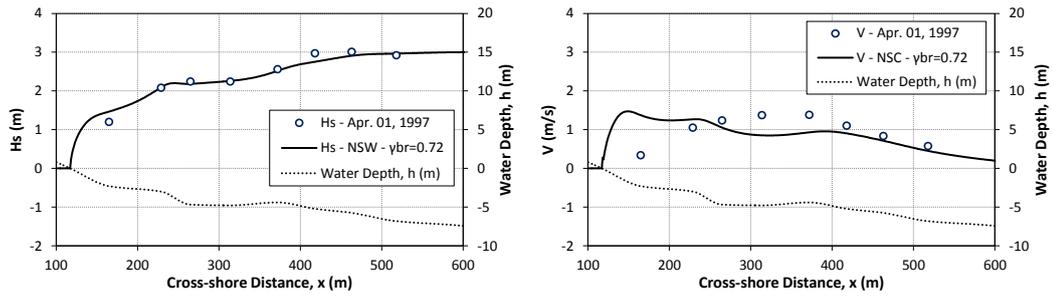
Figure 4.63 The measured and computed significant wave heights (*Hs*) and longshore current velocities (*V*) for the SANDYDUCK, April 01, 1997 Experiment
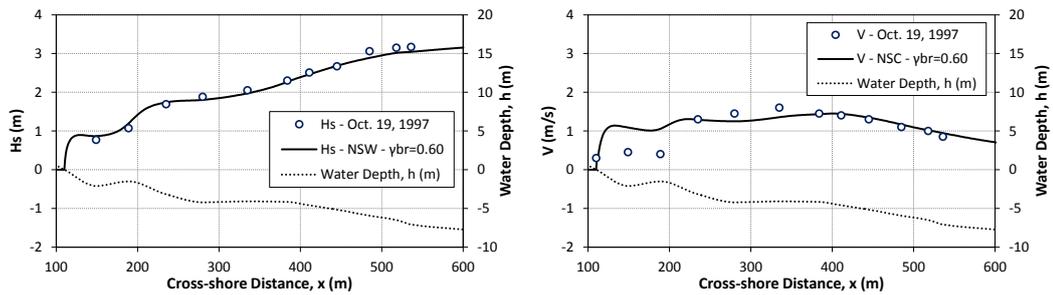
Figure 4.64 The measured and computed significant wave heights (*Hs*) and longshore current velocities (*V*) for the SANDYDUCK, October 19, 1997 Experiment
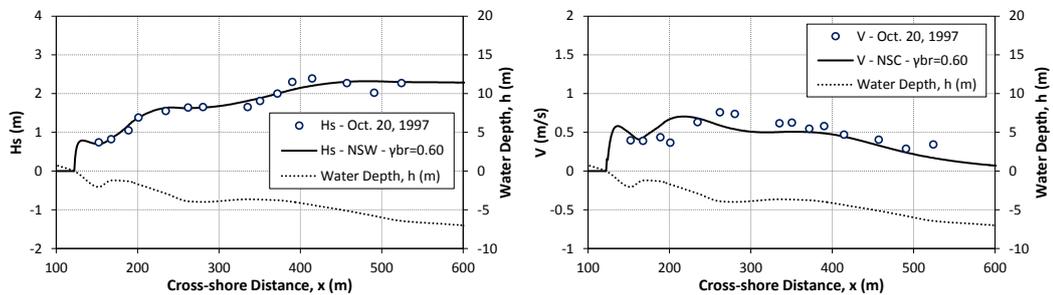
Figure 4.65 The measured and computed significant wave heights (*Hs*) and longshore current velocities (*V*) for the SANDYDUCK, October 20, 1997 Experiment
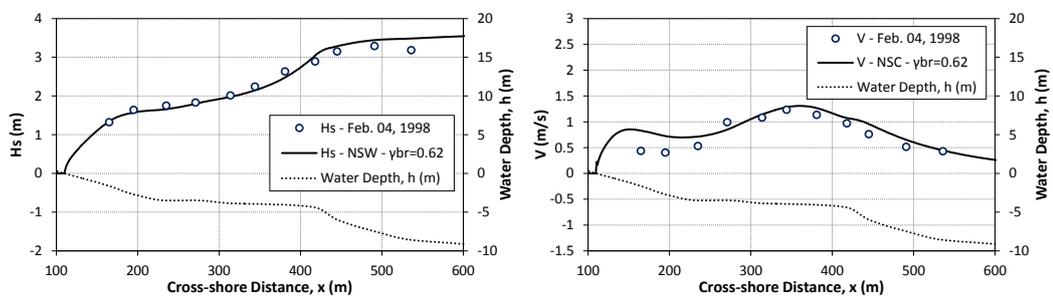
Figure 4.66 The measured and computed significant wave heights (*Hs*) and longshore current velocities (*V*) for the SANDYDUCK, February 04, 1998 Experiment
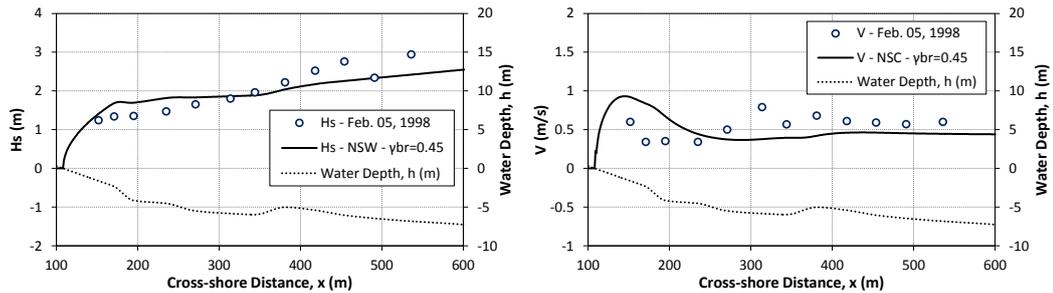
Figure 4.67 The measured and computed significant wave heights (Hs) and longshore current velocities (V) for the SANDYDUCK, February 05, 1998 Experiment

Figure 4.59 - Figure 4.67 show that the computed nearshore wave heights and the longshore current velocities are in good agreement with the measured data both qualitatively and quantitatively especially for the October 19-20, 1997 and February 04, 1998 experiments. The disparities between the measured and computed longshore velocities are mostly due to the accuracy of the computed wave heights. The disparities between the measured and computed wave heights might be attributed mainly to the changing offshore wave conditions during the experiments and the accuracy and the resolution of the available dataset. Moreover, the performance of the wave model and the random wave breaking method utilized depends mainly on the bottom profile and the wave steepness in the absence of significant ambient currents.

For the computation of longshore sediment fluxes, the significant or *rms* wave heights, maximum orbital velocities at the bottom, mean approach angles and the rates of dissipation of wave energies due to random wave breaking computed with the NSW model and the measured current velocities interpolated at the respective positions of the measured sediment transport rates are used. The A coefficient in the Watanabe (1992) formulation is taken as 2.0 for the SANDYDUCK experiments. The computed and measured local total longshore sediment fluxes computed using Watanabe (1992), SED1 and SED2 approaches are given in Figure 4.68 - Figure 4.72.
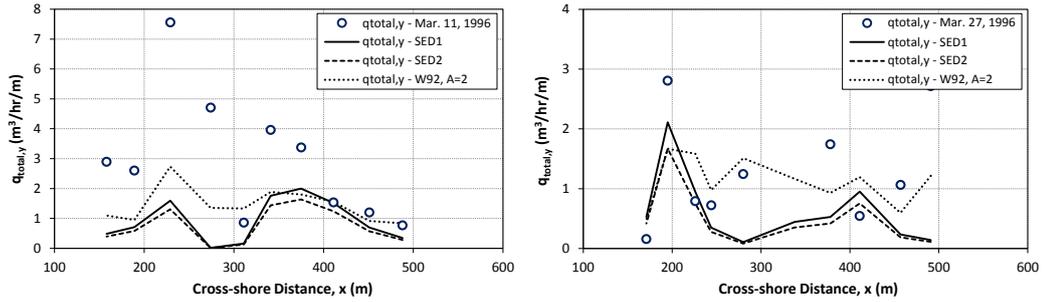
Figure 4.68 The measured and computed local total sediment transport rates ($q_{total,y}$) for SANDYDUCK, March 11, 1996 (left) and March 27, 1996 (right) Experiments
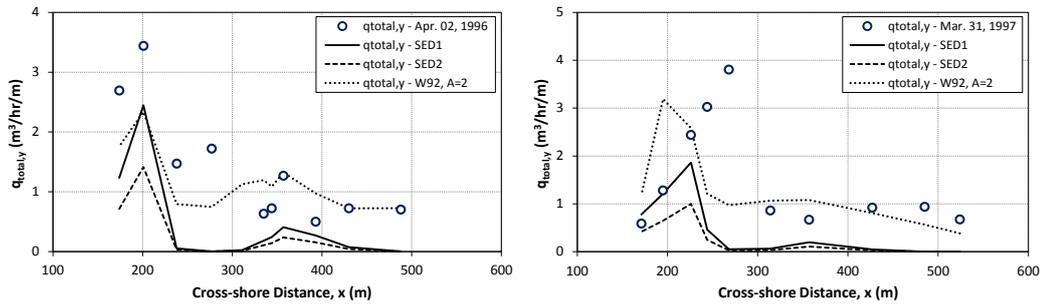
Figure 4.69 The measured and computed local total sediment transport rates ($q_{total,y}$) for SANDYDUCK, April 02, 1996 (left) and March 31, 1997 (right) Experiments
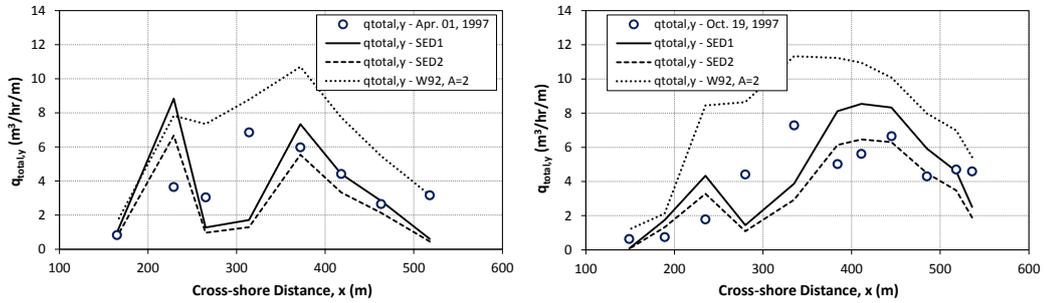
Figure 4.70 The measured and computed local total sediment transport rates ($q_{total,y}$) for SANDYDUCK, April 01, 1997 (left) and October 19, 1997 (right) Experiments
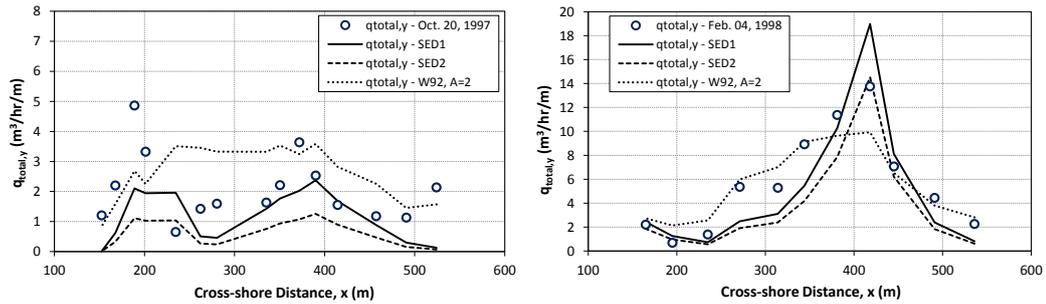
Figure 4.71 The measured and computed local total sediment transport rates ($q_{total,y}$) for SANDYDUCK, October 20, 1997 (left) and February 04, 1998 (right) Experiments
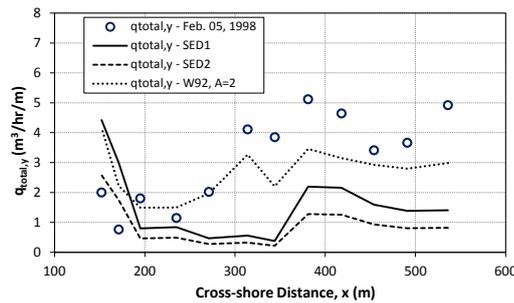
Figure 4.72 The measured and computed local total sediment transport rates ($q_{total,y}$) for SANDYDUCK, February 05, 1998 Experiment

Figure 4.68 - Figure 4.72 shows that the predicted $q_{total,y}$ rates by the SED1 approach are in good agreement with the measured data both qualitatively and quantitatively. The performance of SED2 approach where the ε_{Ba07} parameter is used to compute the $q_{total,y}$ rates is in better agreement with the field experiments compared to the LSTF experiments as the wave conditions are more effective compared to critical stresses to mobilize the sediment grains which has almost the same median diameter ($d_{50,SANDYDUCK}$=0.17 mm) with the sediment used in the LSTF experiments ($d_{50,LSTF}$=0.15 mm). The computed sediment flux values with the Watanabe formulation shows better agreement with the measured values both qualitatively and quantitatively compared to the SED1 and SED2. For the February 04, 1998 and October 19, 1997 experiments, the SED1 and SED2 gives better predictions than Watanabe (1992) which might be explained by that the deep water significant wave heights are the highest for these cases, the sediment transport is dominated by the suspended load under the influence of the turbulence due to breaking of these highly energetic wave conditions and the computed nearshore wave heights and the dissipation rates are in very good agreement with the measurements as seen from Figure 4.64 and Figure 4.66. For the April 01, 1997 and October 20, 1997 experiments, the predicted transport rates by the SED1 and SED2

125

approaches are consistent with the measured data as the computed nearshore wave heights are in agreement with the measurements as seen from Figure 4.63 and Figure 4.65. Over- or under-estimated transport rates for the October 20, 1997 experiment by SED1 or SED2 approaches results from the fact that the waves are less energetic (deep water significant wave height decreases to 2.2 m) and correspond to swell conditions where the effect of turbulence on the transport is reduced. For the April 02, 1996 and March 31, 1997 experiments, only the trend in the cross-shore distribution of total longshore sediment rates agrees with the SED1 and SED2 predictions and Watanabe (1992) predicts better rates outside the surf zone as the flow is less turbulent in this zone. The waves in these experiments have smaller wave heights (1.7-1.8 m) and break close to shore and the nearshore wave heights computed by the NSW model shows a qualitative agreement with the measurements (Figure 4.61 and Figure 4.62) which might be given as another reason for the disagreement between the SED1, SED2 and the measured data. For the experiment conducted on February 05, 1998, both SED1 and SED2 approaches underestimate the transport rates as the computed nearshore wave heights are not in good agreement with the measured data as it is seen from Figure 4.67 which might be explained by the low deep water wave steepness ratio (s_{os}=0.018) of the experiment wave conditions. Finally, the predicted transport rates for the March 11 and March 27, 1996 experiments shows minimum agreement with the measured data which might be attributed to the dissipation rates computed by the NSW model and the accuracy and the resolution of field measurements.

It is a fact that the difficulties governing the field measurements, which severely affect the accuracy of the measurements under continuously changing complex physical processes in coastal areas, create questions when the comparative studies are carried out between the theoretical approaches, laboratory experiments and field measurements.

To determine the relationship between the measured flux values and the $D_b \cdot v/(\rho_s-\rho)/(1-p)/w_s$ values, they are plotted against each other and the slope of the best fitting line (y=mx) for the data gives the ε parameter to be equal to 0.0018 (Figure 4.73). Predicted flux values with the Watanabe (1992), SED1 and SED2 approaches are plotted against measured flux values in Figure 4.74 - Figure 4.76.
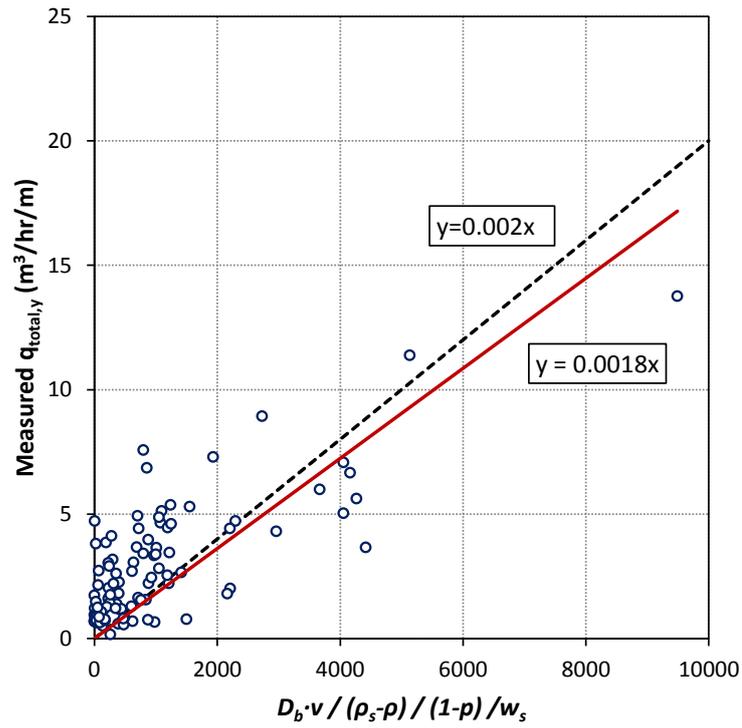
Figure 4.73 Measured flux values are plotted against $D_b \cdot v/(\rho_s-\rho)/(1-p)/w_s$ values for LSTF Movable Bed Experiments (Gravens and Wang, 2007 and Wang et al., 2002a)
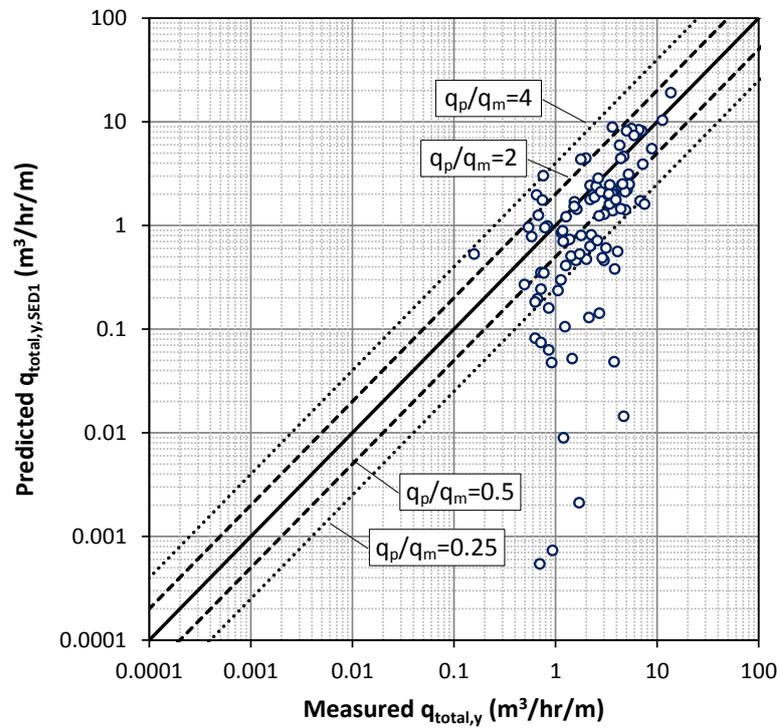
Figure 4.74 Measured transport rates versus predicted by the SED1 approach (ε=0.002) for SANDYDUCK Experiments (Miller, 1999)
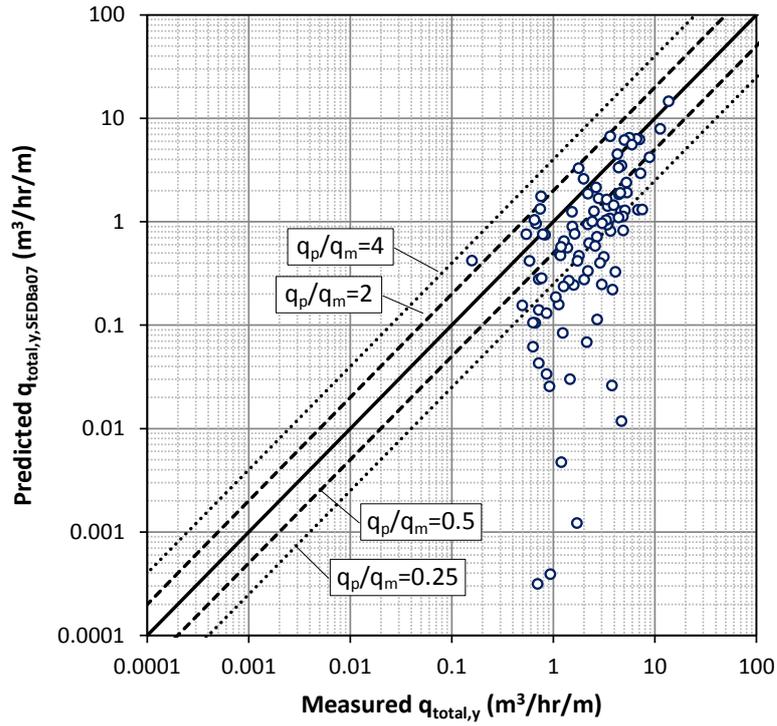
Figure 4.75 Measured transport rates versus predicted by the SED2 approach ($\varepsilon=\varepsilon_{Ba07}$) for SANDYDUCK Experiments (Miller, 1999)
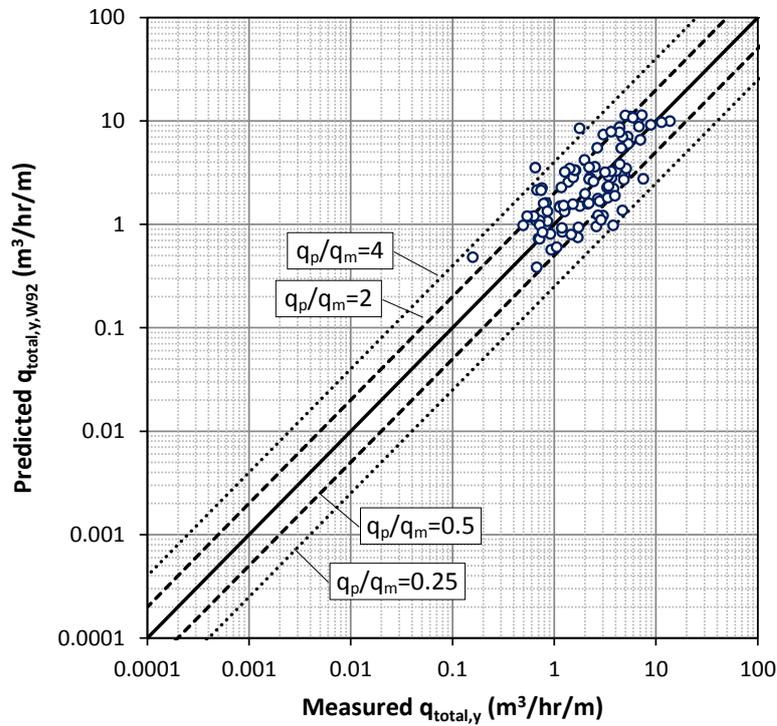
Figure 4.76 Measured transport rates versus predicted by the Watanabe (1992) formulation for SANDYDUCK Experiments (Miller, 1999)

Quantitative and qualitative comparisons are made through computing the mean absolute percent error (E_{mean}), scatter (σ_{rms}) and the percent discrepancy ratios within the limits of 0.5-2.0, 0.25-4.0 and 0.2-5.0 of the measured flux values for both the data set including all of the SANDYDUCK experiments considered in this study (DATA-9) and the selected experiments (DATA-5: March 31, 1997, April 1, 1997, October 20, 1997, February 04 and February 05, 1998) by Bayram et al. (2001) in their comparative study for the Watanabe (1992) and other distributed load approaches. The computed mean absolute errors, scatters and the discrepancy ratios for both of the datasets are given for the two data sets in Table 4.24. The computed values of scatter and discrepancy ratios for the Watanabe (1992) formulation by Bayram et al. (2001) are given in parentheses.

Table 4.24 Summary of accuracy of the formulas for SANDYDUCK Experiments (Miller, 1999)

	Formulas	Mean Absolute Percent Error, E_{mean} (%)	Scatter, σ_{rms}	Discrepancy Ratio (%)		
				1/2 - 2.0	1/4 - 4.0	1/5 – 5.0
DATA-9	SED1 (ε=0.002)	65.3	0.95	59.4	26.0	21.9
	SED2 ($\varepsilon=\varepsilon_{Ba07}$)	66.3	1.07	72.9	40.6	35.4
	Watanabe (1992) (A=2.0)	64.6	0.27	26.0	2.1	0.0
DATA-5	SED1 (ε=0.002)	62.4	0.95	57.1	21.4	19.6
	SED2 ($\varepsilon=\varepsilon_{Ba07}$)	65.6	1.09	73.2	37.5	33.9
	Watanabe (1992) (A=2.0)	61.7	0.26 (0.35)*	23.2	1.8	1.8 (4.0)*

: Scatter and discrepancy ratio values given by Bayram et al. (2001) for the Sandyduck DATA5

As it is seen from Table 4.24, the SED1 and SED2 approaches show similar mean absolute error with the Watanabe approach (65%) for both data sets, yet, the scatter and discrepancy ratios are higher and the predicted values show higher scatter for all cases. However, the sediment transport in the surf zone under energetic wave conditions, such as February 04, 1998 and October 19, 1997 experiments where the suspended sediment transport dominates the sediment transport in the surf zone, is represented better both qualitatively and quantitatively. The SED2 approach shows similar predictive capability slightly underestimating the flux values. Similar to the results of the LSTF comparison, the mean absolute errors and the discrepancy ratios show that there exists a high uncertainty in the prediction of the sediment transport

rates. Moreover, this uncertainty increases for the field experiments as expected since the governing physical processes is under control for laboratory experiments whereas it is usually not in the field.

The error computation studies for the given laboratory and field experiments are specific to the selected empirical parameters of the model (breaker index, eddy viscosity constant, bottom friction and energy transfer coefficients, A or ε parameters in distributed load computations, directional spreading and diffraction intensity parameter) which are not actually measured, yet selected based on engineering intuition within the given range of each parameter. Moreover, the physical processes which might have occurred during the laboratory and field experiments such as tidal or wind induced currents, wave-wave and wave-current interactions, Coriolis effects etc. are not reflected in the numerical model, COD. Therefore, the error computations are limited to the theoretical benchmark studies and the distributed total longshore computations only.

4.4. Discussion on the Use of Breaker Index Parameter

The benchmark studies carried out for both the field and laboratory experiments shows that the selection of the breaker index parameter determines the performance of the wave model significantly. The list of the laboratory and field data used in the comparisons are tabulated in Table 4.25 in descending order with the respect to the deep water significant wave steepness of the experimental wave conditions. The SANDYDUCK data is excluded as the wave measurements were conducted at different times of the day for different cross-shore locations and the offshore wave conditions change in time. The values of breaker index parameters computed with the Nairn's formula (1990) and resulted in either over- or under-estimation of nearshore wave heights are typed in *italic* with a superscript (*).

Table 4.25 List of laboratory and field experiments sorted with respect to deep water significant wave steepness values

Laboratory Data Set	Bottom Profile	Deep Water Wave Steepness, s_{os}	Breaker Index, $\gamma_{br,N90}$
Wa02a, T1-C1	Irregular	0.091	*0.928**
GW07, TEST-BC1	Irregular	0.081	*0.914**
Wa02a, T5-C1	Irregular	0.055	*0.847**
RB97, SO014	Barred Beach	0.053	*0.840**
Ba98, J3	Mixed Uniform (1/10 close to shoreline)	0.049	**0.823**
BJ78, R2	Uniform, 1/20	0.046	*0.812**
BJ78, R15	Barred Beach	0.043	*0.797**
OK92, Case-3	Barred Beach	0.042	**0.790**
OK92, Case-2	Uniform, 1/20	0.036	**0.753**
Ba98, J2	Mixed Uniform (1/10 close to shoreline)	0.036	**0.749**
BJ78, R13	Barred Beach	0.028	**0.687**
Wa02a, T3-C1	Irregular	0.027	**0.620**
HE01, TEST-8E	Uniform, 1/30	0.026	**0.690**
Ta08, Case-2	Uniform, 1/100	0.022	*0.640**
HORF, March 28, 1989	Barred Beach	0.022	**0.632**
BJ78, R3	Uniform, 1/21	0.021	**0.621**
HORF, April 04, 1989	Barred Beach	0.019	*0.600**
Wa02a, T6	Irregular	0.017	*0.565**
DELILAH, October 11, 1990	Barred Beach	0.015	*0.560**
Ta08, Case-1	Uniform, 1/40	0.01	*0.510**
DELILAH, October 14, 1990	Barred Beach	0.006	*0.457**

From Table 4.25, It can be said that the Nairn's formula works best for the deep water waves having significant steepness values within the range of 0.026-0.042 and the type of the beach profile seems to have no significant effect on the selection of breaker index value except for very mild or steep slopes as in the cases of J3 experiment of Baldock et al. (1998) and Case-2 experiment of Tang et al. (2008).

4.5. Conceptual Benchmarks

In order to observe the behavior of the numerical beach evolution model, several simulations are performed for the conceptual cases. The first case in the conceptual

benchmark studies is the modeling of rip currents around beach cusps under perpendicular wave approach. The second case is the modeling of beach evolution next to a groin perpendicular to an initially straight shoreline under oblique wave approach. The third and fourth cases are the modeling of beach evolution in the lee of T-type groin and series of offshore breakwaters respectively.

4.5.1. Rip Currents around Beach Cusps: Park and Borthwick (2001)

To study the nearshore wave-induced circulation in case of arbitrary bathymetries, a conceptual benchmark study has been carried out based on the Park and Borthwick's (2001) study on nearshore currents at a sinusoidal beach which is similar to the beach cusps in nature. The water depths, $h(x,y)$, over the sinusoidal bathymetry in the benchmark problem is defined as

$$h(x,y) =$$
$$\begin{cases} 0.8 - x/20 & for \quad x < 11m \quad and \quad x > 16m \\ 0.05\left\{(15-x) - 0.75\sin\left[\frac{\pi(15-x)}{5}\right]\left[1 + \sin\left(\frac{3\pi}{2} - \frac{2\pi y}{4}\right)\right]\right\} & for \quad 11m \leq x \leq 16m \end{cases}$$

(4.11)

where x is the cross-shore coordinate (from 0 to 17 m) and y is the longshore coordinate (from 0 to 28 m) of the point of interest. The length between the sinusoidal beach cusps is taken as 4 m for the problem. The bottom slope beyond 0.25 m water depth is taken as 1/20 up to the offshore boundary where the water depth is 0.80 m. At the offshore boundary, uni-directional random waves with a significant wave height of 0.062 m and significant period of 1.0 sec are generated perpendicular to the bottom contours. The breaker index is taken as γ_{br}=0.78, bottom friction coefficient is taken as c_f=0.015, energy transfer coefficient is taken as α=0.5 and the effects of lateral mixing are disregarded in the simulation. The results of the simulation are shown in Figure 4.77.

132
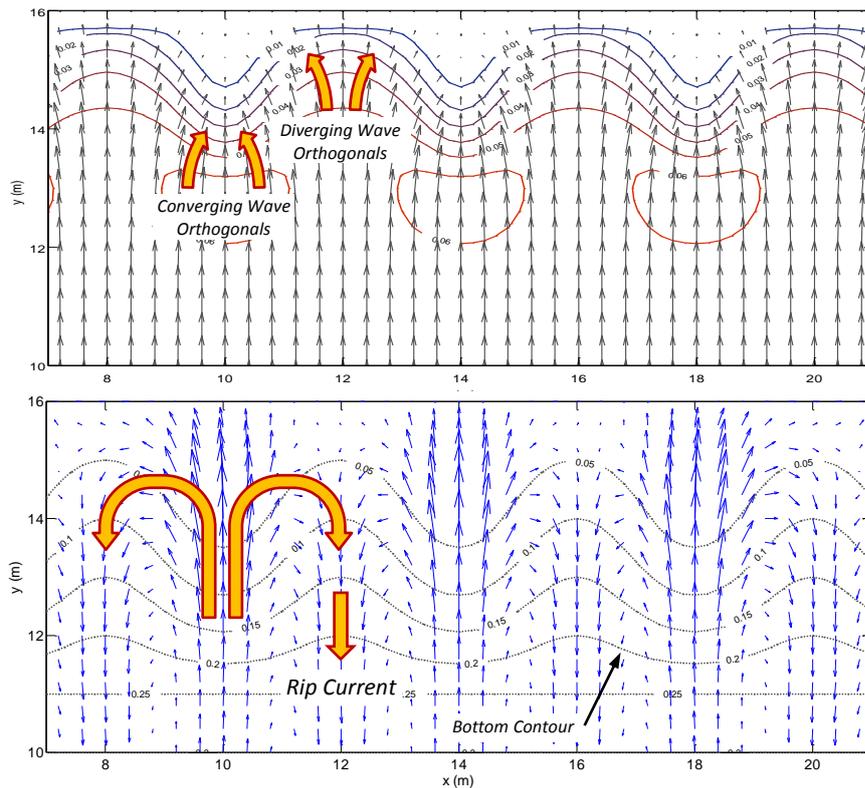
Figure 4.77 The vectorial representation of the computed wave (upper) and current (lower) fields around the beach cusps

As it is seen from Figure 4.77, the waves increase in height around cusps and the wave orthogonals converge to the cusps as expected. The wave crests tend to align themselves with respect to bottom contours and decrease in height as the wave orthogonals diverge from each other. The rip currents are formed due to the diverted flows from the cusps.

4.5.2. Beach Evolution around a Single Groin under Oblique Wave Approach

To observe the behavior of the numerical beach evolution model (COD) in the case of a single groin under oblique wave approach on an initially straight shoreline with uniform bottom slope, a simulation with the COD model is performed. In the simulation, the deep water significant wave height is taken H_{s0}=2.0 m, and significant wave period as T_s=5.7 sec, the deep water mean approach angle is taken as θ=30°, the grid spacing is 25 m in both x and y directions, the breaker index, eddy constant, bottom friction, surface roller constants, median grain size diameter and A coefficient in Watanabe (1992)

formulation are taken as γ_{br}=0.78, Λ=0.5, c_f=0.005, α=0.5, d_{50}=0.15 mm and A=2 respectively. The length of the groin is taken 500 m reaching to a depth of 20 m on a 1:25 uniform bottom slope. The computed bottom contours after 200 hours of simulation is given in Figure 4.78.
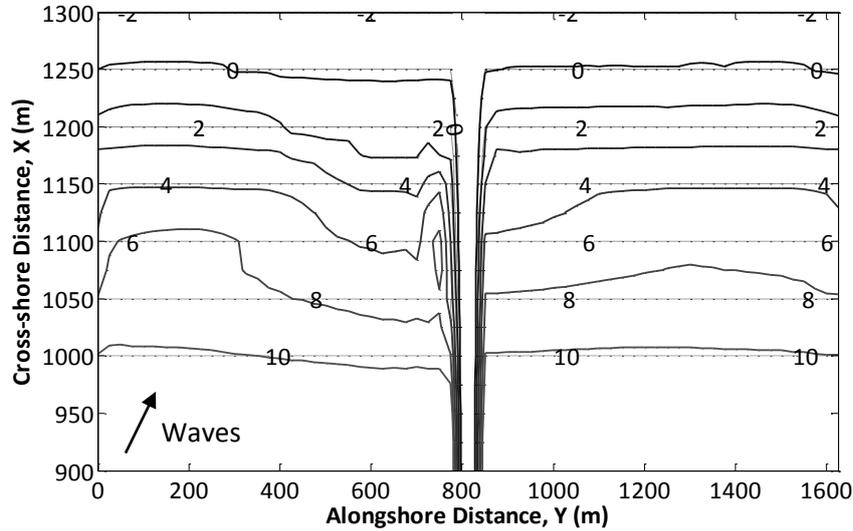
Figure 4.78 The change in the nearshore bathymetry around a single groin after 200 hours of simulation (--- initial bottom contours, — final bottom contours)

As it is seen from Figure 4.78, the shoreline recedes in the shadow zone of the structure and at the far upstream of the beach and the bottom contours tend to align according to the shoreline. At the upstream of the groin, the accretion occurs and the shoreline moves offshore confirming the expected bottom evolution around a single groin.

4.5.3. Beach Evolution around a Series of Offshore Breakwaters under Oblique Wave Approach

To observe the behavior of the numerical beach evolution model (COD) in the case of a series of offshore breakwaters under oblique wave approach on an initially straight shoreline with uniform bottom slope (1:25), a simulation with the COD model is performed. In the simulation, the deep water significant wave height is taken H_{s0}=2.0 m, and significant wave period as T_s=5.7 sec, the deep water mean approach angle is taken as θ=30°, the grid spacing is 25 m in both x and y directions, the breaker index, eddy constant, bottom friction, surface roller constants, median grain size diameter and A coefficient in Watanabe (1992) formulation are taken as γ_{br}=0.78, Λ=0.5, c_f=0.005, α=0.5,

d_{50}=0.15 mm and *A*=2 respectively. Three offshore breakwaters with a 150 m length and 150 m spacing between them are located at a depth of 5 m which is 125 away from the shoreline. The computed bottom contours after 200 hours of simulation is given in Figure 4.78.
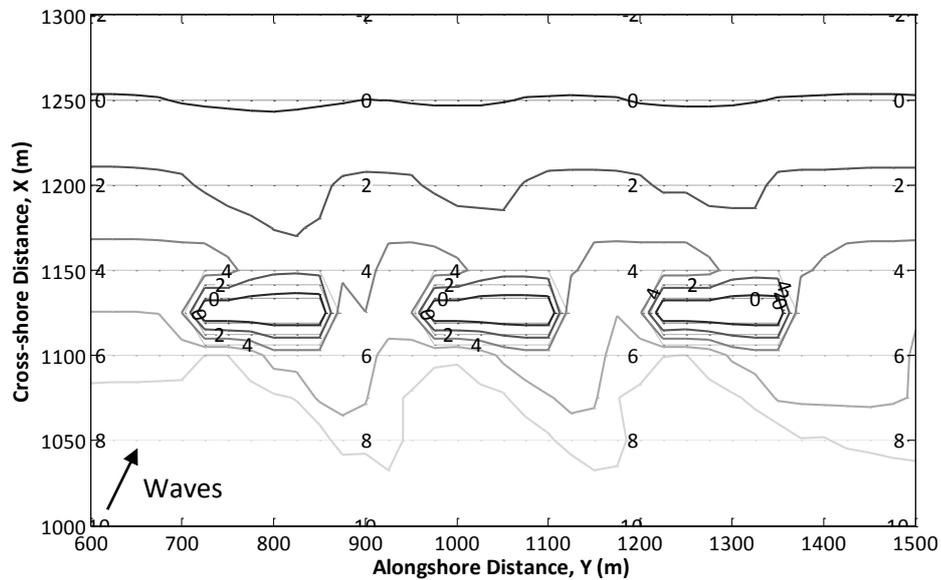
Figure 4.79 The change in the nearshore bathymetry around three offshore breakwaters after 200 hours of simulation (--- initial bottom contours, — final bottom contours)

As it is seen from Figure 4.79, the accretion starts at the upstream end of the beach and the shoreline recedes at the downstream, the bottom contours are eroded between the breakwaters due to return flows and the bottom contours move offshore behind the breakwaters due to current field behind the structures confirming the expected bottom evolution around a series of offshore breakwaters.

CHAPTER 5

A CASE STUDY: COASTAL EROSION AT THE KIZILIRMAK RIVER MOUTH

In this chapter, an application of the developed numerical beach evolution model (COD) to a case study is given. The coastal erosion problem encountered at the Kızılırmak river mouth at the Bafra alluvial plain is briefly given focusing on the causes, previous attempts of physical and numerical modeling of the problem and the remedial measures taken by the General Directorate of State Hydraulic Works (DSİ) and Bafra Plain Irrigation Project Directorate of DSİ. The COD model is run to simulate the shoreline changes at a groin field constructed in 1999 to the east of the river mouth for the representative wave conditions obtained through a wave hindcasting study for the years 1999-2003. In the wave hindcasting study, the hourly average wind data measured by Sinop Meteorological Station for the respective years is used. The hourly average wind data is provided by the General Directorate of Meteorological Affairs (DMİGM).

5.1. General Information about the Site

In most of the developing countries, denser the population in coastal areas, the more vulnerable they become to severe environmental problems such as coastal erosion, exploitation and depletion of natural resources and extinction of endangered species. Wetlands at coastal areas are one of the most adversely affected areas due to their diverse floras and faunas. In Turkey, there are 13 sites designated as "Wetlands of International Importance" with a total surface area of 179,898 ha and 5 of these sites are located at coastal areas. One of these sites is Bafra alluvial plain (Kızılırmak Delta) where the Kızılırmak River discharges into the Black Sea. The site was designated as RAMSAR Area in 15.04.1998. It has a surface area of 21,700 ha including dunes, beaches, shallow lakes, seasonal marshes and wooded areas (URL-3). Numerous species of water

birds, several of which are globally threatened, breed at this site. Over 92,000 water birds of various species winter at the site. In recent years, eutrophication, deforestation, illegal constructions and coastal erosion have become increasingly problematic in Kızılırmak coastal wetland (Kuleli et al., 2011).
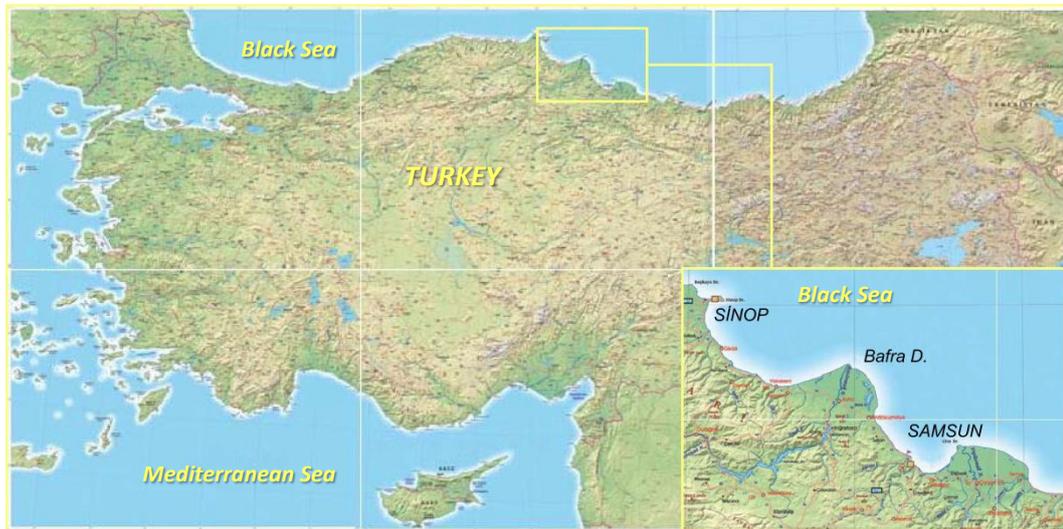
Figure 5.1 Location of Bafra alluvial plain

Figure 5.2 Bafra alluvial plain and plan view of the existing shore protection system at the Kızılırmak River mouth (Google Earth, 2011)

The location of Bafra alluvial plain is shown in Figure 5.1 and Figure 5.2. The sea level variations of the Black Sea, where semidiurnal tides are dominant with a spring tidal

range of 8-12 cm, has been largely controlled by a seasonal variation (inter-annual change) of 20–40 cm maximum in June (Alpar, 2009; Vigo et al., 2005; Bondar, 2007). The inter-decadal sea level variations have a period of 30 years and are in the order of 16 cm (Trifonova and Grudeva, 2002). The sea level variations produced by the atmospheric pressure changes or by sudden changes of wind direction could reach 10-20 cm with periods of 1-5 hours (Bondar, 2007). In the computations, the effects of these sea level variations are disregarded.

The Kızılırmak River, which rises in the Eastern Anatolian Mountains, flows in a northwestern direction and discharges into the Black Sea by forming a conic alluvial delta (Figure 5.2). It is the longest river in Turkey, with a length of 1,355 km, draining a basin of 74,515 km^2 (Kökpınar et al., 2007). The amount of sediment carried by the Kızılırmak River was 23.1 million tons/year till 1960's prior to any flow regulatory structures and decreased to 18 million tons/year following the construction of Hirfanlı Dam in 1960, and almost came to a cease with the total amount of 0.46 million tons/year after the constructions of Altınkaya Dam in 1988 and Derbent Dam in 1991 (Hay, 1994). This drastic decrease in the amount of sediment carried by the Kızılırmak River resulted in severe erosion with a maximum 1 km wide band of shoreline since 1988 according to the Regional Directorate of State Hydraulic Works and from local residents (Kökpınar et al., 2007).

Regarding the coastal erosion problem at Bafra alluvial plain, Kuleli et al. (2011) focused on the shoreline change rate analysis by automatic image analysis techniques using multi-temporal Landsat images and Digital Shoreline Analysis System (DSAS) along five Ramsar wetlands of Turkey. For Kızılırmak Delta, they have used three satellite images for the years 1989, 1999 and 2009 and found 16.1 m/year erosion rate for the Kızılırmak Delta.

The first remedial measure against this severe coastal erosion problem at the river mouth was held in 2000 by State Hydraulic Works (DSİ) based on the findings of the physical and mathematical model studies conducted at the Hydraulic Model Laboratory of DSİ, in Ankara, Turkey (Kökpınar et al., 2007). The shoreline changes around several combinations of different types of groins (I, Y and T-type groins) were studied through

physical model experiments carried out in a wave basin of 8 m wide and 25 m long with a uni-directional regular wave generator, by mathematical model studies using numerical one-line and parabolic bay shape methods. It was composed of two Y-type and one I-type groins constructed at the eastern shoreline of the river mouth (Figure 5.2). Ergin et al. (2006) studied the shoreline changes around these structures with the numerical shoreline change model, CSIM, using the shoreline measurements taken in 1999 (April) and 2003 (January) by DSİ. Despite utilizing T-groins instead of Y-groins and despite the numerical model's lack of capability of modeling tombolo formation, the model results was in good agreement quantitatively with the field measurements, especially at western sides (updrift) of second and third groins.

After the construction of first remedial system (two Y-type and one I-type groins), the shoreline retreat slowed down between the groins and trapping of sediment initiated. However, recession at the shoreline due to wave action continued to the east from the third groin (I-groin) as almost no sediment is carried by the Kızılırmak River. Later, two jetties were constructed at the west and east sides of river mouth between the years 2001-2004 to prevent seasonal closure of the river mouth. Between the years 2004-2005, the coastal defense system was extended with the construction five more I-type groins to prevent the collapse of drainage channel. Although, the drainage channel has been saved against wave action constructing the new series of five I-type groins, shoreline retreat at the east side of the defense system could not been prevented and continued to further east. The series of groins are extended further to the east recently.

In this study, the shoreline change between the east groin and the first Y-type groin for the years 1999-2003 is studied using the numerical beach evolution model, COD where the bottom topography measurements were assumed to be more accurate. The corresponding shoreline GPS measurements for the dates April, 1999 and January, 2003 were kindly provided by Regional Directorate of DSİ (Figure 5.3). The nearshore bathymetry for the groin field is approximated from the measured bottom contours on April 25, 2004 by DSİ and the navigation maps of Navigation, Hydrography, and Oceanography Department of Turkish Naval Forces (SHODB). The nearshore bottom slope is around 1:65 between the shoreline and 10 m water depth. In the computations, the nearshore bathymetry is discretized to a rectangular grid with 20 m grid spacing

both in cross-shore and longshore directions. The nearshore bathymetry used in the study is given in Figure 5.4.
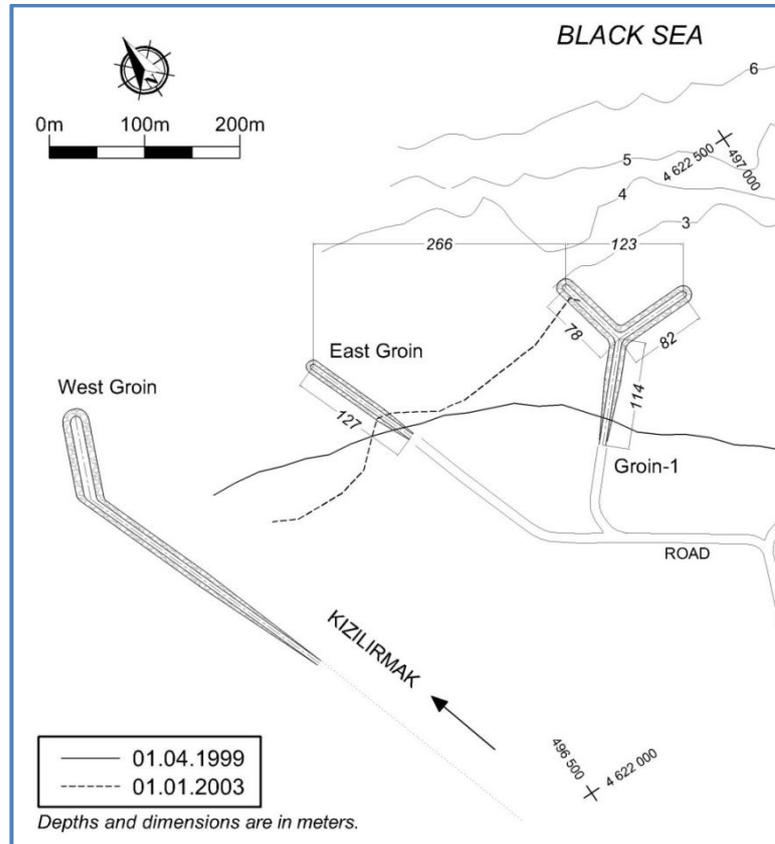
Figure 5.3 The measured shoreline positions at the Kızılırmak River mouth between the East Groin and Y-type Groin-1 plan view
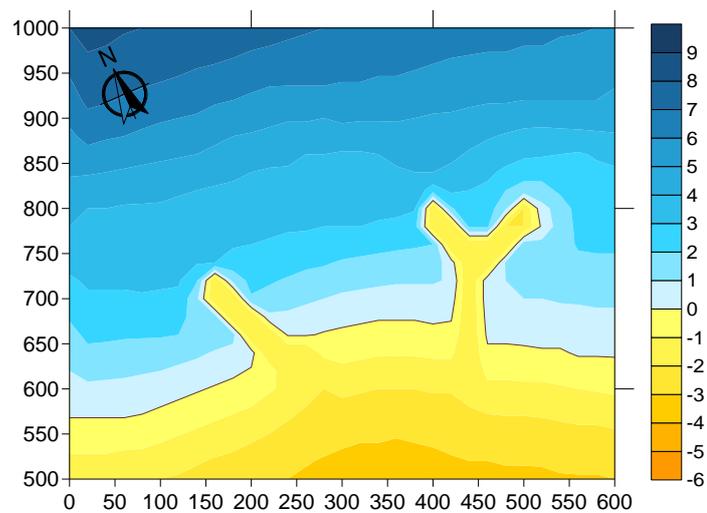
Figure 5.4 The nearshore bathymetry used in the COD model for the groin field at the Kızılırmak river mouth

5.2. Wave Climate Study

Long term geomorphological evolution of coastal areas under wave action results from series of short-term wave events occurring randomly. When there exist no time histories of these wave events or no continuous wave measurements, yet, wind measurements exist for such coastal areas, wave hindcasting studies are performed. For each wave direction, the wind velocities and effective fetch distances are used to hindcast the wave climate history of the site and a long-term wave statistics study is carried out to determine annual deep water wave characteristics.

To determine the wave climate at the region between the years 1999 and 2002, a wave hindcasting study has been performed using the hourly average wind data measured at 10 m above ground level by Sinop Meteorological Station, obtained from DMİGM. The location of the river mouth is open to waves approaching from a wide directional sector from West to East-South-East. The effective fetch distances for the directions in this directional sector are determined from the navigation maps of Navigation, Hydrography and Oceanography Department of Turkish Naval Forces (SHODB). In the computation of effective fetch distances, for each direction, the effective generation area is considered as a sector from $-22.5°$ to $+22.5°$ totally covering an area of $45°$ with $7.5°$ intervals (SPM, 1984). The effective fetch directions and distances are shown in Figure 5.5.

Using the effective fetch distances and the wind data obtained from Sinop Coastal Meteorological Station, deep water wave parameters (H_{s0}, deep water significant wave height; T_s, significant wave period) are obtained for the storms occurred during the years 1999-2002 by using the numerical model, W61, developed at Middle East Technical University, Department of Civil Engineering, Ocean Engineering Research Center (Ergin and Özhan, 1986; Ergin et al., 2008; Ergin et al., 2009).
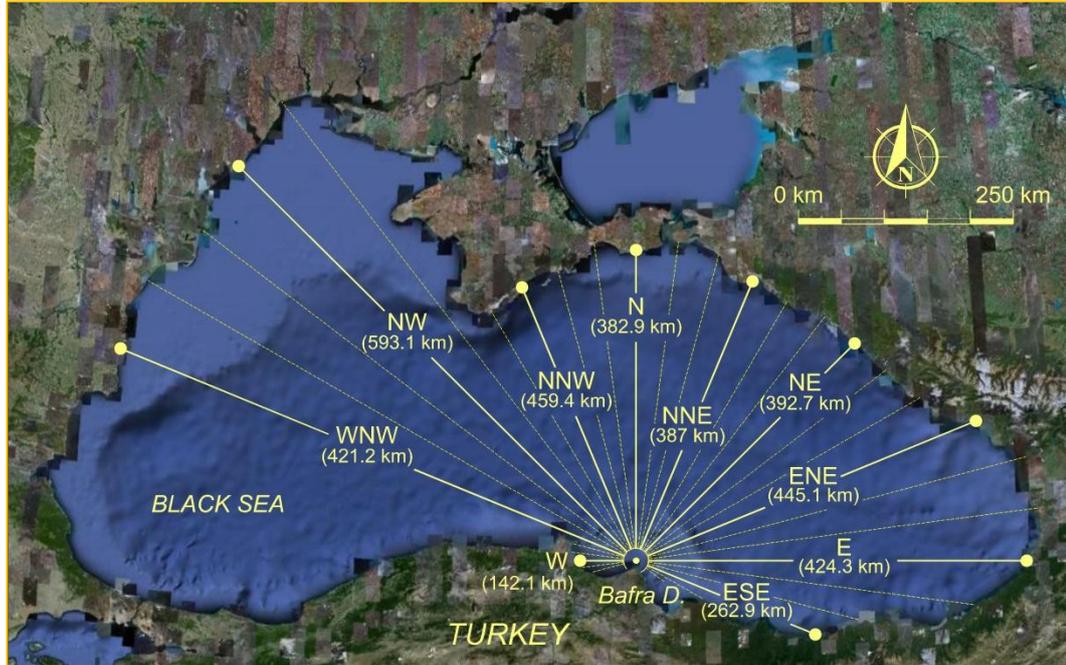
Figure 5.5 Wave directions for Bafra region (Google Earth, 2011)

The characteristic deep water wave steepness value (H_{s0}/L_0), the ratio of deep water significant wave height (H_{s0}) to the corresponding deep water wave length (L_0), for the project area is obtained as 0.040 from deep water significant wave heights and deep water wave lengths computed from corresponding significant wave periods (T_s) of each individual storm ($L_0 = gT_s^2/2\pi$ where g is gravitational acceleration in m/s^2). The hindcasted wave heights for the years 1999-2002 are classified in 0.4 m ranges and the cumulative number of occurrences of each wave height class is plotted on to a semi-log graphical paper. The cumulative exceedance probability of deep water significant wave height, H_{s0}, is given as;

$$Q(> H_{s0}) = exp[(H_{s0} - B)/A]$$ (5.1)

where $Q(>H_{s0})$ is the cumulative exceedance probability of a deep water significant wave height (H_{s0}). This equation indicates that if data points corresponding to H_{s0} and $Q(>H_{s0})$ are plotted on a semi-log graphical paper (H_{s0} on normal, and $Q(>H_{s0})$ on logarithmic scales), they should lie on a straight line with a slope of A and intercept of B when $Q(>H_{s0})$ is the horizontal axis.

Another major assumption in the preparation of wave data input is such that the effects of smaller but more frequent waves are considered to be more appropriate for a better representation of long term wave climate rather than higher waves with less frequency. By using the long-term statistics, the representative deep water significant heights ($H_{rs,0}$) of waves coming from every direction, their periods and annual frequencies in hours are calculated using (Güler, 1997; Güler et al., 1998; Şafak, 2006);

$$H_{rs,0} = \frac{\sum(P_i \cdot H_i)}{\sum P_i} \tag{5.2}$$

where H_i is the wave height and P_i is the occurrence probability of wave height H_i. Occurrence probability (P_i) of wave height (H_i) is computed by using the corresponding occurrence durations within the given range as follows;

$$P_i = Q(H_i - k) - Q(H_i + k) \tag{5.3}$$

where Q is the exceedance probability and k is an assigned range to compute occurrence probability. In Table 5.1, the seasonal wave data input for the model consisting of representative wave heights ($H_{rs,0}$), corresponding periods (T_s) and seasonal occurrence durations (Δt in hours) from all directions is presented.

Table 5.1 Annual representative wave heights, corresponding periods and occurrence durations from all directions

Directions	$H_{rs,0}$ (m)	T_s (sec)	Δt (hrs)
W	3.60	7.62	2
WNW	**2.77**	**6.68**	**196**
NW	**2.83**	**6.76**	**145**
NNW	**2.92**	**6.87**	**50**
N	2.44	6.27	0
NNE	2.57	6.44	4
NE	3.06	7.03	4
ENE	2.76	6.68	10
E	2.90	6.84	3
ESE	2.52	6.38	6

As seen from Table 5.1, for all seasons the highest occurrences of waves within the range of 2.8 m are from West-North-West and North-West.

5.3. Numerical Modeling Study

In the application of the COD model to the site, the median grain size diameter (d_{50}) is taken as 0.23 mm (Kökpınar et al., 2007). It is also assumed that the flow regime of Kızılırmak River does not affect the nearshore waves and the decreased amount of sediment carried by the river due to flow regulation structures is neglected. The wave data input (Table 5.1) used in the simulation is taken as limited to WNW, NW and NNW waves to decrease the computation time and the data order is given from WNW to NNW directions. The bottom friction coefficient c_f is taken as 0.008, the lateral mixing constant is taken as Λ=0.8 and the surface roller constant is taken α=0.5. In the simulation, Watanabe (1992) approach is used to compute the sediment fluxes. The A coefficient is taken as 2 as recommended for random waves. The directional spreading for the deep water waves is taken as s_{max}=10 which is given for wind waves in Table 3.1. The grid spacing in both x and y directions are taken as 20 m and the morphological time step is taken as 1 min. Simulation of 3 consecutive years with the same wave conditions given in Table 5.1 took approximately 9 hours at a personal computer (Intel® Xeon E5530 2.4GHz Processor, 8GB RAM, 32-Bit Windows® 7 Professional Edition). The average significant wave and current fields and the change in the bottom topography are given in Figure 5.6, Figure 5.7 and Figure 5.8.
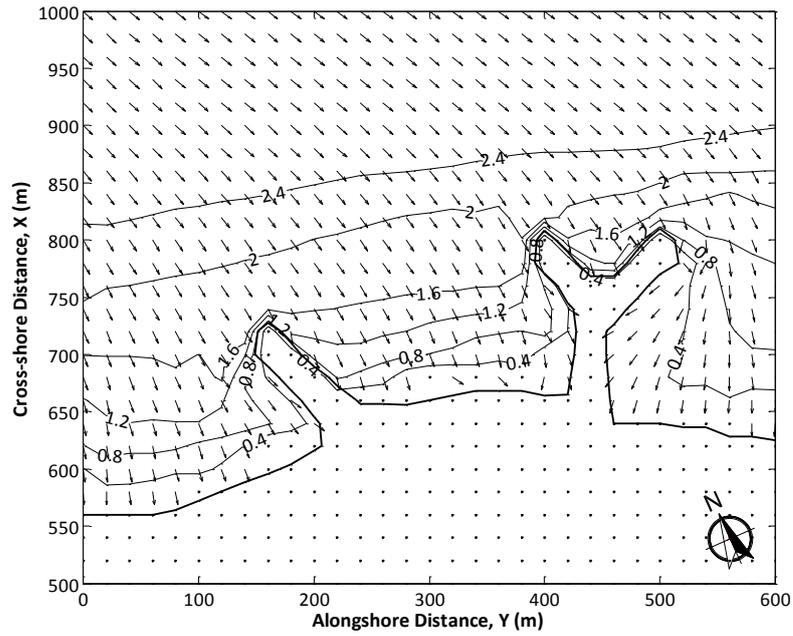
Figure 5.6 The average significant wave height contours and the vectorial representation of the wave orthogonals for the WNW waves
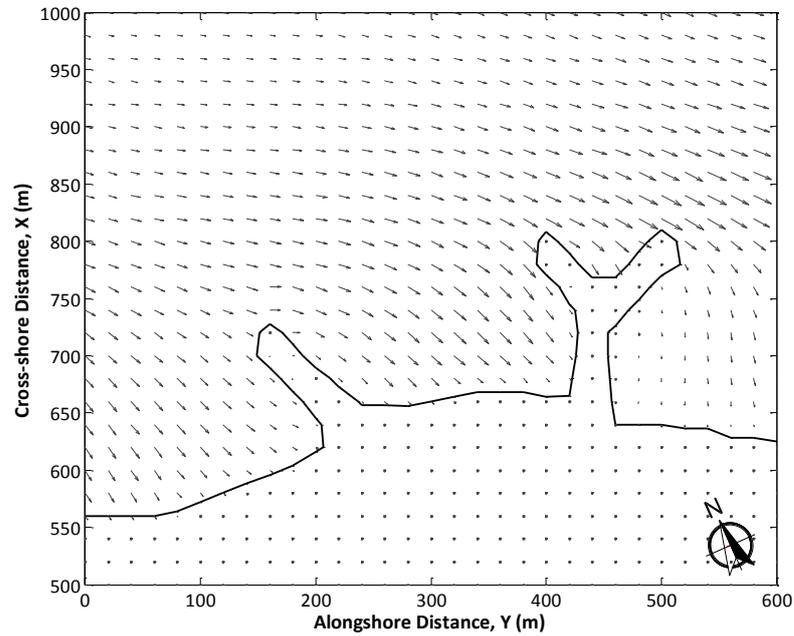
Figure 5.7 The vectorial representation of the average current field during the waves approaching from WNW direction
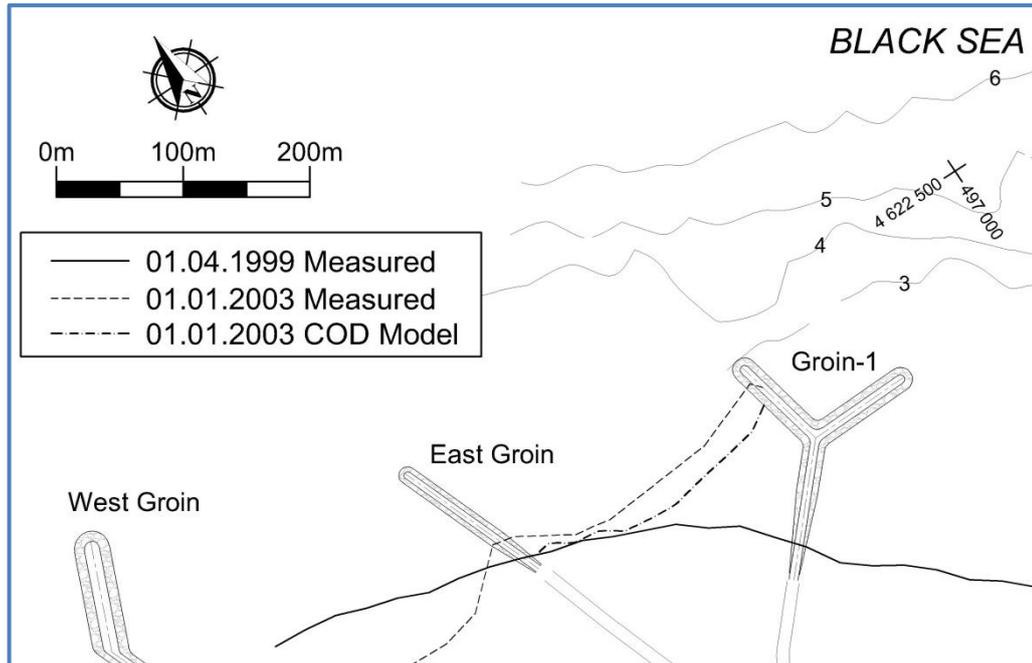
Figure 5.8 The measured and the computed shoreline positions between the East Groin and Groin-1 after 3 years of simulation

As it is seen from Figure 5.8, the computed shoreline change between the East Groin and Y-type Groin-1 is in agreement with the measured shoreline both qualitatively and quantitatively. The modeling of the accretion up to the branch of Groin-1 is significant which cannot be simulated using the typical one-line models. The amount of sediment in accumulated between the two groins may also be computed more accurately with the adjustment of the 'A' parameter used in the Watanabe (1992) formulation.

The bottom topographies having a spatial resolution higher than the numerical grid resolution before and after the duration of beach evolution under consideration, measurements of deep water or nearshore wave and current characteristics during the respective duration, detailed information about the sediment grain size distribution at the beach and the information on the locations of hard substrates at the sea bottom would further improve the accuracy of the computations. The actual time series of wave data might also be considered for detailed investigations. Moreover, decreasing the grid spacing around the structures would increase the numerical accuracy of the wave and flow fields.

CHAPTER 6

CONCLUSION

"There and back again"
J.R.R. Tolkien, The Hobbit

The scope of this study was to develop a base structure of a two-dimensional depth-averaged numerical 'BeaCh EvOlution MoDel', (COD), which will be applicable to both medium-term (weeks to months) and long-term beach evolution events (years to decades). The model structure is mainly composed of four main sub-models. The first sub-model is a phase-averaged spectral wave transformation model based on energy balance equation. The second sub-model is a two-dimensional depth-averaged numerical circulation model based on non-linear shallow water equations. The effects of surface rollers both in cross-shore and longshore directions are included in the nearshore circulation computations for accurate representations near bar formations in the surf zone. The third sub-model is a sediment transport model based on Watanabe (1992) distributed total sediment load formulation. The fourth sub-model is a bottom evolution model which computes the changes in the bottom topography due to sediment transport under wave action only. The developed sub-models are compared and validated with an extensive data set of laboratory and field experiments. The developed sub-models are also applied to conceptual benchmark cases including simulation of rip currents around beach cusps. The numerical model, COD, reflected the physical concepts well for the selected cases. Finally, the developed beach evolution model is applied to a case study of a coastal erosion problem at the Bafra alluvial plain where the Kızılırmak River discharges into the Black Sea. Within the boundaries of the study area, the COD model gave results in agreement with the measurements both qualitatively and quantitatively.

Within the scope of this study, to compute the distributed total longshore sediment transport rates over the arbitrary bathymetries an alternate approach has been

proposed based on the assumption that the local total sediment transport rates across the surf zone are proportional to the product of rate of dissipation of wave energies due to wave breaking and wave-induced depth-averaged current velocities. The validation of the proposed approach has been done by the available data sets of laboratory and field experiments. From the comparative studies, it has been found that the proposed approach is in good agreement with the measurements both qualitatively and quantitatively, especially for the cases where the wave conditions are highly energetic (both for plunging and spilling type breakers) and the suspended load is the main mode of sediment transport in the surf zone.

For further improvement of the numerical model, COD, developed within the scope of this study, there exists a loaded future research agenda. Starting from the spectral wave transformation model up to the bottom evolution model, the main headings of the recommended future studies are given below.

The numerical schemes utilized in the NSW and NSC models could be improved to enhance the applicability of the numerical model for irregular bathymetries and various cases of combinations of coastal structures and to increase the predictive capability of the models and acquire more numerically stable solutions.

As for the computation of the wave energy dissipation rates due to random wave breaking for the wave conditions with very low or high steepness values, unsaturated breaking wave conditions observed at steep beaches and the bathymetries with very mild slopes, alternate approaches of wave breaking and the effect of breaker index parameter might be investigated to improve the performance and optional approaches of both wave and current models for such conditions.

Wave-current interactions that can be observed at the river mouths or tidal inlets or at locations with strong ocean, wind-induced or tidal currents are not considered in the wave transformation computations. For the inclusion of the wave-current interactions, the action balance equation need to be adopted instead of energy balance equation in the wave model.

Wave reflection from shore due to sharp bottom gradients and coastal structures, dissipation due to bottom friction, white-capping (steepness controlled dissipation in deep water) and bottom vegetation, transfer of wind energy and Coriolis effects are not considered in the wave model which are recommended as future research topics for further improvement of the wave model.

Alternative bottom friction, lateral mixing and surface roller terms used in the NSC model might be re-considered to increase the performance and optional properties of the model.

The boundary conditions at the wet/dry interfaces in the circulation model should be studied in detail to obtain physically and numerically accurate flow conditions at these boundaries such as shoreline or at wet cells near coastal structures or steep sloped topographical features.

Implementation of a vertically stratified flow conditions would enable to study short term events where the onshore-offshore sediment transport governs more accurately such as bar formations during storms. However, such an effort would also increase the computational demand and decrease the applicability of the model to the medium- and long-term events. In this respect, further research might be carried out to include the effects of onshore-offshore sediment transport more accurately in the numerical model promoting it into a quasi-3D type of model structure.

The time-averaged approach in the sediment transport computations omits two aspects of sediment transport under an oscillatory flow. It ignores the presence of phase shift between sediment and water motions and ignores the asymmetry in the oscillatory flow. These two major aspects should be considered within the scope of improvement of the sediment model.

The proposed approach to compute the distributed total longshore sediment transport rates over the arbitrary bathymetries should be verified with more field and laboratory data carried out under various hydrodynamic and bottom conditions. The proposed

approach might be extended to compute the net cross-shore sediment transport rates considering the above mentioned undertow, phase shift and the asymmetry concepts.

In the bottom evolution computations, non-erodible bottoms are disregarded. The overall beach area where the sediment transport rates are computed (all the wet points and the wet-dry boundary) is assumed to be eroded infinitely till the end of the simulation and there exist no hard substrate under the surface of the bathymetry. This assumption is not realistic for most of the beaches and to extend the model capabilities for various types of bottom topographies it should be considered as a recommended future study.

For a detailed investigation or modeling of the shoreline changes at coastal areas, the bottom topographies having a spatial resolution higher than the numerical grid resolution before and after the duration of beach evolution under consideration, measurements of deep water or nearshore wave and current characteristics during the respective duration, sediment characteristics, the locations of hard substrates at the sea bottom are the main inputs that are needed. Moreover, decreasing the grid spacing around structures would increase the numerical accuracy of the wave and flow fields around such structures. However, such a decrease in the grid spacing would also increase the duration of computations. Therefore, an optimization for both accuracy and the speed of the computations might be necessary for large scale areas or long term events.

In the application of the 2D or 3D beach evolution models to the actual case studies, the amount of data needed for the model is usually much more compared to the one-line models which reflect as a disadvantage of 2D or 3D models. Yet, 2D or 3D models provide better representations of the complex physical processes at coastal areas both qualitatively and quantitatively. Therefore, their popularity and use in engineering applications increase in parallel to the advances in the numerical computing techniques, the computer techonology and increasing knowledge of coastal physical processes.

Above given recommended future studies are recently popular topics in the field of coastal engineering and will also keep their popularity in the near future. In that sense,

the developed numerical beach evolution model will become a base structure for such future studies and will be a developing and effective tool to be utilized in coastal erosion/accretion problems encountered in our country.

REFERENCES

Ackers, P. and White, W.R. (1973). "Sediment transport: new approach and analysis." Journals of Hydraulics Division 99 (1), pp.2041-2060.

Ahrens, J.P. (2000). "The fall-velocity equation." Journal of Waterways, Port, Coastal, Ocean Eng., 126-2, 99–102.

Alpar, B. (2009). "Vulnerability of Turkish coasts to accelerated sea-level rise." Geomorphology 107, pp.58–63

Apotsos, A., Raubenheimer, B., Elgar, S. and Guza, R.T. (2008). "Testing and calibrating parametric wave transformation models on natural beaches," Coastal Engineering Vol.55, pp.224–235

Artagan, S.S. (2006). "A One Line Numerical Model for Shoreline Evolution under the Interaction of Wind Waves and Offshore Breakwaters." M.S. Thesis, METU, Ankara

Bagnold, R.A. (1966). "An approach to the sediment transport problem from general physics." Geological Survey Professional Papers 422-1, Washington, USA.

Bailard, J.A. (1981). "An energetics total load sediment transport model for a plane sloping beach." Journal of Geophsical Research. 86 (C11), 10938-10954.

Bailard, J.A. (1984). "A simplified model for longshore sediment transport." Proc. of the 19th Coastal Eng. Conf., pp.1454-1470.

Bailard, J.A. and Inman, D.L. (1981). "An energetics bedload model for plane sloping beach: local transport." Journal of Geophysical Research 86 (C3), pp.2035-2043.

Balas L., Asu, İ. and İpek. Y.. (2006). "Numerical Modelling of Coastal Currents." Lecture Notes in Computer Science, 3980 (547-555).

Baldock, T.E., Holmes, P., Bunker, S., and Van Weert, P. (1998). "Cross-shore Hydrodynamics within an Unsaturated Surf Zone," Coastal Eng., 34, pp.173-196.

Basco, D.R. and Yamashita, T. (1986). "Toward a Simple Model of the Wave Breaking Transition Region In Surfzones." Proc. of the 20th Conf. on Coastal Eng., ASCE. pp.955-970.

Battjes, J.A. (1972). "Set-up Due to Irregular Waves," Proc. of the 13th Coastal Eng. Conf., American Society of Civil Engineers, pp 1993-2004.

Battjes, J.A. (1975). "Modeling of turbulence in the surf zone," Proc. Symp. Modeling Techniques, pp.1050-1061

Battjes, J.A. and Groenendijk, H. W. (2000). "Wave height distributions on shallow foreshores." Coastal Engineering, Vol.40, no 3, pp.161–182

Battjes, J.A., and Janssen, J. P. F. M. (1978). "Energy Loss and Setup due to Breaking of Random Waves," Proc. of the 16th Coastal Eng. Conf., American Society of Civil Engineers, pp.569-587.

Battjes, J.A. and Stive, M.J.F., (1985). "Calibration and verification of a dissipation model for random breaking waves." J. Geophys. Res. 90, pp.9159–9167.

Baykal, C. (2006). "Numerical Modeling of Wave Diffraction in One-Dimensional Shoreline Change Model." M.S. Thesis, METU, Ankara, Turkey

Baykal, C., Ergin, A., Güler, I. (2011). "Book Chapter: Intervention of Human Activities on Geomorphological Evolution of Coastal Areas: Cases from Turkey." Geomorphology, Intech Open Access Publisher, ISBN 979-953-307-113-7 (in print)

Bayram, A. (2011), personal communication

Bayram, A., Larson, M., and Hanson, H. (2007). "A new formula for the total longshore sediment transport rate." Coastal Eng. 54, pp.700-710.

Bayram, A., Larson, M., Miller, H.C., Kraus, N.C. (2001). "Cross-shore distribution of longshore sediment transport: comparison between predictive formulas and field measurements." Coastal Eng. 44, pp.79-99

Benoit, M., Marcos, F. and Becq, F. (1996). "Development of a third-generation shallow water wave model with unstructured spatial meshing. Proc. 25th Int. Conf. Coastal Eng., ASCE, Orlando, 465-478

Berkhoff, J. C. W. (1972). "Computation of Combined Refraction - Diffraction," Proceedings, 13th International Conference on Coastal Engineering, American Society of Civil Engineers, Vol 1, pp.471-490.

Bijker, E.W., (1967). Some considerations about scales for coastal models with movable bed. Delft Hydraulics Laboratory, Publication 50, Delft, The Netherlands.

Bijker, E.W., (1971). Longshore transport computations. Journal of the Waterways, Harbors and Coastal Eng. Division 97 (4), pp.687-703.

Birkemeier, W.A., Donoghue, C., Long, C.E., Hathaway, K.K., Baron, C.F. (1997). "The DELILAH Nearshore Experiment: Summary Data Report." US Army Corps of Engineers, Waterways Experiment Station, Vicksburg, MS.

Bodge, K.R. (1989). "A literature review of the distribution of longshore sediment transport across the surf zone," Journal of Coastal Research, Vol.5(2), pp.307-328.

Bokaris, J. and Anastasiou, K. (2003). "Solution of the hyperbolic mild-slope equation using the finite volume method." International Journal of Numerical Methods in Fluids. Vol.41. pp225-250

Bondar, C. (2007). The Black Sea level variations and the river-sea interactions, GEO-ECO-MARINA 13/2007, Coastal Zone Processes and Management, Environmental Legislation

Booij, N. (1981). "Gravity waves on water with non-uniform depth and current." Rep. No. 81-1, Dept. of Civ. Eng., Delft Univ. of Technology.

Booij, N., Holthuijsen, L.H., Doorn, N., Kieftenburg, A.T.M.M., (1997). "Diffraction in a spectral wave model." Proc. 3rd Intl. Symposium Ocean Wave Measurement and Analysis WAVES 97. ASCE, New York, pp.243–255.

Booij, N., R.C. Ris and L.H. Holthuijsen. (1999). "A third-generation wave model forcoastal regions, Part I, Model description and validation." J.Geoph.Research, 104, C4, pp.7649-7666

Borgman, L.E. (1984). "Directional spectrum estimation for the Sxy gages." Tech.Rep. Coastal Eng. Research Center, Vicksburg, Miss

Boussinesq, J. (1871). "Théorie de l'intumescence liquide, applelée onde solitaire ou de translation, se propageant dans un canal rectangulaire." Comptes Rendus de l'Academie des Sciences 72: 755–759.

Bouws, E., Gunther, H., Rosenthal, W. and Vincent, C.L. (1985). "Similarity of the wind wave spectrum in finite depth water 1. Spectral form." Journal of Geophysical Research 90 (C1): pp.148-227

Bretherton, F.P. and Garrett, C.J.R. (1968). "Wavetrains in inhomogeneous moving media." Proc. of the Royal Society of London, Series A 302 (1471): 529–554

Bretschneider, C.L. (1968). "Significant waves and wave spectrum, Ocean Industry Feb. 1968, pp.40-46.

Briand, M.H.G., and Kamphuis, J.W. (1993). "Sediment transport in the surf zone: A quasi 3-D numerical model." Coastal Eng., Vol.20, pg.135-156

Bruneau, N., Bonneton, P., Pedreros, R., Dumas, F. and Idier, D. (2007). "A New Morphodynamic Modelling Platform: Application to Characteristic Sandy systems of the Aquitanian Coast, France." Journal of Coastal Research, Special Issue 50, pp.932-936

Burkardt, J. (2010). "Numerical solution of the Shallow Water Equations, MATH 6425 Lectures 23/24." ICAM/Information Technology Department Virginia Tech

Buttolph, A.M., Reed, C.W., Kraus, N.C., Ono, N., Larson, M., Camenen, B., Hanson, H., Wamsley, T., and Zundel, A.K., (2006). "Two-dimensional depth-averaged circulation Model CMS-M2D: Version 3.0, Report 2, Sediment Transport and Morphology Change." Technical Report ERDC/CHL TR-06-9, Coastal and Hydraulics Laboratory, US Army Engineer Research and Development Center, Vicksburg, MS.

Camenen, B. and Larroude, P. (2003). "Comparison of sediment transport formulae for the coastal environment." Coastal Eng. 48, 111–132.

Camenen, B. and Larson, M. (2005). "A general formula for non-cohesive bed load sediment transport." Estuarine, Coastal and Shelf Science 63, 249–260.

Camenen, B. and Larson, M. (2007). "A unified sediment transport formulation for coastal inlet application." Technical report ERDC/CHL CR-07-1, US Army Engineer Research and Development Center, Vicksburg, MS.

Camenen, B. and Larson, M. (2008). "A general formula for noncohesive suspended sediment transport." Journal of Coastal Research 24 (3), 615–627.

Chawla, A., Özkan, H.T., Kirby, J.T. (1998). "Spectral model for wave transformation and breaking over irregular bathymetry." J. Waterways, Port, Coast., Ocean Eng., ASCE 124 (4), pp189–198.

CIRIA. (1996). "Beach Management Manual," CIRIA Report 153, CIRIA, London

CEM. (2003). "Coastal Engineering Manual," U.S. Army Corps of Engineers, Coastal Eng. Research Center, U.S.Government Printing Office

Collins, J. I. (1970). "Probabilities of Breaking Wave Characteristics," Proc. of the 12th Coastal Eng. Conf., American Society of Civil Engineers, pp.1993-2004.

Copeland, G.J.M. (1985). "A Practical Alternative to the Mild- Slope Wave Equation." Coastal Eng., 9. pp125-149

Dabees, M.A. and Kamphuis, J.W. (1998). "ONELINE, a Numerical Model for Shoreline Change." Proc. 27th Int. Conf. On Coastal Engrg., ASCE, Copenhagen, pg.2668-2681

Dabees, M.A. and Kamphuis, J.W. (2000). "NLINE: efficient modelling of 3-D beach change." Proc. 27th Coastal Eng. Conf.. ASCE, pp. 2700–2713.

Dally, W.R. (1990). "Random Breaking Waves: A Closed-Form Solution for Planar Beaches," Coastal Eng., Vol 14, No. 3, pp.233-263.

Dally, W.R. (1992). "Random Breaking Waves: Field Verification of a Wave-by-Wave Algorithm for Engineering Application," Coastal Eng., Vol 16, pp.369-397.

Dally, W.R. and Brown, C.A. (1995). "A modeling investigation of the breaking wave roller with application to cross-shore current." J. Geophys. Res., 100 (C12), pp.873–883.

Dally, W.R., Dean, R.G., and Dalrymple, R. A. (1985). "Wave height variation across beaches of arbitrary profile." J. Geophys. Res., 90(C6), 11, pp.917-927.

De Vriend, H.J. and Stive, M.J.F., (1987). "Quasi-3D modelling of nearshore currents." In: P.P.G. Dyke (Editor), JONSMOD '86. Coastal Eng., 11: 565-601.

De Vriend, H.J., Capobianco, M., Chesher, T., de Swart, H.E., Latteux, B., Stive, M.J.F. (1993). "Approaches to long-term modelling of coastal morphology: a review." Coastal Eng., Elsevier 21, 225–269.

Dean, R.G. and Dalrymple, R.A. (2002). "Coastal Processes with Engineering Applications." Cambridge University Press, Cambridge, UK (2002), 475 pp.

Demirbilek, Z.; Lin, L., and Seabergh, W.C. (2009). "Laboratory and numerical studies of hydrodynamics near jetties." Coastal Engineering Journal 51(2):143-175 JSCE.

DHI, Danish Hydraulic Institute. (2001). "LITPACK Coastline evolution, User's Guide and Reference Manual." Ed. DHI, Lingby, Denmark

Ding, Y., Wang, S.S.Y., and Jia, Y. (2006) "Development and validation of a quasi-three dimensional coastal area morphological model." ASCE, J. of Waterway, Port, Coastal, and Ocean Engineering, 132(6), pp.462-476.

Dolan, R. and Davis, R.E., (1992). "An intensity scale for Atlantic Coast northeast storms." J. Coastal Res. 8 (4), 840–853.

Eldeberky, Y. and Battjes, J.A. (1995). "Parameterization of triad interactions in wave energy models." Proc. Coastal Dynamics Conf. '95, Gdansk, Poland, 140-148

Elgar, S., Guza, R.T., O'Reilly, W.C., Raubenheimer, B., Herbers, T.H.C. (2001). "Wave energy and direction observed near a pier." ASCE J. Waterw. Port Coast. Ocean Eng. 127, 2–6.

Engelund, F., Hansen, E. (1967). "A Monograph On Sediment Transport in Alluvial Streams." Teknisk Forlag, Copenhagen, Denmark.

Ergin, A. and Özhan, E. (1986). "Wave Hindcasting Studies and Determination of Design Wave Characteristics for 15 Regions - Final Report." Middle East Technical University, Department of Civil Engineering,, Feb., 1986, Ankara (in Turkish)

Ergin, A., Baykal, C., İnsel, I. and Esen, M. (2009). "Tsunami and Storm Surge Evaluation for Yenikapı and Üsküdar Stations - Final Report." Middle East Technical University, Department of Civil Engineering, Ocean Engineering Research Center, Ankara, June, 2009

Ergin, A., Güler, I., Yalçıner, A.C., Baykal, C., Artagan A.A. and Safak, I. (2006). "A One-Line Numerical Model for Wind Wave Induced Shoreline Changes." Proc. 7th Int. Congress on Advances in Civil Eng., Istanbul, Turkey

Ergin, A., Yalçıner, A.C., Güler, I., Baykal, C., Esen, M. and Karakuş, H. (2008). "Fugla Beach Protection and Control Project - Final Report." Middle East Technical University, Department of Civil Engineering, Ocean Engineering Research Center, Ankara, December 2008 (in Turkish)

Ergin, A., Yalçıner, A.C., Güler, I., Baykal, C., Şafak, I., Artagan, S.S., Esen, M., and Özyurt, G. (2007). "Side Perissia Perissia Hotel Beach Preservation and Control Project - Final Report." Middle East Technical University, Department of Civil Engineering, Ocean Engineering Research Center, Ankara, Turkey (in Turkish)

Esen, M. (2007). "An implicit one-line numerical model on longshore sediment transport." M.S. Thesis, METU, Ankara, Turkey

Feddersen, F., Guza, R. T., Elgar, S. and Herbers, T. H. C. (1998). "Longshore momentum balances in the nearshore," J. Geophys. Res., 103, 15,667–15,676

Goda, Y. (1975a). "Irregular Wave Deformation in the Surf Zone," Coastal Eng. in Japan, Vol 18, pp.13-26.

Goda, Y. (1975b). "Deformation of irregular waves due to depth-controlled wave breaking," Rept. Port and Harbour Res. Inst. 14 (3), pp. 59-106 (in Japanese).

Goda, Y. (1988). "Statistical variability of sea state parameters as a function of wave spectrum." Coastal Eng. in Japan, Vol.31, No.l, pp.39-52.

Goda, Y. (2002). "A Fast Numerical Scheme for Unsaturated Random Breaking Waves in 3-D Bathymetry," Proc., 28th International Conf. on Coastal Eng.. World Scientific, pp.508-520.

Goda, Y. (2004). "A 2-D random wave transformation model with gradational breaker index." Coast. Eng. J. 46 (1), 1 –38 (JSCE and World Scientific).

Goda, Y. (2006). "Examination of the influence of several factors on longshore current computation with random waves." Coastal Eng. 53 (2006) 157 – 170

Goda, Y. (2008). "Wave setup and longshore currents induced by directional spectral waves - Prediction formulas Based on Numerical Computation Results." Coastal Eng. Journal, Vol. 50, No. 4 (2008) pp.397-440

Goda, Y. (2009). personal communication

Goda, Y. (2010). "Random Seas and Design of Maritime Structures." 3rd Edition. World Scientific Publishing. ISBN-13: 978-981-4282-40-6., 708pp.

Goda, Y. and Suzuki, Y. (1975). "Computation of refraction and diffraction of sea waves with Mitsuyasu's directional spectrum." Tech. Note of Port and Harbour Res. Inst. 230, 1–45 (in Japanese)

Goda, Y., Takayama T. and Suzuki, Y. (1978). "Diffraction diagrams for directional random waves," Proc. 16th Int. Cont. Coastal Engrg. (Hamburg, 1978.) pp. 628-650.

Gravens, M.B. (2011). personal communication

Gravens, M.B. and Wang, P. (2007). "Data report: Laboratory testing of longshore sand transport by waves and currents; morphology change behind headland structures." Technical Report, ERDC/CHL TR-07-8, Coastal and Hydraulics Laboratory, US Army Engineer Research and Development Center, Vicksburg, MS.

Gravens, M.B., Wang, P., Kraus, N.C., Hanson, H. (2006). "Physical model investigation of morphology development at headland structures." Proc. 30th International Conf. on Coastal Eng..World Scientific Press, San Diego, pp. 3617–3629.

Güler, I. (1997). "Investigation on Protection of Manavgat River Mouth." Yüksel Proje International Co. Inc., Research Project Report

Güler, I., Baykal, C., Ergin, A. (2008). "Shore Stabilization by Artificial Nourishment, A Case Study: A Coastal Erosion Problem in Side, Turkey." 7th International Conf. on Coastal and Port Engineering in Developing Countries, 24-28 Feb. 2008, Dubai, UAE

Güler, I., Ergin, A., and Yalçıner, A.C. (1998). "The Effect of the Use of Wave Data for the Numerical Solution of Shoreline Evolution." Journal of Coastal Research, Special Issue No.26, pg. 195-200

Hamilton, D.G. and Ebersole, B.A. (2001). "Establishing uniform longshore currents in a large-scale sediment transport facility." Coast. Eng. 42, 199-218

Hanson, H. and Kraus, N.C. (1989). "Genesis: Generalized Model for Simulating Shoreline Change." Technical Report CERC-89-19, Report 2 of a Series, Workbook and User's Manual. US Army Corps of Engineers, Waterways Experiment Station, Vicksburg, MS, USA.

Hanson, H. and Kraus, N.C. (2011). "Long-Term Evolution of a Long-Term Evolution Model." Journal of Coastal Research, Special Issue, No. 59, pp. 118-129

Hanson, H. and Larson, M. (1998). Seasonal shoreline variations by cross-shore transport in a one-line model under random waves. Proc. of 26th International Coastal Eng. Conf., ASCE, 2,682-2,695.

Hanson, H. and Larson, M. (2000). "Simulating shoreline evolution using a new type of N-line model." Proc. 27th Coastal Eng. Conf. ASCE, pp. 2808–2821.

Hanson, H., Aarninkhof, S., Capobianco, M., Jimenez, J.A., Larson, M., Nicholls, R.J., Plant, N.G., Southgate, H.N., Steetzel, H.J., Stive, M.J.F., de Vriend, H.J. (2003). "Modeling of Coastal Evolution on Yearly to Decadal Time Scales." Journal of Coastal Research, Vol.19, No.4, pg.790-811

Hanson, H., Larson, M. Kraus, N.C. and Gravens, M.B. (2006). "Shoreline response to detached breakwaters and tidal current: Comparison of numerical and physical models." Proc. 30th International Conf. on Coastal Eng., ASCE, 3: 630-642

Hanson, H., Larson, M., and Kraus, N.C. (2001). "A new approach to represent tidal cunents and bathymétrie features in the oneline model concept." Proc., Coastal Dynamics '01, ASCE, 172-181.

Hanson, H., Larson, M., Kraus, N.C., and Capobianco, M. (1997). "Modeling of seasonal variations by cross-shore transport using one-line compatible methods." Proc., Coastal Dynamics '97, ASCE, 893-902.

Hasselmann, K., Barnett, T.P., Bouws, E., Carlson, H., Cartwright, D.E., Enke, K., Ewing, J.A., Gienapp, H., Hasselmann, D.E., Kruseman, P., Meerburg, A., Müller, P., Olbers, D.J., Richter, K., Sell, W. and Walden, H. (1973). "Measurements of wind-

wave growth and swell decay during the Joint North Sea Wave Project (JONSWAP)." Dtsch. Hydrogr. Z. Suppl. A 8(12), 95p.

Hay, B.J. (1994). "Sediment and water discharge rates of Turkish Black Sea Rivers before and after hydropower dam construction." Environmental Geology, Vol.23, pp.276-283.

Hoan, L.X. (2010). "Long-Term Simulation of Coastal Evolution." Ph.D. Thesis, Lund, Sweden

Hoefel, F. and Elgar, S. (2003). "Wave-induced sediment transport and sandbar migration." Science, Vol.299, pp.1885-1887.

Holthuijsen, L.H., Booij, N. and Herbers, T.H.C. (1989). A Prediction Model for Stationary, Short-Crested Waves in Shallow Water with Ambient Currents, Coastal Eng., 13, 23-54.

Holthuijsen, L.H., Herman, A., and Booij, N. (2003). "Phase-decoupled refraction–diffraction for spectral wave models." Coastal Eng. Volume 49, Issue 4, October 2003, Pages 291-305

Houwman, K. T., and P. Hoekstra. (1998). "Tidal ellipses in the nearshore zone (-3 to -10 m); modelling and observations," in Proc. 26th Int. Coastal Eng. Conf., pp. 773–786, Am. Soc. of Civ. Eng., New York

Inman, D.L. and Bagnold, R.A., (1963). "Littoral Processes in the Sea." In: Hill, M.N. (Ed.). Vol. 3. Interscience, New York, pp. 529–533.

Janssen, T.T. (2011). personal communication

Janssen, T.T. and Battjes, J.A. (2007). "A note on wave energy dissipation over steep beaches." Coastal Eng., 54, 711-716

Kamphuis, J.W. (1991). "Alongshore Sediment Transport Rate." Journal of Waterway, Port, Coastal and Ocean Engineering, ASCE, Volume 117, pp. 624-640.

Kamphuis, J.W. (2000). "Introduction to Coastal Engineering and Management." World Scientific Publishing, Singapore

Karlsson, T. (1969). "Refraction of continuous ocean wave spectra." Proc. Amer. Soc. Civil Engrs. 95 (WW4), 471–490.

Katayama, H. and Goda, Y. (1999). "Sediment suspension by random breaking waves evaluated from the CERC formula." Proc. Coastal Sediments 99, Long Island, New York, ASCE, pp. 1019-1033.

Katayama, H. and Goda, Y. (2000). "A sediment pickup rate formula based on energy dissipation rate by random breaking." Proc. 27th Int. Conf. Coastal Eng., Sydney, ASCE, 2859-2872.

Katayama, H. and Goda, Y. (2002). "2DH beach changes due to suspended sediment picked-up by random breaking waves." Proc. 28th Int. Conf., Cardiff, Wales, World Scientific, pp. 2767-2779.

Kennedy, A. B, Chen, Q., Kirby, J. T., and Dalrymple, R. A. (2000). "Boussinesq modeling of wave transformation, breaking and runup. I: One dimension'', J. Waterway, Port, Coastal and Ocean Engrng., 126, 39-47.

Kirby, J.T., Wei, G., Chen, Q., Kennedy, A. B. and Dalrymple, R. A. (1998). "Fully Nonlinear Boussinesq Wave Model, User Manual." Technical Report CACR-98-06, University of Delaware.

Kirby, J.T. and Dalrymple, R.A. (1983). "A parabolic equation for the combined refraction-diffraction of Stokes waves by mildly varying topography." J. Fluid Mech., 136: 453-466.

Kirby, J.T. and Dalrymple, R.A. (1984). "Verification of a parabolic equation for propagation of weakly-nonlinear waves." Coastal Eng., 8: 219-232.

Kobayashi, N., Agarwal, A. and Johnson, B.D. (2007). "Longshore current and sediment transport on beaches." Journal of Waterway, Port, Coastal, and Ocean Engineering, 133 (2007), pp.296-304

Komar, P.D., and Inman, D. L. (1970). "Longshore sand transport on beaches," Journal of Geophysical Research 75(30), 5514-5527.

Komar, P.D. (1997). "Beach processes and sedimentation." 2nd Edition. Prentice Hall, New York

Kökpınar, M.A., Darama, Y., and Güler, I. (2007). Physical and Numerical Modeling of Shoreline Evaluation of the Kızılırmak River Mouth, Turkey, Journal of Coastal Research, Vol. 23, No. 2, pp. 445-456

Kraus, N. C., and Larson, M. (1991). "NMLONG – Numerical model for simulating the longshore current. Report 1: Model development and tests," Technical Report DRP-91-1, U.S. Army Engineer Waterways Experiment Station, Vicksburg, MS.

Kuik, A.J., van Vledder, G.Ph. and Holthuijsen, L.H. (1988). "Proposed method for the routine analysis of pitch-and-roll buoy wave data." J. Phys. Oceanogr., Vol. 18, 7, 1020-1034.

Kuleli, T., Güneroğlu, A., Karslı, F. and Dihkan, M. (2011). "Automatic detection of shoreline change on coastal Ramsar wetlands of Turkey." Ocean Engineering Vol.38, pp.1141–1149

Kuriyama, Y. (2010). "Prediction of cross-shore distribution of longshore sediment transport rate in and outside the surf zone." Rep. Port and Airport Res. Inst., Vol.49, No.2.

Kuriyama, Y., and Ozaki, Y. (1993). "Longshore current distribution on a bar-trough beach, Field measurements at HORF and numerical model," Report of Port and Harbour Research Institute 32(3), Ministry of Transport, Japan, 3-37

Larson, M. and Kraus, N. C. (1991). "Numerical Model of Longshore Current for Bar and Trough Beaches," Journal of Waterway, Port, Coastal, and Ocean Engineering, Vol 117, No. 4, pp.326-347.

Larson, M. and Kraus, N.C. (2002). "NMLONG: numerical model for simulating longshore current; report 2: wave–current interaction, roller modeling, and validation of model enhancements." Technical Report ERDC/CHL TR-02-22, US Army Engineer Research and Development Center, Vicksburg, MS.

Larson, M. and Wamsley, T.V. (2007). "A formula for longshore sediment transport in the swash." Proc. Coastal Sediment'07, ASCE, pp. 1924-1937.

Larson, M., Kraus, N.C, and Connell, K.J. (2006). "Cascade Version 1 : Theory and model formulation." ERDC TNSWWRP-06-7. Vicksburg, Mississippi: U.S. Army Engineer Research and Development Center.

Larson, M., Kraus, N.C, and Hanson, H. (2002). "Simulation of regional longshore sediment transport and coastal evolution - the 'Cascade' model." Proc. of 28th Coastal Eng. Conf., World Scientific Press, Singapore, 2,612-2,624.

Larson, M., Kraus, N.C. and Hanson, H. (1990). "Decoupled numericalmodel of three-dimensional beach range." Proc. 22nd Coastal Eng. Conf.. ASCE, pp. 2173–2185.

Lax, P.D and Wendroff, B. (1960). "Systems of conservation laws." Commun. Pure Applied Math. 13 (2): 217–237

LeMehaute, B. (1962). "On non-saturated breakers and the wave run-up. Proc. 8th Int. Coastal Eng. Conf. Mexico, 1962, p. 77-92,

Leffler, M., Baron, C., Scarborough, B., Hathaway, K., Hodges, P., Townsend, C., (1996). "Annual Data Summary for 1994 CERC Field Research Facility." TR CERC-96-6, WES Vicksburg, MS.

Lin, L. and Demirbilek, Z. (2005). "Evaluation of Two Numerical Wave Models with Inlet Physical Model." Journal of Waterway, Port, Coastal, And Ocean Engineering ASCE, July-August, pp149-161

Lin, L., Z. Demirbilek, H. Mase, J. Zheng, and F. Yamada. (2008). "CMS-Wave: a nearshore spectral wave processes model for coastal inlets and navigation projects." Coastal Inlets Research Program, Coastal and Hydraulics Laboratory Technical Report ERDC/CHL TR-08-13. Vicksburg, MS: U.S. Army Engineer Research and Development Center.

Liu, Z. (2001). "Sediment Transport." Laboratoriet for Hydraulik og Havnebygning Instituttet for Vand, Jord og Miljøteknik Aalborg Universitet

Longuet-Higgins, M.S. (1970). "Longshore current generated by obliquely incident sea waves, 1 & 2" J. Geophys. Res. 75(33), pp.6779-6801.

Longuet-Higgins, M.S. and Stewart, R.W. (1964). "Radiation stresses in water waves; a physical discussion with applications." Deep-Sea Res 11:529–562

Longuet-Higgins, M.S. Cartwright, D.E., Smith, N.D., (1963). "Observations of the directional spectrum of sea waves using motions of a floating buoy." In: Ocean Wave Spectra. Prentice Hall, New York, pp. 111–136.

Luijendijk, A.P., Henrotte, J., Walstra, D.J.R., van Ormondt, M. (2010). "Quasi-3d Modelling of Surf Zone Dynamics." Proc. 32th Int. Conf. on Coastal Eng.

Madsen, P. A., Larsen, J. (1987). "An Efficient Finite-Difference Approach to the Mild-Slope Equation." Coastal Eng., 11: 329-351

Mangor, K. (2004). "Shoreline Management Guidelines." DHI Water and Environment, 294pp

Mase, H., (2001). "Multidirectional random wave transformation model based on energy balance equation." Coastal Eng. Journal 43 (4), 317–337.

Mase, H., Amamori, H., and Takayama, T. (2005). "Wave prediction model in wave-current coexisting field." Proc. of 12th Canadian Coastal Conf., Dartmouth, CSCE

Mase, H., and Kitano, T. (2000). "Spectrum-based prediction model for random wave transformation over arbitrary bottom topography." Coastal Eng. Journal 42(1):111-151.

Masselink, G. and Hughes, M. G. (2003). "Introduction to Coastal Processes and Geomorphology." Edward Arnold, London, 354 pp.

Mei, C.C. and LeMehaute, B. (1966). "Note on the equations of long waves on uneven bottom." Journal of Geophysical Research, 72 (1966), no. 2, 815-827.

Miche, M. (1951). "Le Pouvoir Réfléchissant des Ouvrages Maritimes Exposés à l'Action de la Houle," Annals des Ponts et Chaussess, 121e Annee, pp.285-319 (translated by Lincoln and Chevron, University of California, Berkeley, Wave Research Laboratory, Series 3, Issue 363, June 1954).

Militello, A., Reed, C. W., Zundel, A. K., and Kraus, N. C. (2004). "Two-dimensional depth-averaged circulation model M2D: Version 2.0, Report 1: Documentation and user's guide," ERDC/CHL TR-04-02, U.S. Army Engineer Research and Development Center, Vicksburg, MS.

Miller, H.C. (1998). "Comparison of storm longshore transport rates to predictions." Proc. 26th Int. Conf. Coastal Eng., ASCE, pp.2967-2954.

Miller, H.C. (1999). "Field measurements of longshore sediment transport during storms." Coastal Eng., Vol. 36, p. 301-321

Mitsuyasu, H., (1970). "On the growth of spectrum of wind-generated waves (2)—spectral shape of wind waves at finite fetch." Proc. 17th Japanese Conf. on Coastal Eng., pp.1–7 (in Japanese).

Mitsuyasu, H., Suhaya, T., Mizuno, S., Ohkuso, M., Honda, T., and Rikiishi, K. (1975). "Observations of the directional spectrum of ocean waves using a cloverleaf buoy." J. Phys. Oceanogr., 5, 750–760

Nairn, R.B. (1990). "Prediction of cross-shore sediment transport and beach profile evolution." Ph.D thesis, Imperial College, London, 391 pp.

Nam, P.T., Larson, M., Hanson, H., and Hoan, L.X. (2009). "A numerical model of nearshore waves, currents, and sediment transport." Coastal Eng. 56, pp.1084-1096

Nam, P.T., Larson, M., and Hanson, H. (2010). "Modeling Morphological Evolution In The Vicinity Of Coastal Structures." Proc. of the International Conf. on Coastal Eng., No.32

Nielsen, P. (1992). "Coastal bottom boundary layers and sediment transport," World Scientific, New Jersey, 324 pp.

Nishimura, H., Maruyama, K., Hirakuchi, H. (1983). "Wave field analysis by finite difference method." Proc. 30th Japanese Conf. Coastal Eng, pp. 123 – 127R (in Japanese).

O'Reilly, W.C., and Guza, R.T. (1991). "Comparison of spectral refraction and refraction diffraction wave model." J. Waterway. Port. Coastal Ocean Eng., vol.117. no.3 pp.199-214.

Okayasu, A. and Katayama, H. (1992). "Distribution of undertow and long-wave component velocity due to random waves," Proc. 23rd Coastal Eng. Conf., ASCE, pp.883-893.

Panchang, V.G., Pearce B.R., Wei G., Cushman-Roisin, B.. (1991). "Solution of the Mild-Slope Wave Equation by iteration." Applied Ocean Research, 13 (4): 187-199

Park, K.-Y., and Borthwick, A.G.L. (2001). "Quadtree grid numerical model of nearshore wave-current interaction." Coastal Engineering Vol.42, pp.219-239

Pelnard-Considere, R. (1956). "Essai de Theorie de l'Evolution des Forms de Rivage en Plage de Sable et de Galets." 4th Journees de l'Hydraulique, Les Energies de la Mer, Question III, Rapport No.1, pg.289-298

Penny, W.G., and Price, A.T. (1952). "The Diffraction Theory of Sea Waves by Breakwaters, and the Shelter Afforded by Breakwaters," Philosophical Transactions, Royal Society of London, Series A, Vol.244, pg.236-253

Peregrine, D.H. (1967). "Long waves on a beach." Journal of Fluid Mechanics 27 (4): 815–827

Perenne, N. (2005). "MARS: a Model for Applications at Regional Scale," Documentation Scientifique Ver.1.0. User Manual, 45p.

Pierson, W.J.Jr., and Moskowitz, L. (1964). "A Proposed Spectral Form for Fully Developed Wind Seas Based on the Similarity Theory of S. A. Kitaigorodskii." J. Geophys. Res., 69(24), pp.5181–5190

Pierson, W.J.Jr., Tuttell, J. J. and Woolley, J. A. (1952). "The theory of the refraction of a short crested Gaussian sea surface with applications to the northern New Jersey Coast." Proc. 3rd Conf. Coastal Eng., 685–692.

Radder, A. C. (1979). "On the Parabolic Equation Method for Water-Wave Propagation," Journal of Fluid Mechanics, Vol 95, Part 1, pp.159-176.

Raubenheimer, B., Guza, R.T., Elgar, S. (1996). "Wave transformation across the inner surf zone." J. Geophys. Res. 101, 25589–25597.

Raubenheimer,B. (2002). "Observations and predictions of fluid velocities in the surf and swash zones." J. Geophys. Res. 107, 3190.

Reeve, D., Chadwick, A. and Fleming, C. (2004). "Coastal Engineering: Processes, theory and design practice", Spon Press, Taylor & Francis Group, 461p.

Reniers, A.J.H.M. and Battjes, J.A. (1997). "A laboratory study of longshore currents over barred and non-barred beaches." Coast. Eng. Vol.30, pp.1-22

Requejo, S., Medina, R. and Gonzalez, M. (2008). "Development of a medium-long term beach evolution model." Coastal Eng., Vol.55(12), pp.1074-1088.

Resio, D.T. (1988). "A steady-state wave model for coastal applications." Proc. 21st Int. Conf.Coastal Eng., ASCE, pp. 929–940.

Ribberink, J.S. (1998). "Bed-load transport for steady flows and unsteady oscillatory flows." Coastal Eng., Vol.34, pp.59-82.

Rivero, F.J., Arcilla, A.S., Carci, E. (1997). "An analysis of diffraction in spectral wave models." In: Proc. of the Third International Symposium of Ocean Wave Measurement and Analysis, ASCE, Reston, VA, USA, pp. 431–445.

Roelvink, D., Reniers, A., van Dongeren, A., van Thiel de Vries, J., McCall, R., Lescinski, J. (2009). "Modelling storm impacts on beaches, dunes and barrier islands." Coastal Eng. 56, 1133-1152.

Ruessink, B.G., Houwman, K.T., Hoekstra, P. (1998). "The systematic contribution of transporting mechanisms to the cross-shore sediment transport in water depths 3 to 9 m." Mar. Geol. 152, pp.295–324.

Ruessink, B.G., Miles, J.R., Feddersen, F., Guza, R.T., Elgar, S. (2001). "Modeling the alongshore current on barred beaches." J.Geophys. Res. 106, pp.22451–22463.

Ruessink, B.G., Walstra, D.J.R., Southgate, H.N. (2003). "Calibration and verification of a parametric wave model on barred beaches." Coastal Eng. Vol.48, pp.139–149.

Saint-Cast, F. (2002). "Modélisation de la morphodynamique des corps sableux en milieu littoral." Bordeaux, France: University of Bordeaux I, Ph.D. thesis, 247p.

Saint-Venant, A.J.C.d. (1871). "Theorie du mouvement non-permanent des eaux, avec application aux crues des rivieres et a l'introduction des marees dans leur lit." C. R. Acad. Sc. Paris, 73:147–154, 1871.

Schoonees, J.S., and Theron, A.K. (1993). "Review of the field data base for longshore sediment transport." Coastal Eng. Vol.19, pp.1-25.

Schoonees, J.S. and Theron, A.K. (1996). "Improvement of the most accurate longshore transport formula." Proc. 25th ICCE, Orlando, USA

Shimizu, T., Kumagai, T., Watanabe, A., (1996). "Improved 3-D beach evolution model coupled with the shoreline model (3D-shore)." Proc. 25th Coastal Eng. Conf.. ASCE, pp. 2843–2856.

SPM. (1984). "Shore Protection Manual." Department of the Army, U.S. Corps of Engineers, Washington, DC 20314.

Smith, E.R. (2006). "Longshore Sediment Transport Rate Calculated Incorporating Wave Orbital Velocity Fluctuations." Technical Report, U.S. Army Corps of Engineers, ERDC/CHL TR-06-18, September 2006

Smith, E.R., Ebersole, B. and Wang, P. (2004). "Dependence of Total Longshore Sediment Transport Rates on Incident Wave Parameters and Breaker Type." Technical Report, U.S. Army Corps of Engineers, ERDC/CHL CHETN-IV-62, September 2004

Smith, J.M., and Zundel, A.K. (2006). "Full-Plane STWAVE: I. SMS graphical interface." ERDC/CHL CHETN I-71. Vicksburg, MS: U.S. Army Engineer Research and Development Center

Smith, J.M., Larson, M. and Kraus, N.C. (1993). "Longshore current on a barred beach: Field measurement and calculation," J. Geophys. Res. 98 (C12), 22,717-22,731.

Smith, J.M., Sherlock, A.R. and Resio, D.T. (2001). "STWAVE: Steady-state spectral wave Model User's Manual for STWAVE Version 3.0." CE-ERDC/CHL 1R-01-1, U.S. Army Engineer Research and Development Center, Coastal and Hydraulics Laboratory, Vicksburg, MS

Smith, R. and Sprinks, T. (1975). "Scattering of surface waves by a conical island." J. Fluid Mech. 72, 373 – 384

Sommerfeld, A. (1896). "Mathematische Theorie der Diffraction," Mathematische Annalen, Vol.47, pg.317-374

Soulsby, R. L. and Whitehouse, R. J. S. W. (1997). "Threshold of sediment motion in coastal environments." Proc. Pacific Coasts and Ports '97 Conf., Christchurch, 1, pp. 149154. University of Canterbury, New Zealand

Svendsen, I.A. (1984). "Wave Heights and Setup in a Surf Zone," Coastal Eng., Vol 8, No. 4, pp303-329.

Svendsen, I.A., Haas, K. and Zhao, Q. (2004). "Quasi-3D Nearshore Circulation Model SHORECIRC: Version 2.0." Research Report, Center for Applied Coastal Research, University of Delaware.

Svendsen, I.A. and R.S. Lorenz (1989). "Velocities in combined undertow and longshore currents." Coastal Eng., 13, pp.55-79

Syme, W.J. (1991). "Dynamically Linked Two-Dimensional/One-Dimensional Hydrodynamic Modelling Program for Rivers, Estuaries & Coastal Waters." William Syme, M.Sc. Thesis, Dept of Civil Engineering, The University of Queensland, May (1991)

Şafak, I. (2006). "Numerical Modeling of Wind Wave Induced Longshore Sediment Transport." M.S. Thesis, METU, Ankara

Tajima, Y. and Madsen, O. S. (2003). "Modeling near-shore waves and surface roller" in Proc. 2nd Int. Conf. Asian and Pacific Coasts (APAC 2003), Makuhari, Chiba, Japan, Paper No. 28 in CD-ROM, 12p.

Tajima, Y. and Madsen, O. S. (2006). "Modeling Near-Shore Waves, Surface Rollers, and Undertow Velocity Profiles." Journal of Waterway, Port, Coastal, And Ocean Engineering, 429, ASCE"

Tang, J., (2011). personal communication

Tang, J., Shen, Y.M. and Cui, L. (2008). "Modeling Near-Shore Currents Induced by Irregular Breaking Wave." Journal of Coastal Research, Special Issue 52, pp.245-252, Florida, USA

Tang, Y. and Ouellet, Y., (1992) Models for combined refraction-diffraction of water waves with nonlinear harmonics. In: Proc. of the Annual Conf. of the Canadian Society for Civil Engineering, Quebec, Vol. II, pp. 421-430.

Tang, Y. (1994). "Linear and nonlinear water waves on water with variable depth - theoretical and numerical models for combined refraction-diffraction with reflection." Ph.D. Thesis, Dept. of Civil Engineering, Laval University, Quebec

Tang, Y. and Ouellet Y. (1997). "A New Kind of Nonlinear Mild-Slope Equation for Combined Refraction- Diffraction of Multifrequency Waves." Coastal Eng., 31: 3-36

Thomson, J., Elgar, S., Herbers, T.H.C., Raubenheimer, B., Guza, R.T. (2006). "Tidal modulation of infragravity waves via nonlinear energy losses in the surfzone." Geophys. Res. Lett. 33, L05601

Thornton, E.B. and Guza, R.T. (1983). "Transformation of Wave Height Distribution," Journal of Geophysical Research, Vol 88, No. C10, pp.5925-5938.

Thornton, E.B. and Guza, R.T. (1986). "Surf zone longshore currents and random waves: Field data and models." Phys. Oceanogr. 16, pp.1165-1178.

Thornton, E.B. and Kim, C.S. (1993). "Longshore Current and Wave Height Modulation at Tidal Frequency Inside the Surf Zone." J. Geophysical Research, 98(C9), 16,509 16,519.

Tolman, H.L., (1991) "A third-generation model for wind waves on slowly varying, unsteady and inhomogeneous depths and currents." J. Phys. Oceanogr., 21, 6, 782-797

Trifonova, E. and D. Grudeva. (2002). "Sea Level Surface Variations in Bourgas and Varna Bays." Proc. of Second Int. Conf. on Oceanography of Eastern Mediterranean and Black Sea: Similarities and Differences of Two Interconnected Basins, TUBITAK Publishers, Ankara, Turkey, pp.151-155

Troch, P. (1998). "A numerical model for propagation and transformation of linear water waves." Department of Civil Engineering, Ghent University, Ghent, Belgium, http://awww.ugent.be/en/coastal/research/mildwave/mildwave.php

URL-1: http://chl.erdc.usace.army.mil, last visited on December, 2011

URL-2: http://www.frf.usace.army.mil/SandyDuck/Gallery-SandyDuck.stm, last visited on December, 2011

URL-3: http://www.ramsar.org, last visited on December, 2011

Van Dongeren, A.R., Sancho, F.E., Svendsen, I.A. and Putrevu, U. (1994). "SHORECIRC: A quasi 3-D nearshore model." Proc., 24th Int. Conf. on Coast. Engrg., ASCE, 2741-2754.

Van Maanen, B., de Ruiter, P.J. and Ruessink, B.G. (2009). "An evaluation of two alongshore transport equations with filed measurements." Coastal Eng., Vol.56, pp.313-319.

Van Rijn, L.C. (1984). "Sediment transport: Part I: Bed load transport; Part II: Suspended load transport; Part III: Bed forms and alluvial roughness." Journal of Hydraulic Division 110 (10), 1431-1456; 110 (11) 1613– 1641; 110 (12) 1733-1754.

Van Rijn, L.C. (2004). "Longshore Sediment Transport." Report Z3054.20, Delft Hydraulics, Netherlands.

Van Rijn, L.C. (2009), personal communication

Vigo, I., Garcia, D., Chao, B.F. (2005). "Change of sea level trend in the Mediterranean and Black seas, Journal of Marine Research 63, pp.1085–1100.

Vincent, C.L. and Briggs, M.J. (1989). "Refraction-diffraction of irregular waves over a mound." J. Waterways, Port, Coast., Ocean Eng., ASCE 115 (2), pp269–284.

WAMDI Group. (1988). "The WAM model – a third generation ocean wave prediction model." J. Phys. Oceanogr., 18, 1775–1810

Wang, P., Ebersole, B. A., Smith, E. R., and Johnson, B. D. (2002b). "Temporal and spatial variations of surf-zone currents and suspended sediment concentration." Coastal Eng., 46, pp.175–211.

Wang, P., Ebersole, B.A. and Smith, E.R. (2002c). "Longshore sand transport-initial results from large-scale sediment transport facility." U.S. Army Corps of Engineers, ERDC/CHL CHETN-II-46. 10 pp.

Wang, P., Ebersole, B.A., Smith, E.R. and Johnson, B.D. (2002). "Temporal and spatial variations of surf-zone currents and suspended sediment concentration." Coastal Eng. Vol.46, pp.175–211

Wang, P., Smith, E.R. and Ebersole, B.A. (2002a). "Large-scale laboratory measurements of longshore sediment transport under spilling and plunging breakers." Journal of Coastal Research 18 (1), 118– 135.

Warner, J.C., Sherwood, C.R., Signell, R.P., Harris C.K. and Arangoc, H.G. (2008). "Development of a three-dimensional, regional, coupled wave, current, and sediment-transport model." Computers & Geosciences 34, 1284–1306

Watanabe, A. (1992). "Total rate and distribution of longshore sand transport." Proc. of the 23rd Coastal Eng. Conf., pp. 2528-2541.

Weggel, J.R. (1972). "Maximum Breaker Height." Journal of the Waterways, Harbors and Coastal Eng. Division, Vol 98, No. WW4, pp.529-548.

Wei, G., Kirby, J.T., Grilli, S.T. and Subramanya, R. (1995). "A fully nonlinear Boussinesq model for surface waves. part 1: Highly nonlinear unsteady waves." J. Fluid Mech., 294, pp.71-92

Whitford, D.J. and Thornton, E.B. (1993). "Comparison of wind and wave forcing of longshore currents," Continental Shelf Research, 13 (11) (1993), pp.1205–1218

Whitham, G.B. (1974). "Linear and Nonlinear Waves." Wiley Interscience, 636 pp.

Wiegel, R.L. (1962). "Diffraction of Waves by Semi-infinite Breakwater," Journal of the Hydraulics Division, ASCE, Vol.88, No.HY1, pg.27-44

Wilson, B.W. (1965). "Numerical prediction of ocean waves in the North Atlantic for December, 1959," Deutche Hydr. Zeit 18 (3) (1965), pp. 114-130.

APPENDIX A

SAMPLE CROSS-SHORE DISTRIBUTIONS OF STRESS TERMS IN NON-LINEAR SHALLOW WATER EQUATIONS

To show the order of magnitude of the stress terms existing in the non-linear shallow water equations (Eq.3.28-Eq.3.30), sample simulations are carried out for two different bottom profiles given in the laboratory experiments of Battjes and Janssen (1978). The first bottom profile has a uniform slope of 1:20 and the second bottom profile has a bar with a 1:40 landward slope and 1:20 seaward slope as shown in Figure 4.16. The stress terms in the equation of conservation of momentum in *y*-direction are given below,

$$R_y = \frac{1}{\rho(h+\bar{\eta})}\left(\frac{\partial S_{yx}}{\partial x} + \frac{\partial S_{yy}}{\partial y}\right) \tag{A.1}$$

$$S_y = \frac{1}{\rho(h+\bar{\eta})}\left(\frac{\partial}{\partial x}(E_{sr}\sin 2\bar{\theta}) + \frac{\partial}{\partial y}(2E_{sr}\sin^2\bar{\theta})\right) \tag{A.2}$$

$$F_y = R_y + S_y \tag{A.3}$$

$$T_y = \frac{1}{\rho(h+\bar{\eta})}\left(\frac{2}{\pi}\cdot\rho\cdot c_f\cdot v\cdot u_0\right) \tag{A.4}$$

$$A_y = \frac{\partial}{\partial x}\left[\mu\frac{\partial v}{\partial x}\right] + \frac{\partial}{\partial y}\left[\mu\frac{\partial v}{\partial y}\right] \tag{A.5}$$

where R_y is the stress term due to radiation stress gradients only, S_y is the stress term due to surface rollers only, F_y is the sum of radiation and surface roller stress terms, T_y is the bottom shear stress term and the A_y is the lateral mixing term in y-direction.

In the sample simulations for two bottom profiles, the deep water significant wave height is taken H_{s0}=0.2 m, and significant wave period as T_p=2.0 sec, the deep water mean approach angle is taken as θ=30°, the grid spacing is taken as 0.1 m in both x and y directions, the directional spreading parameter, breaker index, eddy constant, bottom friction and surface roller constants are taken as s_{max}=25, γ_{br}=0.78, Λ=0.5, c_f=0.005 and α=0.5 respectively. For the bottom profile with a uniform slope of 1:20, the computed nearshore significant wave height (H_s), change in the mean water level ($\bar{\eta}$), depth-averaged longshore current velocity (v) and the stress terms in y-direction (R_y, S_y, F_y, T_y and A_y) are given in Figure A.1-A.2.
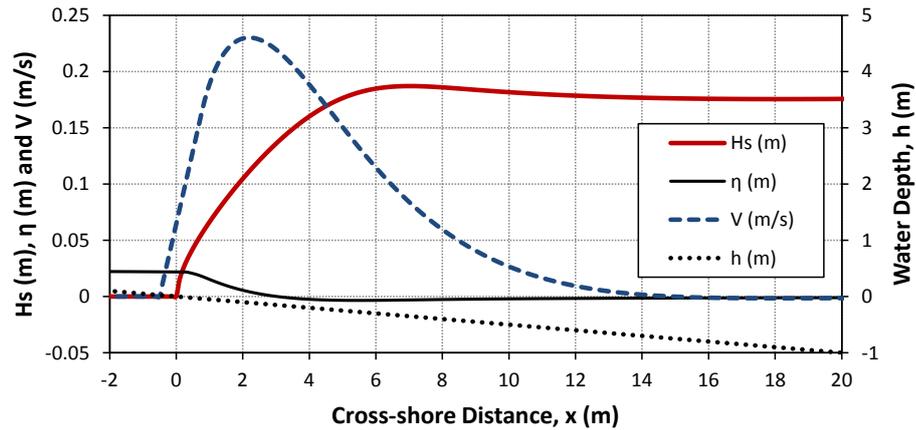

Figure A.1 The computed nearshore significant wave height (H_s), change in the mean water level ($\bar{\eta}$), depth-averaged longshore current velocity (v) for the uniform slope
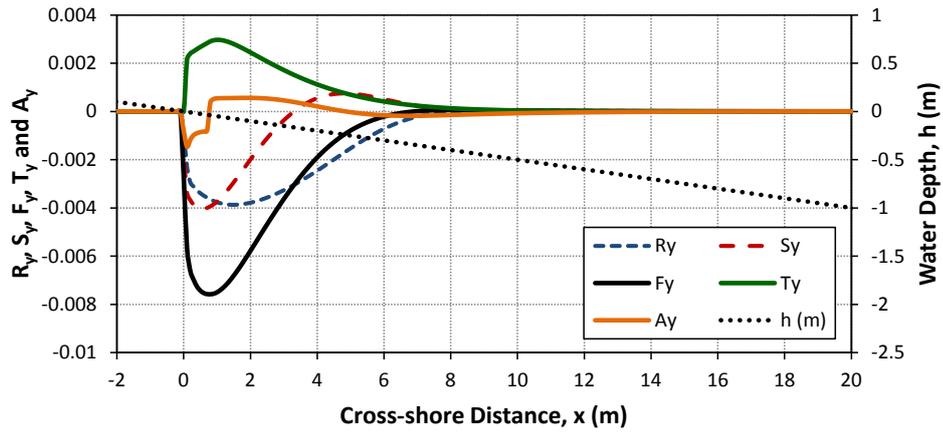
Figure A.2 The computed stress terms in *y*-direction (R_y, S_y, F_y, T_y and A_y) for the uniform slope

For the bar profile, the computed nearshore significant wave height (H_s), change in the mean water level ($\bar{\eta}$), depth-averaged longshore current velocity (*v*) and the stress terms in *y*-direction (R_y, S_y, F_y, T_y and A_y) are given in in Figure A.3-A.4.
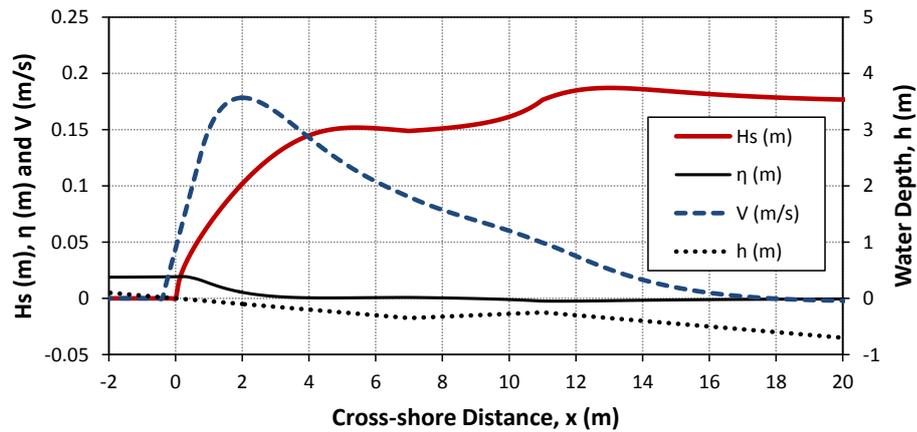
Figure A.3 The computed nearshore significant wave height (H_s), change in the mean water level ($\bar{\boldsymbol{\eta}}$), depth-averaged longshore current velocity (*v*) for the bar profile
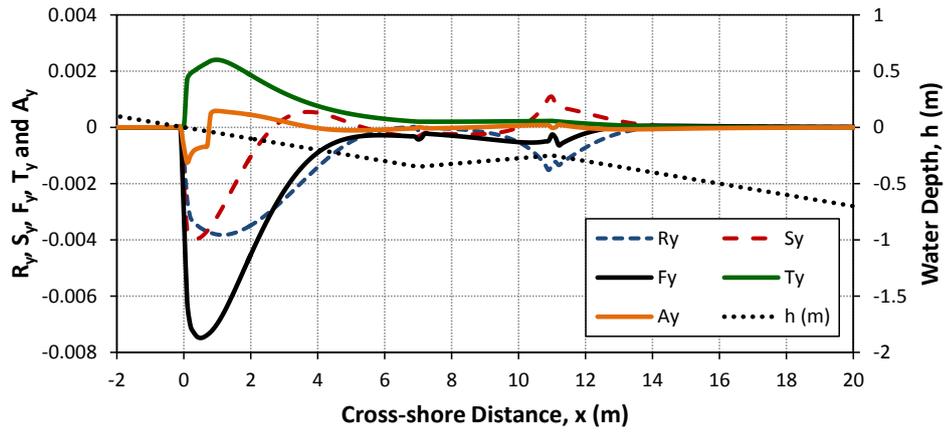
Figure A.4 The computed stress terms in *y*-direction (R_y, S_y, F_y, T_y and A_y) for the bar profile

For the above given sample computations (), it is seen from that the sum of radiation and surface roller stress terms (F_y) is the governing stress term in the conservation of momentum equation in y-direction. The second governing term is the bottom shear stress term (T_y) which acts in the opposite sense with the F_y term.

CURRICULUM VITAE

PERSONAL INFORMATION

Surname, Name   : Baykal, Cüneyt

Nationality   : Turkish (TC)

Date and Place of Birth : 4 July 1980, Eskişehir

Phone   : +90 232 382 06 54

e-mail   : cbaykal@gmail.com

EDUCATION

Degree	Institution	Year of Graduation
MS	METU, Civil Engineering	2006
BS	METU, Civil Engineering	2003
High School	İzmir Karşıyaka Anatolian High School, İzmir	1998

WORK EXPERIENCE

Year	Place	Enrollment
2007-2011	METU, Department of Civil Engineering	Research Assistant
2006	Danish Hydraulic Institute	Intern Engineer
2004-2006	PETEK Design Engineering Construction Co.	Project Engineer

FOREIGN LANGUAGES

English (fluent)

PUBLICATIONS

Baykal, C., Ergin, A., Güler, I. (2011). "Numerical Modeling of Longshore Currents." 7th National Coastal Engineering Symposium, Trabzon, Turkey (in Turkish)

Baykal, C., Ergin, A., Güler, I. (2011). "Book Chapter: Intervention of Human Activities on Geomorphological Evolution of Coastal Areas: Cases from Turkey." Geomorphology, Intech Open Access Publisher, ISBN 979-953-307-113-7 (in print)

Özyurt, G., Ergin, A., Baykal, C. (2010). "Fuzzy Vulnerability Assessment Of Coastal Areas To Sea Level Rise." Proc. of 32nd Int. Conf. on Coastal Engineering, June 30 - July 5, 2010, Shanghai, China

Güler, I., Baykal, C., Ergin, A. (2008). "Shore Stabilization by Artificial Nourishment, A Case Study: A Coastal Erosion Problem in Side, Turkey." 7th International Conference on Coastal and Port Engineering in Developing Countries, 24-28 Feb. 2008, Dubai, UAE

Esen, M., Baykal, C., Güler, I., Ergin, A. (2007). "Yapay Besleme ile Kıyı Dengelenmesi, Örnek Uygulama: Bir Kıyı Aşınımı Sorunu, Side, Türkiye." 6th National Coastal Engineering Symposium, Izmir, Turkey (in Turkish)

Ergin, A., Güler, I., Yalçıner, A.C., Baykal, C., Artagan S.S., Safak, I. (2006). "A One-Line Numerical Model for Wind Wave Induced Shoreline Changes." 7th International Congress on Advances in Civil Engineering, Yıldız Technical University, Istanbul, Turkey

Baykal, C. (2006). "Numerical Modeling of Wave Diffraction in One-Dimensional Shoreline Change Model." M.S. Thesis, METU, Ankara, Turkey

HOBBIES

Movies, Computer Technologies, Table Tennis, Football, Scuba Diving